



**HAL**  
open science

# Revisiting initiation mechanisms of gaseous detonations

Raúl Hernández Sánchez

► **To cite this version:**

Raúl Hernández Sánchez. Revisiting initiation mechanisms of gaseous detonations. Fluids mechanics [physics.class-ph]. Aix-Marseille Université, 2023. English. NNT : 2023AIXM0266 . tel-04789544

**HAL Id: tel-04789544**

**<https://theses.hal.science/tel-04789544v1>**

Submitted on 18 Nov 2024

**HAL** is a multi-disciplinary open access archive for the deposit and dissemination of scientific research documents, whether they are published or not. The documents may come from teaching and research institutions in France or abroad, or from public or private research centers.

L'archive ouverte pluridisciplinaire **HAL**, est destinée au dépôt et à la diffusion de documents scientifiques de niveau recherche, publiés ou non, émanant des établissements d'enseignement et de recherche français ou étrangers, des laboratoires publics ou privés.



Distributed under a Creative Commons Attribution - NonCommercial - NoDerivatives 4.0 International License

# THÈSE DE DOCTORAT

Soutenue à Aix-Marseille Université

le 11 juillet 2023 par

## Raúl HERNÁNDEZ SÁNCHEZ

### Revisiting Initiation Mechanisms of Gaseous Detonations: Theoretical and Numerical Study of One-Dimensional Models

#### Composition du jury

#### Discipline

Sciences pour l'Ingénieur

#### Spécialité

Mécanique et Physique des  
Fluides

#### École doctorale

ED 353 Sciences pour l'Ingénieur :  
Mécanique, Physique, Micro et  
Nanoélectronique

#### Laboratoire

Institut de Recherche sur les  
Phénomènes Hors Équilibre  
(IRPHÉ)

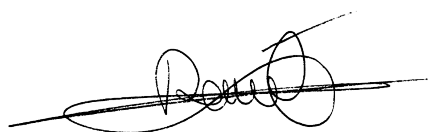
•	Luc VERVISCH	Président du jury
•	Professeur des Universités, CORIA, INSA Rouen Normandie	
•	Nabiha CHAUMEIX	Rapporteuse
•	Directrice de Recherche, ICARE, CNRS	
•	Pierre VIDAL	Rapporteur
•	Chargé de Recherche, PPRIME, CNRS	
•	César HUETE	Examineur
•	Maitre de Conférences, Universidad Carlos III de Madrid	
•	Ratiba ZITOUN	Examinatrice
•	Maitre de Conférences, PPRIME, Université de Poitiers	
•	Bruno DENET	Directeur de thèse
•	Professeur des Universités, IRPHE, Aix-Marseille Université	
•	Paul CLAVIN	Invité
•	Professeur Émérite, IRPHE, Aix-Marseille Université	



I, undersigned, Raúl Hernández Sánchez, hereby declare that the work presented in this manuscript is my own work, carried out under the scientific direction of Bruno Denet, in accordance with the principles of honesty, integrity and responsibility inherent to the research mission. The research work and the writing of this manuscript have been carried out in compliance with both the French National Charter for Research Integrity and the Aix-Marseille University charter on the fight against plagiarism.

This work has not been submitted previously either in this country or in another country in the same or in a similar version to any other examination body.

Signed in Marseille the 11th July, 2023



Cette œuvre est mise à disposition selon les termes de la Licence Creative Commons Attribution - Pas d'Utilisation Commerciale - Pas de Modification 4.0 International.



A mis padres. . .

“Le voyageur qui franchit sa montagne dans  
la direction d’une étoile, s’il se laisse trop  
absorber par ses problèmes d’escalade,  
risque d’oublier quelle étoile le guide.”  
– Antoine de Saint-Exupéry



## Acknowledgements • Remerciements • Agradecimientos

Ce travail a été soutenu par l'ANR (Agence National de la Recherche) dans le cadre du projet ANR-18-CE05-0030 'ReDDT' (Revisiting Deflagration to Detonation Transition in the context of carbon-free energy production).

Je tiens tout d'abord à remercier sincèrement les membres du jury pour le temps qu'ils ont consacré à la lecture et à l'évaluation de mon travail. Je remercie en particulier Nabiha Chaumeix et Pierre Vidal d'avoir accepté de prendre le rôle de rapporteurs pour examiner dans un premier temps l'adéquation de ce dissertation à une soutenance de thèse et de me faire part de leurs remarques pertinentes pour l'amélioration du manuscrit. Je remercie également Luc Versvisch et Ratiba Zitoun d'avoir faire partie du jury de cette thèse en animant la soutenance et en apportant leur expertise à une discussion scientifique enrichissante. *Finalmente, aprovechando que compartimos lengua materna, agradezco individualmente a César Huete su completa disposición a desplazarse a Marsella para participar en este jurado.*

Ce travail de thèse a été développé grâce à l'encadrement et au soutien de mes directeurs de thèse. Je tiens donc à remercier mon directeur de thèse, Bruno Denet, pour avoir accepté d'encadrer cette thèse et pour la liberté qu'il m'a accordée tout au long de ce projet de recherche. Je voudrais également remercier mon co-encadrant, Paul Clavin, pour m'avoir ouvert les portes du réputé laboratoire fondé par lui-même, pour m'avoir guidé à travers les problèmes fondamentaux de la détonation et fixé les limites de la recherche, pour avoir partagé avec moi son expertise sur les développements asymptotiques, pour son esprit critique et ses défis constants pour améliorer le travail et, de manière générale, pour sa vaste contribution à la compréhension des fronts réactifs.

Les collègues et amis avec lesquels j'ai partagé ces années de thèse ont également joué un rôle fondamental dans la réussite de ce travail. La bonne ambiance qui règne entre les doctorants de l'IRPHE a été d'une grande importance pour le développement de cette thèse. Je tiens donc à remercier un par un les doctorants qui m'ont accueilli dans ce groupe : Fabien, Keshav, Sarah, Romain, Pierre, Daphné, qui ont été des modèles d'excellentes doctorants, mais dont j'ai aussi appris de la richesse du français à la magie du terminal Linux en passant par la pratique de l'escalade. Je remercie tout particulièrement Amélie qui, après avoir faire partie du groupe des doctorants modèles, m'a également guidé dans mon expérience d'enseignement à l'IUT avec la bienveillance qui la caractérise toujours. *I also owe a special thanks to my promotion colleagues. We lived together the arduous experience of embarking on a thesis, and only a few months later, without having had time to understand what we had gotten ourselves into, being sent to lock ourselves in our humble rented rooms for weeks in a city strange to most of us, because a virus had declared war on the world. Thanks to the always available support of Tommaso, Ahmed, Rêmi and Tristan, those confusing periods of confinement were finally nothing more than a bump on the road to becoming a doctor.* La richesse et la complicité de ce groupe se sont rapidement élargies avec l'énergies renouvelées et l'humour de Marc, Quentin, Simone, Elisabeth, Hugo, Nihal, Djihane, Florian, Roman, Selim, Elliot et Joris, que je remercie énormément pour leur soutien et leur inspiration quotidiens depuis leur



arrivée. Je n'oublie pas, mais je remercie tout particulièrement Lucas, qui a été un pilier fondamental pour la réussite de cette thèse. La gratitude que méritent nos longues et profondément sincères conversations sur nos préoccupations scientifiques ainsi que sur tout autre aspect de nos vies ne tiennent pas dans ces lignes. *And, even if circumstances beyond our control have hindered our collaboration, I am indebted to Hassan with whom it has always been a pleasure to discuss the challenges of our theses and I have felt his support from the distance.*

Je tiens également à remercier l'ensemble du personnel du laboratoire qui, que ce soit par une partie de pétanque, ou une démonstration d'excellence scientifique, une brève discussion lors d'une pause café ou même un simple sourire, ont contribué d'une manière ou d'une autre à la réussite de ces années de travail. Mes remerciements s'adressent également à l'ensemble du personnel du département Métiers de la Transition et de l'Efficacité Énergétiques pour m'avoir accueilli à l'IUT et m'avoir permis de terminer cette thèse dans les meilleures conditions, avec un remerciement particulier à Jean-Luc, Hervé, Jean-Marie, Laurence, Bruno et Pierre pour m'avoir initié à leurs activités d'enseignement.

*Sin el incondicional apoyo de mi familia, este trabajo no habría sido posible. Quiero extender mi agradecimiento a mis padres, cuyo esfuerzo y trabajo incansable me han permitido llegar a defender esta tesis. A mis hermanos, cuyo ejemplo de dedicación y sabios consejos han guiado mi camino académico. Y a Olivia, quién siempre está dispuesta a recordarnos que todo es un juego más que disfrutar.*

Et finalement et surtout, un grand merci à Loïse, ma plus importante découverte après des années de recherche. Ton soutien et ta patience pendant la thèse ont été cruciaux pour l'achèvement de ce projet. Ton aide pour l'intégration en France a adouci chaque difficulté rencontrée. Sans l'accueil chaleureux de la famille Coiplet et de la grande famille de Fay-en-Montagne, le défi scientifique aurait été plus difficile à relever.

Thank you very much, merci beaucoup y muchas gracias a todos!

## List of Publications and Participation in Conferences

List of publications realized in the framework of the thesis project:

- i. P. Clavin, R. Hernández Sánchez, and B. Denet (2021a). “Asymptotic Analysis of the Critical Dynamics of Spherical Gaseous Detonations”. *Journal of Fluid Mechanics* 915, A122. DOI: 10.1017/jfm.2021.196
- ii. R. Hernández Sánchez and B. Denet (2023a). “Numerical Analysis of a Flame Acceleration Runaway Model for Thin Tubes”. *Combustion and Flame, Under Review*

Participation in conferences during the thesis period:

- i. P. Clavin, R. Hernández Sánchez, and B. Denet (2021b). “Study of the Direct Initiation of Spherical Detonations”. XXV International Congress of Theoretical and Applied Mechanics (ICTAM). Milano, Italy
- ii. R. Hernández Sánchez, B. Denet, and P. Clavin (2022). “Critical Dynamics of Direct Initiation of Spherical Detonations”. 28th International Colloquium on the Dynamics of Explosions and Reactive Systems (ICDERS). Naples, Italy
- iii. R. Hernández Sánchez and B. Denet (2023b). “Numerical Study of a 1D Model for DDT at the Tip of a Flame in Narrow Channels”. 11th European Combustion Meeting (ECM). Rouen, France



## Abstract

A combustion front can propagate in the form of two distinct waves: deflagrations, subsonic flames controlled by diffusion processes, and detonations, supersonic waves producing an intense overpressure that can have catastrophic effects. This thesis aims to motivate new approaches to deal with the complex phenomenon of the initiation of gaseous detonations, which represents a physical problem of great interest in different scientific and technological fields from explosion safety to astrophysics, including propulsion.

Based on fundamental principles, mathematical models were developed to describe two primary process of detonation initiation: direct initiation and deflagration-to-detonation transition. A combination of asymptotic and numerical methods was used to analyze the interaction of gas dynamics with the internal structure of the premixed reactive waves. First, the critical dynamics of direct initiation of detonations was studied in the asymptotic limit of small heat release. Analytical and numerical results of this study exhibit similar behaviors to those found in the opposite limit of large Mach number, which underlines the relevance of the small heat release limit. Regarding the critical conditions for direct initiation, the results highlight the critical role of the sonic condition in the transition towards a self-sustained detonation regime. The front curvature is then essential to define critical initiation criteria, since the nonlinear effect of the propagation velocity on the detonation thickness prevents the sonic condition from being reached when the front curvature exceeds a critical value. Secondly, a simplified one-dimensional model for the tip of elongated flames propagating along thin tubes was studied. In this model, flame acceleration is only driven by the expansion of the combustion products and the thermal sensitivity of the rate of combustion reactions. The feedback between both mechanisms generates criticality conditions defined by a maximum flame elongation, beyond which there is no steady solution. Numerical simulations illustrate a flame acceleration runaway mechanism when the critical flame elongation is exceeded. Consequently, the onset of the detonation occurs within the internal structure of the flame when, upon the strong acceleration, the dissipation mechanisms become significant enough to trigger the formation of a shock wave.

The findings reported in this work provide insights into detonation initiation phenomena that in a context of energy decarbonization may be relevant both to ensure the safe use of alternative fuels, such as hydrogen, and to develop a new generation of more efficient combustion engines.

**Key words:** detonation theory, direct initiation, deflagration-to-detonation transition, asymptotic methods, numerical integration



## Résumé

Un front de combustion peut se propager sous la forme de deux ondes distinctes : les déflagrations, flammes subsoniques contrôlées par des processus de diffusion, et les détonations, ondes supersoniques produisant une surpression intense qui peut avoir des effets catastrophiques. Cette thèse vise à motiver de nouvelles approches pour traiter le phénomène complexe de l'initiation des détonations gazeuses, qui représente un problème physique d'un grand intérêt dans différents domaines scientifiques et technologiques tels que la sécurité des explosions et l'astrophysique, y compris la propulsion.

Sur la base des principes fondamentaux, des modèles mathématiques ont été développés pour décrire les deux principaux processus d'initiation des détonations : l'initiation directe et la transition déflagration-détonation. Une combinaison de méthodes asymptotiques et numériques a été utilisée pour analyser l'interaction de la dynamique des gaz avec la structure interne des ondes réactives prémélangées. Tout d'abord, la dynamique critique de l'initiation directe des détonations a été étudiée dans la limite asymptotique d'un faible dégagement de chaleur. Les résultats analytiques et numériques de cette étude montrent des comportements similaires à ceux trouvés dans la limite opposée d'un grand nombre de Mach, ce qui souligne la pertinence de la limite d'un faible dégagement de chaleur. En ce qui concerne les conditions critiques pour l'initiation directe, les résultats mettent en évidence le rôle critique de la condition sonique pour former une onde de détonation auto-entretenu. La courbure du front est alors essentielle pour définir les critères d'initiation critiques, puisque l'effet non linéaire de la vitesse de propagation sur l'épaisseur de la détonation empêche la condition sonique d'être atteinte lorsque la courbure du front dépasse une valeur critique. Deuxièmement, un modèle unidimensionnel simplifié pour la pointe des flammes allongées se propageant le long de tubes minces a été étudié. Dans ce modèle, l'accélération de la flamme est uniquement due à l'expansion des produits de combustion et à la sensibilité thermique de la vitesse des réactions de combustion. La rétroaction entre les deux mécanismes génère des conditions de criticité définies par une élongation maximale de la flamme au-delà de laquelle il n'y a pas de solution stationnaire. Les simulations numériques illustrent un mécanisme d'emballement de l'accélération de la flamme lorsque l'allongement critique de la flamme est dépassé. Par conséquent, la détonation se produit dans la structure interne de la flamme lorsque, suite à une forte accélération, les mécanismes de dissipation deviennent suffisamment importants pour déclencher la formation d'une onde de choc.

Dans le contexte de la décarbonisation de l'énergie, les résultats rapportés dans ce travail donnent un aperçu des phénomènes d'initiation de la détonation qui peuvent être pertinents à la fois pour assurer l'utilisation sûre de carburants alternatifs, tels que l'hydrogène, et pour développer une nouvelle génération de moteurs à combustion plus efficaces.

**Mots clés :** théorie des détonations, allumage direct, transition déflagration-détonation, méthodes asymptotiques, intégration numérique



## Resumen

Un frente de combustión puede propagarse en forma de dos ondas distintas: deflagraciones, llamas subsónicas controladas por procesos de difusión, y detonaciones, ondas supersónicas que producen una intensa sobrepresión que puede tener efectos catastróficos. Esta tesis pretende motivar nuevas aproximaciones para tratar el complejo fenómeno de la iniciación de detonaciones gaseosas, que representa un problema físico de gran interés en diferentes campos científicos y tecnológicos desde la seguridad frente a explosiones hasta la astrofísica pasando por la propulsión.

Basándose en principios fundamentales, se desarrollaron modelos matemáticos para describir dos procesos principales de iniciación de la detonación: la iniciación directa y la transición de deflagración a detonación. Se utilizó una combinación de métodos asintóticos y numéricos para analizar la interacción de la dinámica del gas con la estructura interna de las ondas reactivas premezcladas. En primer lugar, se estudió la dinámica crítica de la iniciación directa de las detonaciones en el límite asintótico de pequeña liberación de calor. Los resultados analíticos y numéricos de este estudio muestran comportamientos similares a los encontrados en el límite opuesto de gran número de Mach, lo que subraya la relevancia del límite de pequeña liberación de calor. En cuanto a las condiciones críticas para la iniciación directa, los resultados destacan el papel crítico de la condición sónica para formar una onda de detonación autosostenida. La curvatura del frente es entonces esencial para definir los criterios críticos de iniciación, ya que el efecto no lineal de la velocidad de propagación sobre el espesor de la detonación impide que se alcance la condición sónica cuando la curvatura del frente supera un valor crítico. En segundo lugar, se estudió un modelo unidimensional simplificado para la punta de llamas alargadas que se propagan a lo largo de tubos delgados. En este modelo, la aceleración de la llama está impulsada únicamente por la expansión de los productos de combustión y la sensibilidad térmica de la velocidad de las reacciones de combustión. La retroalimentación entre ambos mecanismos genera condiciones de criticidad definidas por una elongación máxima de la llama más allá de la cual no hay solución estacionaria. Las simulaciones numéricas ilustran un mecanismo de aceleración de la llama fuera de control cuando se supera el alargamiento crítico de la llama. En consecuencia, el inicio de la detonación se produce dentro de la estructura interna de la llama cuando, tras la fuerte aceleración, los mecanismos de disipación se vuelven lo suficientemente significativos como para desencadenar la formación de una onda de choque.

En el contexto de la descarbonización de la energía, los hallazgos presentados en este trabajo aportan conocimientos sobre los fenómenos de iniciación de la detonación que pueden ser relevantes tanto para garantizar el uso seguro de combustibles alternativos, como el hidrógeno, como para desarrollar una nueva generación de motores de combustión más eficientes.

**Palabras clave:** teoría de la detonación, iniciación directa, transición de deflagración a detonación, métodos asintóticos, integración numérica





---

# Contents

---

<b>Affidavit</b>	<b>ii</b>
<b>Acknowledgements</b>	<b>vi</b>
<b>List of Publications and Participation in Conferences</b>	<b>ix</b>
<b>Abstract</b>	<b>x</b>
<b>Resumé</b>	<b>xi</b>
<b>Resumen</b>	<b>xiii</b>
<b>List of Figures</b>	<b>xxi</b>
<b>List of Tables</b>	<b>xxv</b>
<b>Nomenclature</b>	<b>xxvi</b>
<b>1 Introduction</b>	<b>1</b>
1.1 Motivation . . . . .	5
1.2 Aims and Objectives . . . . .	8
1.3 Methodology . . . . .	9
1.4 Document Structure . . . . .	10
<b>2 One-dimensional compressible flow and premixed combustion waves</b>	<b>11</b>
2.1 General considerations . . . . .	12
2.2 One-dimensional compressible flow . . . . .	15
2.2.1 Unsteady compressible waves . . . . .	15

## Contents

2.2.2	Shock waves . . . . .	19
2.2.3	Strong blast wave . . . . .	26
2.3	Premixed combustion waves . . . . .	29
2.3.1	Deflagrations . . . . .	33
2.3.2	Detonations . . . . .	35
<b>3</b>	<b>Direct initiation of critical detonations in the small heat release asymptotic limit</b>	<b>41</b>
3.1	Introduction . . . . .	42
3.2	Detonation model near the self-sustained regime in the small heat release limit . . . . .	49
3.2.1	General equations . . . . .	49
3.2.2	Physical insights from steady planar detonations . . . . .	52
3.2.3	Small heat release asymptotic limit . . . . .	57
3.2.4	Chemical-kinetics model . . . . .	62
3.3	Dynamics of the combustion products behind a detonation . . . . .	67
3.3.1	Self-similar solution behind a CJ wave . . . . .	68
3.3.2	Overdriven decaying detonation . . . . .	70
3.3.3	Transitory regime in curved waves . . . . .	73
3.4	Direct initiation of a detonation . . . . .	78
3.4.1	Overdriven regimes . . . . .	78
3.4.2	Numerical integration . . . . .	79
3.4.3	Discussion of the critical dynamics . . . . .	86
3.5	Quasi-steady approximation . . . . .	91
3.5.1	Steady internal structure of self-sustained detonations . . . . .	91
3.5.2	Steady internal structure of overdriven waves . . . . .	94
3.6	Summary . . . . .	98
<b>4</b>	<b>Deflagration-to-detonation transition at the tip of a flame in thin tubes</b>	<b>99</b>
4.1	Introduction . . . . .	100
4.2	Elongated flame tip model . . . . .	102
4.2.1	Governing equations . . . . .	102
4.2.2	Steady planar flame . . . . .	106
4.2.3	One-dimensional model at the flame tip . . . . .	114
4.3	Double-discontinuity model . . . . .	118
4.3.1	Self-similar solutions . . . . .	120
4.3.2	Isentropic compression waves . . . . .	122
4.4	Internal flame structure . . . . .	127
4.4.1	Numerical method . . . . .	128
4.4.2	Steady flame propagation . . . . .	132
4.4.3	Slow flame elongation . . . . .	138
4.5	Summary . . . . .	148

<b>5</b>	<b>Conclusions and perspectives</b>	<b>151</b>
5.1	Direct Initiation . . . . .	151
5.1.1	Future work . . . . .	153
5.2	Deflagration-to-Detonation Transition . . . . .	155
5.2.1	Future work . . . . .	157
	<b>Bibliography</b>	<b>159</b>



---

## List of Figures

---

1.1	Laffitte’s streak photography of detonation direct initiation and Ballossier’s schlieren photographs of deflagration-to-detonation transition . . . . .	3
1.2	Bach et al. schlieren photographs showing subcritical and critical initiation of gaseous detonations. . . . .	4
1.3	Photographs of the consequences of the Buncefield accident in 2005 . . . . .	6
1.4	Photograph of the Type Ia supernova SN 1994D . . . . .	7
2.1	Shock formation ahead an accelerating piston . . . . .	18
2.2	Locus of the singularity in the compression wave as a function of the piston velocity law . . . . .	20
2.3	Hugoniot adiabetic curve and Michelson-Rayleigh line . . . . .	22
2.4	Rankine-Hugoniot jump relations in an inert shock wave as a function of the Mach number $M_u$ for different values of the heat capacity ratio $\gamma$ . . . . .	23
2.5	Rankine-Hugoniot jump relations (dotted black line) and linearised Rankine-Hugoniot jump relations (solid red line) for weak shock waves $M_u - 1 \ll 1$ in polytropic diatomic gases $\gamma = 1.4$ . . . . .	24
2.6	Internal structure of a weak shock wave $M_u - 1 \ll 1$ propagating towards the right (i.e., the upstream gas is at $x \rightarrow \infty$ and the shocked gas is at $x \rightarrow -\infty$ ) for a diatomic gas $\gamma = 1.4$ . . . . .	25
2.7	Physical variables distribution in the strong blast wave solution . . . . .	28
2.8	Rankine-Hugoniot curves and Michelson-Rayleigh lines for detonations and deflagrations . . . . .	31
2.9	ZND detonation structure . . . . .	37
2.10	Partially reacted Hugoniot curves and Michelson-Rayleigh lines illustrating the fluid particle path throughout the ZND detonation structure. . . . .	37
2.11	Physical variables distribution behind a strong CJ detonation . . . . .	39

*List of Figures*

3.1	Trajectories propagation velocity vs. front radius with different source energies obtained through numerical simulation . . . . .	45
3.2	Pressure $p$ and velocity $v$ profiles at different time instants $t$ around transition to CJ detonation $t_c$ in the infinitely fast reaction rate limit . . . . .	47
3.3	Temperature and density profiles at the internal structure of a steady planar detonation for different values of $\gamma$ . . . . .	53
3.4	Pressure and relative flow velocity profiles at the internal structure of a steady planar detonation for different values of $\gamma$ . . . . .	54
3.5	Characteristic lines in the internal structure of a steady planar detonation	56
3.6	Detonation structure of a CJ wave with a simplified three-step chemical-kinetics model . . . . .	64
3.7	Reduced heat release distribution $\omega(\xi)$ as a function of the propagation velocity $\dot{\alpha}_\tau$ . . . . .	66
3.8	Flow velocity profile of combustion products behind a CJ detonation . . . . .	70
3.9	Transitory flow velocity at the front behind a decaying detonation wave . . . . .	73
3.10	Transitory flow velocity profile of combustion products behind a planar detonation . . . . .	76
3.11	Transitory flow velocity profile of combustion products behind a cylindrical detonation . . . . .	77
3.12	Transitory flow velocity profile of combustion products behind a spherical detonation . . . . .	77
3.13	Initial solution for the overdriven regime of a stable spherical detonation	81
3.14	Trajectories “propagation velocity $\dot{\alpha}_\tau$ vs. front radius $\tilde{r}_f$ ” for a stable spherical detonation . . . . .	82
3.15	Trajectories “propagation velocity $\dot{\alpha}_\tau$ vs. front radius $\tilde{r}_f$ ” for a stable cylindrical detonation . . . . .	83
3.16	Trajectories “propagation velocity $\dot{\alpha}_\tau$ vs. front radius $\tilde{r}_f$ ” for a stable cylindrical detonation . . . . .	83
3.17	Trajectories “propagation velocity $\dot{\alpha}_\tau$ vs. front radius $\tilde{r}_f$ ” for a weakly unstable spherical detonation . . . . .	84
3.18	Trajectories “propagation velocity $\dot{\alpha}_\tau$ vs. front radius $\tilde{r}_f$ ” for a weakly unstable spherical detonation . . . . .	84
3.19	Trajectories “propagation velocity $\dot{\alpha}_\tau$ vs. front radius $\tilde{r}_f$ ” for a strongly unstable spherical detonation . . . . .	85
3.20	Trajectories “propagation velocity $\dot{\alpha}_\tau$ vs. front radius $\tilde{r}_f$ ” for a stable spherical detonation with lower crossover . . . . .	86
3.21	Slowdown mechanism in successful initiation . . . . .	88
3.22	Slowdown mechanism in detonation failure . . . . .	89
3.23	Comparison between the numerical results considering the internal detonation structure and the self-similar solution for the flow of products behind a discontinuous CJ detonation . . . . .	91
3.24	Flow velocity profile of a CJ detonation . . . . .	92
3.25	Steady-state detonation waves in curved geometries . . . . .	96

3.26	Comparison of the numerical results with the quasi-steady approximations	97
4.1	Internal flame structure in the asymptotic limit of large activation energy and for a finite activation energy	110
4.2	Scheme of the elongated flame model	117
4.3	Curve of self-similar solutions for a shock/flame system	121
4.4	Curve of solutions for a shock/isentropic wave/flame system	123
4.5	Profiles of the physical variables at the initialization of the numerical integration	134
4.6	Evolution towards the self-similar solution of the profiles of the physical variables	136
4.7	Self-similar profiles for different values of burned gases backflow	137
4.8	Temporal evolution of the flame position and absolute flame propagation speed for different values of the backflow of burned gases	138
4.9	Comparison of the relationships between velocities and elongation parameter obtained by the double-discontinuity model and the parametric study of the internal flame structure	139
4.10	Physical variables profiles during a quasi-steady evolution of the elongation parameter	141
4.11	Physical variable profiles in the flame internal structure during a quasi-steady evolution of the elongation parameter	142
4.12	Flame velocities with a time-dependent elongation parameter	143
4.13	Absolute flame velocity with a time-dependent elongation parameter increasing at different paces	144
4.14	Physical variable profiles in the flame internal structure at the onset of the detonation	146
4.15	Physical variable profiles in the flame internal structure at the onset of the detonation	147
4.16	Absolute flame velocity with a time-dependent elongation parameter during the onset of the detonation	148
5.1	Numerical analysis of the quasi-steady approximation	153
5.2	Flow velocity profile at $\tau_s$ when the sonic point reaches the exit of the reaction zone	154





---

## List of Tables

---

3.1	Characteristic lines behind the leading shock of a detonation . . . . .	55
3.2	Sonic regimes behind the leading shock of a detonation . . . . .	57
3.3	Simplified three step kinetic scheme of Clavin and Denet (2018) . . . . .	65
4.1	Thermochemical parameters employed in the numerical study of the internal flame structure . . . . .	128



---

# Nomenclature

---

## Acronyms

- 1D One-dimensional
- CJ Chapman-Jouguet regime
- CT Clavin & Tofaili elongated flame model
- DDT Deflagration-to-Detonation Transition
- DI Direct Initiation
- DJ Deshaies & Joulin theoretical analysis
- DL Darius-Landau hydrodynamic instability
- DNS Direct Numerical Simulation
- ODE Oblique Detonation Engine
- PDE Pulsed Detonation Engine
- RDE Rotating Detonation Engine
- RH Rankine-Hugoniot jump conditions
- ZFK Zeldovich-Frank Kamenetskii asymptotic analysis
- ZND Zeldovich-Neumann-Döring detonation internal structure

## Constants

- $k_B$  Boltzmann constant  $1.380\,649 \cdot 10^{-23}$  J/K

## Nomenclature

$N_A$	Avogadro constant	$6.022\,140\,76 \cdot 10^{23}$ mol
$R$	Universal gas constant, $R = N_A k_B$	8.314 462 618 J/molK

## Dimensionless Numbers

$Le$	Lewis number
$Pr$	Prandtl number
$Re$	Reynolds number

## Greek letters

$\beta$	Zeldovich number, $\beta \equiv \frac{E_a}{k_B T_b} \frac{T_b - T_o}{T_b}$
$\dot{\alpha}_\tau$	First order dimensionless propagation velocity of the leading shock in the small heat release limit, $\dot{\alpha}_\tau \equiv \frac{\mathcal{D} - \mathcal{D}_{oCJ}}{a_u \epsilon}$
$\epsilon$	Small parameter in the small heat release asymptotic expansion, $\epsilon \equiv \sqrt{\frac{q_m}{c_p T_u}}$
$\gamma$	Specific heat ratio, $\gamma \equiv \frac{c_p}{c_v}$
$\lambda$	Thermal conductivity
$\mu$	First order dimensionless flow velocity in the small heat release limit, $\mu \equiv \frac{a_u - (\mathcal{D}_{oCJ} - u)}{a_u \epsilon}$
$\nu$	Kinematic viscosity or momentum diffusivity, $\nu = \mu/\rho$
$\omega$	Reaction rate
$\pi$	First order dimensionless pressure in the small heat release limit, $\pi \equiv \frac{1}{\gamma \epsilon} \ln \left( \frac{p}{p_u} \right)$
$\tau$	Non dimensional time coordinate, $\tau \equiv \frac{t}{t_r} \epsilon$
$\xi$	Non dimensional spatial coordinate, $\xi \equiv \frac{r - r_f(t)}{a_u t_r}$

## Latin letters

$\rho$	Density
$\tilde{b}$	Thermal sensitivity, $\tilde{b} = \frac{T_u}{U_b} \frac{dU_b}{dT_u}$

$a$	Sound speed
$b$	Reduced activation energy, $b = 2(\gamma - 1) \epsilon \frac{E_a}{k_B T_u}$
$C$	Characteristic line
$c_p$	Specific heat capacity at constant pressure
$c_v$	Specific heat capacity at constant volume
$D$	Molecular diffusivity
$d$	Shock thickness
$D_T$	Thermal diffusivity, $D_T = \frac{\lambda}{\rho c_p}$
$E$	Total energy
$e$	Internal thermal energy
$E_a$	Activation energy
$I$	Riemann invariant
$j$	Geometrical parameter for cartesian $j = 0$ , cylindrical $j = 1$ , and spherical $j = 2$ coordinates.
$l$	Mean free path
$l_f$	Flame characteristic length
$l_i$	Induction layer characteristic length
$l_r$	Reactive layer characteristic length
$M$	Mach number
$p$	Pressure
$q_m$	Heat release per unit of mass
$r$	Radius or distance to the origin
$r_f$	Front radius
$t$	Time
$u$	Gas velocity
$u_f$	Flame velocity in the laboratory reference frame

## *Nomenclature*

$V$	Self-similar solution
$v$	Specific volume
$x$	Distance to the front
$z$	Self-similar variable
$\mathcal{D}$	Combustion wave velocity relative to the upstream flow
$\mathcal{P}$	Normalised pressure, $\mathcal{P} = \frac{\gamma + 1}{2\gamma} \left( \frac{p}{p_u} - 1 \right)$
$\mathcal{Q}$	Normalised heat of reaction, $\mathcal{Q} = \frac{\gamma + 1}{2} \frac{q_m}{c_p T_u}$
$\mathcal{V}$	Normalised specific volume, $\mathcal{V} = \frac{\gamma + 2}{2} \left( \frac{\rho_u}{\rho} - 1 \right)$

## **Superscripts and subscripts**

0	Leading edge of the core of stagnant gases
b	Burned state
ext	External flow
f	Front
i	Initial value
N	Neumann state
o	Unperturbed state
s	Shock wave
tr	Transitory flow
u	Unburned state

# CHAPTER 1

---

## Introduction

---

The energy released by a spark in a reactive medium can initiate the propagation of a reactive wave converting the reactants into combustion products. The internal chemical energy stored in the chemical bonds of the reactants that is not involved in the recombination of the products is released in the form of heat. Significant changes in the thermodynamics and gas dynamics states occur across the combustion wave under the effect of this additional energy. The gradients created across the wave lead to physical and chemical processes that drive the self-propagation of the combustion wave.

The propagation of a combustion front in premixed reactive mixtures exhibits two distinct modes: deflagration and detonation. In the deflagration regime, the combustion wave advances a few meters per second with the velocity of a laminar flame (Williams, 1985). Alternatively, the combustion wave may accelerate leading to turbulent flames with velocities of hundred of meters per second (Poinsot and Veynante, 2005). In contrast, the reactive wave in the detonation regime propagates at supersonic velocities of about thousands of meters per second, resulting in an overpressure of around twenty times the atmospheric pressure (Lee, 2008). The wide range of propagation velocities exhibited by such premixed reactive waves implies the existence of a variety of propagation mechanisms.

The propagation of a laminar deflagration is governed by the molecular diffusion of heat and mass from the reaction zone to the unburned mixture, while the propagation of a detonation depends on the adiabatic shock compression of the reactive mixture. In order to sustain a detonation at such a high speed, the compressive and dissipative heating must be large enough to initialize the reactions of combustion which are frozen at ambient temperatures. Detonation is defined as a combustion sustained shock wave



## 1 Introduction

with a significant pressure and density rise across the wave (Fickett and Davis, 2000). The salient feature of detonation waves is the coupled motion of a shock wave with the reaction zone behind it.

The growing number of accidental explosions in coal mines during the latter half of the 19th century motivated the first systematic study of the detonations by Berthelot and Vieille (Manson, 1987). Subsequent investigations by Mallard and Le Chatelier demonstrated that the two propagation regimes, deflagration and detonation, could be observed in the same reactive mixture. This observation suggested that the propagation mechanisms could be controlled by the gas dynamics and not by the intrinsic thermochemical properties of the mixture.

The earliest theory of detonation waves is the classical Chapman-Jouguet (CJ) theory (Chapman, 1899; Jouguet, 1905). This theory allows to compute overall characteristics of a steady detonation such as the jump relations across the wave or the detonation velocities observed experimentally. The CJ theory is based on thermodynamic equilibrium and does not require to investigate the kinetics of the chemical interactions since the detonation is considered as a discontinuity. Hence, it cannot predict the rate-dependent detonation parameters such as the detonation thickness, the critical tube diameter or the critical initiation energy. One of the main results of the CJ theory, is that the flow left behind by a self-sustained detonation is sonic relative to the wave.

Another important contribution to the theory of detonations is the Zeldovich-von Neumann-Döring (ZND) theory (Zeldovich, 1940; von Neumann, 1942; Döring, 1943). This theory considers a one-dimensional steady structure for detonation waves, which consists of a normal shock wave followed by an inviscid induction zone and subsequently by a reaction zone. The reaction zone ends at the CJ or sonic plane, where the predicted equilibrium states correspond to those determined by the CJ theory. Although the one-dimensional ZND structure is rarely observed experimentally due to its intrinsic longitudinal instability, it provides a characteristic length scale for the detonation wave and a qualitative description of its structure.

Beside these classic theories, numerous theoretical (Clavin and Searby, 2016), experimental (Lee, 2008), and computational research (Oran and Boris, 2005) have been conducted over the past decades to further investigate different aspects of gaseous detonations. However, no satisfactory theory has been developed that can accurately predict certain dynamic parameters of gaseous explosions from fundamental principles based on the thermo-chemical properties of a reactive mixture. For instance, it remains unclear what minimum energy is required for the initiation of a detonation, or under which conditions a detonation wave may persist through the passage of a small opening into a large reservoir. Furthermore, it is not possible to determine a priori whether it is possible to detonate a given mixture, nor can it be ascertained under which conditions a deflagration can undergo an acceleration leading to the transition to an explosive regime.

Among the open questions regarding the understanding of detonation phenomena, the process of initiation of a detonation is one of the main concerns when considering the safe use of highly reactive mixtures and control of detonations waves. The processes followed during the initiation of a self-propagating detonation have been categorized into

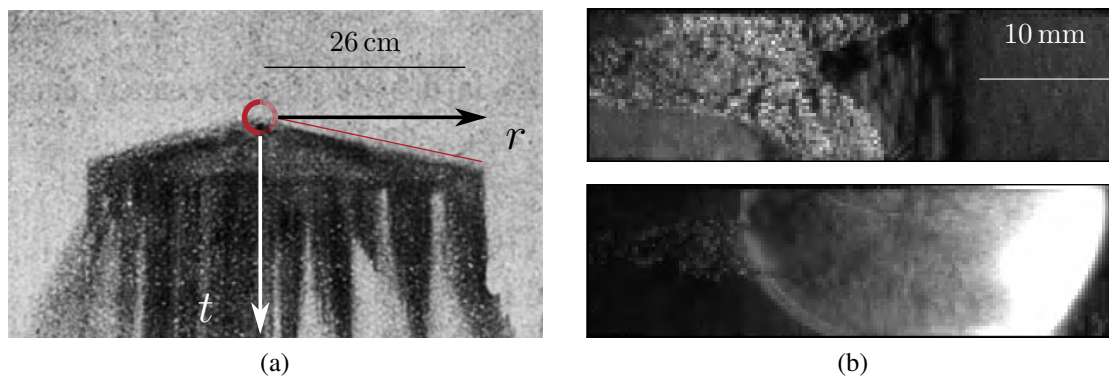


Figure 1.1: (a) Streak photography of the detonation direct initiation process taken by Laffitte (1925). A strong blast wave was ignited through a mercury charge at the center of a balloon filled with a hydrogen-oxygen mixture. (b) Successive schlieren photographs of the deflagration-to-detonation transition taken by Ballossier (2021). A deflagration wave propagating in a 10 mm channel filled with a hydrogen-oxygen mixture abruptly turns into a detonation in the time span of 6  $\mu$ s between photographs.

two distinct categories: Direct Initiation (DI) and Deflagration-to-Detonation Transition (DDT). The former involves a fast transition from a decaying blast wave to a self-sustained detonation, while the latter involves a slower transition from a deflagration to a detonation.

### *Direct Initiation*

Direct Initiation is the process of formation of a detonation in open space without undergoing a predetonation stage of flame acceleration. The conditions required for the onset of the detonation are created directly in the decay of a strong blast wave generated by a powerful concentrated energy source. The feasibility of initiating a detonation in open space was not clear in the early days of detonation research until the first experimental evidences were obtained by Laffitte (1925) under the direction of M. Le Chatelier. Using a powerful igniter with a mercury charge, Laffitte succeeded in initiating a spherical detonation in the center of a spherical glass balloon, as revealed by the streak photographs (see Figure 1.1a). The photographs showed the apparent instantaneous formation of the detonation without the noticeable predetonation period observed in previous experiments. Nevertheless, Laffitte already noted that a remarkably large amount of energy had to be released initially for a direct initiation to occur.

A later experimental study of the direct initiation of spherical detonations by Bach et al. (1969) identified three distinct regimes as a function of the initiation energy:

- i) Subcritical energy regime: When the initiation energy is below the critical value, the reaction front progressively decouples from the leading shock, leading to the rapid deceleration of the shock wave into an acoustic wave. The notable decoupling between the expansion wave and the reactive shell is illustrated by Figure 1.2a.

## 1 Introduction

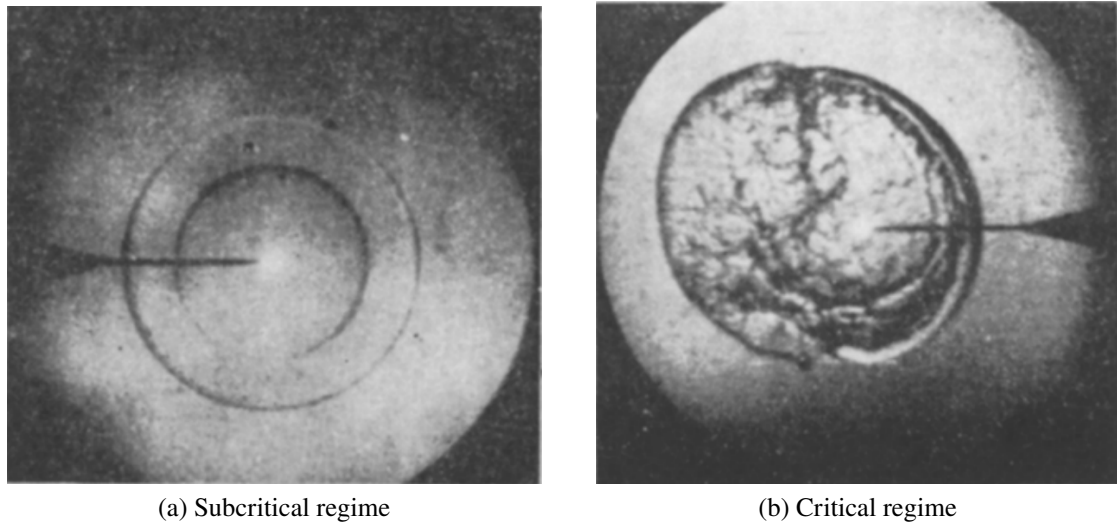


Figure 1.2: Schlieren photographs of direct initiation of a detonation of an stoichiometric acetylene-oxygen mixture. Reprinted from Bach et al., 1969.

- ii) Critical energy regime: For initiation energies close to the critical value, it is observed that the distance between the shock wave and the peak of reactivity initially increases. However, the decoupling stops when the reaction front is a few millimetres behind the shock. The shock and reaction front then propagate steadily, with instabilities developing over time and the reaction front accelerating towards the shock wave. Eventually, this re-acceleration leads to the formation of a self-sustained detonation wave. Figure 1.2b illustrates the asymmetric recoupling of both waves in the critical initiation regime.
- iii) Supercritical energy regime: When the initiation energy is greater than the critical value, no decoupling between the shock and the reaction front is observed. The overdriven spherical detonation gradually decays towards the theoretical CJ velocity and then propagates at constant velocity.

The study of Bach et al. (1969) provided valuable insight into the direct initiation of spherical detonations and particularly into the critical regime.

### *Deflagration-to-Detonation Transition*

In contrast to the Direct Initiation, the Deflagration-to-Detonation Transition starts with the ignition of the combustible mixture by a low energy source that generates a slowly propagating flame. Under appropriate conditions, the flame accelerates and undergoes a transition to detonation. During DDT, the propagation mechanism of the combustion wave shifts from molecular diffusion and convective transport to autoignition by adiabatic shock compression. In the final phase of DDT, the flame is observed to propagate at velocities approaching the speed of sound for a certain period of time and, eventually,

the abrupt onset of a detonation wave occurs (see Figure 1.1b). The systematic study of Urtiew et al. (1966) using pioneering experimental techniques was a milestone that made it possible to visualize with detail the DDT phenomenon.

The two modes of initiation are typically explained by differentiating between two distinct phases. In the case of DI, an initial phase of rapid decay of the blast wave leads to a phase of transition from an overdriven detonation into a CJ detonation regime. The DDT is characterized by an initial phase of flame acceleration that culminates in the sudden onset of an overdriven detonation, which subsequently relaxes to a CJ detonation. Thus, both initiation modes differ mainly in their initial phases. The final phase which culminates with the formation of a self-sustained CJ detonation is seemingly similar in both modes and has been suggested to be universal for DI and DDT (Lee and Higgins, 1999).

This study will look into the transition from an overdriven regime to a CJ detonation in the context of DI, and flame acceleration and onset of a strong detonation in the context of DDT. Particularly, the study will focus on the interplay of gas dynamics with simplified models of chemical kinetics.

## 1.1 Motivation

The destructive potential as well as the energetic interest of the rapid release of chemical energy has motivated extensive research on detonations across a wide range of scientific and technological fields such as explosion safety, detonative propulsion and astrophysics. In the context of explosion safety, the increasing interest in hydrogen as a means decarbonizing the energy sector demands a thorough understanding of the underlying physics of detonations to ensure the safe operation of hydrogen-based industrial processes and the storage of this fuel (Ng and Lee, 2008). The theoretical potential of detonation-based engines to provide higher efficiency and wider operating regimes over traditional engines with a simpler mechanical design (Wolański, 2013) attracts attention from the aerospace and military sectors, which promote the introduction and development of novel designs. Understanding the dynamics of detonation waves is essential for the operation of such engines, so improved detonation control models are fundamental to their development. Additionally, the similarities of terrestrial detonations with astrophysical events, such as some supernovae, have attracted the interest of astronomers and astrophysicists in detonation phenomena (Röpke and Hillebrandt, 2005).

### *Explosion safety*

In the field of explosion safety, the formation of a detonation represents the worst possible accident (Oran et al., 2020) (see Figure 1.3). Understanding the mechanism that govern the initiation of detonations is crucial to ensure the safe operation of industrial processes and the protection of passengers on vehicles powered by combustion engines. Particularly, the growing popularity of hydrogen as a clean energy carrier or diluent of traditional fuels to reduce the carbon footprint of the energy and transportation sectors represents

## 1 Introduction

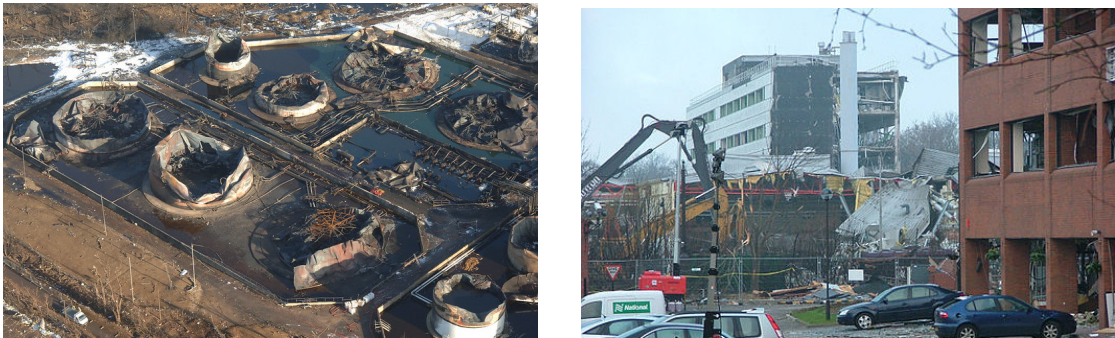


Figure 1.3: Photographs of the aftermath of the 2005 Buncefield accident. A thorough investigation determined that a deflagration-to-detonation transition was the mechanism behind the intense explosion of the vapour cloud originated from a leak in one of the fuel tanks (Johnson, 2010; Chamberlain et al., 2019).

a major risk (Crabtree et al., 2004; Chaumeix et al., 2007). But even when hydrogen is not used directly as a fuel, it can still form spontaneously in severe nuclear accidents (Yanez et al., 2015; Grosseuvres et al., 2019), or by decomposition of products from the semi-conductor industry or nuclear waste storage Mével et al. (2009) and Mével et al. (2015).

The flammability, buoyancy, and permeability of hydrogen mixtures raise concerns about their safe use (Boivin et al., 2022). The wide flammability limits of hydrogen (Cheikhvat et al., 2012; Sánchez and Williams, 2014), its tendency to propagate in the fast flame regime (Cicarelli et al., 2019), or detonative regime (Zitoun et al., 1995; Mével et al., 2016), the embrittlement of materials exposed to hydrogen (Oriani, 1978) and unexpected flame propagation regimes in ultra-lean conditions (Veiga-López et al., 2020) pose new safety challenges compared to traditional fuels. Better insights on detonation phenomena can then be used to design safer equipment and develop effective prevention strategies.

### *Detonative propulsion*

Detonative propulsion is concerned with the design of propulsion systems that rely on the rapid combustion of a reactive mixture in a detonation to produce high-speed thrust. Detonations represent an ideal combustion process for such systems, as they allow for highly efficient energy transfer and can produce high pressures and temperatures. Different implementations of detonative engines include Pulse Detonation Engines (PDE), Rotating Detonation Engines (RDE), and Oblique Detonation Wave Engines (ODWE) engines. PDEs operate by sequentially generating detonation in a combustion chamber (Roy et al., 2004). The momentum produced in the detonation is then directed into a nozzle to produce thrust. RDEs are a more recent innovation that generate a rotating detonation wave in an annular chamber, allowing for a continuous thrust output (Rankin et al., 2017). ODWEs (also known as *shramjet* for shock-induced combustion ramjet),



Figure 1.4: Photograph of the Type Ia supernova SN 1994D (Treffers et al., 1994) taken by the Hubble Space Telescope. The supernova at the lower left exhibits a brightness comparable to that of the entire galaxy NGC 4526.

on the other hand, rely on the geometry of the air inlet to generate supersonic combustion waves (Urzay, 2018).

The control of the detonation waves is crucial in the design of such propulsion systems. For instance, a better understanding of the deflagration-to-detonation transition can be employed to optimize the combustion chamber of a PDE (Sorin et al., 2006). The fundamental analysis of the transmission of a detonation wave from a straight channel to a curved chamber, as occurs within an RDE, is a subject of current research (Melguizo-Gavilanes et al., 2021b). Assessing the impact of non-uniformities of the incoming flow on detonations (Huete et al., 2013; Boulal et al., 2016; Cuadra et al., 2020) is an ongoing research topic. These examples show that the development of detonation-based propulsive systems still requires a deeper understanding of detonation fundamental aspects.

### *Astrophysics*

In astrophysics, the mechanism underlying type Ia thermonuclear supernova (see Figure 1.4) represents an open topic of discussion without a widely accepted explanation (Mazzali et al., 2007; Pomeau et al., 2014). A unified mechanism is thought to govern both unconfined DDT in terrestrial detonations and type Ia supernovae (Poludnenko et al., 2019; Gordon et al., 2021). For instance, Charignon and Chièze (2013) and Charignon (2013) proposed a new mechanism for DDT based on the formation of shock waves by amplification of acoustic waves passing through regions of steep density gradients in the context of thermonuclear supernovae. Understanding the mechanism behind these stellar explosions is essential for developing accurate models of these phenomena, which are used to measure interstellar distances and are therefore fundamental to our understanding

## 1 *Introduction*

of the universe.

The study of the initiation mechanisms of detonations is motivated by its relevance to various scientific and technological fields. Contemporary research on flame and detonation dynamics is mainly based on numerical simulations that attempt to reproduce all known physics in a quest to recreate virtual experiments. Such simulations must accurately describe the strongly transient behaviors that characterize the initiation and propagation of detonation waves to be relevant. From the smallest time and length scales imposed by the detailed chemical kinetics to the large scales that characterize supersonic flows have to be included in the simulations. Therefore, the cost of the simulations required to define safety regulations, design and optimize reliable systems, and gain an in-depth understanding of natural phenomena becomes prohibitive even with state-of-the-art computational capabilities.

The onset and large-scale dynamics of detonation waves is strongly influenced by the internal structure of the wave, whose scales are significantly smaller. The predictive capabilities of numerical simulations have so far been limited. Therefore, new theoretical models of detonation dynamics based on insights into the behavior of the internal structure of these waves are needed to guide numerical simulations or even suggest alternative experimental studies.

### **1.2 Aims and Objectives**

The ultimate goal of this thesis is to propose new approaches to deal with the complex phenomenon of detonation ignition, either to minimise its likelihood, to improve the control and operation of detonation-based engines, or to better understand the underlying physics which could shed light in the understanding of other complex phenomena such as the explosions of stars. In order to achieve this goal, a common approach in combustion science of systematic reduction of the complexity to retain exclusively the fundamental mechanisms responsible for the phenomena will be followed. The analysis will aim to eliminate all mechanisms that may introduce quantitative corrections but are not essential to the problem of detonation ignition at hand. By focusing on the essential mechanisms, the thesis aims to develop a deeper understanding of detonation ignition phenomena.

The distinct behavior exhibited by the direct initiation of detonations and the deflagration-to-detonation transition suggest that they are likely driven by fundamentally different mechanisms. As such, both processes will be studied independently in this thesis and eventual similarities will be discussed.

An enlightening step in the understanding of direct initiation was taken decades ago by inspecting the curvature effects under the overly restrictive assumption of the quasi-steady approximation. An objective of this thesis will then be to inspect the effects of curvature during direct initiation of detonations removing this hypothesis. The asymptotic limit of small heat release, which has proven useful in the study of the longitudinal instability of detonations, could ease this endeavor. Hopefully, the detonation dynamics during the process of direct initiation can also benefit from a better comprehension in the

aforementioned asymptotic limit. In particular, this thesis has the objective to elucidate the physical mechanism behind the rich dynamics observed in the critical regime of initiation in the asymptotic limit of small heat release.

Besides, recent experiments and multidimensional simulations have suggested that deflagration-to-detonation transition may occur in laminar flames. The elimination of the complexities of turbulence, which is still a research topic in itself, facilitates the theoretical study of DDT on the basis of fundamental principles. A flame acceleration runaway mechanism due to the thermal feedback from the gas dynamics that may be relevant in laminar flames propagating in thin tubes will be examined. The objective of this study is to investigate the onset of a detonation in the internal structure of the flame under the acceleration induced by the thermal feedback and by the increment of flame surface area.

### 1.3 Methodology

Detonation initiation phenomena involve the interplay of numerous physico-chemical processes such as molecular transport, gas compressibility, fluid mechanics and chemical interactions. In order to reduce such complexity and validate the pertinence of the simplifications performed, advanced theoretical and analytical tools will be combined with well-established numerical techniques to address the challenging aspects of the mathematical description of detonation dynamics. A differentiating element of the methodological approach will be the attention paid to the gas dynamics in the internal structure of the combustion waves. In the conventional approach, the internal structure is modeled or simply considered as a discontinuity, since its scale is much smaller than that of the rest of the physics of the problem. However, small modifications of the internal structure of the reactive fronts are expected to have major consequences on the overall dynamics of the reactive fronts.

Mathematical modeling will be used to develop analytical descriptions of the detonation and flame dynamics, which can then be used to investigate the underlying physics of the process. It involves creating a mathematical representation of the reactive wave under study, based on empirical data, physical laws, or theoretical assumptions, which can then be used to simulate, analyze or predict the behavior of the reactive wave under different conditions. While mathematical models are not expected to reproduce an exact copy of the system, they capture the essential features of the system and can be used to study the underlying physics of the process. In this thesis, the classical mathematical modeling of premixed reactive waves will be followed and asymptotic and numerical methods will be applied to these models to gain a deeper understanding of the fundamental mechanisms controlling detonation initiation.

Asymptotic methods will be used to analyze the leading order mechanisms controlling the detonation dynamics. Asymptotic methods include mathematical techniques used to study the behavior of a function, equation, or system as a certain parameter or variable approaches a limiting value, such as infinity or zero (Bender and Orszag, 1999). The



## 1 *Introduction*

term asymptotic refers to the behavior of a function as it approaches a limit or an infinite value, rather than its actual value at a specific point. Asymptotic methods are widely used in many areas of science and engineering, such as physics, chemistry, biology, and economics. Some common asymptotic methods include: perturbation methods, matched asymptotic expansions and multiple-scale analysis.

Numerical methods are mathematical techniques used to solve problems that cannot be solved using exact methods (Hirsch, 2007). These problems often involve complex mathematical equations or models that are difficult or impossible to solve analytically. Using numerical methods is it possible to approximate the solution with specified error bounds to such problems following a series of mathematical computations or algorithms. These methods are widely used to solve problems in many different areas of science and engineering. Some common examples of numerical methods include: root finding methods (such as the Newton-Raphson method), interpolation methods (such as the Lagrange interpolation method), numerical integration (such as the Simpson's rule), differentiation methods (such as finite difference methods) and numerical optimization methods (such as the gradient descent method).

### **1.4 Document Structure**

The structure of this thesis manuscript is organized in five different chapters. The introductory Chapter 1 sets the stage for the study. This chapter explains the significance the detonation initiation phenomenon and its relevance to a range of disciplines, highlighting the reasons why this area of research is important. It also provides the background to the study, outlining the motivations, objectives and the methodology used.

Thereafter, the Chapter 2 will review some fundamental concepts of the one-dimensional compressible flow and premixed combustion waves theory. The purpose of this chapter is to summarize the underlying principles used in the following chapters from the classical theories of compressible flow and premixed combustion.

The Chapters 3 and 4 will each focus on a specific research topic related to a particular process of detonation initiation. Chapter 3 will delve into the critical dynamics of detonation initiation, presenting a literature review and detailing the methodology used in the research. It will then present and discuss the results of the research. Chapter 4 will similarly explore the deflagration to detonation transition in thin smooth tubes, providing a literature review, methodology, results and analysis.

Finally, the concluding Chapter 5 of the thesis will summarize the main findings of the research conducted in the previous chapters. It will discuss the conclusions obtained regarding the objectives and motivations of the study. Additionally, it will highlight the limitations of the study and suggest directions for future research in initiation of detonations.

---

## One-dimensional compressible flow and premixed combustion waves

---

In this chapter, some aspects of the classical theories of one-dimensional compressible flow and premixed combustion waves are reviewed. The scope is limited to the classical problems and concepts that will be referred to in the following chapters. Some general considerations of the study of reactive gaseous flows is provided in the first section. Then, in the following section, the theory of one-dimensional flows in compressible gases, including the description and formation of compression and shock waves is discussed. Finally, in the last section, the gas dynamic theory of premixed reactive waves is reviewed with attention to the internal structure and propagation regimes of deflagrations and detonations.

---

2.1	General considerations . . . . .	12
2.2	One-dimensional compressible flow . . . . .	15
2.2.1	Unsteady compressible waves . . . . .	15
2.2.2	Shock waves . . . . .	19
2.2.3	Strong blast wave . . . . .	26
2.3	Premixed combustion waves . . . . .	29
2.3.1	Deflagrations . . . . .	33
2.3.2	Detonations . . . . .	35

## 2.1 General considerations

Combustion is a mass and energy conversion process during which part of the energy stored in the chemical bonds between atoms is released and transformed into thermal energy. A substance, called fuel, reacts with an oxidant, usually the oxygen in the air, to form products such as carbon dioxide and water, which contain a chemical bond energy lower than the sum of the chemical energy contained in the reactants. The detailed description of the reaction mechanism that transform the initial reactants into the final products includes numerous elementary reactions between numerous intermediate chemical elements that evolve over a wide range of time scales. These chemical transformations modify the physical properties of the mixture, such as temperature and density, which in turn affect the rate of chemical reactions. In addition, the physical disturbances are propagated at different velocities beyond the scope of the chemical interactions and interact with the surroundings. As a result, the combustion of gaseous mixtures is realized as a complex process involving interactions between gas dynamics and chemistry over a wide range of time scales.

The global reaction of combustion is irreversible, highly exothermic and has a high activation energy. The combination of these characteristics causes combustion to propagate in a reactive medium as a reactive front. Due to the large activation energy that characterizes the reaction of combustion, an out-of-equilibrium reactive mixture can remain in a metastable state. In this state, combustion reactions proceed so slowly that the energy perturbations generated by the completion of a reaction are dissipated before triggering new combustion reactions. However, upon a large localized energy deposition, termed ignition, the combustion reaction may be fast enough for the released energy to initiate combustion reactions in the surroundings. Combustion then propagates as a front through which the out-of-equilibrium reactive mixture turns into a less energetic steady state releasing the energy required to ignite the unburned mixture ahead of it.

The complex interplay of chemical reactions involved in the combustion process is generally reduced in the theoretical study of combustion to a single chemical reaction. In order to retain the autocatalytic thermal character of combustion, the rate of this overall reaction is modeled with an Arrhenius law with a large activation energy. The temperature-dependent characteristic reaction rate can then be written as

$$\frac{1}{t_r(T)} = B \exp\left(-\frac{E_a}{k_B T}\right) \quad (2.1)$$

where  $E_a$  is the activation energy of the reaction that can be interpreted as the thermal sensitivity of the reaction,  $k_B$  is the Boltzmann constant that serves as conversion factor between the temperature of the mixture and its energy stored in the form of thermal agitation, and  $B$  is a prefactor accommodating the time units. Due to the large activation energy, the characteristic times of the chemical-kinetics of the overall combustion reaction are typically much longer than the characteristic relaxation times for the local thermodynamic equilibrium of a gas volume. Therefore, combustion processes in gaseous

mixtures can be described by the equations of conservation of continuous media with additional reactive terms that account for the heat release as well as consumption and production of chemical species.

### Conservation equations

The fundamental equations that describe the phenomena of gaseous combustion are the equations of continuum mechanics. A volume of reactive gases can be considered as a continuum medium when the characteristic time of evolution of the varying conditions is much larger than the thermodynamic relaxation time. The relaxation time decreases with the size of the gas volume under consideration. Considering a volume containing a few molecules, the relaxation time will be of the order of the collision time between them. Therefore, the collision time sets a lower limit to the characteristic evolution time for which the local thermodynamic equilibrium is valid. The spatial limit in turn is given by the mean free path between particles, so that gas volumes with a characteristic length significantly larger than the mean free path can be analyzed under the local thermodynamic equilibrium simplification. Under this approximation, the thermodynamics laws are valid locally and the evolution is governed by conservation equations in which the molecular transport can be accounted for through transport coefficients. The chemical transformation occurring in a small fraction of collisions between molecules due to high activation energy appear as independent source or sink terms in the conservation equations.

The local balance of total mass is given by the conservation equation, also known as continuity equation,

$$\frac{\partial \rho}{\partial t} + \nabla \cdot (\rho \mathbf{u}) = 0 \quad (2.2)$$

where  $\rho$  is the mass density and  $\mathbf{u}$  is the flow field. Introducing the Lagrangian or material derivative  $D/Dt \equiv \partial/\partial t + \mathbf{u} \cdot \nabla$ , the continuity equation can be written in the Lagrangian formulation

$$\frac{1}{\rho} \frac{D\rho}{Dt} = -\nabla \cdot \mathbf{u}. \quad (2.3)$$

The mass of each chemical species is conserved unless it is consumed or produced by chemical reactions. Introducing the mass fraction of a species  $i$  as  $Y_i = \rho_i/\rho = C_i W_i/\rho$ , where  $C_i = N_i/V$  is the concentration and  $W_i$  is the molecular weight of the species  $i$ , the partial density of each species is  $\rho_i = \rho Y_i$ . The conservation equation for the species  $i$  is

$$\rho \frac{DY_i}{Dt} = \rho \left( \frac{\partial Y_i}{\partial t} + \mathbf{u} \cdot \nabla Y_i \right) = -\nabla \cdot (\rho Y_i \mathbf{V}_i) + \rho \omega_i \quad (2.4)$$

where  $\mathbf{V}_i = \mathbf{u}_i - \mathbf{u}$  denotes the diffusion velocity and  $\omega_i$  the chemical production of species  $i$ . The diffusive flux includes the molecular diffusion of each species  $i$  in the rest of the species of the mixture, the thermophoresis (or Soret effect) related to temperature gradients, the barodiffusion related to pressure gradients and the selective impact of mass

## 2 One-dimensional compressible flow and premixed combustion waves

forces. For simplicity, in combustion problems only the effect of the Fick's law

$$\rho Y_i \mathbf{V}_i = -\rho D_i \nabla Y_i \quad (2.5)$$

is considered. This approximation is accurate under ordinary flame conditions in diluted mixtures where one species is in abundance and  $D_i$  denotes the diffusion coefficient of the species  $i$  in the abundant species.

The conservation of momentum takes the general form

$$\rho \frac{D\mathbf{u}}{Dt} = \rho \left( \frac{\partial \mathbf{u}}{\partial t} + \mathbf{u} \cdot \nabla \mathbf{u} \right) = \nabla \cdot \boldsymbol{\sigma} + \rho \mathbf{f}, \quad (2.6)$$

where  $\mathbf{f}$  denotes the body forces, such as gravity, and the stress tensor for Newtonian fluids is given by

$$\boldsymbol{\sigma} = -p\mathbf{I} + \eta \left[ (\nabla \mathbf{u}) + (\nabla \mathbf{u})^T \right] + \left( \kappa - \frac{2}{3}\eta \right) (\nabla \cdot \mathbf{u}) \mathbf{I} \quad (2.7)$$

where  $p$  is the thermodynamic pressure,  $\eta$  is the shear viscosity and  $\kappa$  is the bulk viscosity.

The total specific energy

$$E = e_T + \frac{|\mathbf{u}|^2}{2} \quad (2.8)$$

that accounts for the specific thermal energy  $e_T$  and the specific kinetic energy  $|\mathbf{u}|^2/2$  is a conserved scalar. The balance of the total energy given by the energy fluxes, the potential energy of the body forces and the heat released by the combustion reactions can be written in the form a energy conservation equation

$$\rho \frac{DE}{Dt} = \rho \left( \frac{\partial E}{\partial t} + \mathbf{u} \cdot \nabla E \right) = -\nabla \cdot \mathbf{q} + \nabla \cdot (\boldsymbol{\sigma} \cdot \mathbf{u}) + \rho \mathbf{f} \cdot \mathbf{u} + \rho q_{m,j} \omega_j \quad (2.9)$$

where  $\mathbf{q}$  is the heat flux and  $q_{m,j}$  is the heat release per unit mass of a reaction  $j$  with a rate of reaction  $\omega_j$ . The heat flux includes the heat transfer by conduction due to temperature gradients and due to mass concentration effect, known as Dufour effect that is the reciprocal phenomenon of the Soret effect. For simplicity, the heat flux it is assumed to satisfy the Fourier's law

$$\mathbf{q} = -\lambda \nabla T \quad (2.10)$$

where  $\lambda$  is the thermal conductivity of the mixture.

The set of mass, species, momentum and energy conservation equations (2.2), (2.4), (2.6) and (2.9) together with the constitutive equations presented here (2.5), (2.7) and (2.10) is often referred as reactive compressible Navier-Stokes equations. When molecular transport effects such as viscous effects, heat conduction and body forces are neglected,

the resulting set of equations is known as reactive Euler equations

$$\frac{\partial \rho}{\partial t} + \nabla \cdot (\rho \mathbf{u}) = 0, \quad \rho \frac{DY}{Dt} = \omega, \quad (2.11)$$

$$\rho \frac{D\mathbf{u}}{Dt} = -\nabla p, \quad \rho \frac{Ds}{Dt} = \frac{q_m}{T} \omega, \quad (2.12)$$

where the energy conservation equation is replaced by the entropy conservation equation which is defined as

$$T ds = de_T - \frac{p}{\rho^2} d\rho. \quad (2.13)$$

## 2.2 One-dimensional compressible flow

Before turning attention to the effects of the combustion reactions that drive detonations, it is useful to study the motion of compressible fluids moving at velocities that may eventually be close or greater than the speed of sound. Waves produced in this regime with finite velocities cannot be studied by means of the linear acoustic theory. In an inert homogeneous mixture without significant velocity and temperature gradients, molecular transport phenomena can be neglected. Under these conditions, all sources of entropy are removed from the problem simplifying the analysis. The isentropic flow of compressible fluids admits an exhaustive mathematical treatment when the state of the gas depends exclusively on time and a single Cartesian coordinate as can be found in multiple references (Courant and Friedrichs, 1948; Landau and Lifshitz, 1987; Anderson, 2003).

The Euler equations (2.11) and (2.12), that govern the motion of isentropic flows, can be written for a one-dimensional geometry as

$$\frac{\partial \rho}{\partial t} + \frac{\partial \rho u}{\partial r} = -\frac{j \rho u}{r}, \quad (2.14)$$

$$\rho \frac{\partial u}{\partial t} + \rho u \frac{\partial u}{\partial r} = -\frac{\partial p}{\partial r}, \quad (2.15)$$

$$\frac{\partial s}{\partial t} + u \frac{\partial s}{\partial r} = 0, \quad (2.16)$$

where  $j = 0$  corresponds to the Cartesian geometry studied in this section.

### 2.2.1 Unsteady compressible waves

The flow described by the evolution of an initially uniform gas through the conservation equations (2.14) to (2.16) is called simple wave. Such waves form when a piston moves in a tube filled with gas. When the piston moves out of the tube, a rarefaction wave is formed in which the gases expand, while a compression wave is formed when the piston moves towards the gases in the tube.

## 2 One-dimensional compressible flow and premixed combustion waves

The mathematical analysis of the problem gets simpler by introducing the dependent variable

$$a^2 = \left( \frac{\partial p}{\partial \rho} \right)_s \quad (2.17)$$

which corresponds to the square of the sound speed. This is the speed of propagation of pressure perturbations propagate relative to the flow. Since the entropy is being assumed to be initially uniform in the flow, it will remain constant and homogeneous throughout the domain as described by equation (2.16). Therefore, the density derivatives of the equation (2.14) can be replaced by pressure derivatives using (2.17) as  $dp = a^2 d\rho$ . Multiplying the resulting equation by  $a/\rho$  gives

$$\frac{1}{\rho a} \frac{\partial p}{\partial t} + \frac{u}{\rho a} \frac{\partial p}{\partial r} + a \frac{\partial u}{\partial r} = 0. \quad (2.18)$$

Adding and subtracting this equation from (2.15) divided by  $\rho$  results in the two equations

$$\frac{\partial u}{\partial t} + (u \pm a) \frac{\partial u}{\partial r} \pm \frac{1}{\rho a} \left[ \frac{\partial p}{\partial t} + (u \pm a) \frac{\partial p}{\partial r} \right] = 0. \quad (2.19)$$

which together with (2.16) are equivalent to the original system. This form of the equations shows the existence of three curves in the  $r - t$  plane

$$C_{\pm} : \quad dr = (u \pm a) dt, \quad \text{and} \quad C_0 : \quad dr = u dt, \quad (2.20)$$

known as characteristics curves, along which the corresponding quantities

$$I_{\pm} = \int_{C_{\pm}} du \pm \int_{C_{\pm}} \frac{dp}{\rho a}, \quad \text{and} \quad I_0 = \int_{C_0} ds, \quad (2.21)$$

known as Riemann invariants, are conserved. For a polytropic gas  $a^2 = \gamma p/\rho$ , the conservation of the invariants  $I_{\pm}$  along a path  $C_{\pm}$  passing through a point where the flow moves with velocity  $u_o$  and the sound speed is  $a_o$ , gives the following relationship between the local sound speed and the flow velocity

$$\frac{a}{a_o} = 1 \pm \frac{\gamma - 1}{2} \frac{u - u_o}{a_o}. \quad (2.22)$$

Applying the equation of state for ideal gases and the relationships for isentropic processes,

the relations

$$\frac{T}{T_o} = \left(1 \pm \frac{\gamma - 1}{2} \frac{u - u_o}{a_o}\right)^2, \quad (2.23)$$

$$\frac{\rho}{\rho_o} = \left(1 \pm \frac{\gamma - 1}{2} \frac{u - u_o}{a_o}\right)^{2/(\gamma-1)}, \quad (2.24)$$

$$\frac{p}{p_o} = \left(1 \pm \frac{\gamma - 1}{2} \frac{u - u_o}{a_o}\right)^{2\gamma/(\gamma-1)}, \quad (2.25)$$

between the thermodynamic variables and the flow velocity that hold in compression and rarefaction waves are obtained.

### *Shock wave formation*

The nonlinearity of the Euler equations leads to the formation of singularities in their solutions, such as shock waves. The position and instant at which a singularity appears in the solutions can be taken as a rough prediction of the instant and position at which a shock wave is formed. The problem of the formation of a shock wave due to the motion of a piston accelerated by a known law was proposed and solved by Landau and Lifshitz (1987). Their solution is reviewed and discussed below.

Consider a piston that starts advancing at  $t = 0$  in an infinite tube filled with gas at rest. The piston accelerates with a velocity given by the law  $u_p(t) = dr_p/dt = \alpha t^n$  where the prefactor  $\alpha > 0$  is constant and positive, so that the piston moves in the positive direction  $r$ , and the exponent  $n \geq 1$  is positive describing a monotonically non-decreasing acceleration. Ahead of the piston, the invariant (2.21) is conserved along the trajectory defined by (2.20), which integrating can be written as

$$r = t(u + a) + f(u), \quad (2.26)$$

where  $f(u)$  is an arbitrary function of the flow velocity. Introducing the relation for the sound speed as a function of the flow velocity (2.22), the trajectory writes

$$r = t \left( a_o + \frac{\gamma + 1}{2} u \right) + f(u). \quad (2.27)$$

Setting the origin of coordinates at the initial position of the piston  $r_p(t = 0) = 0$ , the position of the piston is obtained by integration of its velocity to give  $r_p(t) = \alpha t^{n+1}/(n+1)$ . The boundary condition on the piston  $r = r_p$ , where the gas has to flow at the same speed as the piston  $u = u_p$  determines the function  $f(u) = r_p(t) - t[a_o + (\gamma + 1)/2u_p(t)]$ . By setting  $t$  as a parameter  $\tau$ , the flow velocity profile  $u(r, t)$  in the compression wave



## 2 One-dimensional compressible flow and premixed combustion waves

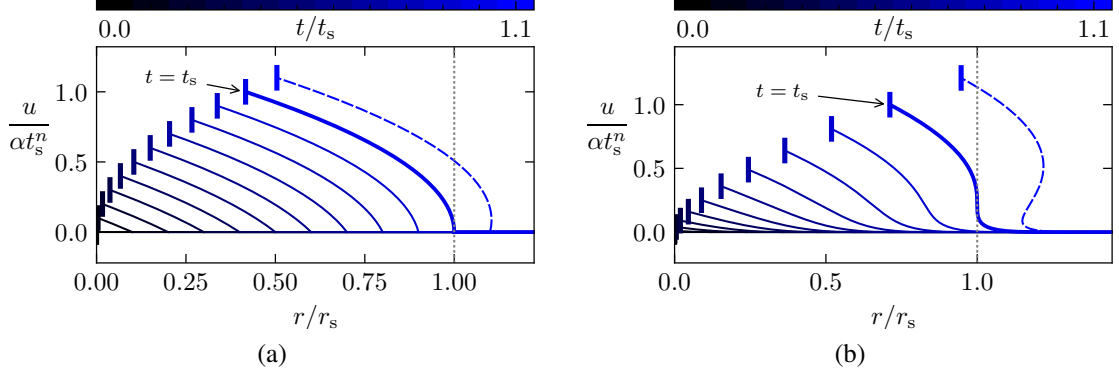


Figure 2.1: Shock formation ahead of an accelerating piston whose velocity is given by the law  $u_p = \alpha t^n$  with (a)  $n = 1$ , and (b)  $n = 2$ . The velocity profiles given by the solution of Landau and Lifshitz (1987) (2.28) are plotted at different time instants. The thick vertical lines indicate the position of the piston.

generated ahead of the piston can be expressed by the parametric formulae

$$\begin{cases} u = \alpha \tau^n, \\ r = \frac{\alpha}{n+1} \tau^{n+1} + (t - \tau) \left( a_o + \frac{\gamma+1}{2} \alpha \tau^n \right). \end{cases} \quad (2.28)$$

The evolution of the flow velocity profile for two values of the exponent  $n$  are represented in Figure 2.1. It is observed that after a certain instant, the solution of the Euler equation becomes multi-valued, i.e., the same position has two solutions for the velocity. This is clearly not a realistic solution that has been obtained passing through a singularity of the Euler equations that can be interpreted as the formation of a shock wave. In fact, as will be seen below, the entropy increases through a shock wave. Therefore, the solution obtained here within the isentropic assumption ceases to be valid when a shock wave is formed.

In the framework of the Euler equations, the formation of a shock wave corresponds to the formation of a singularity in its solutions. The exact instant of time  $t_s$  and the position  $r_s$  of the singularity can be obtained through the mathematical analysis of the velocity distribution given by (2.28). The singularity appears in the velocity gradient which becomes locally infinite, thus, the derivative  $(\partial r / \partial u)_{t_s}$  cancels out

$$\left( \frac{\partial r}{\partial u} \right)_{t_s} = -\frac{a_o}{\alpha n \tau^{n-1}} + \frac{\gamma+1}{2} t_s - \frac{\gamma+1}{2} \frac{1}{n} \left( n + \frac{\gamma-1}{\gamma+1} \right) \tau_s = 0. \quad (2.29)$$

At the same instant, the solution becomes multi-valued, therefore an inflection point appears where the second derivative  $(\partial^2 r / \partial u^2)_{t_s}$  also cancels out.

$$\left( \frac{\partial^2 r}{\partial u^2} \right)_{t_s} = \frac{\gamma+1}{2} (n-1) t_s \tau_s^{-1} - \frac{\gamma+1}{2} \left( n + \frac{\gamma-1}{\gamma+1} \right) = 0 \quad (2.30)$$

Solving the system of equations (2.29) and (2.30), the instant of formation of the singularity

$$t_s = \left[ \frac{2}{\gamma + 1} \frac{a_o}{\alpha} \left( \frac{1}{n - 1} \left( \frac{\gamma - 1}{\gamma + 1} + n \right) \right)^{n-1} \right]^{1/n} \quad (2.31)$$

and the corresponding value of the parameter  $\tau_s$  are obtained. The time instant  $t_s$  determines when the solution of the Euler equations ceases to be valid. The dissipative mechanisms are expected to play a role before  $t_s$  leading to the formation of a shock wave where the entropy increases and the inviscid flow equations are no longer valid.

Using the solutions for  $t_s$  and  $\tau_s$  it is also possible to know the exact position of the singularity through (2.28), which after some algebra can be written as

$$r_s = a_o t_s \left[ 1 - \frac{(n - 1)^2}{(n + 1) \left( \frac{\gamma - 1}{\gamma + 1} + n \right)} \right]. \quad (2.32)$$

This expression shows that for  $n = 1$ , the singularity is formed at the leading edge of the compression wave  $r_o$  propagating with the initial sound speed,  $r_o(t) = a_o t$ . For  $n > 1$ , the singularity appears at an intermediate position between the leading edge of the compression wave and the piston. The distance relative to the piston at which the singularity forms with respect to the distance to the piston from the leading edge of the compression wave as a function of the exponent of the piston velocity law is represented in Figure 2.2. The larger the exponent  $n$ , the closer to the piston the singularity occurs, however, both positions only approach each other asymptotically. That is, under this velocity law and for exponents greater than or equal to unity  $n \geq 1$ , the shock wave is never formed strictly on the piston. For  $n < 1$ , the singularity is formed in the piston at the initial instant since the acceleration of the piston is also singular at that instant. The complete solution to this problem can be found in Landau and Lifshitz (1987).

### 2.2.2 Shock waves

As it has been shown above, in the absence of dissipative or external damping mechanisms the propagation of compression waves leads ultimately to the formation of a singularity. This singularity, characterized by an infinite velocity gradient, is solved when the role of the dissipative mechanisms in the thin regions with large velocity gradients is considered. These regions of strong gradients where the inviscid theory of one-dimensional flow is not valid correspond to what are generally termed shock waves. Fortunately, the irreversible processes controlled by the dissipative mechanisms only occur in narrow zones of the order of the mean free path, while outside of these transition zones the inviscid flow approximation of the Euler equations remains accurate (Courant and Friedrichs, 1948).

## 2 One-dimensional compressible flow and premixed combustion waves

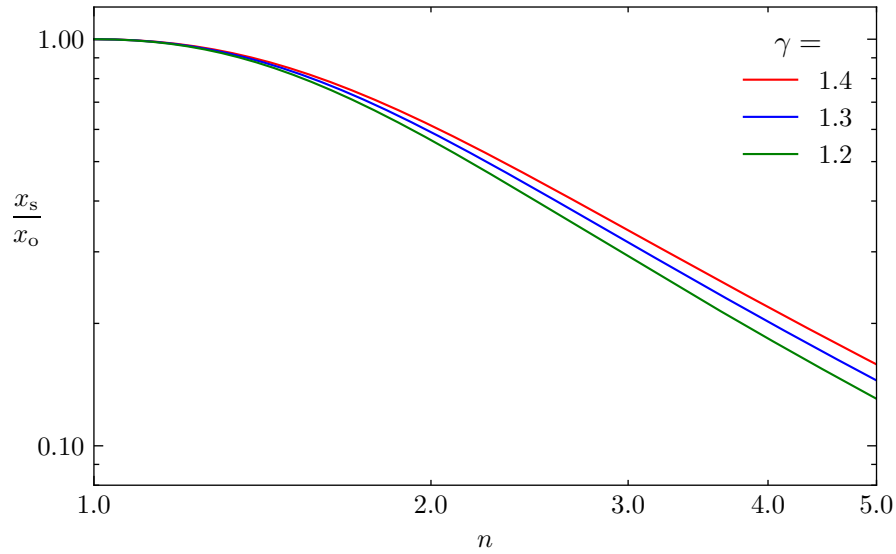


Figure 2.2: Relative position of formation of the singularity in the compression wave  $x_s/x_o = (r_s - r_p(t_s))/(r_o - r_p(t_s))$  as a function of the exponent  $n$  of the piston velocity law  $u_p = \alpha t^n$  for different values of the heat capacity ratio  $\gamma$ .

### Rankine-Hugoniot jump conditions

At scales larger than the mean free path, shock waves can be simply described as supersonic discontinuities. Integration of the conservation equations of mass (2.2), momentum (2.6), and energy (2.9) provides the jump relationships on both sides of the discontinuity without describing the irreversible processes in detail. Considering a plane shock wave propagating at constant velocity, the conservative form of the steady equations (2.2), (2.6) and (2.9) is written as

$$\frac{d}{dx} [\rho (\mathcal{D} - u)] = 0, \quad (2.33)$$

$$\frac{d}{dx} \left[ \rho (\mathcal{D} - u)^2 + p - \mu \frac{du}{dx} \right] = 0, \quad (2.34)$$

$$\frac{d}{dx} \left[ \rho (\mathcal{D} - u) \left( h + \frac{(\mathcal{D} - u)^2}{2} \right) - \lambda \frac{dT}{dx} - \mu (u - \mathcal{D}) \frac{du}{dx} \right] = 0, \quad (2.35)$$

where  $x = r - r_f(t)$  is the direction of propagation in the system of coordinates attached to the shock wave propagating with velocity  $\mathcal{D} \equiv dr_f/dt$  in the reference frame where flow ahead of the shock is at rest, and  $h$  denotes de enthalpy of the gas  $dh = de_T + d(p/\rho) = c_p dT$ .

Integrating the equation of mass conservation from the upstream state, denoted by  $u$  at surface of discontinuity ahead of the wave, to the Neumann state, denoted by  $N$ , at the

## 2.2 One-dimensional compressible flow

post-shock discontinuity surface, results in the conservation of the mass flow rate

$$m \equiv \rho_u \mathcal{D} = \rho (\mathcal{D} - u_N). \quad (2.36)$$

Similarly, integration of the momentum equation and the energy equation, introducing the mass flow rate, leads to

$$p_u + \frac{m^2}{\rho_u} = p_N + \frac{m^2}{\rho_N} \quad (2.37)$$

and

$$h_u + \left( \frac{m}{2\rho_u} \right)^2 = h_N + \left( \frac{m}{2\rho_N} \right)^2, \quad (2.38)$$

where the upstream and Neumann states are assumed to be uniform, so that the terms of heat conduction and momentum transport vanish at the limits of integration. Eliminating the mass flow rate with the help of (2.37) gives the Hugoniot relation

$$h_u - h_N + \frac{1}{2} \left( \frac{1}{\rho_u} - \frac{1}{\rho_N} \right) (p_N - p_u) = 0. \quad (2.39)$$

For a polytropic gas characterized by the equation of state of ideal gases and constant specific heats

$$p = \frac{\gamma - 1}{\gamma} c_p \rho T, \quad h = c_p T = \frac{\gamma}{\gamma - 1} \frac{p}{\rho}, \quad (2.40)$$

the Hugoniot relation (2.39) becomes

$$\frac{\gamma}{\gamma - 1} \left( \frac{p_u}{\rho_u} - \frac{p_N}{\rho_N} \right) + \frac{1}{2} \left( \frac{1}{\rho_u} - \frac{1}{\rho_N} \right) (p_N - p_u) = 0. \quad (2.41)$$

Introducing the normalized pressure and density proposed by Clavin and Searby (2016)

$$\mathcal{P} \equiv \frac{\gamma + 1}{2\gamma} \left( \frac{p}{p_u} - 1 \right), \quad \mathcal{V} \equiv \frac{\gamma + 1}{2} \left( \frac{\rho_u}{\rho} - 1 \right), \quad (2.42)$$

the Hugoniot relation for polytropic gases (2.41) reduces to an hyperbola in the  $\mathcal{P} - \mathcal{V}$  plane independent of the heat capacity ratio  $\gamma$

$$(\mathcal{P} + 1)(\mathcal{V} + 1) = 1. \quad (2.43)$$

Introducing the same notation, the momentum conservation equation (2.37) writes as

$$\mathcal{P} = -M_u^2 \mathcal{V}, \quad (2.44)$$

which describes the linear relationship between the normalized pressure and density through the mass flow rate written as the Mach number of the shock  $M_u = \mathcal{D}/a_u$ , known as Michelson-Rayleigh line. For physically meaningful (not imaginary) Mach numbers of the shock wave, the slope of the Michelson-Rayleigh line is always negative. Therefore,

## 2 One-dimensional compressible flow and premixed combustion waves

for the half plane defined by  $\mathcal{P}\mathcal{V} > 0$ , the RH relations have no solution.

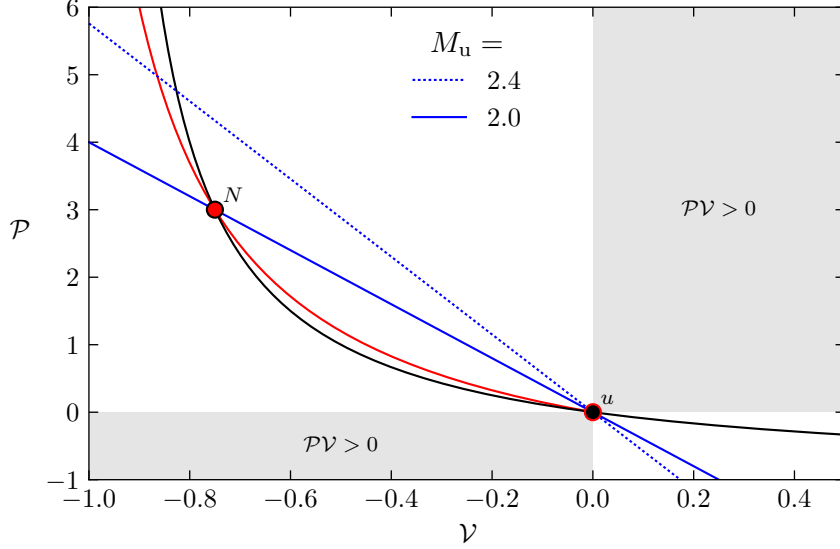


Figure 2.3: Hugoniot adiabat curve (in black) and Michelson-Rayleigh line (in blue) for different values of the Mach number  $M_u$ . The red curve represents the Hugoniot curve that departs from the Neumann state for a heat capacity ratio of  $\gamma = 1.4$ .

The Hugoniot curve (2.43) and the Michelson-Rayleigh line are represented in Figure 2.3 in the  $\mathcal{P} - \mathcal{V}$  plane. Both curves intersect at the initial condition that corresponds to the trivial solution  $\mathcal{P} = \mathcal{V} = 0$  of the system of equations (2.43) and (2.44) and at a compressed state known as Neumann state  $\mathcal{P}_N = M_u^2 - 1 = -M_u^2 \mathcal{V}_N$ . The slope of the Michelson-Rayleigh line steepens with the shock wave Mach number leading to greater compression levels. It is also important to note that the Hugoniot curve depends on the initial state. The red line in Figure 2.3 corresponds to the Hugoniot curve taking the Neumann state as the initial condition, which also passes through its corresponding initial state though it follows a different path.

The non-trivial root of the system of equations (2.43) and (2.44) corresponds to the Neumann state that is yielded by the Rankine-Hugoniot relations for a polytropic gas

$$\frac{\rho_u}{\rho_N} = \frac{\mathcal{D} - u_N}{\mathcal{D}} = \frac{(\gamma - 1)M_u^2 + 2}{(\gamma + 1)M_u^2} \quad (2.45)$$

$$\frac{p_N}{p_u} = \frac{2\gamma M_u^2 - (\gamma - 1)}{\gamma + 1} \quad (2.46)$$

$$\frac{T_N}{T_u} = \frac{[2\gamma M_u^2 - (\gamma - 1)][(\gamma - 1)M_u^2 + 2]}{(\gamma + 1)^2 M_u^2} \quad (2.47)$$

$$M_N^2 = \frac{\mathcal{D} - u_N}{a_N} = \frac{(\gamma - 1)M_u^2 + 2}{2\gamma M_u^2 - (\gamma - 1)} \quad (2.48)$$

which are represented in Figure 2.4 for a range of shock wave Mach numbers and

## 2.2 One-dimensional compressible flow

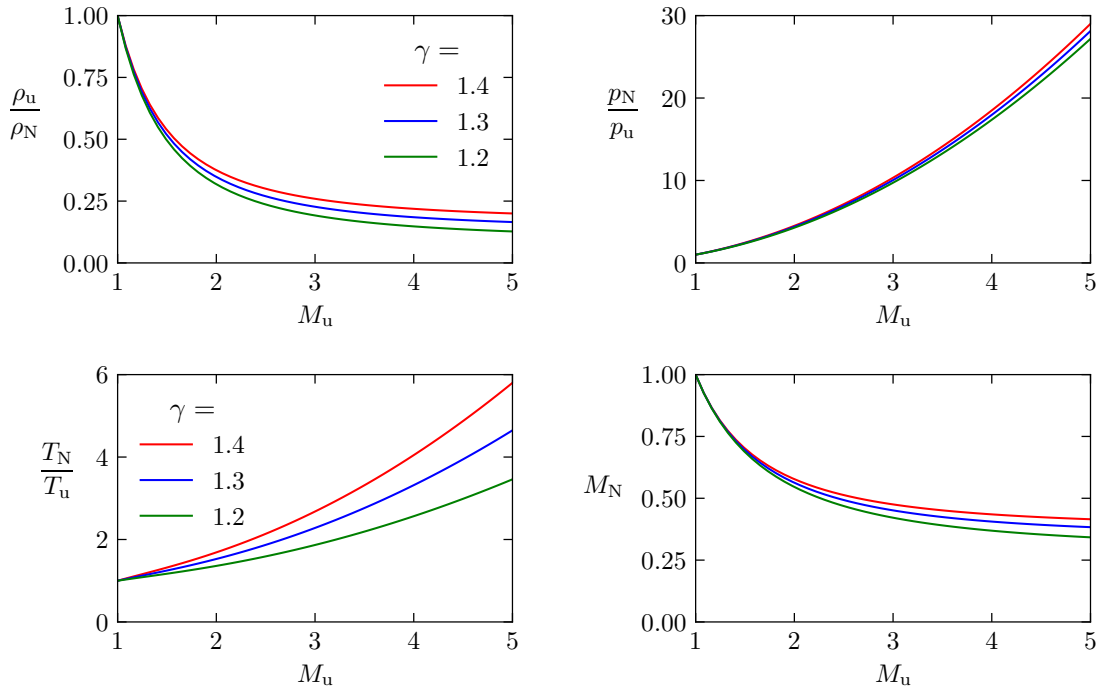


Figure 2.4: Rankine-Hugoniot jump relations in an inert shock wave as a function of the Mach number  $M_u$  for different values of the heat capacity ratio  $\gamma$ .

typical heat capacity ratio values. It is observed that the density jump through a shock wave tends to a limiting value for large Mach numbers given by the heat capacity ratio  $M_u \rightarrow \infty$ :  $\rho_u/\rho_N \approx (\gamma+1)/(\gamma-1)$ . The downstream Mach number relative to the shock wave is always less than unity, which means that through a shock wave a supersonic flow becomes a subsonic flow. Recalling that the square of the Mach number represents the ratio of macroscopic kinetic energy to internal thermal energy  $M^2 = u^2/((\gamma-1)c_p T)$  a shock wave can then be interpreted as a natural mechanism responsible for the conversion of the excess of macroscopic kinetic energy of a gas flow into internal energy. The post-shock Mach number also shows a limiting value for intense shock waves in terms of the heat capacity ratio  $M_u \rightarrow \infty$ :  $M_N \approx (\gamma-1)/2\gamma$ .

### Weak shock wave

The extreme case of a shock wave whose intensity is infinitesimally small serves as an instructive example for the understanding of the shock wave phenomenon. This limit, known as weak shock wave, applies when the Mach number of the wave approaches unity, that is, the propagation velocity of the weak shock approaches the sound speed.

The jump relations across a weak shock wave represent small variations of the physical properties compared with the initial state of the gas. They are determined by the linearised RH jump relations, which are obtained as series expansions of the general RH relations

## 2 One-dimensional compressible flow and premixed combustion waves

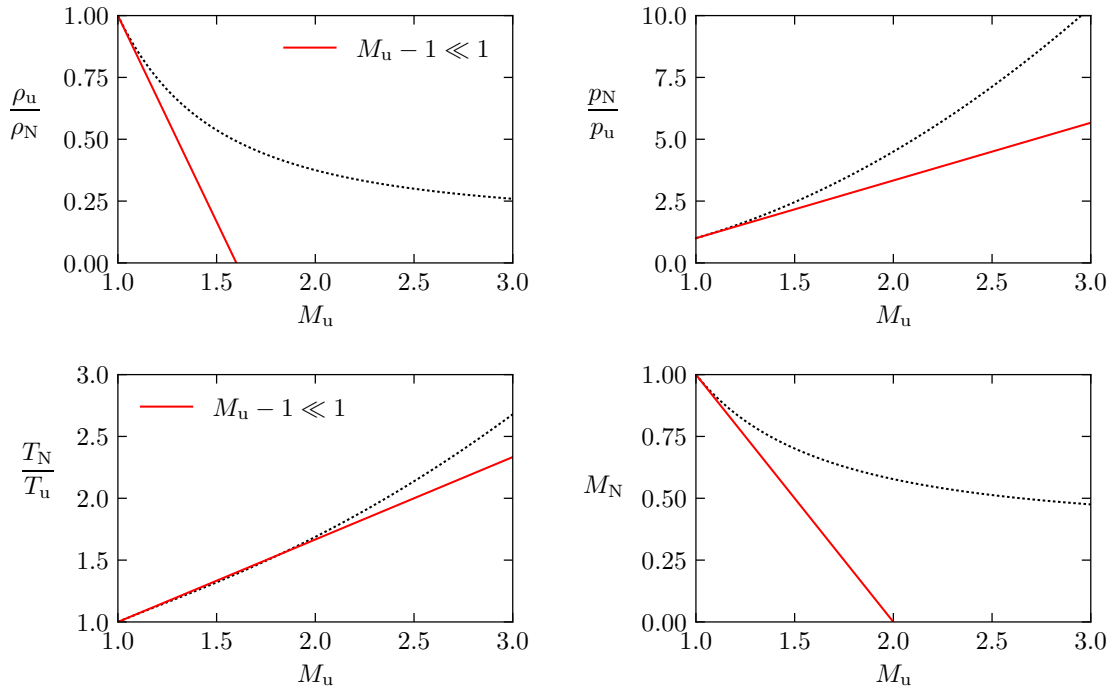


Figure 2.5: Rankine-Hugoniot jump relations (dotted black line) and linearised Rankine-Hugoniot jump relations (solid red line) for weak shock waves  $M_u - 1 \ll 1$  in polytropic diatomic gases  $\gamma = 1.4$ .

(2.45) to (2.48)

$$\frac{\rho_u}{\rho_N} = \frac{\mathcal{D} - u_N}{\mathcal{D}} = 1 - \frac{4}{\gamma + 1}(M_u - 1) + \mathcal{O}[(M_u - 1)^2] \quad (2.49)$$

$$\frac{p_N}{p_u} = 1 + \frac{4\gamma}{\gamma + 1}(M_u - 1) + \mathcal{O}[(M_u - 1)^2] \quad (2.50)$$

$$\frac{T_N}{T_u} = 1 + \frac{4(\gamma - 1)}{\gamma + 1}(M_u - 1) + \mathcal{O}[(M_u - 1)^2] \quad (2.51)$$

$$M_N = 1 - (M_u - 1) + \mathcal{O}[(M_u - 1)^2]. \quad (2.52)$$

These linearised RH jump relations are represented and compared with the general jump relations in Figure 2.5. It is noteworthy that the temperature relation shows a wide range of validity with a relative error below 5% for shock waves as intense as  $M_u = 2$  and the relative flow velocity behind the shock is equal to the local sound speed  $\mathcal{D} - u_N \approx a_N$  to leading order.

The weak shock wave limit also provides a suitable framework for the study of its internal structure through the macroscopic conservation equations. The dissipative mechanisms control the internal structure of a shock wave. In ordinary shock waves, these mechanisms are relevant in a length scale of the order of the mean free path. The

## 2.2 One-dimensional compressible flow

internal structure of the shock wave is then out of equilibrium and must be studied using Boltzmann's equation. However, as the supersonic shock velocity decreases, not only do the jumps through the shock decrease, but also the thickness increases. Indeed, in the weak shock wave limit, the ratio of shock thickness to mean free path diverges. For a weak shock propagating slightly above the speed of sound, the thickness becomes macroscopic, thus, the local equilibrium approximation becomes valid and the fluid mechanics equations can be used to describe the detonation structure. The problem is reduced to solving a one-dimensional steady transonic flow between the initial state and the shocked gas.

Rayleigh (1910) showed that viscosity played as essential a role as heat conduction in the structure of a shock wave. The internal structure of a weak shock wave is then described by the conservation equations (2.33) to (2.35). A perturbation analysis up to the second order of the weak shock wave limit  $M_u - 1 \ll 1$ , reduces this system of second order differential equations to a first order differential equation (Clavin and Searby, 2016). The solution obtained after integration provides to the profiles shown in Figure 2.6. The physical variables evolve from the initial state to the Neumann state given by the linearised RH relations (2.49) to (2.52) in a distance with respect to the mean free path  $l$  that diverges as the shock Mach number goes to unity. The entropy jump throughout the shock wave is a positive quantity of the third order of the approximation. Therefore, the weak shock wave limit also serves to provide insight into the transition from an isentropic compression wave to a weak shock wave.

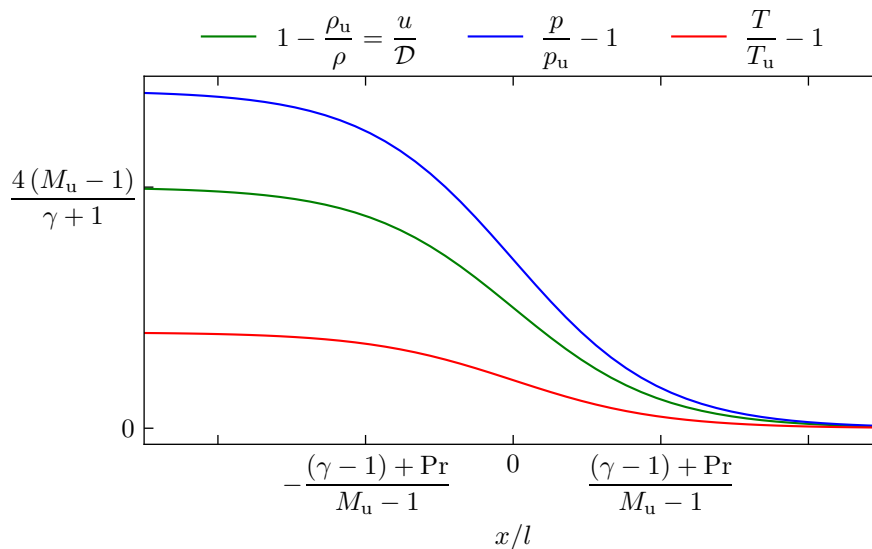


Figure 2.6: Internal structure of a weak shock wave  $M_u - 1 \ll 1$  propagating towards the right (i.e., the upstream gas is at  $x \rightarrow \infty$  and the shocked gas is at  $x \rightarrow -\infty$ ) for a diatomic gas  $\gamma = 1.4$ .



### 2.2.3 Strong blast wave

A shock wave that propagates away from its source and the flow field it leaves behind is known as blast wave. Blast waves are generally formed when a large amount of energy is released during a short period of time in a concentrated location. The propagation of an ideal strong blast wave was first independently described by Sedov (1946) and Taylor (1941). Initially, the motion of the blast wave is determined by the size and distribution of the energy release. Once the radius of the blast and the time elapsed are large enough compared with the spatial and temporal scales that characterize the energy source, the shock motion becomes independent of the initial conditions.

The instantaneous release of a concentrated large amount of energy  $E_0$  (energy per unit length in line sources and energy per unit surface in planar surfaces) leads to the formation of a strong shock wave characterized by a large Mach number  $M_u \gg 1$ . The pressure jump along such a wave is as large as the square of the Mach number

$$M_u \gg 1 : \quad \frac{p_N}{p_u} \approx \frac{2\gamma}{\gamma + 1} M_u^2. \quad (2.53)$$

Therefore, the initial pressure  $p_u$  is negligible compared with the pressure behind the shock wave  $p_N$ . On the contrary, the density reaches a limiting value in the strong shock wave limit

$$M_u \gg 1 : \quad \frac{\rho_N}{\rho_u} \approx \frac{\gamma + 1}{\gamma - 1}. \quad (2.54)$$

The relevant parameters of the problem then include the initial density of the surrounding fluid  $\rho_u$  (which is assumed to be uniform) and the total energy released at the concentrated source  $E_0$ . A dimensionless combination can be formed using these problem parameters and two independent variables of time  $t$  and radial coordinate  $r$  that writes as  $\rho_u r^{j+3} / (E_0 t^2)$ .

Based on this dimensional analysis, Sedov and Taylor anticipated that the position of the shock wave follows the evolution given by

$$r_f(t) = S \left( \frac{E_0 t^2}{\rho_u} \right)^{1/(j+3)} \quad (2.55)$$

where  $S$  is a function of the ratio of heat capacity  $\gamma$  and the geometrical parameter  $j$  whose value can be obtained integrating the energy equation. This prediction of the blast radius as a function of time showed excellent agreement with the evolution of the blast wave extracted from the photographic records of the first atomic explosion in New Mexico (Taylor, 1950b). Furthermore, Taylor was able to approximate with good accuracy the total amount of energy released during the explosion from these results.

The density, pressure, temperature and velocity fields behind the shock wave are governed by the Euler equations. Since the blast radius, which is the only spatial scale of the problem, follows a direct relation with the temporal scale, the strong blast problem admits a self-similar solution.

## 2.2 One-dimensional compressible flow

Defining the non-dimensional functions

$$f(\xi) = \frac{p(r, t)}{\rho_u \mathcal{D}(t)^2}, \quad \psi(\xi) = \frac{\rho(r, t)}{\rho_u} \quad \text{and} \quad \phi(\xi) = \frac{u(r, t)}{\mathcal{D}(t)}, \quad (2.56)$$

of the self-similar variable  $\xi \equiv r/r_f(t)$ , where  $\mathcal{D}(t) \equiv dr_f/dt \gg a_u$  is the propagation velocity of the shock wave, the Euler equations (2.14), (2.15) and (2.18) rewrite as

$$(\phi - \xi)\psi' + \psi\phi' + \frac{j\phi\psi}{\xi} = 0 \quad (2.57)$$

$$(\phi - \xi)\phi' + \chi\phi + \frac{1}{\psi}f' = 0 \quad (2.58)$$

$$(\phi - \xi)f' + 2\chi f + \gamma f\phi' + \frac{\gamma j\phi f}{\xi} = 0, \quad (2.59)$$

where the parameter  $\chi = r_f \mathcal{D}' / \mathcal{D}^2$  has been introduced. For this problem to have a self-similar solution, the system of equations (2.57) to (2.59) must be explicitly independent of time (or front radius). Therefore, the parameter  $\chi$  must be constant

$$\chi = r_f \frac{\mathcal{D}'}{\mathcal{D}^2} = \frac{(\ln \mathcal{D})'}{(\ln r_f)'} = \text{const.} \quad (2.60)$$

After integration, the law for the velocity of propagation of the front  $\mathcal{D} = kr_f^\chi$  is obtained, which according to (2.55) determines value of the parameter through the geometry of the problem as  $\chi = -(j + 1)/2$ .

The mathematical problem defined by the ordinary differential equations (2.57) to (2.59), the boundary conditions at the front  $\xi = 1$  given by the RH relations for strong shock waves

$$M_u \gg 1 : \quad f(1) = \frac{p_N}{\rho_u \mathcal{D}^2} \approx \frac{2}{\gamma + 1} \quad (2.61)$$

$$\psi(1) = \frac{\rho_N}{\rho_u} \approx \frac{\gamma + 1}{\gamma - 1} \quad (2.62)$$

$$\phi(1) = \frac{u_N}{\mathcal{D}} \approx \frac{2}{\gamma + 1}, \quad (2.63)$$

and the rear boundary condition  $\phi(0) = 0$  that imposes the velocity at the origin to vanish due to symmetry, has an exact solution whose analytical closed form can be found in Landau and Lifshitz (1987). Alternatively, the problem can be integrated numerically to obtain the solution shown in Figure 2.7.

The blast wave solution is characterized by the concentration of most of the mass of compressed fluid near the shock wave and a nearly linear velocity profile. An almost empty region of extremely hot gases is observed around the origin of the explosion. The flow velocity evolves in a quasi-linearly from the Neumann velocity imposed by the shock

## 2 One-dimensional compressible flow and premixed combustion waves

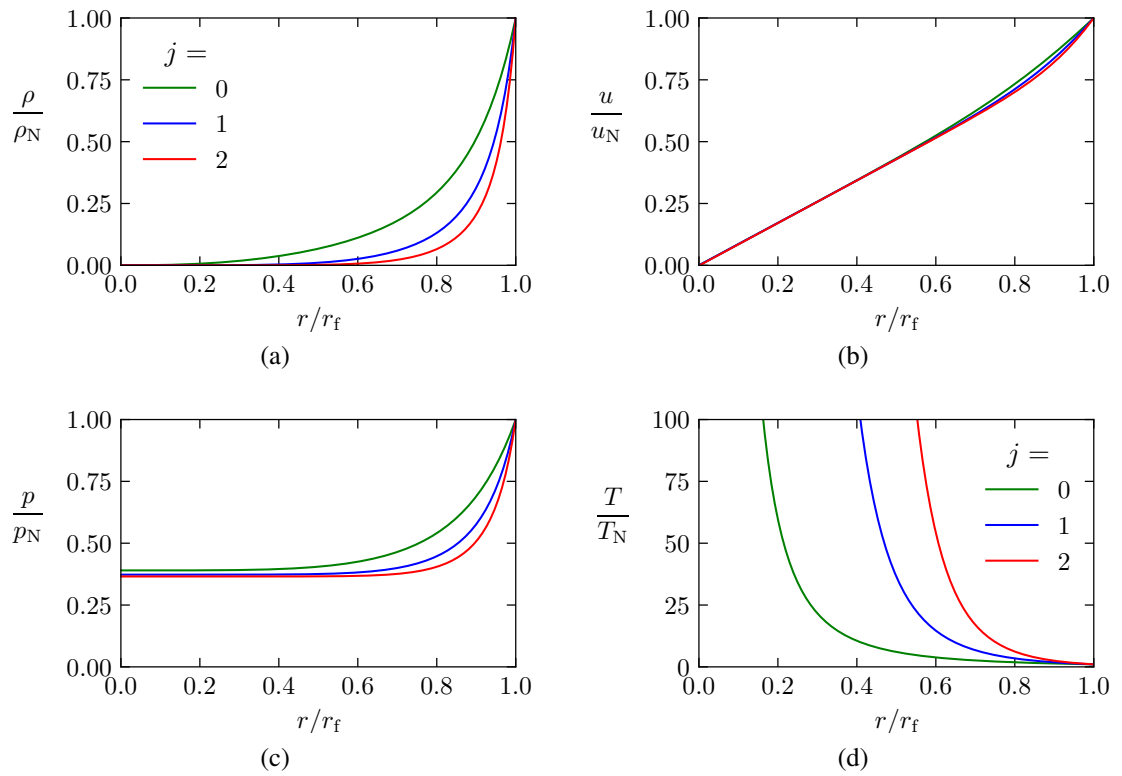


Figure 2.7: (a) Density, (b) velocity, (c) pressure and (d) temperature fields in a strong planar ( $j = 0$ ), cylindrical ( $j = 1$ ) and spherical ( $j = 2$ ) blast wave for a diatomic gas  $\gamma = 1.4$  in the solution of Taylor (1941) and Sedov (1946).

wave to zero at the origin. The flow divergence due to the curvature of the cylindrical and spherical waves introduces only quantitative corrections in the flow field behind the shock wave that further narrow the region where most of the mass is concentrated.

## 2.3 Premixed combustion waves

The theoretical study of combustion waves is generally divided into premixed flames and diffusion, or non-premixed, flames. This categorization is based on the limiting element for the combustion reaction. The study of premixed flames encompasses situations in which fuel and oxidants are perfectly mixed at molecular level, but the thermal agitation of the mixture is not sufficient to initiate the combustion. On the other hand, in diffusion flames the reactants are initially isolated, but the initial conditions allow combustion reactions to start as soon as the reactants are brought into contact. However, it is important to note that this is just a theoretical distinction and under more realistic conditions, such as those found for lifted flames (Liñán et al., 2015), both combustion regimes are indeed intertwined. The present work is limited to combustion fronts propagating in a reactive mixture which is generally the case of interest for accidental flames.

A local increment of the thermal agitation in a reactive mixture ignites a combustion wave which will propagate away from the source transforming reactants into combustion products. Two distinct propagating regimes for these combustion waves are generally identified. Deflagration waves propagate at slow subsonic velocities of the order of a few centimeters per second  $U_L \approx 0.1 - 1 \text{ m/s}$ . Whereas detonation waves are supersonic reactive waves that can cover distances of some kilometers in a second  $\mathcal{D} \approx 1000 \text{ m/s}$ . The fast propagation of a detonation leads to a strong increase in pressure that can be tens of times higher than the initial pressure  $\Delta p/p \approx 30$ , causing significant material damage in its path. In contrast, a deflagration is an expansion wave through which the pressure decreases slightly  $\Delta p/p \approx -10^{-5}$  due to its low velocity.

Such a difference in the propagation speed of both waves is justified by different propagation mechanisms. The slow propagation of deflagration waves is controlled by diffusion mechanisms. The heat released in the chemical reactions of combustion is transferred by conduction towards the fresh mixture of reactive gases. The fresh gases are then heated accelerating the rate of the chemical interactions which are initially frozen. When the chemical reaction takes place, the heat released is in turned transferred forward resulting in a self-propagating wave. This propagation regime is then limited by the random motion of hot particles towards fresh gas zone where the thermal agitation is transmitted to the cold particles through successive collisions giving rise to heat diffusion. Detonations, on the other hand, propagate due to compressibility effects. The ignition of the combustion reactions is triggered by the adiabatic compression of a shock wave leading the detonation front. A reaction zone where heat release occurs after an induction time follows the shock wave. For the detonation wave to persist, the shock wave and the reaction zone must remain coupled, with the shock wave providing the appropriate thermodynamic conditions for a rapid heat release and the reaction zone providing the

## 2 One-dimensional compressible flow and premixed combustion waves

thrust required by the shock wave.

### Reactive Rankine-Hugoniot jump conditions

A first step in the understanding of these reactive waves can be done by considering them as reactive discontinuities and looking at the initial and final state of the gas passing through them. These approach led to the theory of Chapman (1899) and Jouguet (1905) (CJ) of detonations. As in the study of shock waves, the jump relations between the initial state of the reactive mixture and the state of the burned gases behind the reactive front can be obtained by integrating the conservation equations (2.33) to (2.35) along the front. For a reactive front, however, it is necessary to include the heat of reaction in the energy conservation equation (2.35), which is rewritten as

$$\frac{d}{dx} \left[ \rho(u - \mathcal{D}) \left( h + \frac{(u - \mathcal{D})^2}{2} \right) - \lambda \frac{dT}{dx} - \mu(u - \mathcal{D}) \frac{du}{dx} + \rho(u - \mathcal{D}) q_m(1 - Y) \right] = 0, \quad (2.64)$$

where  $q_m$  is the heat of reaction per unit mass of the mixture and  $Y$  is the progress variable of the reaction which is equal to zero in the fresh mixture and one in the burned mixture. Integrating from the uniform mixture of reactive gases to the uniform state of burned gases, denoted by  $b$ , results in

$$h_u + \left( \frac{m}{2\rho_u} \right)^2 + q_m = h_b + \left( \frac{m}{2\rho_b} \right)^2 \quad (2.65)$$

which eliminating the mass flow rate through (2.37), gives the reactive Hugoniot relation

$$h_b - h_u + \frac{1}{2} \left( \frac{1}{\rho_b} - \frac{1}{\rho_u} \right) (p_b - p_u) = q_m, \quad (2.66)$$

that for polytropic gases (2.40) can be written in terms of density and pressure

$$\frac{\gamma}{\gamma - 1} \left( \frac{p_b}{\rho_b} - \frac{p_u}{\rho_u} \right) + \frac{1}{2} \left( \frac{1}{\rho_b} - \frac{1}{\rho_u} \right) (p_b - p_u) = q_m. \quad (2.67)$$

Introducing the normalized heat of reaction proposed by Clavin and Searby (2016)

$$\mathcal{Q} \equiv \frac{\gamma + 1}{2} \frac{q_m}{c_p T_u}, \quad (2.68)$$

the reactive Hugoniot relation for polytropic gases corresponds to an hyperbola in the  $\mathcal{P} - \mathcal{V}$  plane

$$(\mathcal{P} + 1)(\mathcal{V} + 1) = \mathcal{Q} + 1. \quad (2.69)$$

that lies above the inert Hugoniot curve for exothermic reactive mixtures  $\mathcal{Q} > 0$ . Combining this relation with the still valid Michelson-Rayleigh line (2.44) provides with

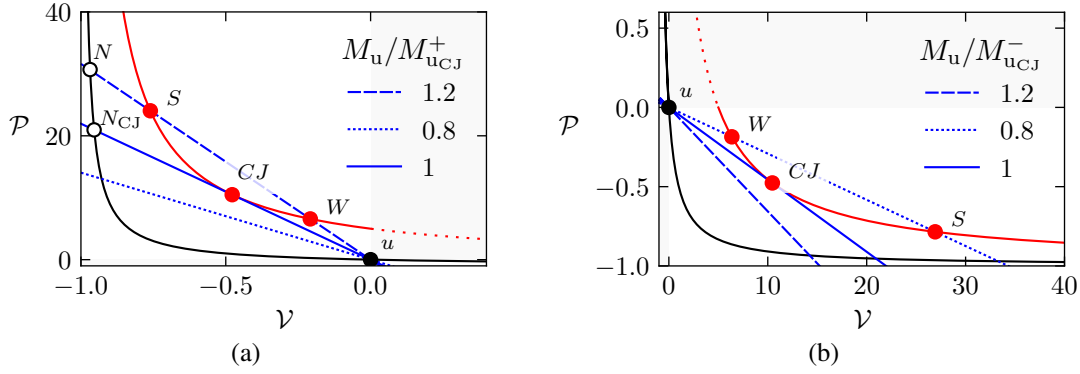


Figure 2.8: Hugoniot curves and Michelson-Rayleigh lines for (a) detonations and (b) deflagrations. Black curve corresponds to inert Hugoniot curve and red curve to reactive Hugoniot for a normalized heat of reaction  $Q = 5$ . Michelson-Rayleigh lines are traced in blue for different values of the Mach number  $M_u$  with respect to the Chapman-Jouguet regime  $M_{u,CJ}$ .

the jump relations across a reactive discontinuity

$$\mathcal{P}_b = -M_u^2 \mathcal{V}_b = \frac{M_u^2 - 1}{2} \left[ 1 \pm \sqrt{1 - \frac{4QM_u^2}{(M_u^2 - 1)^2}} \right] \quad (2.70)$$

which presents a marginal solution when the discriminant of the square root cancels out, i.e.,  $4QM_u^2 = (M_u^2 - 1)^2$ . Solving for the Mach number of the reactive front provides the propagating regime of this marginal solution, known as Chapman-Jouguet regime, in terms of the heat of reaction

$$M_{u,CJ} = \sqrt{Q+1} \pm \sqrt{Q}. \quad (2.71)$$

The possible solutions for steady reactive waves are then restricted to fronts that propagate faster than  $M_{u,CJ}^+ = \sqrt{Q+1} + \sqrt{Q}$  or slower than  $M_{u,CJ}^- = \sqrt{Q+1} - \sqrt{Q}$  with the intermediate values corresponding to imaginary solutions of (2.70) without physical meaning.

The Hugoniot curves and some representative Michelson-Rayleigh lines are represented in Figure 2.8 in order to illustrate the different solutions. For  $M_u \geq M_{u,CJ}^+ = \sqrt{Q+1} + \sqrt{Q}$ , density and pressure are larger behind the reactive wave and the solutions obtained correspond to detonation waves. In particular, when  $M_u > M_{u,CJ}^+$  two solutions are obtained which are typically referred as strong (point  $S$ ) and weak (point  $W$ ) detonations. In the Chapman-Jouguet regime  $M_u = M_{u,CJ}^+$ , both solutions collapse to the marginal solution. On the contrary, for  $M_u \leq M_{u,CJ}^-$ , the gas undergoes an expansion process that corresponds to a deflagration. Similarly, deflagration waves exhibit two solutions when  $M_u < M_{u,CJ}^-$  known as strong and weak deflagrations, which collapse to the marginal solution for  $M_u = M_{u,CJ}^-$ . As it will be shown below, the Chapman-Jouguet regime corresponds to the propagation velocity of self-sustained detonation waves. While the

## 2 One-dimensional compressible flow and premixed combustion waves

Chapman-Jouguet regime is not relevant for ordinary deflagrations. This substantial difference is due to the different propagation mechanisms governing each wave.

The range of propagation velocities limited by both Chapman-Jouguet velocities  $M_{u_{CJ}}^- < M_u < M_{u_{CJ}}^+$  has no solution. Therefore, a continuous transition from a self-accelerating deflagration wave to a detonation wave through quasi-steady intermediate solutions is prohibited by the CJ theory. The transition from a deflagration to a detonation has to pass through an unsteady solution of the reactive fronts (Courant and Friedrichs, 1948).

The pressure and density relationships between the burned gas state and the fresh reactive mixture can be expressed in terms of the propagation velocity  $M_u$  and the CJ regime  $M_{u_{CJ}}$  (or, equivalently, the heat of reaction  $\mathcal{Q}$ ) from the solution (2.70) known as reactive Rankine-Hugoniot jump conditions

$$\frac{\rho_u}{\rho_b} = \frac{\mathcal{D} - u_b}{\mathcal{D}} = \frac{(\gamma - 1) M_u^2 + 2}{(\gamma + 1) M_u^2} + \frac{M_u^2 - 1}{(\gamma + 1) M_u^2} \left[ 1 \pm \sqrt{1 - \left( \frac{M_{u_{CJ}} - M_{u_{CJ}}^{-1}}{M_u - M_u^{-1}} \right)^2} \right] \quad (2.72)$$

$$\frac{p_b}{p_u} = \frac{2\gamma M_u^2 - (\gamma - 1)}{\gamma + 1} - \frac{\gamma (M_u^2 - 1)}{\gamma + 1} \left[ 1 \pm \sqrt{1 - \left( \frac{M_{u_{CJ}} - M_{u_{CJ}}^{-1}}{M_u - M_u^{-1}} \right)^2} \right] \quad (2.73)$$

which for  $\mathcal{Q} = 0$ , or  $M_{u_{CJ}} = 1$ , yield consistently the RH relations across an inert shock wave (2.45) and (2.46).

In the Chapman-Jouguet regime, the discriminant of the square root vanishes leading to a unique solution

$$M_u = M_{u_{CJ}} = \sqrt{\mathcal{Q} + 1} \pm \sqrt{\mathcal{Q}} : \quad \frac{\rho_u}{\rho_{b_{CJ}}} = \frac{\mathcal{D}_{CJ} - u_{b_{CJ}}}{\mathcal{D}_{CJ}} = \frac{\gamma M_{u_{CJ}}^2 + 1}{(\gamma + 1) M_{u_{CJ}}^2} \quad (2.74)$$

$$\frac{p_{b_{CJ}}}{p_u} = \frac{\gamma M_{u_{CJ}}^2 + 1}{\gamma + 1} \quad (2.75)$$

$$\frac{a_{b_{CJ}}}{a_{u_{CJ}}} = \frac{\gamma M_{u_{CJ}}^2 + 1}{(\gamma + 1) M_{u_{CJ}}}. \quad (2.76)$$

Algebraic manipulations of the equations (2.74) and (2.76) show that the burned gas flow velocity relative to the front equals the local sound speed  $M_{b_{CJ}} = (\mathcal{D}_{CJ} - u_{b_{CJ}})/a_{b_{CJ}} = 1$  in the CJ regime. Therefore, the CJ wave corresponds to the propagation regime that imposes the sonic condition behind the detonation. It is also interesting to note that the sonic condition applies equally to detonations as to deflagrations in the CJ regime.

The CJ theory that considers the reactive front as a discontinuity provides the jump conditions as well as information regarding the space of solutions of a reactive front. However, it is required to consider the internal structure of the front in order to discriminate which solutions are relevant, as well as to decipher the propagation mechanisms. In the

following, the salient features of the two propagation regimes concerning the internal structure of the reactive fronts as well as the propagation will be introduced.

### 2.3.1 Deflagrations

A deflagration is a subsonic flame front that propagates through a mixture of fuel and oxidizer. According to the CJ theory, deflagrations corresponds to the solutions for reactive fronts that lie on the lower part of the Hugoniot curve. That is, deflagrations propagate always at subsonic speeds  $M_u < 1$ . Indeed, under ordinary conditions, deflagrations generally propagate at markedly subsonic velocities  $M_u \ll 1$ . The Euler equation (2.12) shows that since pressure is roughly equal to the product of the density with the square of the sound speed  $p \approx \rho a^2$ , relative changes in pressure  $\delta p/p \approx \rho u \delta u \approx u \delta u/a^2$  are of the order of the Mach number squared  $\delta p/p \approx M^2$ . For the slow velocities at which deflagrations propagate  $M \ll 1$ , the pressure variations are negligible  $\delta p/p \ll 1$ . Therefore, the analysis of deflagration waves can be performed under the quasi-isobaric approximation.

#### *Quasi-isobaric approximation*

In the quasi-isobaric approximation, heat conduction must increase the temperature of the fresh gases where the chemical reactions are frozen. Therefore, the Euler equations (2.11) and (2.12) cannot describe the structure of a flame. It is necessary to recover the molecular transport terms included in the reactive Navier Stokes equations (2.2), (2.4), (2.6) and (2.9). In the coordinate system attached to the flame  $x = r - r_f(t)$  that propagates at constant velocity  $\mathcal{D} = dr_f/dt$ , the conservation equations under the quasi-isobaric approximation are written as

$$\frac{d}{dx} [\rho (\mathcal{D} - u)] = 0 \quad (2.77)$$

$$\frac{dp}{dx} = 0 \quad (2.78)$$

$$\frac{d}{dx} [\rho (\mathcal{D} - u) c_p T] = \frac{d}{dx} \left( \lambda \frac{dT}{dx} \right) + \rho q_m \omega \quad (2.79)$$

$$\frac{d}{dx} [\rho (\mathcal{D} - u) Y] = \frac{d}{dx} \left( \rho D \frac{dY}{dx} \right) + \rho \omega, \quad (2.80)$$

where not only the pressure is constant but also kinetic energy variation vanishes. The quasi-isobaric assumption simplifies the analysis of the flame propagation of a flame since it allows to decouple the conservation of energy from the hydrodynamic problem.



## 2 One-dimensional compressible flow and premixed combustion waves

The thermal propagation of a flame gets reduced the thermodiffusive problem

$$\rho(\mathcal{D} - u) c_p \frac{dT}{dx} = \frac{d}{dx} \left( \lambda \frac{dT}{dx} \right) + \rho q_m \omega \quad (2.81)$$

$$\rho(\mathcal{D} - u) \frac{dY}{dx} = \frac{d}{dx} \left( \rho D \frac{dY}{dx} \right) + \rho \omega. \quad (2.82)$$

for which the propagation velocity of the flame is obtained as an eigenvalue of the solution.

### *Large activation energy asymptotic limit*

In the large activation energy asymptotic limit studied by Zeldovich and Frank-Kamenetskii (1938), the thermodiffusive problem (2.81) and (2.82) can be further simplified. When an infinitely large activation energy is considered, the combustion reaction are concentrated in an infinitesimally thin layer. Therefore, a scale separation can be applied to the problem so that outside the infinitesimally thin reactive layer the reactive term is negligible, whereas in the reactive layer the convection-induced temperature gradient is negligible. Thanks to the separation of scales, both problems can be solved independently. The coupling of the solutions provides the eigenvalue of the problem which determines the propagation velocity of the flame in terms of thermo-chemical properties of the reactive mixture. In particular, the burning velocity of the planar flame  $U_b \propto \sqrt{D\omega}$  is determined by the diffusive properties of the mixture and the reaction rate.

### *Flame structure*

The qualitative description of the flame structure in the asymptotic limit of high activation energy is preserved when the thermodiffusive (2.81) and (2.82) problem is integrated numerically for finite values of the activation energy. A preheat region is observed in which the reactive mixture of fresh gases is heated by conduction from the hotter reactive layer. Nevertheless, the chemical reaction are frozen in the preheat region so no heat release occurs. The combustion reactions take place within a much thinner layer than the preheat region.

In conclusion, the mechanism of propagation of deflagrations is the thermal conduction driven by the molecular heat transport. Furthermore, the heat flux is limited by the rate of heat release which, due to the activation energy of the combustion reactions, is much lower than the collision frequency between molecules. Therefore, the propagation of a deflagration must be well below the sound speed. Hence, only the weak deflagration solution of the CJ theory can be explained by this mechanism. The lack of interest of the marginal CJ solution for deflagrations can also be justified by this propagation mechanism. The CJ regime implies the sonic condition behind the flame according to which the flame propagates at the sound speed relative to the burned gases. For this to be possible, the reaction rate would have to be close to the collision frequency. In such a situation, a metastable equilibrium is not justified for the reactive gas mixture, which

would be completely out of equilibrium and would react until completion without the need for a deflagration wave.

### 2.3.2 Detonations

Detonations are supersonic exothermic fronts that propagate on a reactive mixture. The systematic study of detonations was initiated independently by Berthelot and Vieille (1881) and Mallard and Le Chatelier (1881) because of the growing concern about accidental explosions in coal mines resulting in loss of life and property damages in the late 19th century. In contrast to deflagrations, detonations propagate at supersonic speed with a large pressure variation leading to significant mechanical impact. In the CJ theory, the detonations thus correspond to the solutions obtained at the higher part of the Hugoniot curve for supersonic regimes  $M_u > 1$ .

#### *ZND structure*

A one-dimensional model to describe the internal structure of a steady detonation wave was proposed independently by Zeldovich (1940), von Neumann (1942), and Döring (1943) although it had been conjectured previously by Mikhel'son (1893) and Vieille (1900). This structure, known as ZND structure after its authors, consists of a leading shock wave followed by an induction zone and a reaction zone. The fresh mixture of reactive gases in a metastable equilibrium state (i.e., chemically frozen) is compressed as it crosses the leading shock wave. The physical transformations experienced by the gaseous mixture during its passage through the shock wave unsettles the metastable equilibrium and initiates the combustion reactions that transform the reactive mixture into less energetic products. However, chemical transformations take an induction time to finalize that is longer than the collision time. Therefore, a scale separation is again possible.

In the leading shock wave, dissipation mechanisms transform the excess macroscopic kinetic energy into thermal energy by slowing down the gases in the shock wave reference frame and increasing their pressure and temperature. The thickness of the shock wave  $d$  is comparable to the mean free path  $l$  which corresponds to the distance travelled by a gas molecule moving at the sound speed during the time between collisions  $l = at_{\text{coll}}$ .

The induction reactions required for heat release take place on a much larger scale. The induction time of the heat release is related to the collision time through an Arrhenius law  $t_r/t_{\text{coll}} \approx \exp(E_a/(k_B T))$  with a large activation energy  $E_a/(k_B T) \gg 1$ . The flow velocity behind the shock wave is of the order of the sound speed. Hence, the length of the induction zone  $l_i \approx at_r$  is much larger than the shock wave thickness  $l_i/d \approx \exp(E_a/(k_B T)) \gg 1$ . Furthermore, the shock wave can be considered inert with little error.

The relevance of molecular transport effects in the induction zone can be assessed through the Reynolds number. Based on the kinetic gas theory, the molecular transport coefficients, such as the kinematic viscosity, are comparable to the square of the sound

## 2 One-dimensional compressible flow and premixed combustion waves

speed multiplied by the collision time  $\nu = a^2 t_{\text{coll}}$ . Using the estimate for the induction zone length aforementioned, the Reynolds number characterizing the induction zone is much larger than unity  $\text{Re}_{l_i} = l_i a / \nu \approx t_r / t_{\text{coll}} \gg 1$ . Therefore, diffusive effects can be neglected in first approximation in the induction zone.

According to these considerations, the induction zone is described by the reactive Euler equations (2.11) and (2.12). The conservative form of the Euler equations for a steady plane detonation in the reference frame of the leading shock  $x = r - r_f(t)$  propagating with velocity  $\mathcal{D} = dr_f/dt$  are written as

$$\frac{d}{dx} [\rho (\mathcal{D} - u)] = 0, \quad (2.83)$$

$$\frac{d}{dx} [\rho (\mathcal{D} - u)^2 + p] = 0, \quad (2.84)$$

$$\frac{d}{dx} \left[ \rho (u - \mathcal{D}) \left( h + \frac{(u - \mathcal{D})^2}{2} \right) + \rho (u - \mathcal{D}) q_m (1 - Y) \right] = 0, \quad (2.85)$$

$$\frac{d}{dx} [\rho (\mathcal{D} - u) Y] = \rho \omega, \quad (2.86)$$

where  $Y$  is a reaction progress variable which is  $Y = 0$  for the initial mixture of fresh gases and  $Y = 1$  after complete combustion. This reaction progress variable can be interpreted as the reduced mass fraction of the combustion products. Integration of this system of equations from the boundary conditions given by the Neumann state (2.45) to (2.47) behind the shock wave for a given reaction rate  $\omega$  provides with the internal structure of the detonation.

An example of the ZND structure for a CJ detonation whose reaction rate is given by

$$\omega(T, Y) = (1 - Y) B \exp \left( -\frac{E_a}{k_B T} \right) \quad (2.87)$$

has been numerically integrated and the results are represented in Figure 2.9. The induction zone for  $x/l_i < 0$  is characterized by a region where the evolution of the physical variables is negligible followed by a reaction zone where most of the heat is released. A pronounced evolution of the physical variables is observed at the end of the induction zone. Along the induction zone, an expansion process takes place where the gases are slowed down so that at the end of the reaction zone the flow is sonic with respect to the leading shock wave. That is, the ZND structure connects the initial state of the mixture with the sonic condition of the CJ regime.

The internal structure of the detonation described by the ZND model can also be represented on the  $\mathcal{P} - \mathcal{V}$  plane. Since diffusive effects are neglected in the induction zone, the integration of the conservation equations in the induction zone from the Neumann state is equivalent to the integration from the initial conditions to a partially reacted state. Such partially reacted Hugoniot curves correspond to

$$(\mathcal{P} + 1)(\mathcal{V} + 1) = Y \mathcal{Q} + 1 \quad (2.88)$$

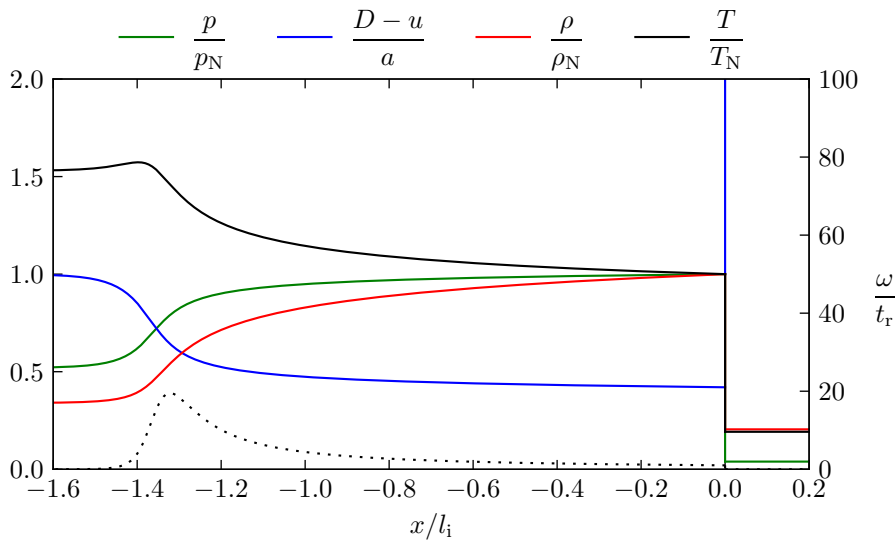


Figure 2.9: Structure of a CJ detonation according to Zeldovich (1940), von Neumann (1942), and Döring (1943). The reactive wave propagating towards the right (i.e., the initial fresh mixture is at  $x > 0$  and the detonation structure at  $x \leq 0$  with  $x = 0$  being the position of the leading shock). The thermo-chemical properties of the mixture are determined by the heat capacity ratio  $\gamma = 1.4$ , the reduced heat release  $\mathcal{Q} = 5$  and the reduced activation energy  $\beta_N = E_a/(k_B T_N) = 15$ .

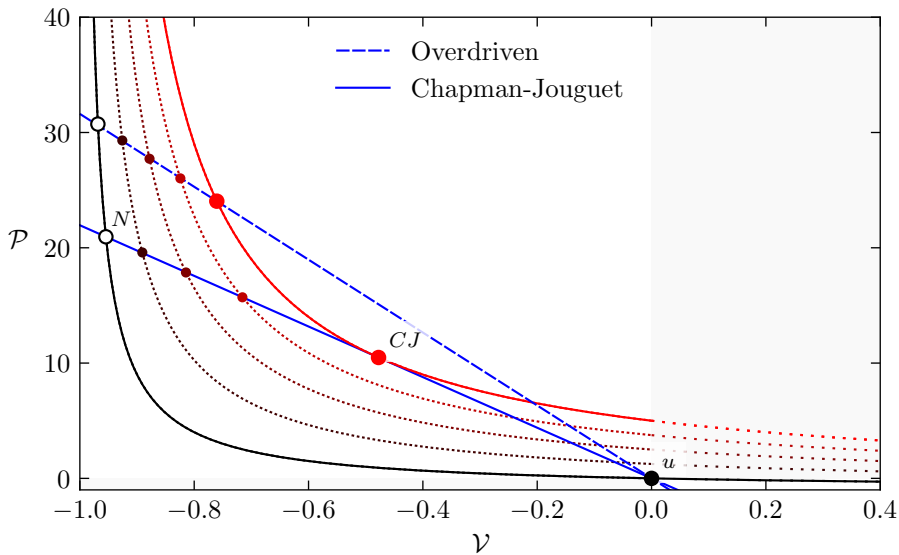


Figure 2.10: Partially reacted Hugoniot curves and Michelson-Rayleigh lines illustrating the fluid particle path throughout the ZND detonation structure.

## 2 One-dimensional compressible flow and premixed combustion waves

and have been represented in Figure 2.10. As it passes through the shock wave, the reactive mixture passes from the initial state, labelled with  $u$ , to the Neumann state, labelled  $N$ . From the Neumann state behind the shock wave, the progress of the reaction results in an expansion which in the  $\mathcal{P} - \mathcal{V}$  plane is represented as a descent down the MR line towards the successive partial Hugoniot curves.

### *Gas flow behind a steady CJ detonation*

The existence of Chapman-Jouguet detonations depends on whether a transient solution for the unsteady expansion of the detonation products can be found to match the steady boundary conditions of the detonation front (Taylor, 1950a). The dynamics of the combustion products behind planar and spherical detonation waves was first independently studied by Zeldovich (1942) and Taylor (1950a).

As in the strong blast wave problem (see Section 2.2.3), the unique spatial scale of the problem given by the radius of the detonation is directly related to time through the propagation velocity of the front. Therefore, the problem of a gas flow behind a CJ wave also lacks of scales and a self-similar solution can be sought.

The dynamics of the gas flow behind a CJ detonation can be studied using the same non-dimensional functions as in the blast wave problem and the self-similar independent variable  $\xi \equiv r/r_f(t)$  that transform the Euler equations (2.14), (2.15) and (2.18) into the system of ordinary equations (2.57) to (2.59). However, in this case, since the detonation front propagates at constant CJ velocity, the entropy generated by the front is constant and therefore the entire gas flow behind the front is homentropic. The last equation (2.59) can then be simply replaced by the isentropic relationship and the constant propagation speed causes the parameter  $\chi$  to vanish. In addition, a new non-dimensional function for the sound speed is introduced  $\beta(\xi)^2 = a^2/\mathcal{D}^2 = \gamma f/\psi$  to replace the function  $\psi$ .

The mathematical problem is composed by the ordinary differential equations

$$\phi' = \frac{j\phi\beta^2}{\xi [(\phi - \xi)^2 - \beta^2]} \quad (2.89)$$

$$\beta' = -\frac{\beta(\gamma - 1) \left( \phi' + \frac{j\phi}{\xi} \right)}{2(\phi - \xi)}, \quad (2.90)$$

the boundary conditions at the front  $\xi = 1$  given by the reactive RH relationships for a strong Chapman-Jouguet detonation

$$M_{u_{\text{CJ}}} \gg 1 : \quad \phi(1) = \frac{u_{\text{bCJ}}}{\mathcal{D}} \approx \frac{1}{\gamma + 1} \quad (2.91)$$

$$\beta(1) = \frac{a_{\text{bCJ}}}{\mathcal{D}} \approx \frac{\gamma}{\gamma + 1} \quad (2.92)$$

and the rear boundary condition  $\phi(0) = 0$  that imposes the velocity to vanish at the origin to conserve the symmetry of the problem.

### 2.3 Premixed combustion waves

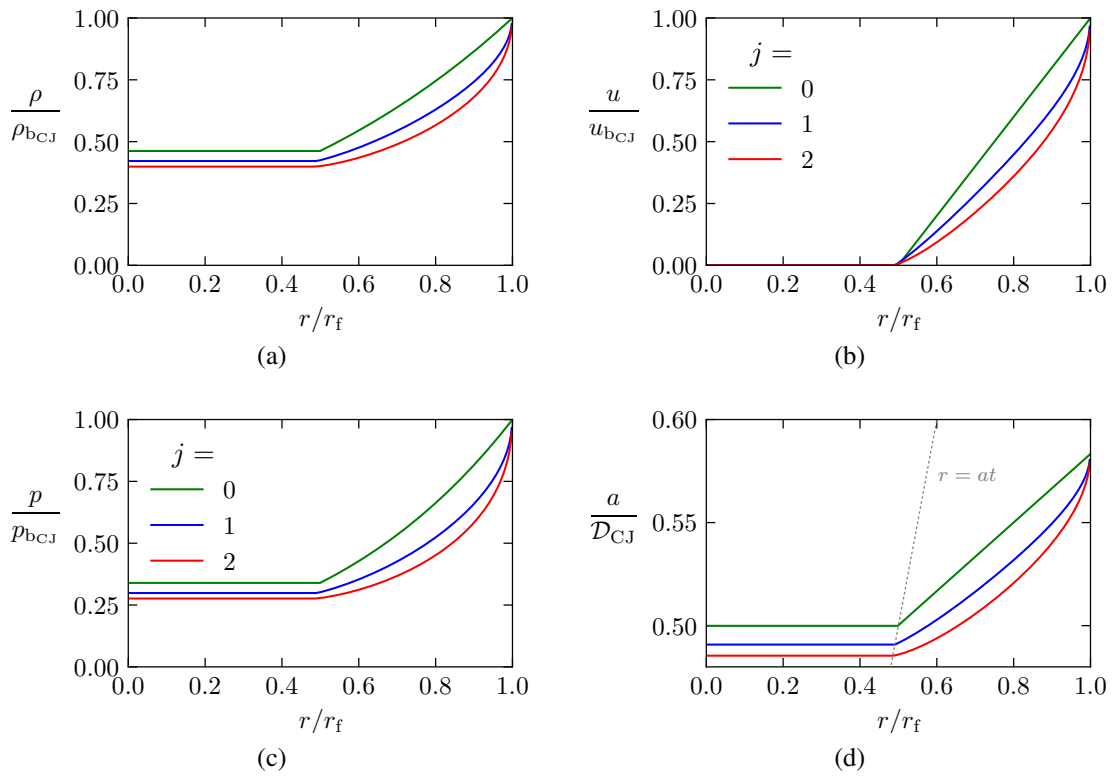


Figure 2.11: (a) Density, (b) velocity, (c) pressure and (d) sound speed fields in planar ( $j = 0$ ), cylindrical ( $j = 1$ ) and spherical ( $j = 2$ ) geometry behind a strong CJ detonation wave for a diatomic gas  $\gamma = 1.4$  in the solution of Zeldovich (1942) and Taylor (1950a).

## 2 One-dimensional compressible flow and premixed combustion waves

For planar detonations, the non-trivial solution is obtained by cancelling the denominator of (2.89), so that a linear profile is obtained that links the conditions behind the front with a growing core of gases at rest ( $\phi = 0$ ) at  $\xi = 1/2$  where  $\beta = 1/2$ . In cylindrical and spherical geometries, the system of equations (2.89) and (2.90) must be integrated numerically from the boundary conditions (2.91) and (2.92). However, using these boundary conditions in the front, the denominator of (2.89) cancels out and the derivative  $\phi'$  diverges due to the curvature effect. Therefore, it is not possible to start the numerical integration strictly from the front. A series expansion near the front  $1 - \xi \ll 1$  must be performed to obtain valid boundary conditions to initialize the numerical integration from a position slightly inside the expansion wave as explained in detail in (Lee, 2016). The solutions obtained for the profiles of the physical variables behind planar, cylindrical and spherical detonations are represented in Figure 2.11.

The rarefaction wave that develops behind a strong Chapman-Jouguet detonation is characterized by a core of stagnant gases growing from the origin. This core of stagnant gases propagates at the velocity of the local sound speed which is roughly half of the leading shock velocity in the strong detonation limit. A linear profile connects the boundary conditions on the front with the state on the core of stagnant gases in planar geometries. In contrast, in cylindrical and spherical geometries, the sonic condition behind the CJ wave results in an infinite gradient. Taylor (1950a) justified this singularity by stating that it resulted from the approximation of the detonation wave as a discontinuity. This approximation would not be valid when the detonation radius is comparable to its thickness. Yet given the large activation energy required to initiate a detonation, with such a small radius the detonation will be highly overdriven. It can also be seen that all the variables are distributed similarly in the rarefaction wave, differing only in the scale and boundary values. This is so since the entropy is uniform throughout the rarefaction wave and, thus, the state of the gas is defined by a single state variable.

To conclude, the propagation mechanism of detonations is the compressive heating produced by the leading shock wave. Since the flow behind a shock wave is always subsonic with respect to it, a shock wave can be damped by the rear conditions. Therefore, the CJ propagation velocity of the shock wave results in the conditions for which after expansion in the induction zone, the flow is sonic with respect to the shock wave, isolating it from disturbances coming from behind. Unlike deflagrations, detonation propagation is a purely gas-dynamic problem. Hence, its propagation velocity can be assessed by a global integration of the reactive front without considering its internal structure. Strong detonations can form when an external support such as a piston pushes the reactive front from behind so that there are no rear disturbances that may dampen the shock wave. Conversely, there is no steady structure that can connect the initial state with the solution for a weak detonation wave. Since the shock wave is the only steady solution for a compression wave, the weak solution requires the heat to be released within the thickness of the shock wave. As in the case of strong deflagrations, this requires that the reaction rate be comparable to the collision frequency. If that were the case, the initial mixture would be in a fully out of equilibrium state and the combustion would proceed without the need for the leading shock wave of the combustion front.

---

## Direct initiation of critical detonations in the small heat release asymptotic limit

---

This chapter presents a study on the critical dynamics of direct initiation of gaseous detonations in the small heat release asymptotic limit, considering unsteadiness, curvature effects, and the evolution of the rear rarefaction wave. The study employs a nonlinear hyperbolic equation, derived from the Euler equations, describing the slow detonation dynamics governing the overall evolution of the detonation. The study identifies the slowdown that occurs as the sonic point approaches the inner detonation structure as the key mechanism controlling the critical dynamics. The quasi-steady approximation is revisited, incorporating the insights gained from the study of the rarefaction wave and compared with the numerical results.

---

3.1	Introduction . . . . .	42
3.2	Detonation model near the self-sustained regime in the small heat release limit . . . . .	49
3.2.1	General equations . . . . .	49
3.2.2	Physical insights from steady planar detonations . . . . .	52
3.2.3	Small heat release asymptotic limit . . . . .	57
3.2.4	Chemical-kinetics model . . . . .	62
3.3	Dynamics of the combustion products behind a detonation . . . . .	67
3.3.1	Self-similar solution behind a CJ wave . . . . .	68



### 3 *Direct initiation of critical detonations in the small heat release asymptotic limit*

3.3.2	Overdriven decaying detonation . . . . .	70
3.3.3	Transitory regime in curved waves . . . . .	73
3.4	Direct initiation of a detonation . . . . .	78
3.4.1	Overdriven regimes . . . . .	78
3.4.2	Numerical integration . . . . .	79
3.4.3	Discussion of the critical dynamics . . . . .	86
3.5	Quasi-steady approximation . . . . .	91
3.5.1	Steady internal structure of self-sustained detonations . . . . .	91
3.5.2	Steady internal structure of overdriven waves . . . . .	94
3.6	Summary . . . . .	98

## 3.1 Introduction

Direct initiation is the process of formation of a detonation in open space without undergoing a predetonation stage of flame acceleration. The conditions required for the onset of the detonation are created directly in the decay of a strong blast wave generated by a powerful concentrated energy source. This process is sometimes referred to as being instantaneous in comparison to the deflagration-to-detonation transition, which requires a previous phase of flame acceleration to reach the necessary conditions for detonation.

As a detonation is essentially a shock wave sustained by the release of chemical energy in its wake, it is reasonable to assume that direct initiation requires the creation of a strong shock of sufficient duration by the ignition device. Following the works of Laffitte, various experimental procedures have been established for the direct initiation of a detonation utilizing different energy sources (see Lee (2008) and references therein). It has been observed that the onset of a detonation is consistent across the various energy sources used. The decay of the initial inert blast wave is dependent on the amount of ignition energy as described by the self-similar solutions of Sedov (1946) and Taylor (1950a). Hence, the direct initiation phenomenon can be accurately described as the instantaneous deposition of a substantial quantity of energy at an ideally concentrated point, line, or plane (Knystautas and Lee, 1976).

#### *Zeldovich criterion*

Nearly a century since the first experimental observation of the direct initiation of spherical detonations by Laffitte (1925), the large amount of energy required to successfully initiate a detonation without a preceding stage of flame acceleration continues to be a subject of intense research in the scientific community (Knystautas and Lee, 1976; Lee, 1977; Lee et al., 1978; Knystautas et al., 1979; Clarke et al., 1986; Carnasciali et al., 1991; He and Clavin, 1994; Zitoun et al., 1995; He, 1996; Lee and Higgins, 1999; Eckett et al., 2000; Radulescu et al., 2000; Ng and Lee, 2003; Kamenskihs et al., 2010; Zhang et al., 2011, 2012; Shen and Parsani, 2017). The critical energy required for the direct initiation process was systematically investigated by Zeldovich et al. (1956).

An initial energy threshold was found below which the detonation wave fails to reach the self-sustained regime. In a first attempt to explain this high energy requirement, Zeldovich et al. suggested that the time taken for the initial blast wave to reach the self-sustained detonation regime should be larger than the reaction time. According to this criterion, the reactive wave should propagate faster than in the self-sustained regime as its front expands beyond a critical radius, which is on the order of the detonation thickness. However, experimental results by Lee et al. (1966) indicated that the Zeldovich criterion significantly underestimated the initiation energy. A critical radius greater than the detonation thickness below which the blast fails to initiate a self-sustained detonation have been consistently identified experimentally (Lee, 1977, 1984).

#### *Detonation-wave model*

Pioneering numerical simulations of direct initiation of detonations by concentrated sources were conducted by Korobeinikov (1971) in the infinitely fast reaction limit. The resulting reactive front, which becomes a discontinuity, was called “detonation-wave model” by Korobeinikov. In this limit, the thickness of the detonation is much smaller than its radius, and the detonation wave can be treated as a supersonic reactive discontinuity that satisfies the reactive jump conditions.

Experimental measurements of the critical radius supported the validity of the discontinuous approximation, as it was found to be much larger than the detonation thickness. However, the discontinuous wave approximation neglects modifications to the internal structure of the detonation through the jump conditions. As a result, there is no critical energy under the discontinuous approximation. Regardless of the initially deposited amount of energy, the overdriven detonation created by the blast wave relaxes systematically to the self-sustained regime.

#### *Critical curvature model (CC)*

A successful theory for direct initiation should provide an analytic expression from which the critical energy can be determined based on fundamental mixture properties. He and Clavin (1994) proposed such a theory considering the modification of the internal structure of a steady self-sustained detonation due to its curvature. The quasi-steady analysis of He and Clavin (1994) for curved self-sustained detonations was performed in the limits of large Mach number and large activation energy using the square-wave model. The square-wave model assumes that the totality of the chemical energy is released instantaneously after an induction time. In the limit of large activation energy, the induction time is governed by an Arrhenius law with a strong thermal sensitivity, resulting in a proportional increase of the detonation thickness which amplifies the impact of the curvature on the reactive wave.

This analysis led to a nonlinear relation between the propagation velocity of a curved self-sustained detonation and the front radius. The corresponding curve propagation velocity versus front radius presents a turning point for a critical front radius interpreted

### 3 *Direct initiation of critical detonations in the small heat release asymptotic limit*

as a quasi-steady curvature-induced quenching. There is no quasi-steady solution for a spherical self-sustained wave with a radius smaller than the critical one, which is larger than the detonation thickness essentially due to the large activation energy.

The critical energy predicted by this theory was in agreement with the experimental results in order of magnitude. However, the quasi-steady analysis is not entirely satisfactory, even though the numerical simulations of He and Clavin (1994) (one-step model) and He (1996) (detailed scheme for the combustion of hydrogen-oxygen mixtures) are in satisfactory agreement with the critical radius, at least concerning its order of magnitude.

Despite the agreement in the order of magnitude of the critical radius, the unsteady effects play a significant role near criticality. For instance, critical regimes of initiation characterized by a quasi-quenching of the detonation with a propagation velocity decreasing well below the self-sustained regime followed by a sudden re-ignition cannot be explained on the basis of a quasi-steady approximation.

#### *Internal structure unsteadiness*

Lee and Higgins (1999) discussed in an exhaustive review on direct initiation of gaseous detonations several successful semi-empirical theories used to estimate the critical energy required for initiation, emphasizing the importance of unsteadiness in the critical regime. According to their analysis, no criterion based solely on curvature effects could capture the essential mechanism of initiation in the critical regime. The SWACER (Shock Wave Amplification by Coherent Energy Release) mechanism, proposed by Lee et al. (1978) in the context of photochemical initiation of gaseous detonations, was given particular attention. This mechanism suggests that the detonation wave re-acceleration, following the quasi-steady period in the critical regime, occurs because the chemical energy release is synchronized with the propagation of a pressure pulse within the supersonic reactive wave. The review also highlighted numerical simulations of the Euler equations by Mazaheri (1997) with a single-step kinetics, which encountered difficulties in obtaining a well-defined value of critical initiation energy. In a single-step chemistry model the mixture always reacts to completion, so that, in the absence of losses, the initiation of a detonation always results in a successful ignition after a sufficiently long time. When a re-acceleration of the front occurred from very slow propagating regimes close to the acoustic regime, a reignition by shock waves was observed. This observation might suggest that the final stages of DDT and direct initiation would be universal if the chemistry allowed for it.

#### *Critical decay rate model (CDR)*

The importance of unsteadiness in the critical regime was further emphasized by Eckert et al. (2000). Numerical simulations of the spherical direct initiation served as a basis for their study (see, for instance, Figure 3.1). The post-processing of the numerical results showed that the unsteady terms of the equation viewed by fluid particles in the

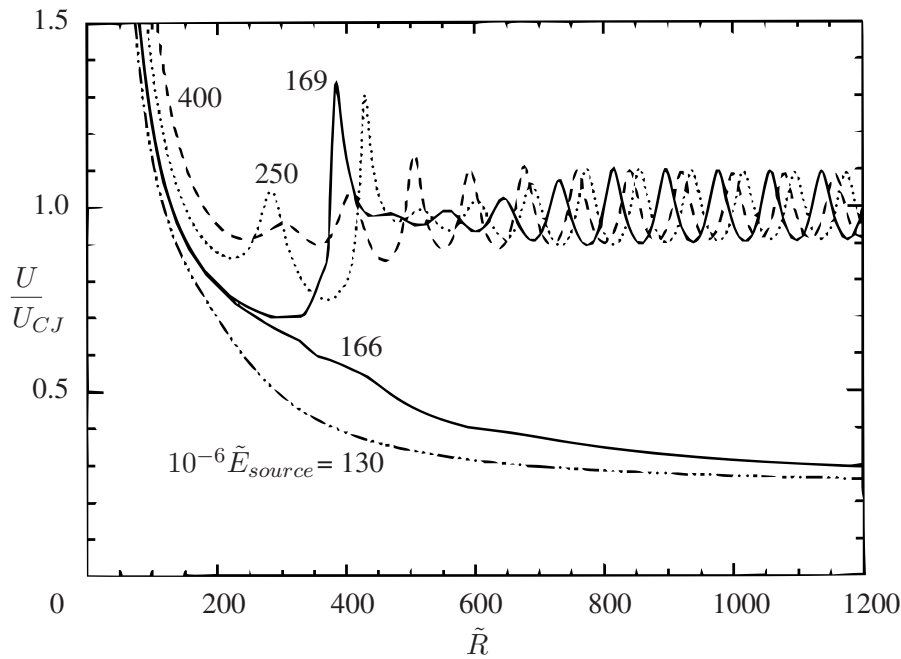


Figure 3.1: Trajectories propagation velocity vs. front radius with different source energies obtained through numerical simulations of the reactive Euler equations for flows with spherical symmetry. Reprinted from Eckett et al. (2000).

subcritical regime were larger than the curvature term. Based on this observation, the authors concluded that unsteadiness in the induction zone resulting from the wave front deceleration was the primary failure mechanism of a detonation. The quasi-steady assumption proposed by He and Clavin (1994) was deemed to be inappropriate for direct initiation and a critical decay rate model was proposed. The critical decay rate model was based on an analysis of the unsteady one-dimensional reaction-zone structure, relying on an appropriate reaction mechanism given by the mixtures and the overdriven detonation wave decay model proposed by Korobeinikov (1971).

A recent study by Weng et al. (2021) compared the predictions from the CC model of He and Clavin (1994) and the CDR model of Eckett et al. (2000). The comparison is made possible applying to both models the wave decay law given by the Sedov (1946) & Taylor (1941) self-similar solution. This study shows that the ratio of the critical initiation energy predicted by the CC and the CDR model is actually much lower than the ratio obtained using different wave decay laws. The critical initiation energy predicted by both models differs from the experimental results by a factor  $10$ — $10^2$ .

The authors of the study also noted that the critical initiation energy predicted by the CC model was consistently larger than the prediction of the CDR model. This tendency is attributed to the fact that the critical conditions of the critical decay rate model can be reached more easily than those of the critical curvature model.

### 3 *Direct initiation of critical detonations in the small heat release asymptotic limit*

#### *Curvature-unsteadiness model*

A general theory of detonation waves considering both curvature and unsteadiness was developed later by Kasimov and Stewart (2005). They derived a dynamical law governing the shock evolution in the asymptotic limit of weakly curved slowly varying detonation waves. The resulting evolution equation exhibited successful detonation initiation and failure, and a steady propagation velocity vs. front radius curve with a turning point, similar to that of He and Clavin (1994). By integrating backwards the evolution equation from a detonation failure solution just below the unstable branch they determined the ignition separatrix curve, which separates solutions with initial conditions that lead to ignition from those that lead to failure. However, this curvature-unsteadiness model still over-predicted the critical initiation energy. The authors noted that this over-prediction of the critical initiation energy seems to be a general feature of critical curvature models that define criticality based on the turning point of the quasi-steady curve. They suggested that the actual onset of unsteady self-sustained detonation at radii much below the quasi-steady critical radius may explain this discrepancy. A similar analysis of the critical curvature conditions for detonation considering the slow dynamics was performed by Vidal (2009) for non-uniform initial temperature and composition distributions.

#### *Near front flow upon onset of the self-sustained regime*

More recently, Liñán et al. (2012) reconsidered the discontinuous detonation model in the context of direct initiation with a finite rate of initial energy release. This study provided new insights into the transition from the strong blast wave solution (Taylor, 1941; Sedov, 1946) to the products dynamics solution behind an intense spherical CJ detonation (Zeldovich, 1942; Taylor, 1950a). At early times, the flow includes a neatly defined core of very hot expanding gas, similar to the flow resulting from a concentrated external heat source in inert mixtures (Kurdyumov et al., 2003). The contact surface delimiting this almost empty region acts as a piston that drives the overdriven detonation. As energy deposition ceases, an expansion wave develops behind the overdriven detonation, which reduces its velocity towards the CJ regime. The curvature of the geometry introduces an additional flow divergence effect that causes the transition to the CJ regime to occur within a finite time. The authors conducted a thorough analysis of the flow structure near the detonation front during the transition to the CJ regime (see Figure 3.2). A Burgers-like equation was included to describe the transonic flow field after the transition for planar waves.

#### *Detonation analog*

A Burgers' equation with a forcing term, which captures many of the behavior of detonations in gaseous reactive mixtures was presented by Kasimov et al. (2013). This model exhibits steady wave solutions, instability of the steady solutions and the onset of chaos. The detonation model is similar to the Fickett's simple analog for detonations (Fickett, 1985), which could not reproduce the observed unstable behavior of detonations

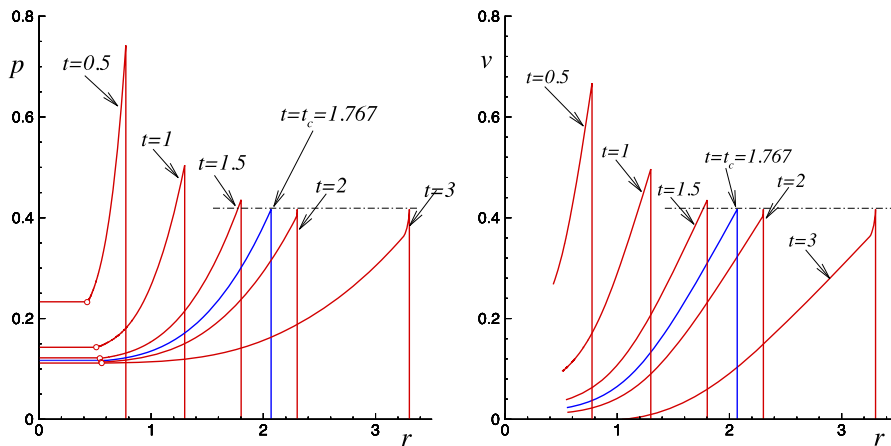


Figure 3.2: Pressure  $p$  and velocity  $v$  profiles at different time instants  $t$  around transition to CJ detonation  $t_c$  in the infinitely fast reaction rate limit. Reprinted from Liñán et al. (2012)

until it was extended by Radulescu and Tang (2011). Further extensions of this model considered generic losses, such as curvature and friction (Faria and Kasimov, 2015), and cellular structures in multidimensional detonations (Faria et al., 2015).

#### *Small heat release asymptotic limit*

A series of works were presented by Clavin and Denet (2018), Clavin (2019), and Clavin and Denet (2020) on the small heat release limit coupled with the Newtonian approximation, providing with a systematic framework for studying the two-time-scales problem of detonation dynamics near the self-sustained regime. The decay of planar overdriven detonations to the self-sustained regime has been described analytically in Clavin and Denet (2018), where the problem was reduced to an integral equation for the velocity of the leading shock. The direct initiation of spherical detonations is studied in Clavin and Denet (2020) in the same asymptotic limit, investigating successful initiation far from the critical radius and neglecting the small gradient of the burnt-gas flow. They demonstrated that, near the self-sustained regime, the outwards-running compressible mode is the main contributor to the inner structure unsteadiness, controlling the delayed response of the detonation structure to the burnt-gas flow. The time-dependent velocity of the leading shock of the curved detonation is obtained equivalently as the solution of an integral equation investigated for stable and weakly unstable detonations.

#### *Critical dynamics of gaseous detonations*

The purpose of the present study is to further explore the impact of unsteadiness combined with the curvature effects. There are two distinct unsteady effects. One is a result of the driving mechanism of the detonation decay, specifically the rarefaction wave in the burnt gas behind the detonation front. The other is the intrinsic dynamics of the inner detonation structure that controls the response to fluctuations in the boundary conditions.

### 3 *Direct initiation of critical detonations in the small heat release asymptotic limit*

The complexity of the complete problem rules out the possibility of obtaining general analytical solutions. Not only the dynamics of the inner structure present a significant challenge but also the rarefaction wave depends on the dynamics of the detonation decay. Furthermore, separating the inner structure from the inert rarefaction wave in spherical geometry is a difficult task.

The characteristic time of evolution of the blast wave, according to the Sedov-Taylor self-similar solution, is of the order of the blast radius divided by the propagation velocity, which is larger than the transit time of a fluid particle through the detonation structure by a factor of the detonation radius to the detonation thickness in the vicinity of criticality. This does not guarantee the accuracy of a quasi-steady approximation, as the response time of the inner structure is also larger than the transit time.

The cumulative effect of feedback loops that control the inner dynamics can be summarized as follows. Disturbances introduced at the leading shock by velocity variations propagate inwards towards the burnt gas with two modes, an inward-running acoustic mode and an entropy wave. The modification of heat release rate that results from this perturbation affects the flow and, in turn, the leading shock velocity after a time delay associated with the outward-running acoustic mode. When approaching the self-sustained detonation regime, the flow near the end of heat release becomes nearly sonic, and the delay of the outward-running mode is larger than those associated with the inward-running modes, including the entropy wave. At the first order of a multiple-time-scale analysis, the leading order terms of the downstream-running modes can be considered instantaneous, and the long time dynamics are primarily controlled by the slow upstream-running mode.

The key unsteady mechanism during direct initiation when approaching the self-sustained detonation regime is the time delay for transferring the rarefaction-wave-induced deceleration to the leading shock. Due to the nearly sonic flow at the exit of the internal detonation structure, the delay increases and diverges at the self-sustained detonation velocity, producing a significant unsteady effect on the dynamics. This topic has not yet been addressed in the context of the direct initiation process, and the present work aims to address this gap through an asymptotic analysis that reduces the problem to a single nonlinear hyperbolic equation.

The current study focuses exclusively on the end of the detonation decay, with a particular emphasis on the critical regime. The dynamics during a supercritical initiation have been analysed in the same framework previously by Clavin and Denet (2020).

#### *Structure of the chapter*

The remaining sections of this chapter, which contains the study of the direct initiation of gaseous detonations in the small heat release limit, are structured as follows: Section 3.2 presents the detonation model utilized in the analysis, derived from the general conservation equations; Section 3.3 examines the rarefaction wave behind a detonation considered as a discontinuity; Section 3.4 investigates the dynamics near criticality, taking into account modifications to the inner structure; Section 3.5 revisits the quasi-steady

### 3.2 Detonation model near the self-sustained regime in the small heat release limit

approximation of the internal structure using the solution obtained for the rarefaction wave behind an overdriven detonation; and finally, conclusions and future perspectives are summarized in Section 3.6.

## 3.2 Detonation model near the self-sustained regime in the small heat release limit

The dynamics of direct initiation of a gaseous detonation are studied utilizing the model of Clavin and Williams (2002) including curvature effects and extending its application to the rarefaction wave that follows the detonation. The model proposed by Clavin and Williams adopts the classical ZND detonation structure that consists of an inert leading shock followed by an inviscid reaction layer. It describes the dynamics of gaseous detonations in mixtures with a heat of reaction that is significantly lower than thermal enthalpy of the unperturbed reactive mixture. This model is applicable in detonations propagating at velocities sufficiently close to the Chapman-Jouguet regime.

In this section, the extended model is derived from the general conservation equations taking into account physical insights obtained from steady planar detonations. Additionally, a simplified chemical-kinetics model suitable for describing the direct initiation of detonations in small heat release mixtures is introduced.

### 3.2.1 General equations

The analysis of the direct initiation of a detonation requires investigating the interaction between a detonation wave propagating through a reactive mixture at rest and a rarefaction wave developed between the supersonic reactive wave and a core of stagnant gases at the locus of energy deposition. The internal structure of the detonation is bounded by an inert shock wave, as in the ZND detonation model, and the exit of the reaction zone where the reactive mixture has been fully consumed. The leading shock wave compresses and heats the reactive mixture to the Neumann state given by the Rankine-Hugoniot jump relations. The compressed flow velocity relative to the shock wave is nearly sonic, resulting in a convective flux that is significantly faster than the transport by diffusion. The flow is then accurately described by the macroscopic laws of conservation, neglecting viscous effects, heat conduction, and molecular diffusion, known as Euler equations including reactive terms that account for the release of chemical heat and the progress of the chemical reactions. This inviscid flow condition persists in the near-front rarefaction wave, which can be analysed by extending the application of the Euler equations into the flow at chemical equilibrium.

#### *Reactive one-dimensional Euler equations*

The dimensional form of the reactive Euler equations in one-dimensional symmetrical geometry (i.e.  $\mathbf{u}' = (u', 0, 0)$ ,  $\nabla \mathbf{u}' = (\partial u'/\partial r', 0, 0)$ ,  $\nabla \cdot \mathbf{u}' = \partial u'/\partial r' + ju'/r'$ ) is



### 3 Direct initiation of critical detonations in the small heat release asymptotic limit

written as

$$\left(\frac{\partial \rho'}{\partial t'} + u' \frac{\partial \rho'}{\partial r'}\right) + \rho' \frac{\partial u'}{\partial r'} = -j \frac{\rho' u'}{r'}, \quad \left(\frac{\partial u'}{\partial t'} + u' \frac{\partial u'}{\partial r'}\right) + \frac{1}{\rho'} \frac{\partial p'}{\partial r'} = 0, \quad (3.1)$$

$$\left(\frac{\partial s'}{\partial t'} + u' \frac{\partial s'}{\partial r'}\right) = \frac{q'_m}{T'} \omega', \quad \left(\frac{\partial Y}{\partial t'} + u' \frac{\partial Y}{\partial r'}\right) = \omega', \quad (3.2)$$

where  $t'$  and  $r'$  are the independent variables of time and space,  $\rho'$ ,  $p'$ ,  $u'$  and  $Y$  are respectively the density, the pressure, the radial velocity in the laboratory reference frame (where gas ahead the detonation is at rest), and the reaction progress variable ( $Y = 0$  in the initial mixture and  $Y = 1$  in the burned gas),  $\gamma \equiv c'_p/c'_v$  is the ratio of specific heat and  $q'_m$  is the chemical heat release per unit mass of the mixture,  $t'_{\text{RN}}$  is the reaction time at the Neumann state of the CJ wave,  $\omega'$  is the heat release rate, and  $j$  corresponds respectively to planar ( $j = 0$ ), cylindrical ( $j = 1$ ) and spherical ( $j = 2$ ) geometries.

The first two equations (3.1) constitute the fluid mechanics problem ensuring the conservation of mass and momentum respectively. Energy conservation is assured by the first equation in (3.2) which is written in terms of the entropy defined by the Gibbs' relation for a polytropic gas as  $T' ds' = de'_T + p' dv'$ . This form of the equation highlights the fact that heat release is the only source of entropy, with viscous dissipation, heat conduction and molecular diffusion being negligible behind the leading the shock wave. The last equation in (3.2) corresponds to a simplified notation for the progress  $Y$  of an arbitrary model for the chemical kinetics of the combustion processes. In compressible flows, the fluid mechanics problem is coupled to the conservation of energy through the equation of state which for ideal gases is

$$p' = (\gamma - 1)c'_v \rho' T', \quad a'^2 = (\gamma - 1)c'_p T', \quad \gamma \equiv \frac{c'_p}{c'_v} = \text{const.} \quad (3.3)$$

The gas flow in a detonation wave is conveniently studied in the moving coordinate system attached to the leading shock wave. The radial position of the leading shock wave  $r'_f(t')$  advances with velocity  $\mathcal{D}' \equiv dr'_f/dt'$  through a reactive mixture initially at rest. In the coordinate system of the leading shock wave

$$x' \equiv r' - r'_f(t'), \quad \frac{\partial}{\partial r'} \rightarrow \frac{\partial}{\partial x'}, \quad \frac{\partial}{\partial t'} \rightarrow \frac{\partial}{\partial t'} - \mathcal{D}' \frac{\partial}{\partial x'}, \quad (3.4)$$

the conservation laws are written as

$$\frac{D\rho'}{Dt'} + \rho' \frac{\partial u'}{\partial x'} = -j \frac{\rho' u'}{x' + r'_f}, \quad \frac{Du'}{Dt'} + \frac{1}{\rho'} \frac{\partial p'}{\partial x'} = 0, \quad (3.5)$$

$$\frac{Ds'}{Dt'} = \frac{q'_m}{T'} \omega', \quad \frac{DY}{Dt'} = \omega', \quad (3.6)$$

### 3.2 Detonation model near the self-sustained regime in the small heat release limit

with the introduction of the differential operator

$$\frac{D}{Dt'} \equiv \frac{\partial}{\partial t'} - (\mathcal{D}' - u') \frac{\partial}{\partial x'}. \quad (3.7)$$

Replacing  $T'$  for  $\rho'$  through the ideal gas law (3.3) and adding the continuity equation (3.5) divided by  $\rho'$ , the entropy equation (3.6) can be written in terms of  $p'$  and  $u'$  as

$$\frac{1}{\gamma p'} \frac{Dp'}{Dt'} + \frac{\partial u'}{\partial x'} = \frac{q'_m}{c'_p T'} \omega' - j \frac{u'}{x' + r'_f}. \quad (3.8)$$

Mass and momentum conservation equations (3.5) can then be replaced by its hyperbolic form for  $u'$  and  $p'$  when the equation for conservation of momentum (3.5) divided by  $a' = \gamma p' / (a' \rho')$  is added to (3.8)

$$\frac{1}{\gamma p'} \frac{D^+ p'}{Dt'} + \frac{1}{a'} \frac{D^+ u'}{Dt'} = \frac{q'_m}{c'_p T'} \omega' - j \frac{u'}{x' + r'_f(t')}. \quad (3.9)$$

and subtracted

$$\frac{1}{\gamma p'} \frac{D^- p'}{Dt'} - \frac{1}{a'} \frac{D^- u'}{Dt'} = \frac{q'_m}{c'_p T'} \omega' - j \frac{u'}{x' + r'_f(t')}. \quad (3.10)$$

where the differential operators

$$\frac{D^+}{Dt'} = \frac{\partial}{\partial t'} + (a' - \mathcal{D}' + u') \frac{\partial}{\partial x'} \quad \text{and} \quad \frac{D^-}{Dt'} = \frac{\partial}{\partial t'} - (a' + \mathcal{D}' - u') \frac{\partial}{\partial x'} \quad (3.11)$$

have been introduced.

When the reaction rate in terms of the thermodynamic variables  $\omega' = \omega'(T', Y)$  is known, the hyperbolic equations of the hydrodynamic problem (3.9) and (3.10) and the two conservation equations of the reactive problem (3.2) together with the ideal gas law (3.3) form a closed set of equations for  $\rho'$ ,  $p'$ ,  $u'$ ,  $T'$  and  $Y$ .

#### *Rankine-Hugoniot boundary conditions*

The Neumann state of the gas behind the leading shock wave is determined by the propagation velocity  $\mathcal{D}'$  of the wave and the initial state of the unperturbed gas stream. Focusing on the initiation conditions, the unperturbed gas ahead of the leading shock is considered homogeneous and chemically frozen, so the boundary conditions at the front are given by the Rankine-Hugoniot jump relations as a function of the leading shock

### 3 Direct initiation of critical detonations in the small heat release asymptotic limit

wave Mach number  $M_u \equiv \mathcal{D}'/a'_u$

$$x' = 0 : \quad \frac{\rho'_u}{\rho'} = \frac{\mathcal{D}' - u'}{\mathcal{D}'} = \frac{(\gamma - 1)M_u^2 + 2}{(\gamma + 1)M_u^2}, \quad (3.12)$$

$$\frac{p'}{p'_u} = \frac{2\gamma M_u^2 - (\gamma - 1)}{\gamma + 1}, \quad (3.13)$$

$$\frac{T'}{T'_u} = \frac{[2\gamma M_u^2 - (\gamma - 1)][(\gamma - 1)M_u^2 + 2]}{(\gamma + 1)^2 M_u^2}, \quad (3.14)$$

where the subscript  $u$  denotes the upstream reactive mixture at rest. Since the gas is assumed to be chemically frozen while flowing through the shock wave, the boundary condition for the progress variable is

$$x' = 0 : \quad Y = Y_u. \quad (3.15)$$

#### 3.2.2 Physical insights from steady planar detonations

The unsteady one-dimensional problem described by the Euler equations in a reactive mixture is still too complex for a general analytical solution. Further simplifications derived from physical insights into planar steady detonations are still required to decipher the fundamental mechanisms involved in the detonation direct initiation. Two properties of steady planar detonations used to simplify the problem are presented and analysed in the following. The first concerns the identification and balance of the heating mechanisms experienced by a fluid particle as it passes through the detonation structure and the second consists of identifying and exploiting the existence of two different time scales that characterise the unsteady dynamics of a detonation wave. The two aforementioned characteristics will be used to simplify the problem at hand. This simplification involve ignoring negligible effects and limiting the scope of the study on specific conditions that highlight the relevant physics underlying the direct initiation phenomenon.

##### *Heating mechanisms in a detonation wave*

Using the definition of entropy for a polytropic gas in the form

$$ds' = c'_p \frac{dT'}{T'} - c'_p \frac{\gamma - 1}{\gamma} \frac{dp'}{p'}, \quad (3.16)$$

the entropy equation (3.6) can be rewritten to describe the relative temperature evolution of a fluid particle

$$\frac{1}{T'} \frac{DT'}{Dt'} = \frac{\gamma - 1}{\gamma} \frac{1}{p'} \frac{Dp'}{Dt'} + \frac{q'_m}{c'_p T'} \omega'. \quad (3.17)$$

The two physical mechanisms responsible for temperature changes in inviscid compressible reactive flows are highlighted in this form of the equation. On the one hand, the temperature of a gas decreases due to adiabatic compressional cooling during expansion. On the other

### 3.2 Detonation model near the self-sustained regime in the small heat release limit

hand, the heat released from combustion increases temperature of the gas. An order of magnitude estimate of the right hand side terms of equation (3.17) yields the approximate contribution of each mechanism to relative temperature variations. During the reaction time, adiabatic compressional effects for unit relative pressure variations are of order  $(\gamma - 1)/\gamma$ , while the release of reaction heat accounts for  $q'_m/(c'_p T'_u)$ .

In ordinary reactive mixtures, the heat capacity ratio  $\gamma$ , which governs the relationship between relative changes in pressure and temperature, varies between 1.3 and 1.4. The profiles of the physical variables in the inner structure of an ordinary steady planar detonation are represented in Figures 3.3 and 3.4 for  $\gamma = 1.3, 1.4$  and the limit  $\gamma \rightarrow 1$ . It can be observed that changes in  $\gamma$ , even in the limit  $\gamma \rightarrow 1$ , do not affect qualitatively the evolution of the physical variables and the largest quantitative difference found in the burnt temperature value is below a 15%. This is justified by the fact that ordinary detonations are characterized by the dominant balance

$$\frac{\gamma - 1}{\gamma} \ll \frac{q'_m}{c'_p T'_u}. \quad (3.18)$$

Specifically, although compressive heating is an essential heating mechanism within the shock wave, leading to a drastic reduction of the induction time, its impact is negligible behind the shock wave compared to the heat released by the chemical reaction.

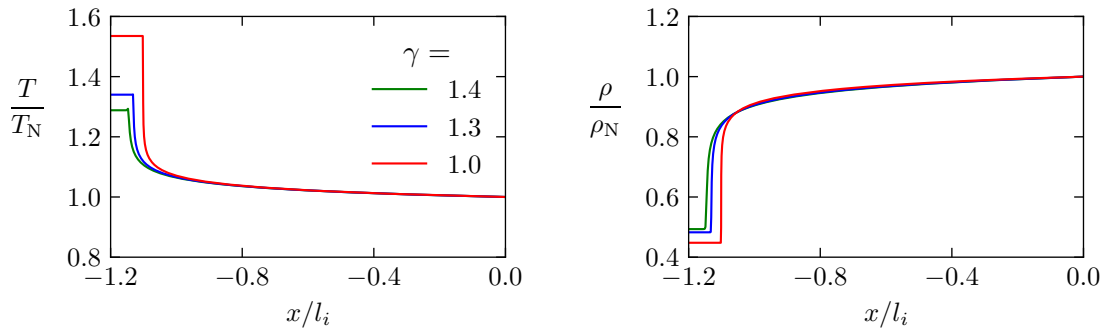


Figure 3.3: Temperature and density profiles at the internal structure of a steady planar detonation for different values of  $\gamma$  with  $q'_m/(c'_p T'_u) = 1$ ,  $\beta_N = 40$ ,  $M_u = 1.01 M_{u_{CJ}}$  (weakly overdriven).

#### *Two time-scale nature of detonation waves*

The method of characteristics, a common approach for solving hyperbolic partial differential equations, can be employed to identify the travelling waves that govern the dynamics of the unsteady flow. The analysis of the characteristic waves provides insights about the timescales involved in the problem. The pair of equations (3.9) and (3.10) establishes a relationship between the propagation of pressure and flow velocity perturbations to the rate of heat release and flow curvature. These equations are the extension of the simple wave equations to reacting gases in divergent geometries.

### 3 Direct initiation of critical detonations in the small heat release asymptotic limit

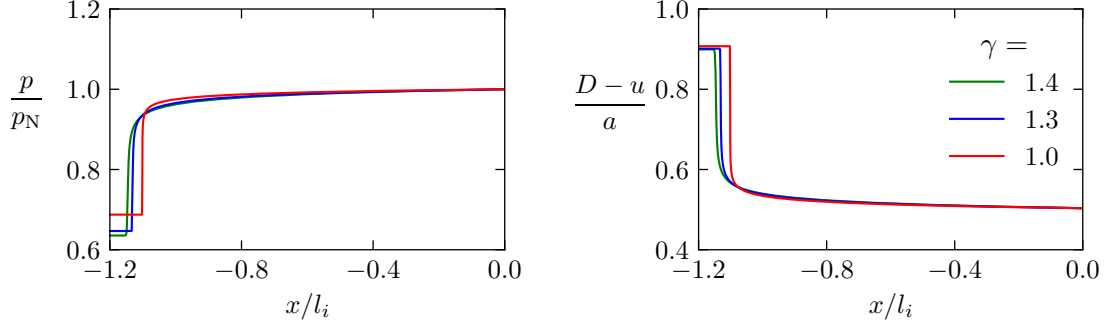


Figure 3.4: Pressure and relative flow velocity profiles at the internal structure of a steady planar detonation for different values of  $\gamma$  with  $q'_m/(c'_p T'_u) = 1$ ,  $\beta_N = 40$ ,  $M_u = 1.01 M_{u_{CJ}}$  (weakly overdriven).

The specific paths satisfying the equation

$$dx' = (a - \mathcal{D}' + u')dt' \quad (3.19)$$

are called outward-running characteristic lines  $C_+$ . Along these lines, the evolution of pressure changes  $dp' = (\partial p'/\partial t')dt' + (\partial p'/\partial x')dx'$  is constrained to

$$dp' = \left[ \frac{\partial p'}{\partial t'} + (a' - \mathcal{D}' + u') \frac{\partial p'}{\partial x'} \right] dt'. \quad (3.20)$$

and, similarly, for the velocity  $du' = (\partial u'/\partial t')dt' + (\partial u'/\partial x')dx'$ ,

$$du' = \left[ \frac{\partial u'}{\partial t'} + (a' - \mathcal{D}' + u') \frac{\partial u'}{\partial x'} \right] dt', \quad (3.21)$$

Substituting (3.20) and (3.21) into (3.9), the compatibility equation

$$\frac{dp'}{\gamma p'} + \frac{du'}{a'} = \left[ \frac{q'_m}{c'_p T'} \omega' - j \frac{u'}{x' + r'_f(t')} \right] dt' \quad (3.22)$$

that holds along the characteristic line  $C_+$  is obtained. Likewise, the inward characteristic lines  $C_-$  can be depicted from (3.10). The trajectory of these characteristic lines is

$$dx' = -(a + \mathcal{D}' - u')dt' \quad (3.23)$$

and the corresponding compatibility equation is

$$\frac{dp'}{\gamma p'} - \frac{du'}{a'} = \left[ \frac{q'_m}{c'_p T'} \omega' - j \frac{u'}{x' + r'_f(t')} \right] dt' \quad (3.24)$$

Integrating (3.22) along the outward characteristic line  $C_+$ , the transported acoustic

### 3.2 Detonation model near the self-sustained regime in the small heat release limit

perturbation evolves on time as

$$\int \frac{dp'}{\gamma p'} + \int \frac{du'}{a'} = \int \left[ \frac{q'_m}{c'_p T'} \omega' - j \frac{u'}{x' + r'_f(t')} \right] dt' \quad (\text{along a } C_+ \text{ characteristic}) \quad (3.25)$$

while evolution of acoustic perturbations along the inward characteristic line  $C_-$  is obtained by integration of (3.24)

$$\int \frac{dp'}{\gamma p'} - \int \frac{du'}{a'} = \int \left[ \frac{q'_m}{c'_p T'} \omega' - j \frac{u'}{x' + r'_f(t')} \right] dt' \quad (\text{along a } C_- \text{ characteristic}). \quad (3.26)$$

Considering only small perturbations, the transported scalars (left-hand side of equations (3.22) and (3.24)) can be written as  $J_+ \equiv \delta p' / (\gamma p') + \delta u' / a'$  and  $J_- \equiv \delta p' / (\gamma p') - \delta u' / a'$ . These scalars correspond in fact to the Riemann invariants for simple waves. However, in this case, the scalars are not conserved due to the flow divergence introduced by the curvature of the geometry and the release of reaction heat.

In this context, fluid particle paths can be interpreted as a third type of characteristic lines  $C_0$  described by

$$dx' = -(\mathcal{D}' - u')dt'. \quad (3.27)$$

Along these lines, the set of compatibility equations obtained from the entropy and reaction progress conservation equations (3.6) describe the evolution of  $ds'$  and  $dY$  as

$$ds' = \frac{q'_m}{c'_p T'} \omega' dt' \quad \text{and} \quad dY = \omega' dt'. \quad (3.28)$$

Integration of these equations along the particle path  $C_0$

$$s'(t') = s'(t'_0) + \int_{t'_0}^{t'} \frac{q'_m}{c'_p T'} \omega' dt' \quad (\text{along the particle path } C_0)$$

$$Y(t') = Y(t'_0) + \int_{t'_0}^{t'} \omega' dt' \quad (\text{along the particle path } C_0)$$

provides the time evolution of the entropy and the reaction progress variable of a fluid particle crossing the reactive flow.

Characteristic line	Propagated small perturbations	Propagating velocity
$C_+$	$J_+ = \delta p' / (\gamma p') + \delta u' / a'$	$V'_+ = a' - \mathcal{D}' + u'$
$C_-$	$J_- = \delta p' / (\gamma p') - \delta u' / a'$	$V'_- = -a' - \mathcal{D}' + u'$
$C_0$	$\delta s'$ and $\delta Y$	$V'_0 = -\mathcal{D}' + u'$

Table 3.1: Characteristic lines behind the leading shock of a detonation

### 3 Direct initiation of critical detonations in the small heat release asymptotic limit

The method of characteristics shows that the unsteady dynamics of the inner structure of the detonation and the rarefaction wave are controlled by three travelling waves summarised in Table 3.1. These waves propagate flow perturbations along the characteristics lines  $C_+$ ,  $C_-$  and  $C_0$  with an associated velocity of  $V'_+$ ,  $V'_-$  and  $V'_0$ , respectively. Figure 3.5 shows the characteristic lines of an illustrative planar detonation that propagates at constant velocity.

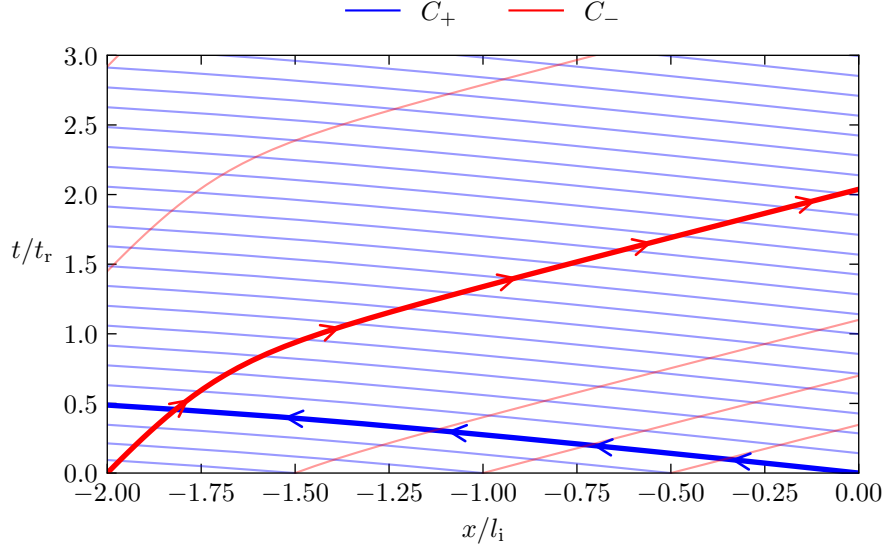


Figure 3.5: Characteristic lines in the internal structure of a steady planar detonation with a one-step Arrhenius law for  $q'_{\text{m}}/(c'_p T'_u) = 5$ ,  $\beta_N = 10$ ,  $M_u = 1.01 M_{u\text{CJ}}$  (weakly overdriven). The characteristic lines issued from the shock wave and the exit of the reaction zone are highlighted with thicker line.

In the shock wave frame of reference, the flow velocity behind a shock wave is always subsonic  $\mathcal{D}' - u'_N < a'_N$ . Near the shock wave, the outward-running characteristic wave  $C_+$  propagates the perturbations from the inner structure towards the front while the inward-running characteristic modes  $C_-$  and  $C_0$  propagate front perturbations through the inner structure. However, since the velocity of the fluid particle  $u'$  decreases from the Neumann velocity  $u'_N > \mathcal{D}' - a'_N > 0$  to zero at the core of stagnant gases, there exists a point in the flow where the outward propagating velocity changes its sign (see Table 3.2). This is a sonic point (or sonic surface in a three-dimensional geometry) where the flow speed with respect to the shock is equal to the local sound speed. Beyond this point the so-called outward propagating waves actually propagate inward. Consequently, the flow between the front and the sonic point is isolated from perturbations coming from beyond the sonic point. Moreover, in the vicinity of the sonic point, the flow is transonic. Given that the outward propagation velocity  $V'_+$  tends to zero at the sonic point, outward perturbations propagate much slower than the inward perturbations. Hence, two different time scales characterise the propagation of perturbations in opposite directions around the sonic point.

The relaxation of an overdriven detonation towards the steady self-sustained regime

### 3.2 Detonation model near the self-sustained regime in the small heat release limit

	Fluid particle velocity	Relative fluid particle velocity	Outward waves velocity
Shock wave	$u'_N > 0$	$\mathcal{D}' - u'_N < a'_N$	$V'_+ > 0$
Subsonic region	$u' \in (u'_s, u'_N)$	$\mathcal{D}' - u' < a$	$V'_+ > 0$
Sonic point	$u'_s = \mathcal{D}' - a'_s$	$\mathcal{D}' - u'_s = a'_s$	$V'_+ = 0$
Supersonic region	$u' \in (0, u'_s)$	$\mathcal{D}' - u' > a$	$V'_+ < 0$
Stagnant gases	$u' = 0$	$\mathcal{D}' > a_0$	$V'_+ < 0$

Table 3.2: Sonic regimes behind the leading shock of a detonation

must be controlled by the largest timescale. Therefore, the two-time scale nature of the detonation allows to simplify the relaxation of the overdriven regime towards the self-sustained regime by considering front perturbations to propagate instantaneously through the detonation structure and focusing the attention on the outward running waves. Unfortunately, the quasi-transonic regime leading to the clear distinction of two time scales does not apply to the entire induction zone of ordinary detonations. In order to extend rigorously the quasi-transonic regime to the entire detonation structure, the analysis must be narrowed down to an appropriate limit of study.

#### 3.2.3 Small heat release asymptotic limit

The two-timescale nature of the detonation dynamics is enlightened in the asymptotic limit of small heat release. The small parameter  $\epsilon$  which introduces a hierarchy of problems corresponding to the different timescales is defined as the square root of the reaction heat to unperturbed gas enthalpy ratio

$$\epsilon \equiv \sqrt{\frac{q'_m}{c'_p T'_u}} \ll 1. \quad (3.29)$$

In order to preserve the ordering of heating mechanisms in the inner structure of a detonation, the small heat release limit needs to be coupled with the Newtonian approximation

$$\gamma - 1 \ll \epsilon \quad (3.30)$$

which establishes that adiabatic compressional effects on temperature are less important than those produced by the release of reaction heat.

In the Newtonian approximation, the effect of the compressive heating on the relative temperature evolution of a fluid particle (3.17) at the reaction timescale  $t'_{rN}$  simplifies to

$$\frac{t'_{rN}}{T'_u} \frac{DT'}{Dt'} = \frac{q'_m}{c'_p T'_u} t'_{rN} \omega' + \mathcal{O}(\epsilon^2) = \mathcal{O}(\epsilon^2). \quad (3.31)$$



### 3 Direct initiation of critical detonations in the small heat release asymptotic limit

Since the pressure dependence is eliminated from the temperature evolution equation, the unsteady effects of the flow only enter into the reactive problem through the temperature jump at the shock wave. Recalling equation (3.6), the reaction progress variable of a fluid particle is also unaffected by the unsteady flow dynamics. Therefore, assuming that the reaction rate depends only on temperature and reaction progress variable  $\omega' = \omega'(T', Y)$ , the reactive problem gets partially decoupled from the unsteady hydrodynamic problem. In other words, the temperature and reaction progress variable distribution are exclusively determined by the temperature jump produced at the leading shock wave.

Furthermore, the relative temperature changes of a fluid particle at the timescale of the reaction rate in the Newtonian approximation (3.31) are of the order of the heat of reaction to upstream gas enthalpy ratio which in the small heat release limit (3.29) becomes a second order term. Equivalently, the changes in the sound speed, which in the ideal gas model is proportional to the square root of the temperature  $a' \propto \sqrt{T'}$  are second order terms. Neglecting second order terms, the technical difficulty introduced by the modification of the sound speed through the detonation wave is avoided and both the temperature and the sound speed become constant

$$T' \approx T'_u \quad \text{and} \quad a' \approx a'_u. \quad (3.32)$$

A Taylor development of the Mach number of a detonation wave in the Chapman-Jouguet regime for small values of heat release shows that the corresponding detonation structure is led by a weak shock wave

$$M_{u\text{CJ}} = \frac{D'_{\text{CJ}}}{a'} = 1 + \epsilon + \mathcal{O}(\epsilon^2). \quad (3.33)$$

Following the same procedure, the fluid particle velocity behind the weak shock wave reads

$$\frac{u'_{\text{NCJ}}}{a'} = 2\epsilon + \mathcal{O}(\epsilon^2). \quad (3.34)$$

Therefore, the characteristics velocities with respect to the sound behind the weak shock wave become

$$\frac{V'_+}{a'} = \epsilon + \mathcal{O}(\epsilon^2), \quad (3.35)$$

$$\frac{V'_-}{a'} = -2 + \epsilon + \mathcal{O}(\epsilon^2) \quad \text{and} \quad (3.36)$$

$$\frac{V'_0}{a'} = -1 + \epsilon + \mathcal{O}(\epsilon^2). \quad (3.37)$$

In a steady detonation, the fluid particle velocity  $u'$  decreases monotonically from its value behind the shock to zero at the core of stagnant gases. Hence, the propagation velocity of the outward acoustic wave with respect to the sound is an order  $\epsilon$  quantity  $V'_+/a' = \mathcal{O}(\epsilon)$ , while both the inward acoustic propagation velocity  $V'_-/a' = \mathcal{O}(1)$  and the fluid particle velocity with respect to the shock  $V'_0/a' = \mathcal{O}(1)$  are order unity quantities. This means

### 3.2 Detonation model near the self-sustained regime in the small heat release limit

that acoustic perturbations propagating towards the front travel through the detonation on a larger timescale than those propagating in the opposite sense. In conclusion, a larger timescale must be considered to study the transport of  $J_+$  along  $C_+$ , during which the transport of  $J_-$ ,  $\delta T'$  and  $\delta Y$  through the characteristics  $C_-$  and  $C_0$  is instantaneous.

An order of magnitude estimate of the curvature term can also be extracted from the conditions behind the shock. Anticipating that the rarefaction wave is smaller than the detonation radius  $\Delta r'/r'_f = \mathcal{O}(\epsilon)$ , the curvature radius along the rarefaction wave can be considered constant and equal to the radius at the front. Then, for a fluid velocity of the order of the sound speed  $u = u'/a' = \mathcal{O}(1)$ , curvature is a first order term  $u/r_f = \mathcal{O}(\epsilon)$  of the approximation. The transit time of the inward acoustic waves  $V_- = V_-'/a' = \mathcal{O}(1)$  through the detonation is  $\Delta r/V_- = \mathcal{O}(\epsilon)$  a first order term. Therefore, the curvature effect on the inward acoustic wave, estimated as the product of the curvature term by the transit time, is actually a second order term  $\epsilon^2$  of the approximation.

Given that the two terms on the right hand side of (3.10) are second order terms  $\epsilon^2$  of the small heat release approximation, their effect is negligible and  $J_-$  is conserved to first order

$$\frac{1}{\gamma p'} \frac{D^- p'}{Dt'} - \frac{1}{a'} \frac{D^- u'}{Dt'} = \mathcal{O}(\epsilon^2). \quad (3.38)$$

Hence, the relation  $\delta p'/(\gamma p') = u'/a'$  holds throughout the entire domain. The long time flow dynamics is thus controlled by the slow characteristic wave  $C_+$  whose governing equation (3.9) simplifies using (3.38) to

$$\frac{1}{a'} \left[ \frac{\partial u'}{\partial t'} + (a' - \mathcal{D}' + u') \frac{\partial u'}{\partial x'} \right] = \frac{1}{2} \frac{q'_m}{c'_p T'} \omega' - \frac{j}{2} \frac{u'}{x' + r'_f(t')}. \quad (3.39)$$

This first order quasilinear hyperbolic equation modified by a reaction and a curvature term constitutes the basis of the study of the direct initiation phenomenon near criticality. A straightforward mathematical development that reduces the Euler equations to a simple equation of this type is presented in the following subsection.

Lastly, it may be questionable whether it is still correct to consider the leading shock wave as a discontinuity compared to the reaction layer in the weak shock limit. The thickness of a shock  $a'_u t'_{\text{coll}}/(M_u - 1)$  increases as the Mach number gets close to unity. However, it will remain thinner than the reaction layer as long as the ratio between the reaction time and the collision time is sufficiently large  $(M_u - 1)t'_{\text{RN}}/t'_{\text{coll}} \gg 1$ . That is, the leading shock can be considered as a discontinuity as long as the small heat release limit remains bounded by the limit of large activation energy limit  $t'_{\text{RN}}/t'_{\text{coll}} \gg 1$ .

#### *Nondimensional quantities and the slow timescale*

The formal application of the asymptotic analysis requires to nondimensionalize the coordinates of time and space based on the characteristic scales of the problem. A natural time scale of the detonation dynamics is given by time required for a complete combustion at the Neumann temperature of a CJ detonation, denoted as  $t'_{\text{RN}} = 1/\omega' (T'_{\text{NCJ}})$ . As the

### 3 Direct initiation of critical detonations in the small heat release asymptotic limit

velocity of a fluid particle relative to the leading shock is of the same order as the sound speed, an appropriate length scale for the detonation thickness can be determined by taking into account the distance covered by a fluid particle during the aforementioned time scale, which is expressed as  $l' = a'_u t'_{rN}$ . Thus, the nondimensional spatial and time coordinates can be defined as follows

$$\tau_r \equiv \frac{t'}{t'_{rN}} \quad \text{and} \quad \xi \equiv \frac{x'}{a'_u t'_{rN}}. \quad (3.40)$$

In the small heat release limit, where the parameter  $\epsilon$  is much smaller than unity, it is expected that the deviation of the physical variables from the Neumann state of a CJ wave will be of order  $\epsilon$ . Hence, the dimensionless variables can be expressed as follows

$$\frac{\mathcal{D}'_{CJ} - u'}{a'_u} = 1 - \mu \epsilon, \quad \frac{\mathcal{D}' - \mathcal{D}'_{CJ}}{a'_u} = \dot{\alpha}_\tau \epsilon, \quad \text{and} \quad \ln \frac{p'}{p'_u} = \gamma \pi \epsilon, \quad (3.41)$$

where  $\mu$ ,  $\dot{\alpha}_\tau$  and  $\pi$  are the dimensionless quantities of order unity for flow velocity, propagation velocity of the leading shock and pressure, respectively. However, temperature changes in the small heat release coupled with the Newtonian approximation are second order terms, according to equation (3.31). As a result, the dimensionless temperature writes

$$\frac{T'}{T'_u} = 1 + \theta \epsilon^2. \quad (3.42)$$

where  $\theta$  is the dimensionless quantity of order unity that accounts for temperature modifications. Thus, it is important to note that the sound speed, which for ideal gases is proportional to the square root of temperature, remains constant up to the second order of the approximation.

$$\frac{a'}{a'_u} = \sqrt{1 + \theta \epsilon^2} = 1 + \frac{\theta}{2} \epsilon^2 + \mathcal{O}(\epsilon^3). \quad (3.43)$$

Within the new set of coordinates and dependent variables, the differential operators (3.7) and (3.11) become after multiplication by  $t'_{rN}$

$$t'_{rN} \frac{D}{Dt'} = \frac{\partial}{\partial \tau_r} - [1 - (\mu - \dot{\alpha}_\tau) \epsilon] \frac{\partial}{\partial \xi}, \quad (3.44)$$

$$t'_{rN} \frac{D^+}{Dt'} = \frac{\partial}{\partial \tau_r} + (\mu - \dot{\alpha}_\tau) \epsilon \frac{\partial}{\partial \xi} \quad \text{and} \quad (3.45)$$

$$t'_{rN} \frac{D^-}{Dt'} = \frac{\partial}{\partial \tau_r} - [2 + (\mu + \dot{\alpha}_\tau) \epsilon] \frac{\partial}{\partial \xi}. \quad (3.46)$$

The current problem exhibits the presence of two distinct time scales. The propagation velocities governing the operators (3.44) and (3.46) are of order unity, while inward-running perturbations (3.45) propagate at a velocity of order  $\epsilon$ . As the slow scale

### 3.2 Detonation model near the self-sustained regime in the small heat release limit

$t'_{\text{rN}}/\epsilon$  ultimately determines the overall dynamics of the detonation, the appropriate time coordinate is defined as

$$\tau \equiv \frac{t'}{t'_{\text{rN}}/\epsilon} = \tau_r \epsilon. \quad (3.47)$$

#### *Flow curvature in critical detonations*

Previous experimental and numerical studies have consistently demonstrated that the critical front radius is much larger than the detonation thickness (Lee, 1977). Accordingly, the scope of this study is limited to weakly curved detonations, where the detonation thickness is smaller than the front radius by a factor of  $\epsilon$ . The dimensionless front radius of order unity is expressed as

$$\tilde{r}_f \equiv \frac{r'_f}{a'_u t'_{\text{rN}}} \epsilon. \quad (3.48)$$

Within these scales, the radius of curvature along the detonation thickness remains constant, with corrections of order  $\epsilon$

$$\frac{r'}{a'_u t'_{\text{rN}}/\epsilon} = \frac{x' + r'_f}{a'_u t'_{\text{rN}}/\epsilon} = \tilde{r}_f + \xi \epsilon. \quad (3.49)$$

The temporal evolution of the front radius is governed by the front velocity, as expressed by  $dr'_f/dt' = \mathcal{D}'$ . Integration of the front velocity from the initial front radius  $\tilde{r}_{\text{fi}}$  at  $\tau = 0$  in the reduced variables shows that for  $\tau = \mathcal{O}(1/\epsilon)$  the front radius grows linearly with time

$$\tilde{r}_f(\tau) = \tilde{r}_{\text{fi}} + \int_0^\tau M_u d\tau' = \tilde{r}_{\text{fi}} + \int_0^\tau [1 + (1 + \dot{\alpha}_\tau)\epsilon] d\tau' = \tilde{r}_{\text{fi}} + \tau + \mathcal{O}(\epsilon\tau). \quad (3.50)$$

#### *Hyperbolic equation*

In the reduced variables, the leading order problem that arises from the set of conservation equations (3.6), (3.9) and (3.10) is written as follows

$$\left[ \frac{\partial}{\partial \tau} + (\mu - \dot{\alpha}_\tau) \frac{\partial}{\partial \xi} \right] (\pi + \mu) = \omega - j \frac{1 + \mu}{\tilde{r}_f} \quad (3.51)$$

$$\frac{\partial}{\partial \xi} (\pi - \mu) = 0 \quad (3.52)$$

$$\frac{\partial \theta}{\partial \xi} = \frac{\partial Y}{\partial \xi} = -\omega \quad (3.53)$$

with the boundary conditions given by equations (3.12) to (3.15) as

$$\xi = 0 : \quad \mu = 1 + 2\dot{\alpha}_\tau, \quad \pi = 2 + 2\dot{\alpha}_\tau, \quad \theta = 0, \quad Y = 0. \quad (3.54)$$

### 3 Direct initiation of critical detonations in the small heat release asymptotic limit

The reactive problem is reduced to the differential equation (3.53) where  $\omega \equiv \omega' t_{\text{RN}}'$  denotes a dimensionless reaction rate of order unity. The temperature profile  $\theta(\xi)$  and progress variable profile  $Y(\xi)$  at a given time  $\tau$  can be obtained by integrating a specific chemical-kinetics model from the boundary conditions at the shock (3.54) if the chemical-kinetics rate depends only on the temperature and the progress variable  $\omega = \omega(\theta, Y)$ . Solving this reactive problem results in the determination of the reaction rate distribution, represented by  $\omega = \omega(\xi, \tau)$ , which is required to solve the flow dynamics problem. The flow dynamics problem is simplified to a pair of equations given in (3.51) and (3.52). Equation (3.52) describes the propagation of front perturbations towards the reactive zone, and can be integrated from the boundary condition at the front (3.54). This integration results in the relation  $\pi - \mu = 1$  which holds throughout the detonation thickness. Subsequently, the slow dynamics of the detonation are governed by equation (3.51), which takes the form

$$\frac{\partial \mu}{\partial \tau} + (\mu - \dot{\alpha}_\tau) \frac{\partial \mu}{\partial \xi} = \frac{\omega}{2} - \frac{j}{2} \frac{1 + \mu}{\tilde{r}_f} \quad (3.55)$$

$$\xi = 0 : \quad \mu = 1 + 2\dot{\alpha}_\tau. \quad (3.56)$$

This partial differential equation constitutes the basis for the study of the critical dynamics of direct initiation of detonations in the small heat release limit. It should be noted that this equation describing the first order of the formal application of the asymptotic limit is in fact analogous to the equation obtained in the previous subsection for the dynamics of the slow characteristic wave (3.39).

#### 3.2.4 Chemical-kinetics model

The internal structure of a detonation involves intricate chemical transformations that occur during global combustion reactions. A three-step chemical-kinetics model retains the fundamental aspects of these transformations that are relevant to detonation waves and provides a more accurate representation of the chemical processes involved in real detonation structures compared the conventional one-step model. This model simplifies the complex chemical interactions among the various elements involved in the combustion process to three fundamental reactions: chain initiation, chain branching, and chain breaking.

The chain initiation reaction models the slow decomposition of reactants into free radicals. These reactions play a fundamental role in gaseous detonations, while in the propagation of flames, on the other hand, they are less relevant. In the absence of diffusion mechanisms, the initiation reactions are the only source of highly reactive radicals and hence regulate the induction time that characterizes the detonation structure. However in propagating flames, the rate of radical production by chain initiation mechanisms is negligible compared to the diffusive flux of radicals from more reactive regions.

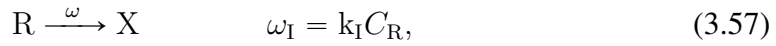
As the concentration of reactive radicals increases, the chain branching reactions trigger further radical production, thereby adding a chemical runaway to the thermal

### 3.2 Detonation model near the self-sustained regime in the small heat release limit

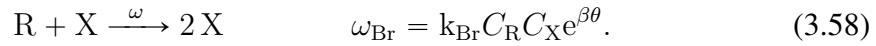
runaway that characterizes combustion reactions. Finally, the reactive radicals undergo transformation into stable products via chain breaking reactions releasing heat.

#### *Three-step simplified kinetic scheme*

The simplified three-step kinetic scheme proposed by Clavin and Denet (2018) is adopted in the current study. This model further simplifies the three-step model by limiting its application to the flow behind a shock wave while retaining the essential features of the detonation structure. Letting R stand for the initial reactants and X for the intermediate radicals, the chain initiation reactions are represented as



where the small constant  $k_I$  provides the ratio of the global reaction time to the chain initiation reaction time. The temperature dependence has been removed for simplicity, limiting the validity of the model to sufficiently strong shock waves so that, at the Neumann temperature, the induction time is finite. The chain-branching elementary reactions are modelled as autocatalytic reactions that are highly dependent on the temperature through a large activation energy  $\beta$  and an Arrhenius pre-exponential factor  $k_{Br}$



Finally, the chain-breaking reactions are represented as fast exothermal reactions transforming the radicals into stable products P at a rate with respect to the global reaction rate given by the constant  $k_R$  with a zero activation energy



#### *Steady-state heat release rate distribution in a CJ wave*

The overall reaction rate used in the construction of the detonation model refers to the rate of heat release. Therefore, the steady-state overall reaction rate corresponds to the rate of exothermic chain-breaking reactions of the three step model  $\omega_{CJ}(\xi) = \omega_R(\xi)$ . The steady-state distribution of heat release rate is thus the solution of the initial value problem

$$\frac{dC_R}{d\xi} = \omega_I + \omega_{Br} = k_I C_R + k_{Br} C_R C_X e^{\beta\theta} \quad (3.60)$$

$$\frac{dC_X}{d\xi} = -\omega_I - \omega_{Br} + \omega_R = -k_I C_R - k_{Br} C_R C_X e^{\beta\theta} + k_R C_X \quad (3.61)$$

$$\frac{d\theta}{d\xi} = \frac{dC_P}{d\xi} = -\omega_R = -k_R C_X \quad (3.62)$$

$$\xi = 0 : \quad C_R = 1 \quad C_X = 0 \quad C_P = 0 \quad \theta = 0. \quad (3.63)$$

### 3 Direct initiation of critical detonations in the small heat release asymptotic limit

This model, which takes into account only irreversible reactions, guarantees that chemical reactions always reach an equilibrium state thus satisfying the boundary condition

$$\xi = \xi_b : \quad C_R = 0 \quad C_X = 0 \quad C_P = 1 \quad \theta = 1. \quad (3.64)$$

where  $\xi_b$  denotes the end of the reaction zone, i.e. the spatial coordinate at which equilibrium is reached. Integration of the system of equations (3.60) to (3.62) from the initial condition (3.63) using the chemical-kinetics parameters summarised in Table 3.3 yields the reaction rates distribution shown in Figure 3.6. The typical structure of a real detonation is recognized: a large induction layer with negligible release of heat from  $\xi = 0$  to  $\xi \approx 0.4$ , a highly reactive layer due to the rapid radical production by chain-branching reactions, and a relaxation tail where all radicals are finally consumed. Furthermore, the example shown in Figure 3.6 satisfies the scaling considerations for the time and spatial reduced coordinates

$$\xi \leq \xi_{b_{CJ}} = -1 : \quad \omega_{CJ}(\xi) = 0 \quad \text{and} \quad \int_{\xi_b}^0 \omega_{CJ}(\xi) d\xi = 1. \quad (3.65)$$

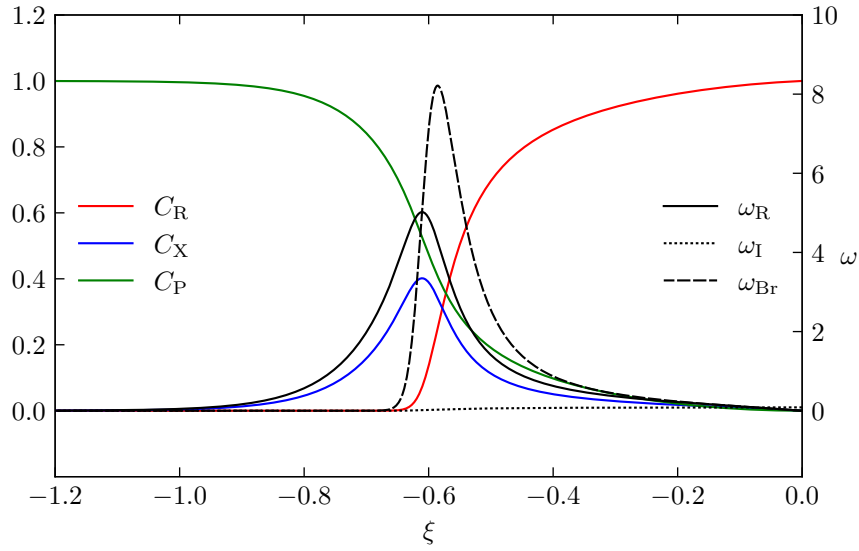


Figure 3.6: Detonation structure of a CJ wave using the three-step chemical-kinetics model of Clavin and Denet (2018): reaction rates in black lines and species concentration in coloured lines.

#### *Heat release rate distribution in unsteady waves*

For unsteady detonation waves with propagation velocities close enough to the CJ velocity  $\dot{\alpha}_\tau = \mathcal{O}(1)$ , the instantaneous distribution of the heat release rate  $\omega(\xi, \tau)$  is governed by the induction length as it was shown by Clavin and He (1996) through numerical computations based on a detailed chemical-kinetics scheme for  $H_2-O_2$

### 3.2 Detonation model near the self-sustained regime in the small heat release limit

	Reaction	k	$\beta$
Chain initiation	$R \longrightarrow X$	$8.5 \cdot 10^{-3}$	0
Chain branching	$R + X \longrightarrow 2X$	12.5	5
Chain breaking	$X \longrightarrow P$	12.5	0

Table 3.3: Simplified three step kinetic scheme of Clavin and Denet (2018)

mixtures. Therefore, the instantaneous distribution of reaction rate is nicely approximated by scaling the steady-state heat release distribution according to the instantaneous induction length  $l_i(\tau)$

$$\omega(\xi, \tau) = \frac{l_{iCJ}}{l_i(\tau)} \omega_{CJ} \left( \frac{l_{iCJ}}{l_i(\tau)} \xi \right). \quad (3.66)$$

For simplicity, the induction length is considered to scale just according to the strong dependence on the Neumann temperature

$$\frac{l_{iCJ}}{l_i(T_N)} = \exp \left[ \frac{E_a}{k_B T_{N,CJ}} \left( 1 - \frac{T_{N,CJ}}{T_N} \right) \right] \quad (3.67)$$

where  $E_a$  is the activation energy of the Arrhenius law controlling the variation of the induction length with the Neumann temperature. Since combustion reactions are characterised by a large activation energy is a large parameter, small temperature variations in the Neumann state must be considered when multiplied by the activation energy even though they are higher order terms neglected in the rest of the analysis. The Neumann temperature dependence on the propagation velocity  $\dot{\alpha}_\tau$  is described by the Rankine-Hugoniot jump condition, which in the small heat release limit coupled to the Newtonian approximation writes as

$$\frac{T_N}{T_u} = 1 + 2(\gamma - 1)(1 + \dot{\alpha}_\tau)\epsilon + \mathcal{O}(\epsilon^2). \quad (3.68)$$

Retaining just the leading order terms, the induction length ratio dependence on the deviation from the CJ propagation velocity  $\dot{\alpha}_\tau$  becomes

$$\frac{l_{iCJ}}{l_i(\dot{\alpha}_\tau)} = e^{b\dot{\alpha}_\tau}, \quad (3.69)$$

where a reduced thermal sensitivity of order unity  $b \equiv 2(\gamma - 1)\epsilon E_a / (k_B T_u) = \mathcal{O}(1)$  has been introduced.

The instantaneous distribution of heat release considering the rescaling with the induction length distance is then described by the equation

$$\omega(\xi, \dot{\alpha}_\tau) = e^{b\dot{\alpha}_\tau} \omega_{CJ} \left( e^{b\dot{\alpha}_\tau} \xi \right). \quad (3.70)$$



### 3 Direct initiation of critical detonations in the small heat release asymptotic limit

Examples of the heat release distributions according to this law are shown in Figure 3.7 for several values of the product  $b\dot{\alpha}_\tau$ .

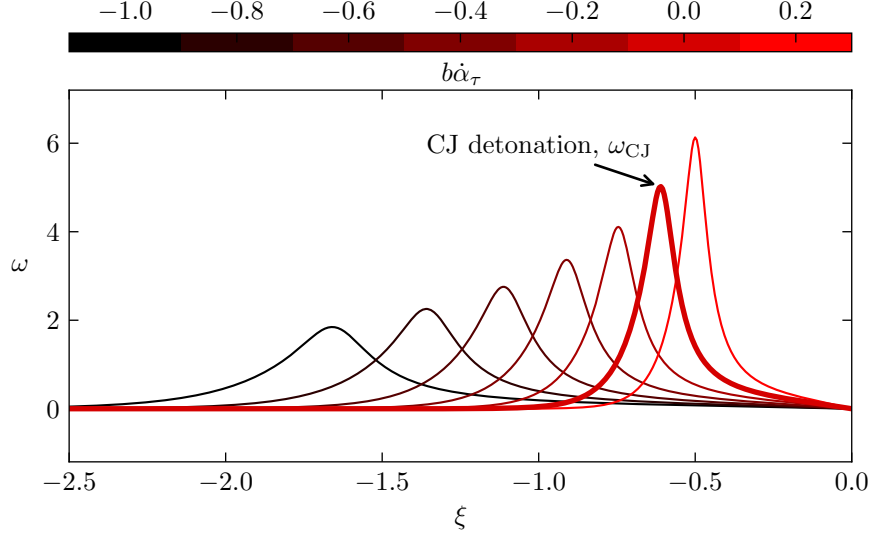


Figure 3.7: Distributions of heat release rate provided by equation (3.70) for a steady heat release rate  $\omega_{\text{CJ}}$  (thick line) obtained by the simplified three-step chemical-kinetics model of Clavin and Denet (2018) for several values of propagation velocity  $\dot{\alpha}_\tau$ .

According to this scaling law (3.70), the end of the reaction zone of the unsteady waves lies on  $\xi_b(\tau) = -e^{-b\dot{\alpha}_\tau}$ , describing a substantial increase of the reaction wave thickness (see Figure 3.7) when the velocity decreases below the CJ velocity  $\dot{\alpha}_\tau < 0$ . However, the variation of  $\dot{\alpha}_\tau$  is intrinsically bounded from below  $\dot{\alpha}_\tau \geq -1$ , since the model is limited to supersonic waves  $D/a > 1$ . Therefore, for reduced temperature sensitivities close to unity, the induction length in the acoustic limit continues to be of the same order of magnitude as in the CJ wave. While on the contrary, ordinary mixtures are known to exhibit a cross-over temperature for which recombination reactions become faster than chain-branching reactions so that the rate of heat release vanishes before reaching the acoustic regime. In fact, this explains why actual detonations are typically observed only for gaseous mixtures with a large enough chemical heat release. The chemical-kinetics quenching can be introduced by multiplying the scaling law by a Heaviside function such that the reaction rate freeze when the front propagation velocity decreases below a crossover value  $\dot{\alpha}_{\tau_c}$

$$\omega(\xi, \dot{\alpha}_\tau) = H(\dot{\alpha}_\tau - \dot{\alpha}_{\tau_c}) e^{b\dot{\alpha}_\tau} \omega_{\text{CJ}}(e^{b\dot{\alpha}_\tau} \xi). \quad (3.71)$$

For hydrogen-oxygen mixtures, the typical Neumann temperature of a CJ wave is around  $T_{\text{N}_{\text{CJ}}} \approx 2000$  K, while the strong increase of induction time is observed at temperatures of  $T_c \approx 1000$  K (Sánchez and Williams, 2014), which is approximately half of the Neumann temperature in the CJ regime. It is reasonable then to establish a value of  $\dot{\alpha}_{\tau_c} = 1/2$  for the propagation velocity at which the crossover temperature is reached.

Nonetheless, the sensitivity of the results to this parameter will be evaluated.

### 3.3 Dynamics of the combustion products behind a detonation

In the study of the flow of combustion products behind a detonation, the detonation can be considered as a discontinuity when the length scale of the flow is significantly larger than the thickness of the detonation. This is true when the detonation radius is greater than the detonation thickness, as it is expected to occur for the critical conditions of initiation. However, the discontinuous model neglects small modifications in the inner structure of the detonation, which are key in the critical dynamics of gaseous detonations. In contrast, the analysis of the unsteady flow of combustion products behind a discontinuity will prove to be a useful preliminary step. This analysis provides with the external solution for the dynamics of the internal structure of the detonation, thereby yielding valuable insight into the study of the detonation initiation.

The derivation of the simplified detonation model, represented by equations (3.55) and (3.56), is based on approximations that remain accurate in the flow of combustion products behind the detonation. However, the characteristic length of the flow of burnt gases is much larger than the detonation thickness. The relevant spatial scale in the dynamics of the combustion products is determined by the length of the rarefaction wave, while the reference time scale continues to be the time taken for an outward wave to traverse the length of the rarefaction wave.

The length of the rarefaction wave, denoted as  $|\xi_0|$ , it is determined by the distance between the leading edge of the core of stagnant gases  $r_0$  and the front  $r_f$ . The front radius evolves as  $dr_f/dt = D$ , while the leading edge of the core of stagnant gases moves at the local sound speed  $dr_0/dt = a$ . The time evolution of the rarefaction wave thickness on the slow timescale of the detonation is given by

$$\frac{d\xi_0}{d\tau} = -(1 + \dot{\alpha}_\tau) + \mathcal{O}(\epsilon) \quad (3.72)$$

As the front radius evolves at the reaction timescale, the initial size of the rarefaction wave is considered to be an order  $\epsilon$  smaller than the initial front radius  $|\xi_{0i}| = r_{fi}\epsilon/(a_u t_r)$ , and this length scale is used to study the combustion products behind a detonation as a discontinuity. The characteristic timescale of the problem is still the time required for an outward propagating wave to cover the spatial domain, so it must also be scaled accordingly. The following transformation is then applied to the independent coordinates

$$\tilde{\xi} \equiv \frac{\xi}{|\xi_{0i}|} = \frac{r - r_f(t)}{r_{fi} - r_{0i}} \quad \text{and} \quad \tilde{\tau} \equiv \frac{\tau}{|\xi_{0i}|} = \frac{t}{(r_{fi} - r_{0i})/(a_u \epsilon)}. \quad (3.73)$$

The dynamics of combustion products are governed by a simplified version of the equations (3.55) and (3.56) in which the reactive term has been removed since it is

### 3 Direct initiation of critical detonations in the small heat release asymptotic limit

assumed that the detonation products are in chemical equilibrium

$$\frac{\partial \mu^{\text{ext}}}{\partial \tilde{\tau}} + (\mu^{\text{ext}} - \dot{\alpha}_\tau) \frac{\partial \mu^{\text{ext}}}{\partial \tilde{\xi}} = -\frac{j}{2} \frac{1 + \mu^{\text{ext}}}{1 + \tilde{\tau}}. \quad (3.74)$$

The boundary condition at the front corresponds to the burnt state behind the detonation wave, which is determined by the reactive RH jump conditions

$$\tilde{\xi} = 0 : \quad \mu^{\text{ext}} = \sqrt{2\dot{\alpha}_\tau}. \quad (3.75)$$

Another boundary condition can be defined at the core of stagnant gases, where the flow velocity must decrease to zero

$$\tilde{\xi} = \tilde{\xi}_0(\tilde{\tau}) : \quad \mu^{\text{ext}} = -1. \quad (3.76)$$

#### 3.3.1 Self-similar solution behind a CJ wave

A CJ detonation propagates with constant velocity (i.e.  $\dot{\alpha}_\tau = 0$ ), resulting in a linear growth of the length of the rarefaction wave with time. A problem like this is said to lack a characteristic length scale and therefore admit a solution of self-similarity. This observation was made by Zeldovich (1942) and Taylor (1950b) in their investigation of the dynamics of combustion products in the limit of large Mach number (see Section 2.3.2). The same condition applies to the opposite limit of small heat release. The ratio of the spatial coordinate  $\xi$  to the rarefaction wave length, which for a CJ wave is given by  $|\tilde{\xi}_0(\tilde{\tau})| = 1 + \tilde{\tau}$ , provides the self-similar variable of the problem

$$z \equiv \frac{\tilde{\xi}}{1 + \tilde{\tau}} = \frac{\xi}{|\xi_0(\tau)|}, \quad \frac{\partial}{\partial \tilde{\xi}} \rightarrow \frac{1}{1 + \tilde{\tau}} \frac{d}{dz}, \quad \frac{\partial}{\partial \tilde{\tau}} \rightarrow -\frac{z}{1 + \tilde{\tau}} \frac{d}{dz}. \quad (3.77)$$

The flow of combustion products behind a steady CJ detonation has a self-similar solution  $V = V(z) = 1 + \mu^{\text{ext}}(\xi, \tau)$  which can be written in terms of the self-similar variable. The introduction of the self-similar variable transforms the partial differential equation (3.74) into an ordinary differential equation

$$(V - 1 - z) \frac{dV}{dz} = -\frac{j}{2} V. \quad (3.78)$$

with boundary conditions

$$z = 0 : \quad V = 1, \quad (3.79)$$

$$z = -1 : \quad V = 0. \quad (3.80)$$

For planar geometry  $j = 0$ , the only solution satisfying both boundary conditions is a linear distribution

$$V_0(z) = 1 + z \quad (3.81)$$

Cylindrical and spherical geometries ( $j = 1, 2$ ) require dividing by  $V^{1+2/j}$  to obtain the

### 3.3 Dynamics of the combustion products behind a detonation

equation

$$\frac{1}{V_j^{2/j}} \frac{dV_j}{dz} + \frac{d}{dz} \left( \frac{jz+1}{2 V_j^{2/j}} \right) = 0 \quad (3.82)$$

whose exact differential form writes differently according to the value of  $j$ . In cylindrical geometry  $j = 1$ , the corresponding exact differential is

$$\frac{d}{dz} \left( \frac{1z+1}{2 V_1^2} - \frac{1}{V_1} \right) = 0. \quad (3.83)$$

Integrating from the boundary condition (3.79) and retaining the solution satisfying the boundary condition (3.80) increasing function, the self-similar solution is described by the expression

$$V_1(z) = 1 - \sqrt{-z} \quad (3.84)$$

Finally, for spherical geometries  $j = 2$ , the exact differential takes the form

$$\frac{d}{dz} \left( \ln V_2 + \frac{z+1}{V_2} \right) = 0. \quad (3.85)$$

Integrating from the boundary condition (3.79) the following transcendental equation is obtained

$$V_2 \ln V_2 - V_2 + 1 + z = 0. \quad (3.86)$$

whose roots describe the velocity distribution and automatically satisfies the boundary condition (3.80).

The small heat release limit solutions corresponding to each geometry are depicted in Figure 3.8. Similar to the solutions derived by Zeldovich (1942) and Taylor (1950a) in the opposite limit of large Mach number  $M_{u_{CJ}} \gg 1$  (see Figure 2.11), the solutions of (3.78) for cylindrical and spherical detonation in the limit of small heat release are singular on the front where the flow gradient becomes infinite. This singular behavior can be verified by introducing the solutions (3.84) and (3.86) in equation (3.78) and examining the limit at the front, i.e.  $z \rightarrow 0^-$  and  $V \rightarrow 1^-$ ,

$$j = 1 : \quad \lim_{z \rightarrow 0^-} \frac{dV}{dz} = \lim_{z \rightarrow 0^-} -\frac{1}{2} \frac{1 - \sqrt{-z}}{-\sqrt{-z} - z} = \infty,$$

$$j = 2 : \quad \lim_{V \rightarrow 1^-} \frac{dV}{dz} = \lim_{V \rightarrow 1^-} -\frac{1}{\ln V} = \infty.$$

The gradient at the inner boundary, however, remains finite with the spherical rarefaction wave being tangent to the core of stagnant gas

$$j = 1 : \quad \lim_{z \rightarrow -1^+} \frac{dV}{dz} = \lim_{z \rightarrow -1^+} -\frac{1}{2} \frac{1 - \sqrt{-z}}{-\sqrt{-z} - z} = \frac{1}{2},$$

### 3 Direct initiation of critical detonations in the small heat release asymptotic limit

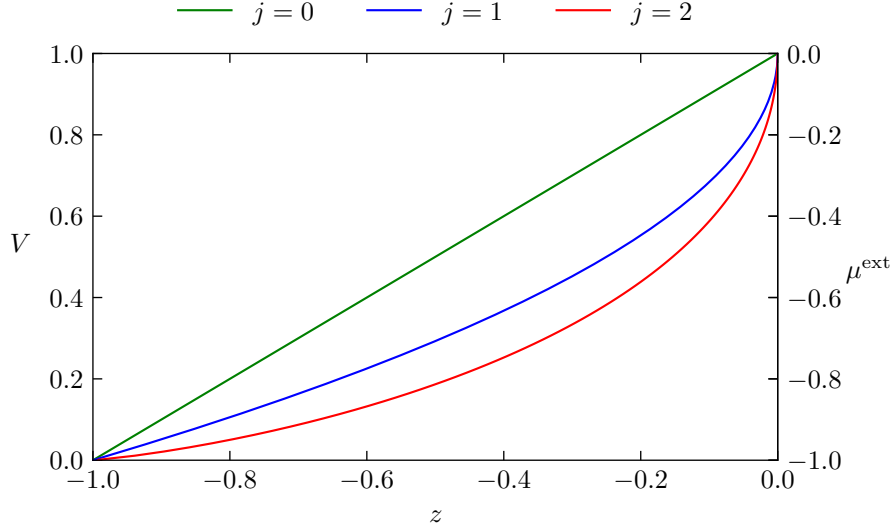


Figure 3.8: Self-similar solution of (3.78) for the flow of combustion products behind a small heat release CJ detonation in planar, cylindrical and spherical geometry ( $j = 0, 1$  and  $2$  respectively). The reduced flow  $V = 1 + \mu^{\text{ext}} = u/\epsilon a$  is plotted in the self-similar variable  $z = \tilde{\xi}/(1 + \tilde{\tau}) = \xi/|\xi_0(\tau)| = (r - r_f(t))/(r_f(t) - r_0(t))$ .

$$j = 2 : \quad \lim_{V \rightarrow 0^+} \frac{dV}{dz} = \lim_{V \rightarrow 0^+} -\frac{1}{\ln V} = 0.$$

In conclusion, the spherical rarefaction wave behind a CJ detonation sustained by a small heat release is qualitatively similar to the self-similar solution for large Mach number (see Figure 2.11). The differences are only quantitative with the extension of the rarefaction wave being smaller than the detonation radius by a factor  $M_{\text{CJ}} - 1 \ll 1$  in the small heat release limit, while it is roughly equal to half of the detonation radius in the large Mach number limit.

#### 3.3.2 Overdriven decaying detonation

Unlike the steady CJ wave, the rarefaction wave developed in the decay of an overdriven detonation cannot be expected to be self-similar, as the rarefaction wave length and the propagation velocity may evolve independently. The decay of an overdriven detonation in the discontinuous model is conveniently studied in the coordinate system attached to the leading edge of the core of gases at rest  $\tilde{\xi}_0$ . The transformation to this coordinate system is achieved through the change of variable

$$\tilde{\eta} = \tilde{\xi} - \tilde{\xi}_0(\tilde{\tau}), \quad \frac{\partial}{\partial \tilde{\tau}} \rightarrow \frac{\partial}{\partial \tilde{\tau}} - \frac{d\tilde{\xi}_0}{d\tilde{\tau}} \frac{\partial}{\partial \tilde{\eta}} \quad \text{and} \quad \frac{\partial}{\partial \tilde{\xi}} = \frac{\partial}{\partial \tilde{\eta}}.$$

The spatial coordinate of the core of stagnant gases at any given time  $\tilde{\xi}_0(\tilde{\tau})$  is obtained by integration of the time evolution (3.72) denoting by  $\xi_{0i}$  the initial position at time  $\tilde{\tau} = 0$ .

### 3.3 Dynamics of the combustion products behind a detonation

In this coordinate system, the propagation velocity  $\dot{\alpha}_\tau$  dependence disappears from the governing equation (3.74) which becomes

$$\frac{\partial \mu^{\text{ext}}}{\partial \tilde{\tau}} + (\mu^{\text{ext}} + 1) \frac{\partial \mu^{\text{ext}}}{\partial \tilde{\eta}} = -\frac{j}{2} \frac{1 + \mu^{\text{ext}}}{1 + \tilde{\tau}} \quad (3.87)$$

and the boundary condition of zero flow velocity at the core of stagnant gases (3.76) is rewritten as

$$\tilde{\eta} = 0 : \quad \mu^{\text{ext}}(\tilde{\eta}, \tilde{\tau}) = -1. \quad (3.88)$$

The initial solution is characterised by the initial flow velocity at the front  $\mu_{\text{f}}^{\text{ext}}$  so that an initial condition can be defined as

$$\tilde{\tau} = 0 : \quad \mu^{\text{ext}}(\tilde{\xi} = 0, \tilde{\tau}) = \mu_{\text{f}}^{\text{ext}}. \quad (3.89)$$

Anticipating the decay of the overdriven detonation with time and the boundary condition at the core of stagnant gases, a solution to this differential equation is searched in the form

$$\mu^{\text{ext}}(\tilde{\eta}, \tilde{\tau}) = \frac{X(\tilde{\eta})}{T(\tilde{\tau})} - 1$$

so denoting the derivatives  $X' = dX/d\tilde{\eta}$  and  $\dot{T} = dT/d\tilde{\tau}$ , equation (3.87) becomes

$$-\frac{X}{T^2} \dot{T} + \frac{X X'}{T} = -\frac{j}{2} \frac{1}{1 + \tilde{\tau}} \frac{X}{T}.$$

After multiplication by  $T^2/X$  the partial differential equation can be written in separated variables form so that both sides of the equality can be set to a fixed constant  $k$  obtaining a set of two ordinary differential equations

$$X' = k \quad \text{and} \quad \dot{T} = \frac{j}{2} \frac{1}{1 + \tilde{\tau}} T + k. \quad (3.90)$$

The spatial dependence described by the first equation is obtained straightforward leading to a uniform gradient

$$X(\tilde{\eta}) = k\tilde{\eta}$$

On the other hand, functional time dependence requires the integration of the second differential equation specific to each geometry. In planar geometry  $j = 0$ , time integration is straightforward resulting in a linear time decay

$$T_0(\tilde{\tau}) = k\tilde{\tau} + T_{i0}$$

with a constant of integration  $T_{i0}$  whose value can be rewritten in terms of the initial

### 3 Direct initiation of critical detonations in the small heat release asymptotic limit

condition (3.89) to provide

$$\mu_0^{\text{ext}}(\tilde{\xi}, \tilde{\tau}) = \frac{\tilde{\xi} - \tilde{\xi}_0(\tilde{\tau})}{\theta_i + \tilde{\tau}} - 1. \quad (3.91)$$

where the parameter  $\theta_i \equiv -\tilde{\xi}_{0i}/(1 + \mu_{fi}^{\text{ext}})$  represents the initial conditions.

For a cylindrically symmetric geometry  $j = 1$ , the time decay is given by the functional dependence

$$T_1(\tilde{\tau}) = 2k(1 + \tilde{\tau}) + T_{i1}\sqrt{2(1 + \tilde{\tau})}$$

which results in the following expression for the velocity distribution after introducing the initial front flow velocity

$$\mu_1^{\text{ext}}(\tilde{\xi}, \tilde{\tau}) = \frac{\tilde{\xi} - \tilde{\xi}_0(\tilde{\tau})}{\sqrt{1 + \tilde{\tau}} [\theta_i + 2(\sqrt{1 + \tilde{\tau}} - 1)]} - 1 \quad (3.92)$$

The flow of burnt gases behind a spherical detonation  $j = 2$  decays according to

$$T_2(\tilde{\tau}) = k(1 + \tilde{\tau}) \ln(1 + \tilde{\tau}) + T_{2i}(1 + \tilde{\tau}) \quad (3.93)$$

providing the following expression for the velocity distribution

$$\mu_2^{\text{ext}}(\tilde{\xi}, \tilde{\tau}) = \frac{\tilde{\xi} - \tilde{\xi}_0(\tilde{\tau})}{(1 + \tilde{\tau}) [\theta_i + \ln(1 + \tilde{\tau})]} - 1. \quad (3.94)$$

The flow velocity at the front of planar, cylindrical and spherical waves corresponds to the flow velocity obtained for  $\tilde{\xi} = 0$

$$\mu_{0,f}^{\text{ext}}(\tilde{\tau}) \equiv \mu_0^{\text{ext}}(\tilde{\xi} = 0, \tilde{\tau}) = \frac{-\tilde{\xi}_0(\tilde{\tau})}{\theta_i + \tilde{\tau}} - 1 \quad (3.95)$$

$$\mu_{1,f}^{\text{ext}}(\tilde{\tau}) \equiv \mu_1^{\text{ext}}(\tilde{\xi} = 0, \tilde{\tau}) = \frac{-\tilde{\xi}_0(\tilde{\tau})}{\sqrt{1 + \tilde{\tau}} [\theta_i + 2(\sqrt{1 + \tilde{\tau}} - 1)]} - 1 \quad (3.96)$$

$$\mu_{2,f}^{\text{ext}}(\tilde{\tau}) \equiv \mu_2^{\text{ext}}(\tilde{\xi} = 0, \tilde{\tau}) = \frac{-\tilde{\xi}_0(\tilde{\tau})}{(1 + \tilde{\tau}) [\theta_i + \ln(1 + \tilde{\tau})]} - 1 \quad (3.97)$$

which are represented in Figure 3.9 for the same initial profile corresponding to a slightly overdriven wave. Here, it is observed that the flow velocity decays towards the sonic condition  $\mu^{\text{ext}}(\tilde{\xi}_s, \tilde{\tau}) = \dot{\alpha}_\tau(\tilde{\tau})$  at the front which in the discontinuous model, according to the boundary condition (3.75), corresponds to  $\mu_f^{\text{ext}} = 0$ . In planar geometry, the sonic condition for the detonation as a discontinuity is only reached asymptotically in the long time limit. In contrast, in cylindrical and spherical geometries, the flow velocity crosses and continues to decrease after the sonic condition.

To conclude, in the rarefaction wave behind slightly overdriven detonations the flow velocity decreases linearly from its value at the front given by the reactive RH jump conditions to zero at a core of stagnant gases advancing at the sound speed. The rate of

### 3.3 Dynamics of the combustion products behind a detonation

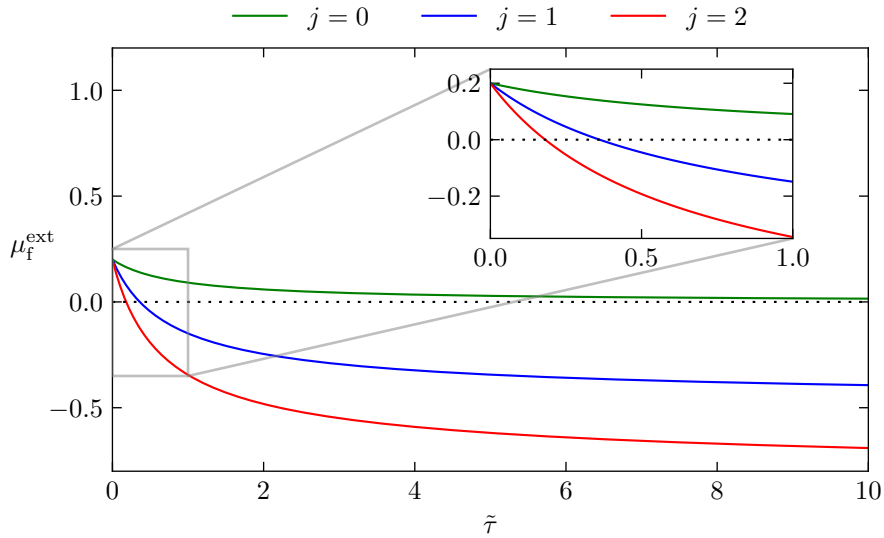


Figure 3.9: Flow velocity at the front behind a decaying detonation wave treated as a discontinuity for planar, cylindrical and spherical geometries  $j = 0, 1$  and  $2$  respectively. The initial solution is determined by the parameters  $\mu_{\text{fi}}^{\text{ext}} = 0.2$  and  $\tilde{\xi}_{0i} = -1$ .

decay of this linear profile depends on the geometry of the detonation wave. In planar waves, the flow velocity at the front decays asymptotically towards the sonic condition. The curved waves decay faster and the sonic condition at the front is quickly reached and overcome. Actually, once the sonic condition reaches the front, the rarefaction wave cannot continue to slow down the detonation as shown here. This solution was obtained by integrating from the core of stagnant gas and is not valid around the front when the sonic condition prevents the propagation of  $C_+$  waves towards the front. A transitory solution shall appear in this situation to match the rarefaction wave behind an overdriven detonation with the self-similar solution behind a CJ wave.

#### 3.3.3 Transitory regime in curved waves

The rarefaction wave behind the CJ wave and behind the overdriven decaying detonation wave are presented in the previous sections. Whereas the decay of planar detonations terminates in the self-similar solution for CJ waves, the way the rarefaction wave in curved geometries behind an overdriven detonation reaches the self-similar solution corresponding to the CJ wave requires more attention. This transition, described in this section in the small heat release limit, is similar to the transition described by Liñán et al. (2012) in the opposite limit  $M_{u_{\text{CJ}}} \gg 1$ .

The flow velocity behind the decaying detonation and the CJ wave vanish at the leading edge of the spherical core of stagnant gas. But, in curved geometries, the flow gradient is uniform and finite in the first case, while it is infinite at the detonation front in the second case. For planar detonations, the overdriven detonation decays asymptotically to the self-similar solution that has no singularity at the front, i.e., the sonic condition is reached



### 3 Direct initiation of critical detonations in the small heat release asymptotic limit

in the long time limit  $\tilde{\tau}_{t,0} \rightarrow \infty$ . While in cylindrical and spherical detonations the sonic condition which is initially located at a finite distance from the front reaches it at a finite time  $\tilde{\tau}_t$  due to the curvature damping effect. The transition time  $\tilde{\tau}_t$  is determined by the time instant when the flow velocity at the front reaches the sonic condition  $\mu_f^{\text{ext}}(\tilde{\tau}_t) = 0$  which leads to a quadratic and a transcendental equation in the cylindrical and spherical cases respectively. However, in the limit of small overdrive  $\mu_{\text{fi}}^{\text{ext}} \ll 1$ , both relations are simplified and the transit time is determined by the initial flow velocity at the front independently of the initial thickness of the rarefaction wave in the cylindrical  $\tilde{\tau}_{t,1} \approx 2\mu_{\text{fi}}^{\text{ext}}$  and spherical  $\tilde{\tau}_{t,2} \approx \mu_{\text{fi}}^{\text{ext}}$  case.

Within the framework of the discontinuous model, the velocity of the burnt gas relative to the lead shock cannot become smaller than the sound speed on the detonation front. According to the boundary condition (3.75), neither  $\dot{\alpha}_\tau$  nor  $\mu_f^{\text{ext}}$  can take negative values. At the transit time  $\tilde{\tau} = \tilde{\tau}_t$ , both variables must simultaneously reach zero and maintain this value for all subsequent periods. Therefore, the slowdown of  $\mu_f^{\text{ext}}$  stops suddenly at  $\tilde{\tau}_t$ . A sudden stop of the detonation decay is thus produced at  $\tilde{\tau}_t$  on the detonation front, introducing a weak discontinuity in the solution which propagates inwards separating the two rarefaction wave solutions. The flow gradient on the detonation front, which is finite for  $\tilde{\tau} \leq \tilde{\tau}_t$ , becomes abruptly infinite at  $\tilde{\tau} = \tilde{\tau}_t$  and stays infinite afterwards as in the self-similar solution. Recalling that no boundary condition is used on the front to derive the flow behind a decaying detonation, this flow is still solution of the rarefaction wave for  $\tilde{\tau} > \tilde{\tau}_t$  far from the detonation front. The transitory flow matching the linear profiles (3.92) and (3.94) to the self-similar solutions (3.84) and (3.86), denoted  $\mu^{\text{ext,tr}}(\tilde{\xi}, \tilde{\tau})$  in the following, is solution of (3.74) for a flow velocity at the front kept equal to its CJ value after  $\tilde{\tau}_t$

$$\tilde{\tau} \geq \tilde{\tau}_t : \quad \frac{\partial \mu^{\text{ext,tr}}}{\partial \tilde{\tau}} + \mu^{\text{ext,tr}} \frac{\partial \mu^{\text{ext,tr}}}{\partial \tilde{\xi}} = -\frac{j}{2} \frac{1 + \mu^{\text{ext,tr}}}{1 + \tilde{\tau}}, \quad \tilde{\xi} = 0 : \mu^{\text{ext,tr}} = 0.$$

The singular perturbation which is generated instantaneously at  $\tilde{\tau} = \tilde{\tau}_t$  on the front is propagated inwards by the last outward wave  $C_+^*$  that reached the front. Since  $\dot{\alpha}_\tau = 0$  for  $\tilde{\tau} > \tilde{\tau}_t$ , the outward wave (which actually propagates inward behind the sonic condition) propagates with velocity

$$\frac{d\tilde{\xi}_{C_+^*}}{d\tilde{\tau}} = \mu_{C_+^*}^{\text{ext}}(\tilde{\tau}).$$

where  $\mu_{C_+^*}^{\text{ext}}(\tilde{\tau}) = \mu^{\text{ext}}(\xi_{C_+^*}(\tilde{\tau}), \tilde{\tau})$  is the flow velocity on the characteristic line. Along this characteristic line, the governing equation (3.74) for  $\tilde{\tau} > \tilde{\tau}_t$  rewrites as

$$\xi = \xi_{C_+^*}(\tilde{\tau}) : \quad \frac{d\mu_{C_+^*}^{\text{ext}}}{d\tilde{\tau}} = -\frac{j}{2} \frac{1 + \mu_{C_+^*}^{\text{ext}}}{1 + \tilde{\tau}}$$

and can be integrated from  $\tilde{\tau} = \tilde{\tau}_t : \mu_{C_+^*}^{\text{ext}} = 0$  to determine the flow velocity transported

### 3.3 Dynamics of the combustion products behind a detonation

by this characteristic

$$\tilde{\tau} \geq \tilde{\tau}_t : \quad \mu_{C_+^*}^{\text{ext}}(\tilde{\tau}) = \left( \frac{1 + \tilde{\tau}_t}{1 + \tilde{\tau}} \right)^{j/2} - 1.$$

The integration of the characteristic velocity from  $\tilde{\xi}_{C_+^*}(\tilde{\tau} = \tilde{\tau}_t) = 0$  provides an analytical description of the characteristic curve. The characteristic curve that separates the overdriven rarefaction wave from the CJ self-similar solution in cylindrical geometry writes

$$\begin{aligned} \tilde{\tau} \geq \tilde{\tau}_t : \quad \tilde{\xi}_{C_{+,1}^*}(\tilde{\tau}) &= 2\sqrt{(1 + \tilde{\tau}_t)(1 + \tilde{\tau})} - 2 - \tilde{\tau} - \tilde{\tau}_t \\ &= (2 + \tilde{\tau}_t)(\sqrt{1 + \tilde{\tau}} - 1) - \tilde{\tau} + \mathcal{O}(\tilde{\tau}_t^2). \end{aligned} \quad (3.98)$$

while in spherical geometry is

$$\begin{aligned} \tilde{\tau} \geq \tilde{\tau}_t : \quad \tilde{\xi}_{C_{+,2}^*}(\tilde{\tau}) &= (1 + \tilde{\tau}_t) \ln \left( \frac{1 + \tilde{\tau}}{1 + \tilde{\tau}_t} \right) - (\tilde{\tau} - \tilde{\tau}_t) \\ &= (1 + \tilde{\tau}_t) \ln(1 + \tilde{\tau}) - \tilde{\tau} + \mathcal{O}(\tilde{\tau}_t^2). \end{aligned} \quad (3.99)$$

These theoretical results are compared with the numerical solution of the general problem for the dynamics of combustion products. The governing equation (3.74) is integrated numerically with the upwind differencing scheme. A forward finite difference scheme is used to approximate the temporal derivative while the spatial derivative is approximated with a backward difference scheme when the local advection velocity  $\mu^{\text{ext}} - \dot{\alpha}_\tau$  is positive or with a forward difference scheme otherwise. Thus, this method naturally deals with the sonic condition at the front. Initially, the sonic condition lies at a finite distance from the front so that the local advection velocity points outside the numerical domain at both boundaries and no numerical boundary conditions are required. The detonation propagation velocity  $\dot{\alpha}_\tau$  is computed through the boundary condition (3.75) from the flow velocity at the front. When the sonic condition, defined by a zero advection velocity, reaches the front, the advection term vanishes and the flow velocity at the front is constrained by the boundary condition (3.75) to non-negative values.

Examples of the numerical results obtained with the solution of the flow behind an overdriven decaying detonation initially defined by the parameters  $\mu_{\text{fi}}^{\text{ext}} = 0.5$  and  $\xi_{0i} = -1$  are shown in Figures 3.10 to 3.12. In the planar geometry (Figure 3.10, the transitory flow approaches asymptotically the self-similar CJ solution following the decay predicted for the straight velocity profiles. The examples for cylindrical and spherical geometries (Figures 3.11 and 3.12) show the transitory flow composed by the self-similar solution between the front and the last characteristic  $C_+^*$  and the straight profiles down to the core of gases at rest at the opposite side.

In conclusion, it has been observed that the dynamics of planar and curved detonations exhibit two distinct behaviours. In the absence of the curvature damping mechanism, detonation waves approach the CJ regime, which is described by the self-similar solution

### 3 Direct initiation of critical detonations in the small heat release asymptotic limit

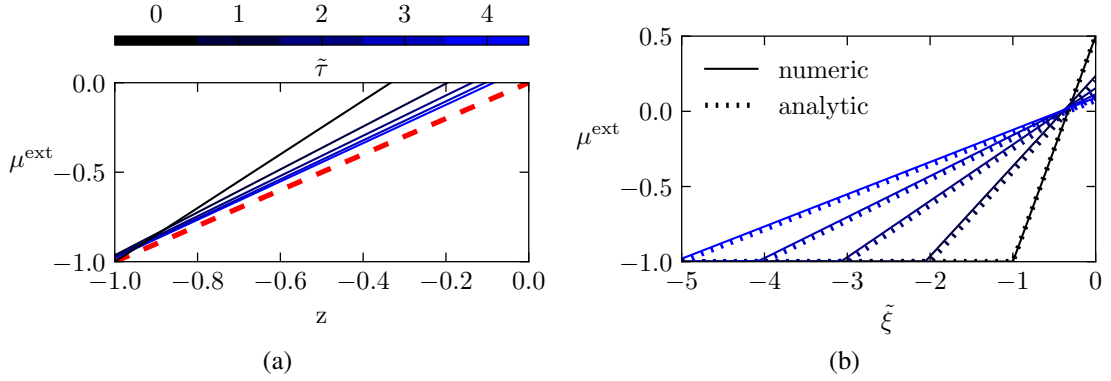


Figure 3.10: Flow velocity profile obtained by numerical integration of (3.74) and (3.75) with  $j = 0$  at different time steps  $\Delta\tilde{\tau} = 1$  from the initial profile at  $\tilde{\tau} = 0$  (black) to  $\tilde{\tau} = 3$  (blue) describing the evolution of the transitory flow  $\mu^{\text{ext},\text{tr}} = u^{(\text{tr})}/(\epsilon a) - 1$  behind a planar wave initialized as a straight line with  $\mu_{\text{fi}}^{\text{ext}} = 0.5$  and  $\tilde{\xi}_{0i} = -1$ . (a) Results presented in the self-similar variable obtained by reducing the dimensionless distance to the front with the thickness of the rarefaction wave  $z \equiv \tilde{\xi}/(1 + \tilde{\tau})$  and compared with the self-similar solution (3.81) in thick dashed red line. (b) Results plotted in the reduced spatial variable and compared with the straight profiles (3.91) in dotted line.

(3.81). This solution is reached asymptotically in the long time limit, as described by equation (3.91). The planar waves do not exhibit any critical conditions that might impede the successful initiation of a detonation.

In contrast, curvature-induced damping drives curved detonations abruptly towards the CJ regime, which is characterized by the sonic condition. At this point, the rarefaction wave can no longer penetrate the internal structure of the detonation, and a disturbance is propagated inward by the characteristic  $\tilde{\xi}_{C_+^*}$ . This disturbance divides the transitory solution into two parts. The flow ahead of the leading edge of this disturbance, where  $\tilde{\xi} > \tilde{\xi}_{C_+^*}(\tilde{\tau})$ , is described by the self-similar solution of the rarefaction wave behind a CJ wave with an infinite slope at the front (equations (3.84) and (3.86)). The flow corresponding to  $\tilde{\xi} \leq \tilde{\xi}_{C_+^*}(\tilde{\tau})$  is described by a linear profile that represents the rarefaction wave behind a decaying overdriven detonation with a uniform slope decreasing to zero (equations (3.92) and (3.94)). During the transitory regime, it is noted that the flow velocity at the front cannot decrease below the that of the CJ regime.

As noted by Korobeinikov (1971), the discontinuous model is unable to provide a critical initiation condition. However, as put forth by Taylor (1950a) “it is unlikely that the radial rate of change of velocity becoming infinite would be true in a real explosive where the time of reaction is not zero”. This observation suggests that the identification of critical conditions requires an examination of the internal structure of the detonation.

### 3.3 Dynamics of the combustion products behind a detonation

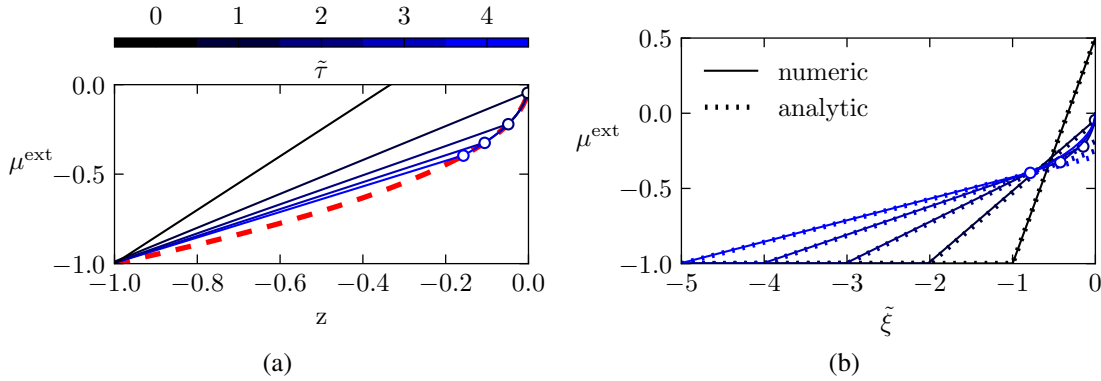


Figure 3.11: Flow velocity profile obtained by numerical integration of (3.74) and (3.75) with  $j = 1$  at different time steps  $\Delta\tilde{\tau} = 1$  from the initial profile  $\tilde{\tau} = 0$  (black) to  $\tilde{\tau} = 3$  (blue) describing the evolution of the transitory flow  $\mu^{\text{ext},\text{tr}} = u^{(\text{tr})}/(\epsilon a) - 1$  behind a cylindrical wave initialized as a straight line with  $\mu_{\text{fi}}^{\text{ext}} = 0.5$  and  $\tilde{\xi}_{0i} = -1$ . The position of the critical characteristic  $\tilde{\xi}_{C^*_{+,1}}$  as predicted by (3.98) is indicated with empty circles. (a) Results presented in the self-similar variable  $z \equiv \tilde{\xi}/(1 + \tilde{\tau})$  obtained by reducing the dimensionless distance to the front with the thickness of the rarefaction wave and compared with the self-similar solution (3.84) in thick dashed red line. (b) Results plotted in the reduced spatial variable and compared with the straight profiles (3.92) in dotted line.

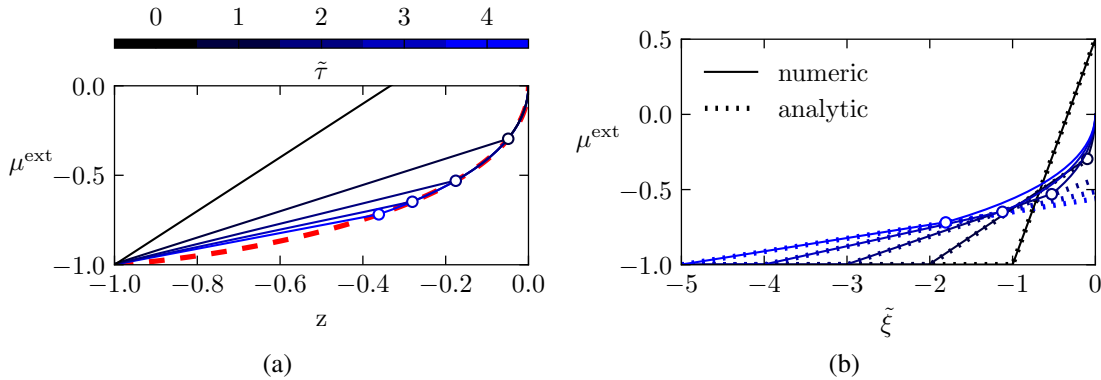


Figure 3.12: Flow velocity profile obtained by numerical integration of (3.74) and (3.75) with  $j = 2$  at different time steps  $\Delta\tilde{\tau} = 1$  from the initial profile  $\tilde{\tau} = 0$  (black) to  $\tilde{\tau} = 3$  (blue) describing the evolution of the transitory flow  $\mu^{\text{ext},\text{tr}} = u^{(\text{tr})}/(\epsilon a) - 1$  behind a spherical wave initialized as a straight line with  $\mu_{\text{fi}}^{\text{ext}} = 0.5$  and  $\tilde{\xi}_{0i} = -1$ . The position of the critical characteristic  $\tilde{\xi}_{C^*_{+,1}}$  as predicted by (3.99) is indicated with empty circles. (a) Results presented in the self-similar variable  $z \equiv \tilde{\xi}/(1 + \tilde{\tau})$  obtained by reducing the dimensionless distance to the front with the thickness of the rarefaction wave and compared with the self-similar solution (3.86) in dashed red line. (b) Results plotted in the reduced spatial variable and compared with the straight profiles (3.94) in dotted line.

### 3.4 Direct initiation of a detonation

The direct initiation of a detonation in the discontinuous model is characterised by a sudden transition from an overdriven regime to a CJ detonation. However, this behavior does not correspond to what is observed in experimental studies and numerical simulations. This abrupt transition leads to the formation of a singularity at the front with an infinite velocity gradient just behind the discontinuous detonation. In order to gain a better understanding of the origin of this singularity, it is necessary to examine the internal structure of the detonation. Hence, this section will examine the critical dynamics of detonation initiation in the limit of small heat release when modifications to the internal structure are taken into account.

When attention is focused on the internal structure  $\xi = \mathcal{O}(1)$ , the time-dependent velocity of the lead shock  $\dot{\alpha}_\tau(\tau)$  is obtained as an eigenfunction of the system (3.55) and (3.56) that requires an additional boundary condition at the exit of the reaction zone  $\mu_b(\tau) = \mu(\xi_b, \tau)$ . In contrast to (Clavin and Denet, 2020), where, considering the burnt-gas flow as uniform, the decelerating flow  $\mu_b(\tau)$  was imposed, the solution of (3.55) and (3.56) will be matched now with the non-uniform flow of the rarefaction wave  $\mu^{\text{ext}}(\xi, \tau)$ , solution to the external problem (3.74) to (3.76). In overdriven regimes, this external flow field is given by the analytical expressions (3.91), (3.92) and (3.94).

#### 3.4.1 Overdriven regimes

In an overdriven detonation, the burnt gas flow at the exit of the reaction zone is subsonic relative to the lead shock  $\mu(\xi_b, \tau) > \dot{\alpha}_\tau$ . The sonic point, where  $\mu(\xi_s(\tau), \tau) = \dot{\alpha}_\tau(\tau)$ , is located within the rarefaction flow, behind the internal structure of the combustion wave. The larger the overdrive factor, defined as  $\mu^{\text{ext}}(\xi_b, \tau) - \dot{\alpha}_\tau(\tau)$ , is the larger is the distance between the sonic point and the exit of the reaction zone. The characteristic  $C_+$  is inward running behind the sonic point, while it is outward running ahead the sonic point. Under these conditions, the characteristic  $C_+$  cannot propagate perturbations from the internal structure of the combustion wave towards the rarefaction flow in the burnt gas, which is still described by (3.94)

$$\xi \leq \xi_b : \mu(\xi, \tau) = \mu^{\text{ext}}(\xi, \tau) = \frac{\xi - \xi_{0i} + \tau [1 + Y(\tau)]}{\tilde{r}_f(\tau) \left[ \frac{-\xi_{0i}}{1 + \mu_{fi}^{\text{ext}}} + \ln \left( \frac{\tilde{r}_f(\tau)}{\tilde{r}_{fi}} \right) \right]} - 1 \quad (3.100)$$

where  $Y(\tau) \equiv \frac{1}{\tau} \int_\tau^0 \dot{\alpha}_\tau(\tau') d\tau'$ .

The external flow  $\mu^{\text{ext}}(\xi, \tau)$  decreases linearly with the radius, regardless of the time-dependent velocity of the front  $\dot{\alpha}_\tau(\tau)$  from its value at the front to zero. The dependence of  $\mu^{\text{ext}}(\tau)$  on the past of the unknown solution  $\dot{\alpha}_\tau(\tau)$  through the integral  $Y(\tau)$  comes from the increase of the thickness of the rarefaction wave with the time. To summarize, for overdriven regimes, the boundary condition in the burnt gas to apply to the system (3.55) and (3.56) is (3.100).

Introducing the decomposition

$$\mu(\xi, \tau) = \mu^{\text{ext}}(\xi, \tau) + \hat{\mu}(\xi, \tau)$$

and subtracting (3.74) from (3.55)

$$\tau \leq \tau_s : \quad \frac{\partial \hat{\mu}}{\partial \tau} + (\hat{\mu} - \dot{\alpha}_\tau) \frac{\partial \hat{\mu}}{\partial \xi} = \frac{\omega}{2} - \frac{\hat{\mu}}{\tilde{r}_f} - \frac{\partial}{\partial \xi} (\mu^{\text{ext}} \hat{\mu}) \quad (3.101)$$

the dynamics of the lead shock  $\dot{\alpha}_\tau(\tau)$  during the decay of a combustion wave in the overdriven regime corresponds to the eigenfunction of (3.101) subject to the boundary conditions

$$\xi = 0 : \quad \hat{\mu} = 1 + 2\dot{\alpha}_\tau(\tau) - \mu^{\text{ext}}_f(\tau) \quad (3.102)$$

$$\xi \leq \xi_b = -e^{-b\dot{\alpha}_\tau(\tau)} : \quad \hat{\mu} = 0 \quad (3.103)$$

where  $\mu^{\text{ext}}(\xi, \tau)$  is given by (3.100) and  $\tau_s$  denotes the time at which it reaches for the first time the exit of the reaction zone.

Typically, an increase in  $\xi_s$  is observed when  $\dot{\alpha}_\tau(\tau)$  decreases, so that the sonic point approaches the end of the reaction  $\xi_b$ . Once the sonic point crosses the exit of the reaction zone  $\tau = \tau_s$ , the overdriven propagation regime is no longer valid, and the external flow which is solution of (3.74) is perturbed by the reactive transonic flow. For  $\tau > \tau_s$ , the boundary conditions (3.102) and (3.103) are no longer applicable, and the rarefaction wave can no longer be accurately represented by the analytical expression (3.100) everywhere in the burnt gas. In essence, shortly after  $\tau_s$ , the rarefaction flow behind the end of the reaction is perturbed by the heat released in the region bounded by the end of the reaction zone and the sonic point. However, as in the discontinuous model, the solution is recovered downstream until the arrival of the disturbance carried by the characteristic  $C_+$ .

### 3.4.2 Numerical integration

In order to study the dynamics for  $\tau \geq \tau_s$ , it is necessary to perform a numerical analysis of (3.55) and (3.56) with an initial condition at  $\tau = \tau_s$  obtained from the solution of the eigenvalue problem (3.101) to (3.103).

#### *Numerical method*

The numerical integration was performed by utilizing a splitting strategy that follows the algorithm

$$\mu^{n+1} = \mathcal{S}^{(\Delta t)} \mathcal{C}^{(\Delta t)} \mu^n$$

where the superscript  $n$  represents the time step number. The algorithm proceeds first integrating the convective term, then the obtained solution is used to integrate both the curvature and the reactive terms. The convective operator  $\mathcal{C}$  corresponds to the application of the high-resolution central scheme presented in Kurganov and Tadmor,

### 3 Direct initiation of critical detonations in the small heat release asymptotic limit

2000 for nonlinear conservation laws to the hyperbolic equation

$$\frac{\partial \mu}{\partial \tau} + (\mu - \dot{\alpha}_\tau) \frac{\partial \mu}{\partial \xi} = 0.$$

At the boundaries of the numerical domain, a first-order upwind scheme is employed to approximate the spatial derivatives. This approach utilizes the direction of the local advection velocity, represented by  $\mu - \dot{\alpha}_\tau$ . At the front, where the flow is subsonic relative to the lead shock  $\mu - \dot{\alpha}_\tau > 0$ , a backward difference scheme is utilized. On the other hand, at the end of the domain on the origin side, where the flow is supersonic relative to the front  $\mu - \dot{\alpha}_\tau < 0$ , a forward difference scheme is employed. The reactive and curvature operator  $\mathcal{S}$  refers to the integration of the following equation

$$\frac{\partial \mu}{\partial \tau} = \frac{\omega}{2} - \frac{1 + \mu}{\tilde{r}_f}$$

using a 2nd order Runge-Kutta explicit method. At the end of every time step, the value of the propagation velocity  $\dot{\alpha}_\tau$  is updated from the solution through the boundary condition (3.56).

#### *Initial conditions*

In a real initiation process, the initial trajectory of the lead shock is determined by the strong blast wave that is generated at the origin due to a nearly instantaneous release of energy. According to the self-similar solution of Sedov (1946) and Taylor (1950b) (see Section 2.2.3), this strong blast wave depends only on the amount of energy deposited. A detailed discussion about the effects of finite deposition times can be found in the work of Liñán et al. (2012). This initial stage corresponds to a high Mach number, which is beyond the scope of the asymptotic analysis for small heat release.

The critical condition of initiation is investigated here through a parametric study of the initial conditions given by (3.100). Three parameters of order unity are involved at  $\tau = 0$ : the initial radius  $\tilde{r}_{fi}$ , the initial thickness of the rarefaction wave  $|\xi_{0i}|$ , and the initial flow velocity at the front  $\mu_{fi}^{\text{ext}}$ . The initial propagation velocity  $\dot{\alpha}_{\tau,i}$  is related to the initial flow velocity through the boundary condition (3.56). This study focused on weakly overdriven detonations with an initial velocity close to that of the CJ regime  $\dot{\alpha}_{\tau,i} = 0.5$  and an initial extension of the rarefaction wave much larger than the detonation thickness  $|\xi_{0i}| = 10$ , as in real initiation processes close to criticality.

The numerical integration of (3.55) and (3.56) is initialized at  $\tau = 0$  by igniting the exothermal reaction in the inert flow (3.100)

$$\tau = 0 : \quad \mu(\xi) = \mu_{fi} - \frac{1 + \mu_{fi}}{\xi_{0i}} \xi$$

This initial conditions lead quickly, on a time scale shorter than unity, to formation of the overdriven detonation structure previously described.

### 3.4 Direct initiation of a detonation

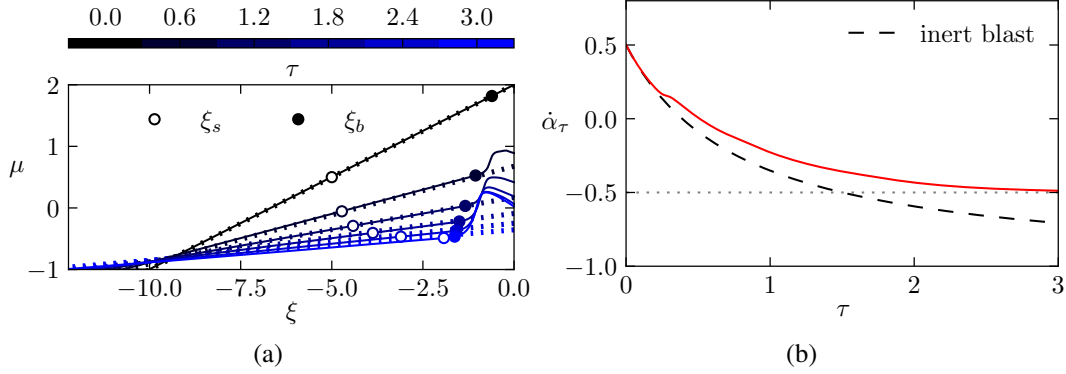


Figure 3.13: Initial solution obtained by numerical integration of (3.55) and (3.56) for a stable spherical detonation with  $b = 1$ ,  $j = 2$  and  $\dot{\alpha}_\tau = -0.5$  during the overdriven regime. (a) Flow velocity profiles at different time steps  $\Delta\tau = 0.6$  from the initial solution at  $\tau = 0$  (black) to  $\tau = 3$  (blue). The full points indicate the exit of the reaction zone  $\xi_b$  and the empty circles are the sonic points relative to the leading shock  $\xi_s$ . The discontinuous lines represent the analytical solution (3.100) for the external flow  $\mu^{\text{ext}}$  of overdriven detonations neglecting the integral  $Y(\tau)$  showing excellent agreement behind the exit of the reaction zone. (b) Temporal evolution of the propagation velocity  $\dot{\alpha}_\tau(\tau)$ . The dashed black line represents the decay of an inert blast wave.

An example of numerical results obtained for a stable spherical detonation with  $b = 1$  and  $j = 2$  is shown in Figure 3.13. The flow velocity profiles obtained by numerical integration of (3.55) and (3.56) during the overdriven regime (see Figure 3.13a), before the sonic point  $\xi_s$  reaches the exit of the reaction zone  $\xi_b$  at  $\tau_s$ , are found to be in great agreement with the analytical solution given by (3.100) even when the integral term  $Y(\tau)$  is neglected. The ignition of the exothermal reaction in the initially inert flow is observed at  $\tau = 0.25$  in Figure 3.13b. Afterwards, the wave decay proceeds at a slower rate compared to the blast wave, due to the expansion occurring within the reaction zone. This methodology is followed to obtain the initial conditions in the subsequent parametric analysis.

#### Parametric study

A numerical investigation of the solutions of the solutions of (3.55) and (3.56) for spherical detonations  $j = 2$  was carried out through a parametric study under varying initial front radii  $\tilde{r}_{fi}$  and reduced activation energies  $b$ . The chemical-kinetics rate  $\omega$  follows the scaling law (3.71) of the simplified three-step kinetic scheme of Clavin and Denet (2018) whose instability threshold was identified to be  $b_c = 1.27$ . For the purpose of the analysis, a reduced activation energy of  $b = 1$  was selected as the base case representing a stable detonation and was compared to  $b = 2$  and  $b = 3$  which correspond to weakly unstable detonations and  $b = 5$  which represents an unstable detonation.

The parametric study was extended to cylindrical and planar cases for completeness. However, as anticipated in the framework of the discontinuous model, the dynamics of the



### 3 Direct initiation of critical detonations in the small heat release asymptotic limit

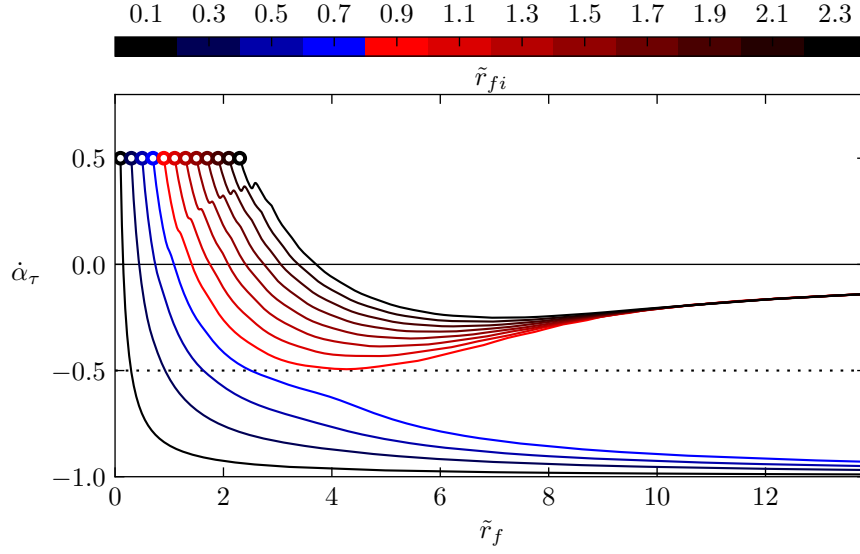


Figure 3.14: Trajectories “propagation velocity  $\dot{\alpha}_\tau$  vs. front radius  $\tilde{r}_f$ ” obtained through numerical integration of (3.55) and (3.56) for a stable spherical detonation with  $b = 1$ ,  $j = 2$  and  $\dot{\alpha}_{\tau,c} = -0.5$ . The failure occurs for a small initial radius  $\tilde{r}_{fi} < 0.8$  due to chemical-kinetics quenching.

cylindrical wave only exhibit quantitative differences with respect to the spherical wave due to the less pronounced effect of curvature. The parametric study in the planar case was limited to the reduced activation energy as the initial front radius is not a parameter of the problem. Additionally, the impact of the crossover propagation velocity  $\dot{\alpha}_{\tau,c}$  below which the reaction is quenched was evaluated by taking  $\dot{\alpha}_{\tau,c} = -0.5$  as the reference case compared to  $\dot{\alpha}_{\tau,c} = -0.8$ .

The results of the parametric study are presented as the trajectories in the plane  $\dot{\alpha}_\tau - \tilde{r}_f$ . These trajectories correspond to different initial radius  $\tilde{r}_{fi}$ , while the initial velocity is kept fixed  $\dot{\alpha}_{\tau,i} = 0.5$  as the initial thickness of the rarefaction wave which is 10 times larger than the detonation thickness  $|\xi_{0i}| = 10$ .

Successful initiation and detonation failure for a stable case  $b = 1$  are depicted in Figure 3.14 and Figure 3.15 for spherical and cylindrical waves, respectively. The results for cylindrical waves are qualitatively similar to those of spherical waves, albeit with a lesser impact of curvature on the wave dynamics.

In the absence of curvature, the initial front radius is not a parameter of the problem, and therefore the parametric study of the planar wave  $j = 0$  is exclusively based on the reduced activation energies  $b$ . The planar detonation decays asymptotically towards the CJ regime as in the discontinuous model. The decay of plane gaseous detonations in the limit of small heat release has been thoroughly examined previously in Clavin and Denet (2018). This study highlights the intrinsic instability of the inner structure for high activation energy values. Recently, Tofaili et al. (2021) and Tofaili (2022) validated the asymptotic analysis of planar detonations stability by comparing it with numerical simulations based on the one-dimensional reactive Euler equations using high-order numerical methods.

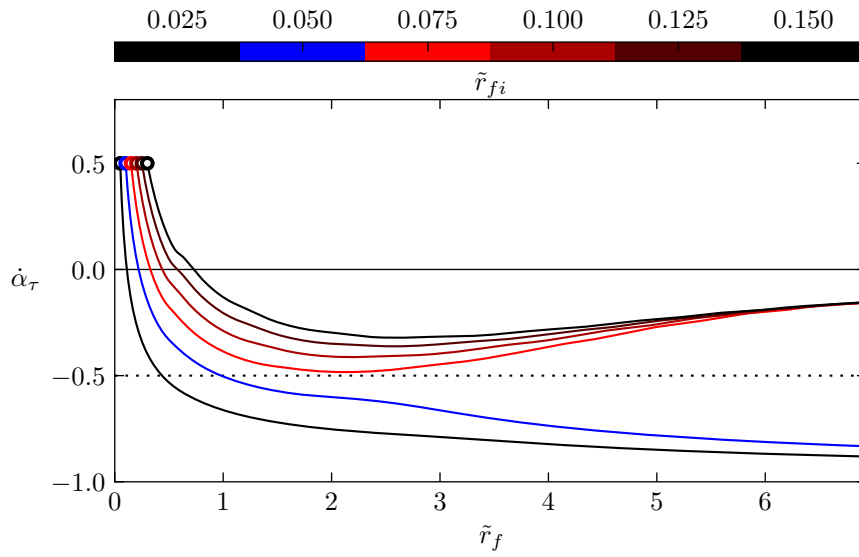


Figure 3.15: Trajectories “propagation velocity  $\dot{\alpha}_\tau$  vs. front radius  $\tilde{r}_f$ ” obtained through numerical integration of (3.55) and (3.56) for a stable cylindrical detonation with  $b = 1$ ,  $j = 1$  and  $\dot{\alpha}_{\tau,c} = -0.5$ . The failure occurs for a small initial radius  $\tilde{r}_{fi} < 0.06$  due to chemical-kinetics quenching.

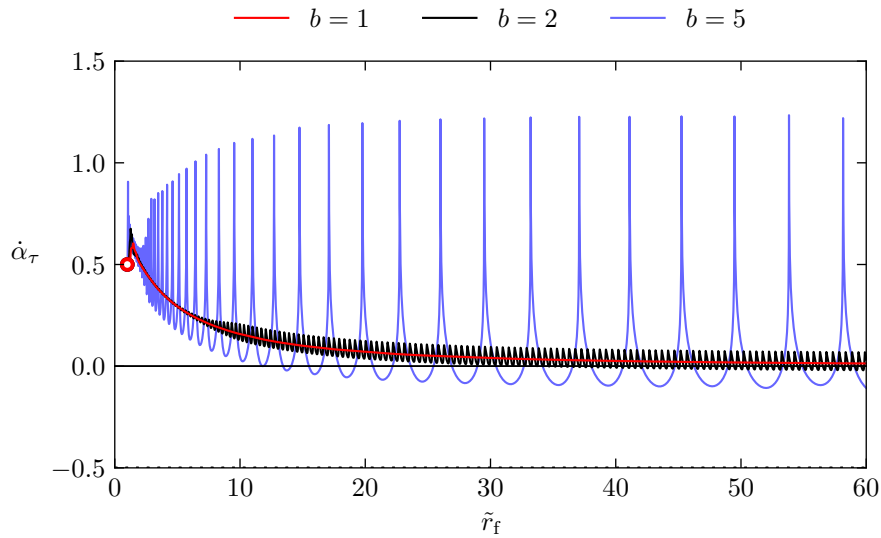


Figure 3.16: Trajectories “propagation velocity  $\dot{\alpha}_\tau$  vs. front radius  $\tilde{r}_f$ ” obtained through numerical integration of (3.55) and (3.56) for a planar detonation for different values of  $b$ .

### 3 Direct initiation of critical detonations in the small heat release asymptotic limit

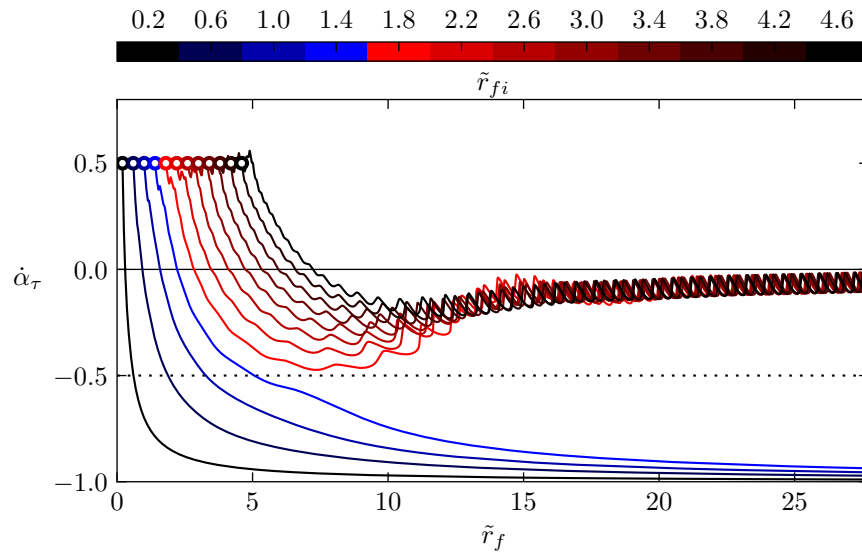


Figure 3.17: Trajectories “propagation velocity  $\dot{\alpha}_\tau$  vs. front radius  $\tilde{r}_f$ ” obtained through numerical integration of (3.55) and (3.56) for a weakly unstable spherical detonation with  $b = 2$ ,  $j = 2$  and  $\dot{\alpha}_{\tau,c} = -0.5$ . The failure occurs for a small initial radius  $\tilde{r}_{fi} < 1.6$  due to chemical-kinetics quenching.

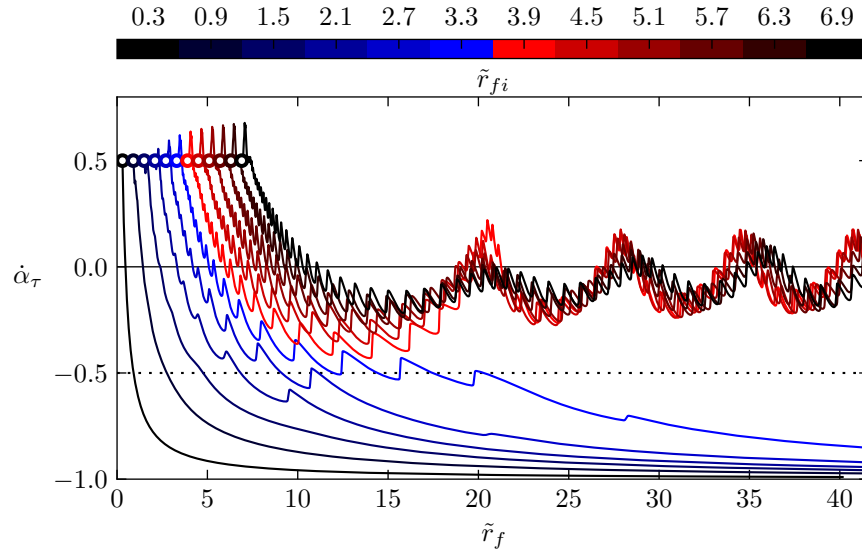


Figure 3.18: Trajectories “propagation velocity  $\dot{\alpha}_\tau$  vs. front radius  $\tilde{r}_f$ ” obtained through numerical integration of (3.55) and (3.56) for a weakly unstable spherical detonation with  $b = 3$ ,  $j = 2$  and  $\dot{\alpha}_{\tau,c} = -0.5$ . The failure occurs for a small initial radius  $\tilde{r}_{fi} < 3.6$  due to chemical-kinetics quenching.

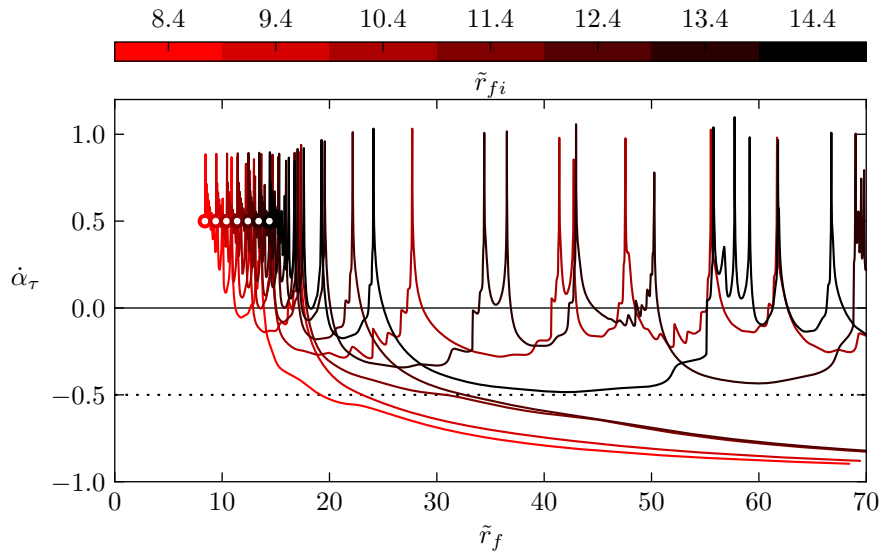


Figure 3.19: Trajectories “propagation velocity  $\dot{\alpha}_\tau$  vs. front radius  $\tilde{r}_f$ ” obtained through numerical integration of (3.55) and (3.56) for a strongly unstable spherical detonation with  $b = 5$ ,  $j = 2$  and  $\dot{\alpha}_{\tau,c} = -0.5$ .

In Figures 3.17 and 3.18, two weakly unstable detonations with  $b = 2$  and  $b = 3$  are presented, respectively. The results for these weakly unstable detonations are consistent with those of stable detonations, except for a nonlinear oscillation superimposed on the trajectories. Additionally, a slight overshoot in the critical trajectories is observed, with the wave initially reaccelerating more strongly than those that are further from the critical regime. This behavior is also observed in the numerical simulations based on the one-dimensional reactive Euler equations reported by He and Clavin (1994), Eckett et al. (2000), and Ng and Lee (2003), although the intensity of the behavior is more pronounced in their findings.

The results for a strongly unstable detonation with  $b = 5$  are shown in Figure 3.19 and exhibit much more complex dynamics. The large oscillations caused by the large activation energy are coupled with curvature effects giving rise to chaotic trajectories in the plan of propagation velocity versus radius of the front. The initiation of strongly unstable detonations constitutes a challenging problem that is left for future works. It is worth noting, however, that there is also a bifurcation in the long time dynamics, with both successful initiation of the detonation and detonation failures.

For moderate values of  $b$ , detonation failure is produced by the chemical-kinetics quenching. This is clearly shown by decreasing the lower bound  $\dot{\alpha}_{\tau,c}$  associated with the chemical-kinetics quenching. For example, considering the case where  $b = 1$  and  $\dot{\alpha}_{\tau,c} = -0.8$ , a successful initiation is observed in Figure 3.20 for  $\tilde{r}_{fi} = 0.5$  which corresponds to a detonation failure for  $\dot{\alpha}_{\tau,c} = -0.5$  in Figure 3.14.

### 3 Direct initiation of critical detonations in the small heat release asymptotic limit

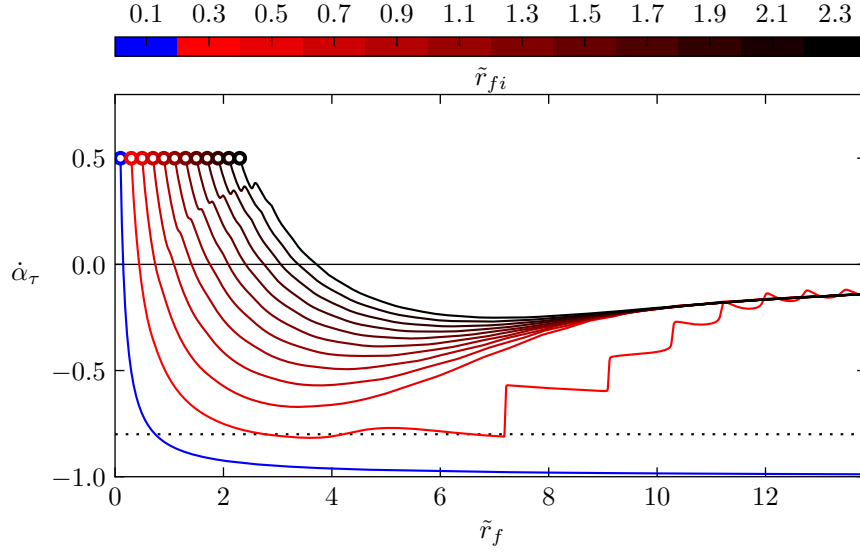


Figure 3.20: Trajectories “propagation velocity  $\dot{\alpha}_\tau$  vs. front radius  $\tilde{r}_f$ ” obtained through numerical integration of (3.55) and (3.56) for a stable detonation with  $b = 1$ ,  $j = 2$  and  $\dot{\alpha}_{\tau,c} = -0.8$ . The trajectory corresponding to  $\tilde{r}_{fi} = 0.1$  describes a failure of initiation  $\dot{\alpha}_\tau(\tau) \rightarrow -1$  and that corresponding to  $\tilde{r}_{fi} = 0.3$  is a successful initiation characterised by sudden detonation accelerations resulting from the formation of shock waves in the induction zone, as explained in the text.

#### 3.4.3 Discussion of the critical dynamics

The dynamics of a detonation are greatly influenced by changes to its inner structure. In contrast to the discontinuous model, detonation failure occurs when the detonation velocity decreases below the CJ velocity at a too small radius (yet larger than the detonation thickness). During the successful initiation of a steady detonation, the CJ velocity is not reached abruptly as in the discontinuous model. In this section, the critical dynamics of detonation initiation observed in the “propagation velocity vs. radius” trajectories will be analyzed and discussed.

##### *Slowdown mechanism of overdriven waves*

Consider initial conditions for which the propagation velocity crosses the CJ velocity  $\dot{\alpha}_\tau(\tau_i) = 0$  with a radius small enough and an overdrive factor large enough so that the flow at the exit of the reaction zone continues to be subsonic well below the CJ velocity. Under this conditions, the sonic point  $\xi_s$  lies on the external flow, which is described by (3.100), where the flow velocity  $\mu^{\text{ext}}$  equals the propagating velocity  $\dot{\alpha}_\tau$

$$\tau < \tau_s : \quad \xi_s(\tau) = \xi_0(\tau) + \tilde{r}_f(\tau) (1 + \dot{\alpha}_\tau(\tau)) \left[ \theta_i + \ln \left( \frac{\tilde{r}_f(\tau)}{\tilde{r}_{fi}} \right) \right]. \quad (3.104)$$

### 3.4 Direct initiation of a detonation

Unfortunately, the trajectory of the sonic point  $\xi_s(\tau)$  is strongly dependent on the instantaneous propagation velocity  $\dot{\alpha}_\tau(\tau)$  which is determined by the eigenvalue problem (3.101) to (3.103) that must be solved numerically. Nevertheless, the direction of motion of the sonic point can be evaluated by examining the time derivative of its trajectory (3.104) which writes

$$\tau < \tau_s : \quad \frac{d\xi_s}{d\tau} = \left[ \theta_i + \ln \left( \frac{\tilde{r}_f}{\tilde{r}_{fi}} \right) \right] \left( 1 + \dot{\alpha}_\tau + \tilde{r}_f \frac{d\dot{\alpha}_\tau}{d\tau} \right).$$

The first factor in brackets within the time derivative of the sonic point trajectory is always positive since  $\theta_i$ , which represents the initial solution parameter, and the logarithmic function of an argument larger than unity are positive. The sign of the second factor depends on the relative values of the propagation velocity  $\dot{\alpha}_\tau$  and its time derivative  $d\dot{\alpha}_\tau/d\tau$ . The sonic point inside the rarefaction flow of burnt gas behind an overdriven detonation moves towards the reaction zone when the detonation decay  $|d\dot{\alpha}_\tau/d\tau|$  is not too large, more precisely when the decay of  $1 + \dot{\alpha}_\tau$  is smaller than the damping rate by curvature

$$\tau < \tau_s : \quad \frac{d\xi_s}{d\tau} > 0 \leftrightarrow \frac{1}{1 + \dot{\alpha}_\tau} \frac{d\dot{\alpha}_\tau}{d\tau} < \frac{1}{\tilde{r}_f}.$$

The exit of the reaction zone  $\xi_b$  moves in the opposite direction when  $\dot{\alpha}_\tau$  decreases

$$\frac{1}{|\xi_b|} \frac{d\xi_b}{d\tau} = b \frac{d\dot{\alpha}_\tau}{d\tau}.$$

Consequently, the overdrive factor  $\mu^{\text{ext}}(\xi_b, \tau) - \dot{\alpha}_\tau(\tau)$  also decreases. As a result, the sonic point may catch the exit of the internal structure of the reaction wave at a later time.

The curvature term present in the right-hand side of (3.55) and the burnt-gas flow at the exit of the reaction zone influences the internal structure of the reaction wave. These two mechanisms exhibit opposing effect on the dynamics of the leading shock, as shown by the following rough arguments. Considering a constant flow at the exit of the reaction zone, the solution of (3.55) and (3.56) describes the dynamics of an overdriven wave which is isolated from the external flow. In the context of direct initiation, if the velocity  $\dot{\alpha}_\tau$  is well below the CJ velocity, namely if  $\dot{\alpha}_\tau$  is negative and not small, the flow velocity  $\mu(\xi, \tau)$  within the internal structure of the combustion wave will be out of equilibrium. In such scenario, the nonlinear relaxation towards equilibrium is expected to result in an increase of  $\dot{\alpha}_\tau$ , specially if the overdrive factor is small, as the equilibrium state would correspond to  $\dot{\alpha}_\tau = 0$ . Hence, the decay of  $\dot{\alpha}_\tau$  should be linked to the rarefaction-wave-induced flow at the exit of the reaction zone  $\mu^{\text{ext}}(\xi_b, \tau)$ . The response of the inner structure in adjusting the propagation velocity  $\dot{\alpha}_\tau$  is delayed by the transit time of the characteristics  $C_+$  leaving the end of the reaction  $\xi_b$  at time  $\tau$  to reach the point  $\xi_{C_+}(\tau, \tau') > \xi_b$  at a later time  $\tau' > \tau$ . With the exception of the integral term  $Y(\tau)$ , which can be neglected in (3.100), the decay of the velocity  $\dot{\alpha}_\tau(\tau)$  of an overdriven wave can be considered to be controlled by the decreasing rate of the rarefaction flow  $\mu^{\text{ext}}(\xi_b, \tau)$ , but with the time delay  $\Delta t_+(0, \tau)$  introduced by the characteristics  $C_+$  as

### 3 Direct initiation of critical detonations in the small heat release asymptotic limit

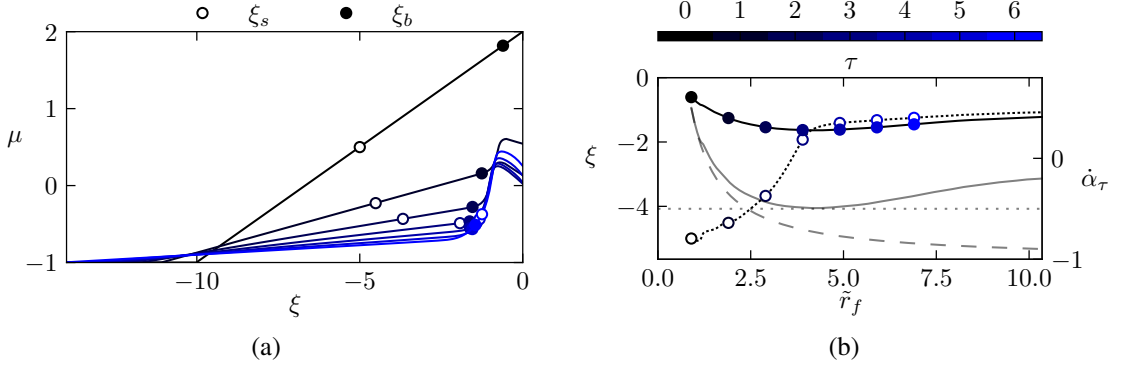


Figure 3.21: Results of the numerical integration of (3.55) and (3.56) for a stable spherical detonation ( $b = 1, j = 2$ ) for  $\dot{\alpha}_{\tau,c} = -0.5$  and  $\tilde{r}_{f,i} = 0.9$  illustrating the slowdown mechanism in a successful initiation. The full points indicate the exit of the reaction zone  $\xi_b$  and the empty circles are the sonic points relative to the lead shock. (a) Profiles of the reduced flow velocity at different time steps  $\Delta\tau = 1$  from the initial solution at  $\tau = 0$  (black) to  $\tau = 6$  (blue). (b) End of reaction  $\xi_b$  and sonic point  $\xi_s$  trajectories with respect to the leading shock in black solid and dotted line, respectively. The trajectory  $\dot{\alpha}_\tau(\tilde{r}_f)$  is plotted in grey line with the horizontal line indicating the chemical-kinetics quenching in dashed line. The grey dashed line represents the trajectory of the inert blast wave.

they travel from the exit of the reaction zone to the leading shock.

The validity of this description of the detonation dynamics extends until a time  $\tau_s$  at which the sonic point catches the exit of the inner structure. As the sonic condition approaches the end of the reaction, the time delay  $\Delta t_+(0, \tau)$  increases strongly. A slowdown of the velocity decay  $d\dot{\alpha}_\tau/d\tau$  should occur then when the sonic point approaches the end of the reaction, due to the time delay of the response becoming notably greater than the characteristic time of the forcing term responsible for the decay, specifically the inverse of the decreasing rate of the rarefaction flow  $\mu^{\text{ext}}(\xi, \tau)$ . Consequently, the derivative  $d\dot{\alpha}_\tau/d\tau$  approaches zero for  $\dot{\alpha}_\tau < 0$  resulting in the observed local minimum, and the decay rate of the propagation velocity is arrested.

In the case where the propagation velocity is greater than the lower bound  $\dot{\alpha}_{\tau,c}$  corresponding to the chemical-kinetics quenching, this scenario occurs when the sonic point traverses the exit of the reaction zone. At this instant, the internal structure becomes isolated from the rarefaction wave and its associated damping rate.

In other words, the driving mechanism behind the decay is deactivated. As previously mentioned, the flow inside the internal detonation structure being out of equilibrium, a non-linear relaxation process towards the steady CJ regime starts, resulting in an increase of the velocity  $\dot{\alpha}_\tau$  after  $\tau_s$  and ultimately leading to a successful initiation.

The slowdown mechanism, leading to a minimum of propagation velocity well below the CJ velocity  $\dot{\alpha}_\tau < 0$  when the sonic point  $\xi_s$  approaches the end of the reaction  $\xi_b$  is clearly observed in Figure 3.21. The minimum propagation velocity  $\dot{\alpha}_\tau = -0.49$  is reached for  $\tilde{r}_f = 4.26$ . During the subsequent re-acceleration of the propagation

### 3.4 Direct initiation of a detonation

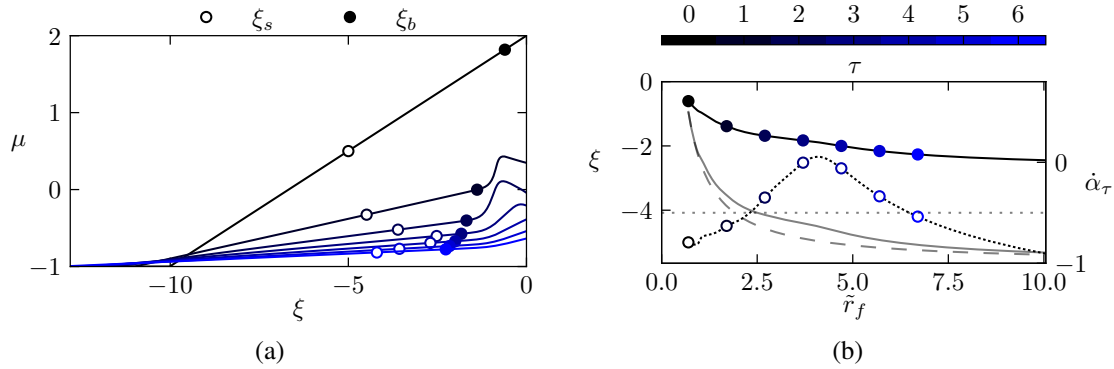


Figure 3.22: Results of the numerical integration of (3.55) and (3.56) for a stable spherical detonation ( $b = 1, j = 2$ ) for  $\dot{\alpha}_{\tau,c} = -0.5$  and  $\tilde{r}_{fi} = 0.7$  illustrating the slowdown mechanism in a detonation failure. The full points indicate the exit of the reaction zone  $\xi_b$  and the empty circles are the sonic points relative to the lead shock. (a) Profiles of the reduced flow velocity at different time steps  $\Delta\tau = 1$  from the initial solution at  $\tau = 0$  (black) to  $\tau = 6$  (blue). (b) End of reaction  $\xi_b$  and sonic point  $\xi_s$  trajectories with respect to the leading shock in black solid and dotted line, respectively. The trajectory  $\dot{\alpha}_\tau(\tilde{r}_f)$  is plotted in grey line with the horizontal line indicating the chemical-kinetics quenching in dashed line. The grey dashed line represents the trajectory of the inert blast wave.

velocity  $\dot{\alpha}_\tau(\tau)$  for  $\tilde{r}_f > 4.26$ , the position of the sonic point remains close to the end of the reaction, as in the solution of a steady and weakly curved self-sustained detonation with large activation energy. Notice that the minimum of propagation velocity  $\dot{\alpha}_\tau(\tau)$  occurs when the sonic point catches the exit of the internal structure of the reaction wave. This means that the external damping rate is balanced by the internal re-acceleration mechanism when the sonic condition is satisfied  $\mu(\xi_b, \tau) = \dot{\alpha}_\tau(\tau_s)$ .

The same mechanism is illustrated in Figure 3.22 in the case of a detonation failure. In this case, the decay in the propagation velocity induced by the external flow decreases as the sonic point gets closer to the end of the reaction, leading to a slowdown of the front trajectory with respect to the inert case. However, the propagation velocity drops below the chemical-kinetics quenching propagation velocity limit  $\dot{\alpha}_{\tau,c} = -0.5$  before the sonic point reaches the internal structure of the detonation, causing the reaction to freeze. At this point, there is no longer a stable self-sustained regime and the internal re-acceleration mechanism disappears, leading to the decay of the leading shock towards the acoustic regime.

To summarize, if the propagation velocity decreases below the leading shock propagation velocity which is necessary to heat the reactive mixture up to the crossover temperature before the sonic condition, then the initiation process is hindered.



### 3 Direct initiation of critical detonations in the small heat release asymptotic limit

#### *Shock wave formation in the internal structure*

In the induction zone, where the heat release is negligible, the curvature term on the right hand side of (3.55) makes the unsteady flow profile gradient negative near the leading shock. This leads to a velocity profile with a maximum value in the inner structure of the reaction wave, as illustrated in Figure 3.21a. A similar peak in pressure was observed in numerical simulations using the one-dimensional reactive Euler equations by Ng and Lee (2003), which they proposed to be the driving mechanism behind the re-acceleration of the wave and the initiation of detonation in the critical regime.

A negative gradient of flow velocity in the direction of propagation enables the formation of shock waves within the induction zone. This has been observed in the numerical solutions of (3.55) and (3.56) obtained for a low bound of the chemical-kinetics quenching  $\dot{\alpha}_{\tau,c}$  when the minimum of the trajectories  $\dot{\alpha}_{\tau}(\tau)$  is close to this threshold. This occurs when the initial radius is small enough, for example on the trajectory corresponding to  $\tilde{r}_{fi} = 0.3$  in Figure 3.20.

The physical relevance of a detonation propagating so close to the acoustic regime  $\dot{\alpha}_{\tau} \approx -1$  is questionable, as it corresponds to a cross-over temperature for the chemical-kinetics quenching that is close to the initial temperature. Mazaheri (1997) has also observed the formation of shocks during the re-acceleration of a detonation in numerical simulations of the one-dimensional reactive Euler equations for a one-step kinetic rate law. Lee and Higgins attributed this phenomenon to the simplicity of the single-step rate model, which lacks a crossover between chain-branching and chain-breaking reactions.

Indeed, this issue is also present with the scaling law for the three-step kinetics rate model when there is no crossover temperature or when it is too low. As such, further analysis is necessary to confirm the physical significance of the reignition by shock waves formed within the internal structure of the detonation.

#### *Infinite gradient of the self-similar solution*

The numerical results of successful initiation also serve to clarify the doubts raised due to the infinite gradient in the flow velocity at the front of a spherical rarefaction wave behind a CJ detonation (see Section 2.3.2). A first indication is given by the instantaneous profiles of the burnt-gas flow behind the reaction zone in Figure 3.21b after  $\tau = 3$ . Once the sonic point reaches and stays close to the end of the reaction zone, the rarefaction wave and the detonation internal structure get decoupled due to the sonic condition. While the rarefaction wave continues to be dampened by the curvature, the internal structure of the detonation re-accelerates towards the CJ regime, resulting in an increase in the flow velocity gradient at the sonic point and a narrowing of the reaction zone. The gradient at the front becomes infinite at the scale of the rarefaction wave, whose length increases linearly over time. When the numerical results for the reduced flow velocity are plotted in the self-similar variable (3.77), they approach asymptotically the self-similar solution (3.86) in the long time limit, as shown in Figure 3.23.

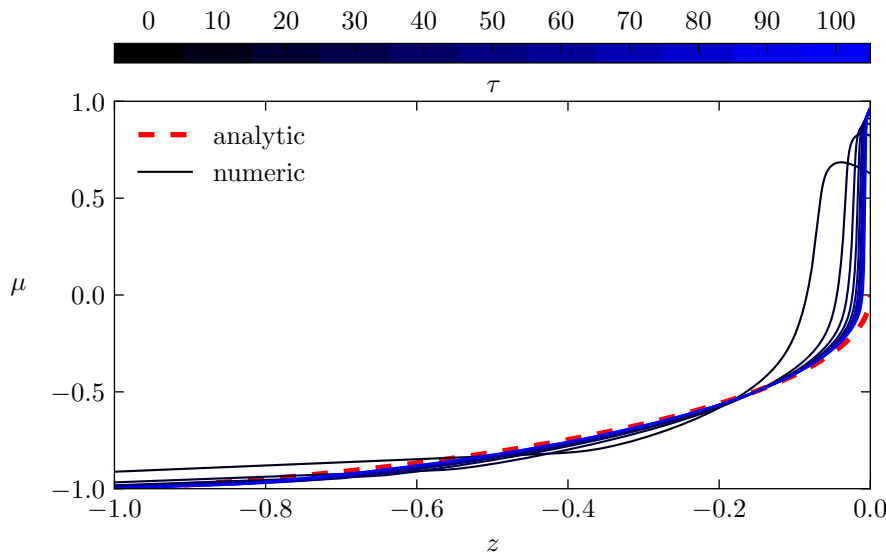


Figure 3.23: Flow velocity profile at different time steps  $\Delta\tau = 10$  from the initial profile at  $\tau = 0$  (black) to  $\tau = 100$  (blue) compared to the self-similar solution for the spherical rarefaction flow behind a CJ detonation considered as a discontinuity. The reduced flow profiles  $\mu(\xi, \tau)$  obtained numerically for a stable spherical detonation with  $b = 1$ ,  $j = 2$  and  $\dot{\alpha}_{\tau,c} = -0.5$  are plotted in the self-similar coordinate  $z = \xi/|\xi_0| = (r - r_f)/(r_f - r_0)$ . The dashed red line represents the self-similar solution (3.86).

## 3.5 Quasi-steady approximation

The internal structure of a detonation can be effectively described through the quasi-steady approximation when the response time of the wave is significantly shorter than the characteristic time of evolution of the boundary conditions. The study of He and Clavin (1994) revealed that, under the quasi-steady approximation, the flow divergence due to the curvature causes the emergence of a critical radius below which there is no steady solution for a detonation. This critical radius has been established in the small heat release limit (Clavin, 2019; Clavin and Denet, 2020). The critical radius appears as a turning point in the quasi-steady solutions, where the rate of change of the detonation propagation velocity is actually infinite. Therefore, the critical dynamics near the critical radius cannot be accurately described by the quasi-steady approximation. However, the quasi-steady approximation remains useful for the understanding of the dynamics of detonation initiation. It anticipates the existence of the critical radius, below which there is no steady solution for a detonation, and provides the steady solution for weakly curved detonations far enough from the critical point.

### 3.5.1 Steady internal structure of self-sustained detonations

The steady-state solution of the internal structure of the detonation corresponds to the solution of (3.55) and (3.56) when the unsteady term becomes negligible compared with

### 3 Direct initiation of critical detonations in the small heat release asymptotic limit

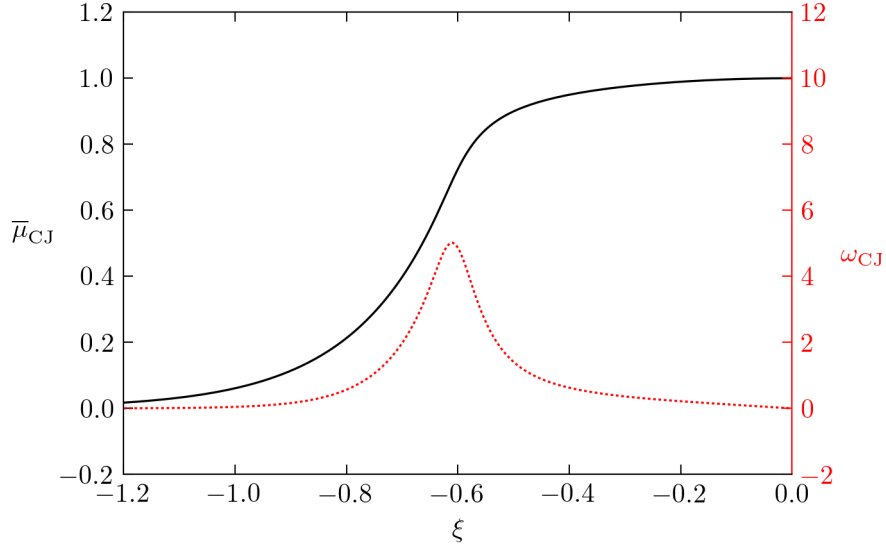


Figure 3.24: Flow velocity profile, in black line, in the internal structure of a CJ detonation for the simplified three-step kinetics rate model of Clavin and Denet (2018) whose corresponding reaction rate is represented in dotted red line.

the rest of the terms in the equation

$$\frac{\partial \bar{\mu}}{\partial \tau} = -(\bar{\mu} - \bar{\alpha}_\tau) \frac{\partial \bar{\mu}}{\partial \xi} + \frac{\omega}{2} + \frac{j}{2} \frac{1 + \bar{\mu}}{\tilde{r}_f} \approx 0 \quad (3.105)$$

$$\xi = 0 : \quad \bar{\mu} = 1 + 2\bar{\alpha}_\tau. \quad (3.106)$$

#### *CJ detonation waves*

In planar geometry, the self-sustained detonation regime is the so-called CJ regime and the internal structure of the detonation is described by

$$\bar{\mu}_{\text{CJ}} \frac{\partial \bar{\mu}_{\text{CJ}}}{\partial \xi} = \frac{\omega_{\text{CJ}}}{2}. \quad (3.107)$$

where the curvature term has been removed  $j = 0$  and  $\bar{\alpha}_{\tau\text{CJ}} = 0$  by definition. Integrating from the Neumann state at the front  $\bar{\mu}(\xi = 0) = 1$ , as given by (3.106), the flow velocity profile is given by  $\bar{\mu}_{\text{CJ}}(\xi) = \sqrt{1 - \int_\xi^0 \omega_{\text{CJ}}(\xi') d\xi'}$ . The velocity profile obtained for the simplified three-step kinetics rate of Clavin and Denet (2018) is represented in Figure 3.24.

#### *Steady curved self-sustained waves*

The steady-state solutions for weakly curved self-sustained waves in the small heat release limit has been extensively studied in a series of works by Clavin (2019), Clavin and Denet (2020), and Clavin et al. (2021a). The propagation velocity  $\bar{\alpha}_{\tau\text{CJ}}$  of weakly curved

### 3.5 Quasi-steady approximation

self-sustained detonations for a given front radius  $\tilde{r}_f$  is obtained through integration of (3.105) within the internal structure of the detonation.

As illustrated in Figure 3.21, the sonic point in self-sustained detonations is consistently located close to the end of the reaction zone. Therefore, the difference between  $\xi_{s_{CJ}}$  and  $\xi_{b_{CJ}}$  has limited effect on the analysis. Neglecting this difference is all the more justified since the heat released in the region delimited by these points is negligible given the long tail of the reaction rate distribution. Consequently, as discussed in detail in Clavin and Denet (2020), the sonic condition can be considered to hold at the end of the reaction zone

$$\xi = \xi_s \approx \xi_b : \quad \bar{\mu} = \bar{\alpha}_\tau. \quad (3.108)$$

Integration of (3.105) from  $\xi_b$  to  $\xi = 0$ , using the boundary conditions (3.106) and (3.108), yields

$$\frac{1}{2} (1 + \bar{\alpha}_\tau)^2 = \frac{1}{2} - \frac{j}{2} \frac{1}{\tilde{r}_f} \int_{\xi_b}^0 [1 + \bar{\mu}(\xi)] d\xi \quad (3.109)$$

recalling that by definition  $\int_{\xi_b}^0 \omega(\xi) d\xi = 1$ . The term on the left-hand side of the equation quantifies the amount of advection required in the internal structure to sustain the propagation of the detonation with a velocity  $\bar{\alpha}_{\tau_{CJ}}$ . The unity quantity on the right-hand side accounts for the expansion of the combustion products, which push the wave forward. The second term on the right-hand side appears due to the additional advection required to propagate the front with a curved internal structure. It is clear that the expansion of the combustion products suffices to propagate a CJ wave with its corresponding velocity  $\bar{\alpha}_{\tau_{CJ}} = 0$ . However, for curved detonations, the expansion of the combustion products must also balance the flow divergence introduced by the curved geometry, resulting in a slower propagation velocity  $\bar{\alpha}_\tau < \bar{\alpha}_{\tau_{CJ}} = 0$ .

The non-linear relationship between the propagation velocity  $\bar{\alpha}_\tau$  and the front radius  $\tilde{r}_f$  is given by the following expression where the variable of integration has been scaled with the thickness of the reaction zone  $|\xi_b| = e^{-b\bar{\alpha}_\tau}$

$$\bar{\alpha}_\tau + \frac{\bar{\alpha}_\tau^2}{2} = -\frac{j}{2} \frac{e^{-b\bar{\alpha}_\tau}}{\tilde{r}_f} \left[ 1 + \int_{-1}^0 \bar{\mu}(e^{-b\bar{\alpha}_\tau} \xi) d\xi \right]. \quad (3.110)$$

The difficulty in determining the value of the integral of the flow velocity profile in a curved wave can be addressed by focusing on propagation regimes that are close enough to the CJ regime  $\bar{\alpha}_\tau \ll 1$ , such that the flow velocity profile  $\bar{\mu}(\xi)$  can be approximated by the velocity profile of the CJ wave  $\bar{\mu}_{CJ}(\xi)$ . Under this approximation, the non-linear relation (3.110) can be simplified to

$$\bar{\alpha}_\tau \ll 1 : \quad \bar{\alpha}_\tau \approx -\frac{j}{2} \frac{e^{-b\bar{\alpha}_\tau}}{\tilde{r}_f} \lambda \quad (3.111)$$

### 3 Direct initiation of critical detonations in the small heat release asymptotic limit

where  $\lambda$  is a constant of order unity defined as

$$\lambda \equiv 1 + \int_{-1}^0 \bar{\mu}_{\text{CJ}}(\xi) d\xi. \quad (3.112)$$

Introducing the notation

$$x \equiv \frac{2}{j} \frac{\tilde{r}_f}{\lambda b} \quad \text{and} \quad y \equiv b \bar{\alpha}_\tau \quad (3.113)$$

for the front radius and the propagation velocity, respectively, the non-linear relationship is given by the transcendental equation free from parameter

$$y \ll 1/b : \quad y = -\frac{e^{-y}}{x}. \quad (3.114)$$

The roots of equation (3.114), represented in Figure 3.25, exhibit a turning point at  $y^* = -1$  and  $x^* = e$ , similarly to the opposite limit of large Mach number He and Clavin (1994). For front radii below the critical value  $\tilde{r}_f < \tilde{r}_f^* = e\lambda bj/2$ , there is no steady-state solution for a curved detonation wave. Above the critical radius, the roots of the equation provide the nonlinear relationship between the steady propagation velocity  $\bar{\alpha}_\tau$  and the front radius  $\tilde{r}_f$  with two branches of solutions. As mentioned above, the curved self-sustained detonations propagate slower than the CJ velocity  $\bar{\alpha}_\tau < \bar{\alpha}_{\tau\text{CJ}} = 0$ . The solutions on the upper branch approach the CJ regime  $\bar{\alpha}_\tau \rightarrow 0$  as the radius increases  $x \rightarrow \infty$  (i.e. the curvature fades away) while the solutions from the lower branch keep decelerating as the curvature vanishes. While the behavior of the upper branch allows the coupling between the curved solution and the CJ solution, the behavior of the lower branch lacks physical significance. Additionally, the lower branch solutions are unstable, since any infinitesimal acceleration of the wave will cause a reacceleration towards the upper branch.

It should be noted that the nonlinear relationship (3.114) is derived under the assumption that the propagation velocity is close to the CJ velocity  $\bar{\alpha}_\tau \ll 1$ . Therefore, the validity of this relationship near the turning point  $\bar{\alpha}_{\tau\text{CJ}}^* \sim -1/b$  is limited to still larger activation energies  $b \gg 1$ .

#### 3.5.2 Steady internal structure of overdriven waves

In this subsection, the quasi-steady approximation of the internal structure is revisited considering an overdriven wave with a burned gas flow given by the external solution developed in Section 3.3. The quasi-steady approximation for such a wave corresponds to the solution of (3.101) to (3.103) when the unsteady term is negligible with respect to the rest of the terms in the equation

$$\frac{\partial \bar{\hat{\mu}}}{\partial \tau} = -(\bar{\hat{\mu}} - \bar{\alpha}_\tau) \frac{\partial \bar{\hat{\mu}}}{\partial \xi} + \frac{\omega}{2} - \frac{\bar{\hat{\mu}}}{\tilde{r}_f} - \frac{\partial}{\partial \xi} [\bar{\mu}^{\text{ext}}(\tau) \bar{\hat{\mu}}] \approx 0 \quad (3.115)$$

### 3.5 Quasi-steady approximation

$$\xi = 0 : \quad \bar{\mu} = 1 + 2\bar{\alpha}_\tau - \mu_f^{\text{ext}}(\tau) \quad (3.116)$$

$$\xi = \xi_b : \quad \bar{\mu} = 0 \quad (3.117)$$

Integrating equation (3.115) from the end of the reaction zone (3.116) to the leading shock (3.117) results in an implicit relationship between the propagation velocity and the front radius  $\bar{\alpha}_\tau(\tilde{r}_f)$  involving the solution of the velocity profile in the internal structure  $\bar{\mu}(\xi)$

$$\bar{\alpha}_\tau + \mu_f^{\text{ext}}\bar{\alpha}_\tau = -\frac{j}{2}\frac{1}{\tilde{r}_f}\int_{\xi_b}^0\bar{\mu}(\xi)d\xi + \frac{(\mu_f^{\text{ext}})^2}{2} \quad (3.118)$$

For propagation velocities that are close enough to the CJ regime  $\bar{\alpha}_\tau \ll 1$ , a closed equation linking the propagation velocity  $\bar{\alpha}_\tau$  and the front radius  $\tilde{r}_f$  through the external flow velocity solution  $\mu_f^{\text{ext}}$  can be derived by replacing the velocity profile  $\bar{\mu}(\xi)$  with the velocity profile of the CJ solution  $\bar{\mu}_{\text{CJ}}(e^{b\bar{\alpha}_\tau}\xi)$

$$\bar{\alpha}_\tau \ll 1 : \quad \bar{\alpha}_\tau(1 + \mu_f^{\text{ext}}) \approx -\frac{j}{2}\frac{e^{-b\bar{\alpha}_\tau}}{\tilde{r}_f}(\lambda - 1) + \frac{(\mu_f^{\text{ext}})^2}{2} \quad (3.119)$$

By utilizing the notation introduced in (3.113), the nonlinear relationship between the front radius  $\tilde{r}_f$  and the propagation velocity  $\bar{\alpha}_\tau$  for an overdriven wave with a burnt-gas flow  $\mu_f^{\text{ext}}$  is expressed by the following transcendental equation

$$\bar{\alpha}_\tau \ll 1 : \quad y(1 + \mu_f^{\text{ext}}) = -\frac{\lambda - 1}{\lambda}\frac{e^{-y}}{x} + \frac{b(\mu_f^{\text{ext}})^2}{2} \quad (3.120)$$

The roots of equation (3.120) are plotted in Figure 3.25 for various values of the burnt-gas flow  $\mu_f^{\text{ext}}$ . These relationships also exhibit a turning point, similar to that observed for the relationship (3.114), although it is slightly shifted. For  $\mu_f^{\text{ext}} = 0$ , the turning point lies on  $y^* = -1$  and  $x^* = e(\lambda - 1)/\lambda$ . Consequently, a small correction is made to the critical front radius  $\tilde{r}_f^* = ej(\lambda - 1)b/2$ , which still corresponds to a non-dimensional front radius  $\tilde{r}_f/b$  of order unity.

Examples of the trajectories propagation velocity  $\bar{\alpha}_\tau$  versus front radius  $\tilde{r}_f$  obtained from numerical integration of (3.55) and (3.56) are presented in Figure 3.26 and compared to the solutions obtained for the quasi-steady approximation. In all cases, it is observed that the successfully initiated detonations follow the solution of the quasi-steady approximation for self-sustained waves in curved geometries. The minimum of propagation velocity in all trajectories is also located in the region bounded by the steady-state curve for self-sustained detonations and that of overdriven waves with a critical value of the burnt-gas flow  $\mu_f^{\text{ext}} = 0$ .

In conclusion, the quasi-steady approximation cannot describe accurately the critical dynamics of direct initiation of spherical detonations. However, it does provide valuable insight as it gives an approximate location for the critical radius below which there is no solution for a self-sustained detonation. The quasi-steady approximation has been revisited for overdriven detonations with a specified burnt-gas flow. In this case, the

### 3 Direct initiation of critical detonations in the small heat release asymptotic limit

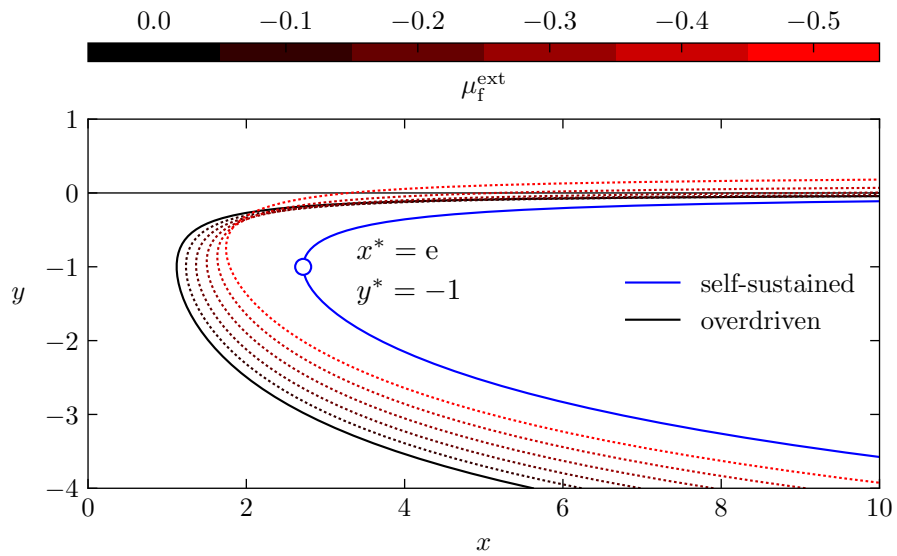


Figure 3.25: Steady-state detonation waves in curved geometries in terms of the variables  $y \equiv b\bar{\alpha}_\tau$  and  $x = \tilde{r}_f/(b\lambda j/2)$ . The blue line in the plot represents the roots of (3.114), which depict the relationship between the front radius and the propagation velocity of self-sustained curved detonation waves in steady-state. A turning point can be observed at  $(x^*, y^*)$ . The roots of (3.120), which depict the relationship between the front radius and the propagation velocity of overdriven waves in steady-state, are plotted in dashed lines, ranging from black to red, for different values of the burnt-gas flow  $\mu_f^{\text{ext}}$ . The solid black line corresponds to the critical value of burnt-gas flow in the discontinuous model  $\mu_f^{\text{ext}} = 0$ .

### 3.5 Quasi-steady approximation

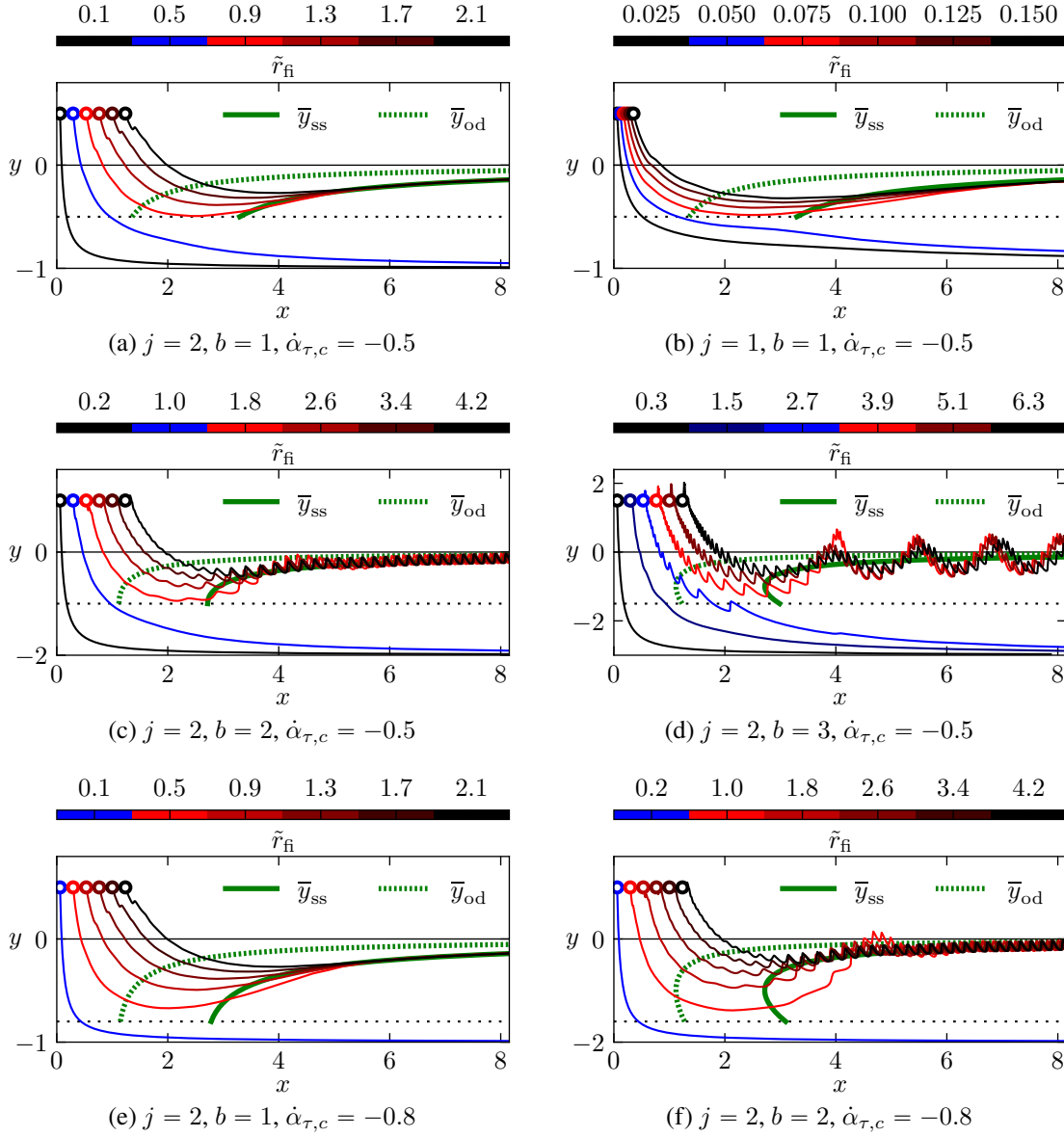


Figure 3.26: Comparison of the trajectories propagation velocity vs. front radius obtained by numerical integration of (3.55) and (3.56) with the nonlinear relationships of steady-state detonation waves. The green solid line represents the roots of (3.114) for self-sustained detonation waves in steady state while the dashed solid line represents the roots of (3.120) for overdriven waves with a burnt-gas flow  $\mu_f^{\text{ext}} = 0$ . (a) Spherical stable detonation wave. (b) Cylindrical stable detonation wave. (c-d) Spherical weakly unstable detonation waves. (e-f) Spherical detonation waves with a low chemical-quenching limit.



### 3 Direct initiation of critical detonations in the small heat release asymptotic limit

critical radius becomes slightly smaller, but retains the same order of magnitude. The critical radius of steady overdriven detonations is obtained for a dimensionless front radius  $\tilde{r}_f/b$  of order unity

$$\frac{r_f^*}{a_u t_{rN}} = \frac{j}{2} \frac{b}{\epsilon} e \int_{-1}^0 \mu_{CJ}(\xi) d\xi. \quad (3.121)$$

The numerical results represented as trajectories in the propagation velocity versus front radius plane show a minimum in the propagation velocity. This local extreme of the detonation velocity lies within the limits given by the quasi-steady solutions for a self-sustained wave and an overdriven wave. In the long time limit, these trajectories also exhibit good agreement with the steady-state solutions for self-sustained detonation waves in curved geometries.

## 3.6 Summary

The direct initiation process, through which a self-sustained detonation is generated in the decay of a initially inert blast wave, has been investigated in the limit of small heat release coupled with the Newtonian approximation, with a particular focus on the critical regime. The detonation model derived from general conservation equations in this limit has been used to investigate the dynamics of the combustion products behind a supersonic reactive discontinuity, the dynamics of a detonation when considering its internal structure, and the steady-state solutions.

First, analytical expressions have been found for the rarefaction wave behind an infinitesimally thin detonation in both the self-sustained regime and the decaying overdriven regime. The transitory regime from the overdriven to the self-sustained regime has been described in terms of the propagation of a weak discontinuity along the corresponding characteristic curve that separates the two solutions. Both regimes described by analytical expressions, as well as the transitory regime, have been verified by comparing them with results obtained by numerical integration.

Then, the problem of direct initiation has been investigated considering the internal structure of the detonation by numerical methods. The analysis of the numerical results for the critical dynamics has helped to clarify the slowdown observed prior to the onset of self-sustained detonation. The slowdown is shown to be related to the setting of the sonic condition in the internal structure of the detonation.

Finally, new analytical expressions of the quasi-steady approximation have been provided for the establishment of the sonic condition in the overdriven decaying regime. The numerical results that take into account the internal structure of the detonation have been compared with these new quasi-steady solutions as well as with the quasi-steady solutions determined in previous works for the self-sustained detonations in the small heat release limit.

---

## Deflagration-to-detonation transition at the tip of a flame in thin tubes

---

This chapter examines a one-dimensional flame model that reproduces the runaway mechanism for Deflagration-to-Detonation Transition in elongated flames propagating throughout thin tubes. This flame acceleration mechanism is driven by the thermal feedback of compression waves on the flame speed and flame surface area increase due to the interaction of the flame with the tube walls. The nonlinear relationship between the flame velocity and the elongation parameter are investigated through the double-discontinuity model where the precursor shock wave and the flame are considered to be infinitesimally thin. Two different relations are obtained for a steady and a quasi-steady regime with a uniform flow and an isentropic compression wave between discontinuities, respectively. These relationships are compared with numerical results obtained through integration of the Navier-Stokes equations. The results demonstrate that the double feedback loop of the elongated flame model can cause a flame acceleration runaway within a finite time with the potential to initiate the formation of a strong shock wave that triggers the onset of a detonation.

---

4.1	Introduction . . . . .	100
4.2	Elongated flame tip model . . . . .	102
4.2.1	Governing equations . . . . .	102
4.2.2	Steady planar flame . . . . .	106

## 4 Deflagration-to-detonation transition at the tip of a flame in thin tubes

4.2.3	One-dimensional model at the flame tip	114
4.3	Double-discontinuity model	118
4.3.1	Self-similar solutions	120
4.3.2	Isentropic compression waves	122
4.4	Internal flame structure	127
4.4.1	Numerical method	128
4.4.2	Steady flame propagation	132
4.4.3	Slow flame elongation	138
4.5	Summary	148

### 4.1 Introduction

The Deflagration-to-Detonation Transition (DDT) is a poorly understood phenomenon in combustion that has been studied for over a century. Since the pioneering experiments of Urtiew et al. (1966), numerous efforts have been devoted to the investigation of this phenomenon and continues to be so, as attested by a number of recent reviews by Oran and Gamezo (2007), Dorofeev (2011), and Oran (2015). Despite this amount of research, the fundamental mechanisms of DDT, through which a subsonic reaction-diffusion flame abruptly turns into a supersonic reaction wave, has not yet been agreed upon. Various forms of DDT have been observed in experiments suggesting different mechanisms (see Lee (2008) and Clavin and Searby (2016) and references therein), rendering challenging the quest of an universal mechanism

A first attempt at proposing an universal mechanism was made by Shelkin (1940) (Zeldovich et al., 1985) related to the development of a turbulent flow due to the non-slip condition on the tube walls along which the flame propagates. When a flame propagates from the closed end of a tube, the expansion of the combustion products induces a flow in the fresh gases. The friction of this flow with the tubes generates a velocity gradient that bends the flame surface increasing the propagation velocity. When the Reynolds number characterizing the induced flow is sufficiently large, the flow becomes turbulent and a positive feedback mechanism can develop. The turbulence of the fresh gases wrinkles the flame front increasing the propagation velocity and in turn increasing the turbulence intensity.

The plausible explanation of DDT from Shelkin spread among the scientific community the view that flame acceleration is impossible without turbulence. For this reason, the theoretical study of DDT was precluded by the study of turbulent combustion, which is a key problem in combustion science (Clavin, 1985; Ronney, 1995; Veynante and Vervisch, 2002). Even if the difficulties of combustion are forgotten, turbulence itself remains a matter of controversy even in the simplest configurations (Pomeau and Manneville, 1980; Hof et al., 2004). Therefore, the explanation of Shchelkin never materialized in a theory for DDT capable of describing the process in detail and predicting its occurrence.

The Darius-Landau (DL) hydrodynamic instability, which causes an amplification of the perturbations of a planar flame to be further amplified due to the density jump through

the flame, was later proposed as a mechanism for flame acceleration (Darrieus, 1938; Landau, 1944). The corrugation of the flame introduced by this instability increases the surface area of the flame which accelerates its propagation velocity. However, recent studies of the DL instability for realistic values of expansion through the flame show that the acceleration induced by this instability in narrow tubes is too short and too weak to initiate a detonation (Bychkov and Liberman, 2000).

A different mechanism for DDT based on the friction-induced adiabatic compression has been discussed in (Brailovsky and Sivashinsky, 2000; Kagan and Sivashinsky, 2008; Brailovsky et al., 2012). Under sufficient friction, the fresh gases undergo a process of adiabatic compression which increases its temperature. This mechanism, termed hydraulic resistance, has been extensively studied through one-dimensional models.

Recent experiments (Wu et al., 2007; Kuznetsov et al., 2010; Liberman et al., 2010; Wu and Wang, 2011; Ballossier et al., 2021; Melguizo-Gavilanes et al., 2021a; Bykov et al., 2022) and multidimensional direct numerical simulations (Liberman et al., 2010; Melguizo-Gavilanes et al., 2021a; Liu et al., 2022) have contributed to a more comprehensive understanding of DDT. The results presented by these studies support the idea that turbulence has a supplementary role in flame acceleration (Kagan and Sivashinsky, 2003; Ott et al., 2003). It is observed that the onset of the detonation is a localized phenomenon, occurring within or close to the internal flame structure, and that DDT can occur in the absence of turbulence.

A simple one-dimensional model leading to the runaway mechanism of DDT has been recently proposed and examined (Clavin and Tofaili, 2021; Clavin and Champion, 2022; Clavin, 2022; Tofaili, 2022) whose critical conditions correspond with the experimental and numerical observations of Kuznetsov et al. (2010), Liberman et al. (2010), and Ivanov et al. (2011). This model builds on an earlier theoretical study by Deshaies and Joulin (1989) who derived the self-similar solutions of the double-discontinuity model using the weak shock approximation and a high thermal sensitivity of the laminar flame speed, along with the introduction of a folding parameter to account for the flame acceleration resulting from surface wrinkling. They showed that due to the thermal feedback of the lead shock on the flame speed, self-similar solutions no longer exist above a critical value of the folding parameter. Similarly, Clavin and Tofaili (2021) and Tofaili (2022) (CT) have established a novel one-dimensional (1D) model for elongated flames, where the folding parameter is replaced by an elongation parameter. An additional feedback mechanism is introduced through the piston effect of a back-flow of burned gas towards the tip of the elongated flame, which is caused by the expansion of the combustion products from the flame skirt and is therefore proportional to the burning velocity. The self-similar solutions neglect the dynamics of the compression waves between the flame and the leading shock assuming the flow in between remains uniform. In the vicinity of the critical point, where the flame acceleration diverges, the uniform flow approximation cannot be valid due to the rapid emission of compression waves. Nonetheless, the CT model is also suitable for investigating the unsteady compression waves that lead similarly to a finite-time singularity (Clavin, 2022).

The goal of this study is to explore the impact of the backflow of burned gases

## 4 Deflagration-to-detonation transition at the tip of a flame in thin tubes

introduced by the CT model on the unsteady internal flame structure through numerical integration within the framework of the DDT. This chapter presents the numerical results obtained for the CT model considering chemical-kinetics of a one-step reaction model with a rate governed by an Arrhenius law. A 1D unsteady flow of perfect gas has been simulated with the boundary conditions imposed by the CT model through the numerical integration of the reactive compressible Navier-Stokes (NS) equations.

### *Structure of the chapter*

The subsequent sections of this chapter investigate the deflagration-to-detonation transition occurring at the tip of elongated flames propagating in laminar regime along thin tubes. The structure of this sections is as follows: Section 4.2 presents the one-dimensional flame model utilized in this study. Section 4.3 examines the external flow generated by the interaction between a flame propagating in a semi-closed tube and the leading shock wave, when both waves are considered as a discontinuity. Section 4.4 extends the analysis by numerically integrating the conservation equations in the internal structure of the flame. Finally, the conclusions and future perspectives of the study are summarized in Section 4.5.

## **4.2 Elongated flame tip model**

The dynamics of the transition from a deflagration to a detonation are investigated utilizing the model of Clavin and Tofaili (2021) to study the consequences of the flame self-acceleration at the tip of elongated flames propagating in narrow channels. The model proposed by Clavin and Tofaili considers the propagation of a one-dimensional laminar flame, which undergoes an acceleration as a consequence of the development of a backflow of the combustion products from the flame skirt adjacent to the channel wall. This backflow acts as a piston behind the flame tip. In the framework of this model, mechanisms such as hydraulic resistance and heat losses to the walls are assumed to play a less significant role at the centerline of the channel, along which the flame tip propagates.

In this section, the mathematical formulation that will be used in the study is presented, along with a description of the proposed model. Additionally, certain simplifying assumptions related to the thermochemical aspects of the problem are introduced. These assumptions serve to reduce the complexity of the problem, allowing a careful examination of the gas dynamics aspects.

### **4.2.1 Governing equations**

The analysis of the deflagration-to-detonation transition requires investigating the interplay between a premixed flame and compressible waves such as shock waves or unsteady compression waves. The internal structure of a flame consists of a thin reactive layer where chemical reactions of combustion occur, and a preheating zone where heat is

transported by diffusion ahead of the reactive layer. The heat of reaction is released in the reactive layer, and a portion of this heat is transferred through conduction to the fresh mixture, which subsequently reacts and propagates the flame. Although the propagating velocity resulting from this mechanism is markedly subsonic, compressible effects are retained in order to explore their interaction with the flame. The unsteady propagation of a one-dimensional flame is then described by the mass, momentum, and energy conservation laws known as Navier-Stokes equations supplemented with conservation equations for the different chemical species (Williams, 1985).

### Reactive one-dimensional Navier-Stokes equations

This study considers the application of the reactive Navier-Stokes equations in a one-dimensional rectangular geometry, where the velocity vector is  $\mathbf{u}' = (u', 0, 0)$ , the gradient operator  $\nabla \mathbf{u}' = (\partial u' / \partial r', 0, 0)$ , and the divergence operator  $\nabla \cdot \mathbf{u}' = \partial u' / \partial r'$ . In dimensional units, these equations can be written as follows

$$\frac{\partial \rho'}{\partial t'} + \frac{\partial(\rho' u')}{\partial r'} = 0, \quad (4.1)$$

$$\rho' \left( \frac{\partial u'}{\partial t'} + u' \frac{\partial u'}{\partial r'} \right) + \frac{\partial p'}{\partial r'} = \frac{\partial}{\partial r'} \left( \mu' \frac{\partial u'}{\partial r'} \right), \quad (4.2)$$

$$\rho' \left( \frac{\partial E'}{\partial t'} + u' \frac{\partial E'}{\partial r'} \right) + \frac{\partial(\rho' u')}{\partial r'} \partial r' = \left( \lambda' \frac{\partial T}{\partial r'} \right) + \frac{\partial}{\partial r'} \left( \mu' u' \frac{\partial u'}{\partial r'} \right) + \rho' q'_m \omega', \quad (4.3)$$

$$\rho' \left( \frac{\partial Y}{\partial t'} + u' \frac{\partial Y}{\partial r'} \right) = \frac{\partial}{\partial r'} \left( \rho' D' \frac{\partial Y}{\partial r'} \right) + \rho' \omega'. \quad (4.4)$$

Equations (4.1) and (4.2) represent the conservation of mass and momentum, respectively, for Newtonian fluids. The third equation (4.3) describes the conservation of total specific energy  $E'$ , which is defined as the sum of internal thermal specific energy and specific kinetic energy of the gas  $E' = e'_T + u'^2/2$ . Equation (4.4) represents the conservation of a product of the combustion, while it can also be written for a reactant by changing the sign ahead of the reaction rate.

For compressible flows, the conservation of energy is coupled with the fluid mechanics problem through an equation of state. For ideal gases, this equation of state can be expressed as

$$p' = (\gamma - 1) c'_v \rho' T' \quad (4.5)$$

where  $\gamma \equiv c'_p / c'_v$  is the ratio of specific heat capacities.

The primary goal of this study is to examine the fundamental physical mechanisms that govern the internal structure of the flame. In order to achieve this objective, the thermophysical properties of the mixture, including viscosity  $\mu'$ , thermal conductivity  $\lambda'$ , and the specific heat capacities at constant pressure  $c'_p$  and constant volume  $c'_v$ , are assumed to be constant

#### 4 Deflagration-to-detonation transition at the tip of a flame in thin tubes

##### *Conservative form*

Numerical methods employed for gas dynamics problems involving of shock waves are typically designed to solve purely conservative equations. The set of conservation equations (4.1) to (4.4) can be expressed in a conservative form where only the non conservative terms related to the effects of molecular collisions remain on the left-hand side with the right-hand side representing a purely conservative problem. This can be accomplished by subtracting the continuity equation (4.1) multiplied by the corresponding transported quantity from the equations (4.2) to (4.4), resulting in

$$\frac{\partial(\rho'u')}{\partial t'} + \frac{\partial(\rho'u'^2)}{\partial r'} + \frac{\partial p'}{\partial r'} = \mu' \frac{\partial^2 u'}{\partial r'^2}, \quad (4.6)$$

$$\frac{\partial(\rho'E')}{\partial t'} + \frac{\partial(\rho'E'u')}{\partial r'} + \frac{\partial(p'u')}{\partial r'} = \lambda' \frac{\partial^2 T'}{\partial r'^2} + \frac{\partial}{\partial r'} \left( \mu' u' \frac{\partial u'}{\partial r'} \right) + \rho' q'_{\text{m}} \omega', \quad (4.7)$$

$$\frac{\partial(\rho'Y)}{\partial t'} + \frac{\partial(\rho'Y u')}{\partial r'} = \rho' D' \frac{\partial^2 Y}{\partial r'^2} + \rho' \omega'. \quad (4.8)$$

This approach facilitates the use of numerical methods that preserve conservation properties of the equations, enabling more accurate and physically meaningful solutions to be obtained.

##### *Chemical-kinetics model*

The set of conservation equations (4.1) and (4.6) to (4.8), in which the constitutive relations for the viscous stresses, heat and molecular transfer have already been incorporated, together with the ideal gas law (4.5) form a closed set of equations for  $\rho'$ ,  $p'$ ,  $u'$ ,  $T'$  and  $Y'$  when a reaction rate is defined in terms of the thermodynamic variables  $\omega' = \omega'(T', Y')$ . In an effort to simplify the problem and retain only its fundamental aspects, the simplest description of the chemical interactions underlying the overall reaction is employed. These interactions are modelled as a single, irreversible exothermic reaction, represented as



where an inelastic collision between  $\nu$  molecules of a single reactant R gives rise to  $\nu$  molecules of a less energetic product P, releasing the energy difference as heat. The reaction rate is controlled by a law of mass action that is proportional to the product of reactant concentrations, which, in this simple model, corresponds to the power  $\nu$  of the reactant concentration  $C_R$ . The rate of product generation in this simplified model can be then expressed mathematically as

$$\frac{1}{C'_{\text{P,b}}} \frac{dC'_P}{dt'} = \left( \frac{C'_R}{C'_{\text{P,b}}} \right)^\nu \frac{1}{t'_r}. \quad (4.10)$$

where  $C'_{P,b}$  represents the concentration of the products in the burned mixture at equilibrium and is introduced for the nondimensionalization of the equation. The rate of chemical transformations resulting from inelastic collisions, denoted by  $1/t'_r$ , is only a small fraction of the rate of elastic collisions  $1/t'_{coll}$  which can be described by an Arrhenius law

$$\frac{1}{t'_r} = \frac{1}{t'_{coll}} B \exp\left(-\frac{E'_a}{k_B T'}\right). \quad (4.11)$$

where  $E'_a$  is the activation energy, which is much larger than the thermal agitation in the burnt gas,  $k_B'$  is the Boltzmann constant, which relates the average kinetic energy of the particles to the thermodynamic temperature,  $B$  is the dimensionless pre-exponential factor, and  $1/t'_{coll}$  is the frequency of elastic collision. The exponential term in the equation accounts for the fraction of reactant molecules that possess enough thermal energy to overcome the activation energy barrier, as determined by the Maxwell-Boltzmann distribution. The value of this part term from zero, when all molecules lack sufficient energy to undergo chemical transformation, to one in the ideal but impossible situation where all molecules possess enough energy to react upon collision. The pre-exponential factor  $B$  represents the fraction of energetic collisions that result in a chemical transformation. The molecular-level intricacies of chemical transformations, such as the steric hindrance, can restrict the fraction of energetic collisions that result in successful reactions, leading to a value of  $B$  smaller than unity. The definition of the molecular concentration  $C'_i \equiv N'_i/V'$  where  $N'_i$  denotes the number of molecules in a volume  $V'$ , is used to determine the mass fraction of a species  $i$ , which is nondimensional by definition, given by  $Y_i = C'_i W'_i / \rho'$ . The rate of product mass fraction increase is expressed as

$$\omega' = \frac{dY}{dt'} = (1 - Y)^\nu \frac{B}{t'_{coll}} \exp\left(-\frac{E_a}{k_B T}\right). \quad (4.12)$$

This is the minimal model that demonstrates the role of thermal feedback in flame propagation.

### Initial conditions

When examining the mechanism that can drive the Deflagration-to-Detonation Transition under controlled laboratory conditions within a tube, the reactive gas mixture is considered to be initially motionless, chemically frozen and homogeneous. Specifically, the boundary conditions far ahead of the flame are

$$x \rightarrow \infty : \quad \rho' = \rho'_o, \quad u = 0, \quad p' = p'_o, \quad T' = T'_o, \quad Y = 0 \quad (4.13)$$

$$\frac{d\rho'}{dx'} = \frac{du'}{dx'} = \frac{dp'}{dx'} = \frac{dT'}{dx'} = \frac{dY}{dx} = 0. \quad (4.14)$$

Here,  $\rho'_o$ ,  $p'_o$  and  $T'_o$  denote the unperturbed density, pressure and temperature, respectively



### 4.2.2 Steady planar flame

The internal structure of a steady flame is conveniently studied in the moving coordinate system attached to an arbitrary position moving with the reactive wave  $r_f$ , such as the position of maximum reaction rate or the position of an isovalue in the reactant mass fraction for instance. The position of the front  $r'_f(t')$  advances with a velocity denoted  $u'_f \equiv dr'_f/dt'$  through a reactive mixture initially at rest. In the coordinate system of the wave

$$x' = r' - r'_f(t), \quad \frac{\partial}{\partial r'} \rightarrow \frac{\partial}{\partial x'}, \quad \frac{\partial}{\partial t'} \rightarrow \frac{\partial}{\partial t'} - u'_f \frac{\partial}{\partial x'} \quad (4.15)$$

the conservation equations (4.1) and (4.6) to (4.8) are written as

$$\frac{\partial \rho'}{\partial t'} - \frac{\partial m'}{\partial x'} = 0, \quad (4.16)$$

$$\frac{\partial(\rho'u')}{\partial t'} - \frac{\partial(m'u')}{\partial x'} + \frac{\partial p'}{\partial x'} = \mu' \frac{\partial^2 u'}{\partial x'^2}, \quad (4.17)$$

$$\frac{\partial(\rho'E')}{\partial t'} - \frac{\partial(m'E')}{\partial x'} + \frac{\partial(p'u')}{\partial x'} = \lambda' \frac{\partial^2 T'}{\partial x'^2} + \mu' \frac{\partial}{\partial x'} \left( u' \frac{\partial u'}{\partial x'} \right) + \rho' q'_m \omega', \quad (4.18)$$

$$\frac{\partial(\rho'Y)}{\partial t'} - \frac{\partial(m'Y)}{\partial x'} = \rho' D' \frac{\partial^2 Y}{\partial x'^2} + \rho' \omega'. \quad (4.19)$$

where  $m' \equiv \rho'(u'_f - u') = \rho'U'$  denotes the mass flux trough the wave and  $U'$  is the velocity of the flame with respect to the flow.

When considering the internal structure of a flame that is propagating in a steady regime, the various terms in the conservation equations (4.16) to (4.19) must balance each other, resulting in the elimination of unsteady terms. As a result, the steady internal structure of the flame can be described by the following system of equations

$$\frac{dm'}{dx'} = 0, \quad (4.20)$$

$$\frac{d(m'u')}{dx'} - \frac{dp'}{dx'} + \mu' \frac{d^2 u'}{dx'^2} = 0, \quad (4.21)$$

$$\frac{d(m'E')}{dx'} - \frac{d(p'u')}{dx'} + \lambda' \frac{d^2 T'}{dx'^2} + \mu' \frac{d}{dx'} \left( u' \frac{du'}{dx'} \right) + \rho' q'_m \omega' = 0, \quad (4.22)$$

$$\frac{d(m'Y)}{dx'} + \rho' D' \frac{d^2 Y}{dx'^2} + \rho' \omega' = 0. \quad (4.23)$$

where the first equation, which represents mass conservation, indicates that the mass flux through a steady deflagration wave remains constant,  $m' = \text{const.}$ .

#### *Isobaric approximation*

The thermal propagation of a flame relies on the molecular transport of heat from the burned gases to the fresh mixture. This results in the propagation velocity of the flame

being significantly slower than the sound speed, which is related to the mean velocity of the molecules. Therefore, the low Mach number limit provides an accurate approximation to describe the internal structure of the flame. To the leading order of the low Mach number limit, the velocity gradient is not large enough to produce a significant pressure gradient. Thus, the equation for the conservation of momentum simplifies to a constant pressure equation, establishing that pressure remains constant throughout the internal structure of the flame

$$\frac{U_b}{a_b} \ll 1 : \quad \frac{dp'}{dx'} = 0. \quad (4.24)$$

Similarly, pressure and kinetic energy variations in the energy conservation equation are negligible when compared with the heat released during combustion. Therefore, the total energy conservation equation can be written in the form of an equation for the conservation of thermal enthalpy without dissipative terms

$$\frac{U_b}{a_b} \ll 1 : \quad m' c'_p \frac{dT'}{dx'} + \frac{d}{dx'} \left( \lambda' \frac{dT'}{dx'} \right) + \rho' q'_m \omega' = 0 \quad (4.25)$$

A enthalpy conservation equation, which is independent of the reaction rate can be obtained by subtracting equation (4.23) multiplied by the reaction heat per unit mass  $q'_m$  from the thermal enthalpy conservation equation (4.25)

$$m' \frac{d}{dx'} (c'_p T' - q'_m Y) + \frac{d}{dx'} \left( \lambda' \frac{dT'}{dx'} - \rho' D' q'_m \frac{dY}{dx'} \right) = 0. \quad (4.26)$$

Integrating this equation from the boundary condition given by the state of the fresh gases far away from the flame

$$x \rightarrow \infty : \quad T' = T'_o, \quad Y = 0, \quad \frac{dT'}{dx'} = \frac{dY}{dx'} = 0 \quad (4.27)$$

to the boundary condition given by the state of the burned gases far from the flame, where the gas mixture is expected to be in equilibrium

$$x \rightarrow -\infty : \quad T' = T'_b, \quad Y = 1, \quad \frac{dT'}{dx'} = \frac{dY}{dx'} = 0, \quad (4.28)$$

provides a relation between the adiabatic flame temperature  $T'_b$  and the initial temperature of the fresh mixture  $T'_o$  in terms of heat per unit mass  $q'_m$  which is written as

$$T'_b = T'_o + \frac{q'_m}{c'_p}. \quad (4.29)$$

After determining the burned gas temperature in terms of the mixture properties, a

#### 4 Deflagration-to-detonation transition at the tip of a flame in thin tubes

normalized temperature can be defined as

$$\theta \equiv \frac{T' - T'_o}{T'_b - T'_o} = \frac{T'_b - T'_o}{q'_m/c'_p} \quad (4.30)$$

allowing to remove the parameter of heat per unit mass from the equations.

Replacing the thermal conductivity  $\lambda'$  by the thermal diffusivity  $D'_T = \lambda' / (\rho' c'_p)$  and introducing the dimensionless Lewis number

$$\text{Le} \equiv \frac{D'_T}{D'}, \quad (4.31)$$

which accounts for the considered constant relationship between the thermal diffusivity and the molecular diffusivity, the internal structure of a isobaric flame is described by a pair of convective-diffusion equations with a strongly nonlinear reaction term

$$m' \frac{d\theta}{dx'} + \rho' D'_T \frac{d^2\theta}{dx'^2} + \rho' \omega' = 0, \quad (4.32)$$

$$m' \frac{dY}{dx'} + \rho' \frac{D'_T}{\text{Le}} \frac{d^2Y}{dx'^2} + \rho' \omega' = 0. \quad (4.33)$$

with the boundary conditions

$$x' \rightarrow +\infty : \quad \theta = 0, \quad Y = 0, \quad \frac{d\theta}{dx'} = \frac{dY}{dx'} = 0 \quad (4.34)$$

$$x' \rightarrow -\infty : \quad \theta = 1, \quad Y = 1, \quad \frac{d\theta}{dx'} = \frac{dY}{dx'} = 0 \quad (4.35)$$

Under the isobaric approximation  $p' \propto \rho' T' = \text{const.}$ , the reaction rate can be expressed in terms of the normalized temperature  $\theta$  and the product mass fraction  $Y$  as

$$\omega'(\theta, Y) = \frac{1}{t'_{\text{rb}}} \frac{(1 - Y)^\nu}{[1 - (1 - \theta)q_m/(c_p T_b)]^\nu} \exp \left[ \frac{-\beta(1 - \theta)}{1 - (1 - \theta)q_m/(c_p T_b)} \right] \quad (4.36)$$

where the dimensionless pre-exponential factor  $B$  is assumed to follow the relationship  $B D_T / t_{\text{coll}} = \text{const.}$ , based on the kinetic theory of gases (Huang, 1987). The characteristic reaction time  $t'_{\text{rb}}$  is determined as the reaction rate at the burned gas temperature

$$\frac{1}{t'_{\text{rb}}} = \frac{B}{t_{\text{coll}}} \exp \left( -\frac{E_a}{k_B T_b} \right). \quad (4.37)$$

The Zeldovich dimensionless number

$$\beta \equiv \frac{E_a}{k_B T_b} \frac{q_m}{c_p T_b}, \quad (4.38)$$

which accounts for the thermal sensitivity, is introduced in the expression of the reaction

rate

The problem at hand is not well-posed mathematically, as the reaction rate does not vanish in the fresh gases. This is a documented difficulty in the literature as the “cold boundary difficulty”. However, this is only a formal problem that arises due to the idealization of an infinite domain and the nature of the Arrhenius law. The reaction rate does not vanish at a far distance from the heat source, regardless how low the temperature is. In other words, the reactive mixture is out of equilibrium even in the far field region.

When the reactive mixture is supplied at a finite location, or when a cut-off temperature is introduced by multiplying the reaction rate by a Heaviside function  $H(T' - T'_i)$  where  $T'_i$  is the ignition temperature, the cold boundary difficulty is no longer present. However, the introduction of an ignition temperature  $T'_i$  implies the introduction of an additional parameter that cannot be interpreted as an intrinsic property of the mixture.

In the large activation energy asymptotic limit, discussed next, the reaction rate at  $T'_u$  becomes vanishingly small, and hence it can be safely neglected without introducing any significant error. For the reaction to occur, the mixture needs to be at a temperature that is close to the adiabatic flame temperature  $T'_b$ , which is essentially the ignition temperature.

### *Large activation energy asymptotic analysis*

In 1938, Zeldovich and Frank-Kamenetskii (ZFK) performed an asymptotic analysis of the thermal flame propagation in the limit of large activation energy  $\beta \rightarrow \infty$ . This analysis was further extended to the first order of the asymptotic approximation by Bush and Fendell (1970). However, for the purposes of this study, the leading order solution of Zeldovich and Frank-Kamenetskii is adopted. In particular, the development of the solution described in Clavin and Searby (2016) is reviewed below to introduce the description of the internal flame structure and the temperature-sensitive propagation velocity on which the subsequent analysis is based.

In the limit of large activation energy, chemical reactions take place within an infinitesimally thin layer, which allows to consider a separation of spatial scales. On a large scale, the reactive term is constrained to a discontinuity surface and the rest of the domain is referred to as the external solution. In the external solution, convective effects are balanced by diffusive effects that transport the heat of reaction by conduction and mix the fresh and burned gases. On the small scale of the reactive zone, convective effects are negligible compared to diffusive effects, which evacuate heat and combustion products.

When  $\beta$  is large, the reaction rate given by (4.36) is only significant where the normalized temperature  $\theta$  is close to unity. Therefore, the reactive layer is characterized by the magnitude relationship  $1 - \theta = \mathcal{O}(1/\beta)$ . For  $\beta \gg 1$ , the exponent on the Arrhenius law makes the reaction term negligible as soon as  $\theta$  is considerably below unity. This simplifies the expression for the reaction rate, given by

$$\beta \gg 1 : \quad \omega = (1 - Y)^\nu e^{-\beta(1-\theta)}. \quad (4.39)$$

As a result, the reaction remains confined to a vanishingly thin boundary layer.

#### 4 Deflagration-to-detonation transition at the tip of a flame in thin tubes

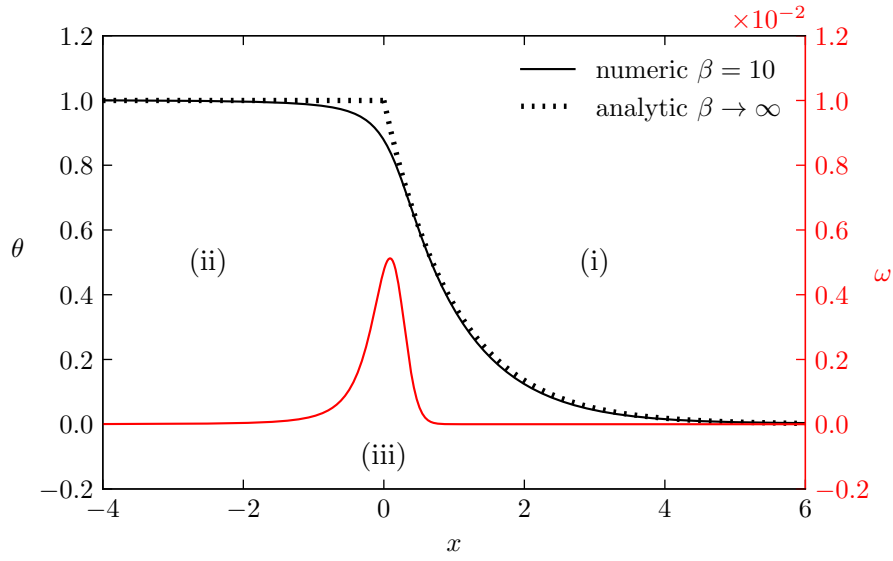


Figure 4.1: Reduced temperature and reaction rate profiles at the internal structure of a steady flame for  $Le = 1$  obtained analytically (4.47) in the asymptotic limit of large activation energy  $\beta \rightarrow \infty$  (discontinuous line) and numerically for  $\beta = 10$  and  $\nu = 2$  (solid line).

The flame structure under these conditions can be divided into three distinct regions (see Figure 4.1): (i) a preheat zone, where the temperature and reactant mass fraction evolve solely due to diffusive transport without any chemical reactions; (ii) a hot and uniform region of burned gases in thermodynamic equilibrium; and (iii) a narrow reactive layer, located at the interface of the preheat zone and the region of burned gases, where high temperature triggers the chemical reaction, leading to the release of the heat of combustion and complete consumption of the reactants.

The characteristic spatial scale of the preheat zone  $l'_f$ , where the diffusive transport is balanced by convective transport, is obtained by dimensional analysis of the convective-diffusion equation for temperature (4.43) to give

$$l'_f = \frac{\rho' D'_T}{m'} = \frac{D'_{Tb}}{U'_b} = \frac{D'_{Tu}}{U'_u} \quad (4.40)$$

where

$$U'_b = u'_f - u'_b \quad \text{and} \quad U'_u = u'_f - u'_u \quad (4.41)$$

denote the velocity of the flame with respect to the flow of burned gases and fresh gases, respectively.

Reducing the problem with this spatial scale and the time scale given by the flame transit time  $t'_f = l'_f/U'_b$  required for a particle moving with velocity  $U'_b$  to cover the distance  $l'_f$  which are written as

$$x \equiv \frac{x'}{l'_f} \quad \text{and} \quad t \equiv \frac{t'}{t'_f} \quad (4.42)$$

The steady propagation of isobaric flames is described by the dimensionless set of equations

$$\frac{d\theta}{dx} + \frac{d^2\theta}{dx^2} + \frac{\rho\omega}{\tau_{rb}} = 0, \quad (4.43)$$

$$\frac{dY}{dx} + \frac{1}{Le} \frac{d^2Y}{dx^2} + \frac{\rho\omega}{\tau_{rb}} = 0. \quad (4.44)$$

where the reaction rate has been reduced by the characteristic reaction time  $\omega = \omega' t'_{rb}$  and  $\tau_{rb} \equiv t_{rb}/t_f$  denotes the ratio of the reaction timescale to the transit time of the flame. The description of the steady propagation of isobaric flames is obtained as the solution of this non-linear eigenvalue problem that determines the temperature  $\theta$  and reactant mass fraction distribution  $Y$  and the timescales ratio  $\tau_{rb}$  that plays the role of an eigenvalue.

Outside the thin reactive layer, the system of equations given by (4.43) and (4.44) reduces to a system of second-order linear equations with constant coefficients

$$\frac{d}{dx} \left( \theta + \frac{d\theta}{dx} \right) = 0, \quad (4.45)$$

$$\frac{d}{dx} \left( Y + \frac{1}{Le} \frac{dY}{dx} \right) = 0. \quad (4.46)$$

which can be easily integrated from the conditions of the fresh mixture far from the flame, as specified by (4.34), to give

$$\frac{d\theta}{dx}(x) = -\theta(x), \quad \frac{1}{Le} \frac{dY}{dx}(x) = -Y(x), \quad \theta(x) = e^{-x}, \quad \text{and} \quad Y(x) = e^{-Le x}, \quad (4.47)$$

where the interface with the thin reaction layer, where  $\theta = Y = 1$ , has been arbitrarily located at the origin of the coordinate system without loss of generality.

Equation (4.47) describes the preheat zone, where a non-reacting gas is heated by thermal conduction from the heat released in the reaction layer and is diluted by molecular diffusion with the products of combustion from the reactive layer. In the preheat zone, the convective fluxes of thermal energy and reactants are everywhere balanced by the corresponding diffusive fluxes.

In the limit of large activation energy, the difference between the normalized temperature and unity must be small, on the order of the inverse of the Zeldovich number  $1 - \theta = \mathcal{O}(1/\beta)$ , for the reactive term to be non-negligible. The thin region where this relationship holds, with a thickness denoted by  $l_r$ , is the reactive layer. Introducing the reduced spatial coordinate of order unity within the reactive layer  $\xi \equiv x'/l'_r$  and the reduced temperature  $\Theta \equiv \beta(1 - \theta)$  of order unity on this region, the system of equations given by (4.43)

#### 4 Deflagration-to-detonation transition at the tip of a flame in thin tubes

and (4.44) is written as

$$\frac{l_f}{l_r} \frac{1}{\beta} \frac{d\Theta}{d\xi} + \left(\frac{l_f}{l_r}\right)^2 \frac{1}{\beta} \frac{d^2\Theta}{d\xi^2} - \frac{\rho\omega}{\tau_{rb}} = 0, \quad (4.48)$$

$$\frac{l_f}{l_r} \frac{dY}{d\xi} + \left(\frac{l_f}{l_r}\right)^2 \frac{1}{Le} \frac{d^2Y}{d\xi^2} + \frac{\rho\omega}{\tau_{rb}} = 0. \quad (4.49)$$

Anticipating that the reactive layer is much thinner than the preheat zone  $l_r/l_f \ll 1$ , a comparison of the orders of magnitude of the terms in (4.48) and (4.49) shows that the convective term is negligible compared with the diffusive term in the reactive layer. Therefore, the reactive layer is described to leading order by the system of equations

$$\frac{l_r}{l_f} \ll 1 : \quad \left(\frac{l_f}{l_r}\right)^2 \frac{1}{\beta} \frac{d^2\Theta}{d\xi^2} - \frac{\rho\omega}{\tau_{rb}} \approx 0, \quad (4.50)$$

$$\left(\frac{l_f}{l_r}\right)^2 \frac{1}{Le} \frac{d^2Y}{d\xi^2} + \frac{\rho\omega}{\tau_{rb}} \approx 0. \quad (4.51)$$

Adding both equations and dividing by the square of the length scales ratio, the following differential equation independent of the rate of reaction is obtained

$$\frac{d^2}{dx^2} \left( \frac{\Theta}{\beta} + \frac{Y}{Le} \right) = 0. \quad (4.52)$$

Integration from the hot and uniform region of burned gases in equilibrium where  $d\Theta/d\xi = dY/d\xi = \Theta = 0$  and  $Y = 1$  yields the relation between the reduced temperature and the product mass fraction within the reactive layer

$$\frac{d}{d\xi} \left( \frac{\Theta}{\beta} + \frac{Y}{Le} \right) = 0 \quad \text{and} \quad \frac{\Theta}{\beta} + \frac{Y}{Le} = \frac{1}{Le}, \quad (4.53)$$

which can be used to remove the mass fraction dependence from the reactive term (4.39)

$$\omega(\Theta) = \frac{Le^\nu}{\beta^\nu} \Theta^\nu e^{-\Theta} \quad (4.54)$$

and reduce the problem (4.50) and (4.51) to a single second order ordinary equation of thermal energy conservation

$$\left(\frac{l_f}{l_r}\right)^2 \frac{1}{\beta} \frac{d^2\Theta}{d\xi^2} = \frac{1}{\tau_{rb}} \frac{Le^\nu}{\beta^\nu} \Theta^\nu e^{-\Theta}. \quad (4.55)$$

After multiplying by  $d\Theta/d\xi$

$$\frac{1}{2\beta} \left( \frac{l_f}{l_r} \right)^2 \frac{d}{d\xi} \left[ \left( \frac{d\Theta}{d\xi} \right)^2 \right] = \frac{1}{\tau_{rb}} \frac{Le^\nu}{\beta^\nu} \Theta^\nu e^{-\Theta} \frac{d\Theta}{d\xi}, \quad (4.56)$$

both sides of the equality can be spatially integrated from the uniform burned gas side  $\xi = 0$ , where  $d\Theta/d\xi = \Theta = 0$ , to the preheat zone  $\xi \rightarrow \infty$  where  $\Theta \rightarrow \infty$  to give

$$\frac{1}{2\beta} \left( \frac{l_f}{l_r} \right)^2 \frac{d\Theta}{d\xi} \Big|_{\xi \rightarrow \infty}^2 = \frac{1}{\tau_{rb}} \frac{Le^\nu}{\beta^\nu} \int_0^\infty \Theta^\nu e^{-\Theta} d\Theta. \quad (4.57)$$

The integral of the left-hand side term is equivalent to the gamma function  $\Gamma(\nu + 1) = \int_0^\infty \Theta^\nu e^{-\Theta} d\Theta$ , which returns the factorial  $\nu!$  when  $\nu$  is an integer. The reduced temperature gradient in the region of overlap with the external solution is therefore given by

$$\frac{1}{\beta} \frac{l_f}{l_r} \frac{d\Theta}{d\xi} \Big|_{\xi \rightarrow \infty} = \sqrt{\frac{1}{\tau_{rb}} \frac{2\nu! Le^\nu}{\beta^{\nu+1}}}. \quad (4.58)$$

The solution to the eigenvalue problem  $\tau_{rb}$  can be obtained through asymptotic matching of the preheat zone with the reactive layer. Precisely, by equating the temperature gradient at the interface with the reactive layer located at  $x = 0$  of the solution for the preheat zone (4.47) with the temperature gradient in the reactive layer in the region of overlap as given by equation (4.58), in comparable spatial and temperature units, leads to the expression for the eigenvalue

$$\frac{1}{\tau_{rb}} = \frac{\beta^{\nu+1}}{2\nu! Le^\nu}. \quad (4.59)$$

Having determined the timescale ratio  $\tau_{rb}$ , an estimation of the order of magnitude estimate of the ratio between the thickness of the reactive layer and the preheat zone for the reactive term to be balanced by the diffusive term (4.50) can be obtained as

$$\frac{l_r}{l_f} = \frac{\sqrt{2\nu!}}{\beta} \quad (4.60)$$

which is asymptotically bounded by  $1/\beta$  up to a constant factor. Consequently, the initial assumption that the reactive layer is significantly thinner than the preheat zone in the large activation energy limit is justified. This also implies that the convective effects can be neglected in comparison to diffusive effects in the reactive layer to leading order.

An additional key finding arising from this analysis relevant to the study of the DDT is the dependence of the flame velocity on the properties of the mixture. The expression for the laminar flame velocity in terms of mixture properties can be obtained by utilizing the



#### 4 Deflagration-to-detonation transition at the tip of a flame in thin tubes

transit time  $t'_f$ , which was defined using the flame velocity. This expression is given as

$$U'_L \equiv U'_b = \sqrt{\frac{2\nu!Le^\nu}{\beta^{\nu+1}} \frac{D'_{Tb}}{t'_{rb}}} \quad (4.61)$$

showing the strong temperature dependence of the flame velocity through the characteristic reaction time  $t'_{rb}$  (4.37), which exhibits an exponential reduction with the adiabatic temperature  $T'_b$ .

Furthermore, the kinetic theory of gases Huang (1987) can provide a rough approximation of the flame velocity with respect to the sound speed. According to this theory, the square of the sound speed is approximately equal to the thermal diffusivity multiplied by the collision frequency  $a'^2 \approx D'_T/t'_{coll}$ . The flame speed to sound speed ratio can then be approximated as

$$\frac{U'_b}{a'_b} \approx \sqrt{\frac{2\nu!Le^\nu}{\beta^{\nu+1}} \frac{t'_{coll}}{t'_{rb}}} \ll 1. \quad (4.62)$$

This relation shows that due to the large activation energy that characterizes combustion processes,  $t'_{coll}/t'_{rb} \ll 1$ , a thermal propagating flame is accurately described by the isobaric approximation for the low Mach number limit  $U'_b/a'_b \ll 1$ .

#### 4.2.3 One-dimensional model at the flame tip

The propagation of an elongated flame from the closed end of a thin tube is studied using a one-dimensional model. Curvature effects at the tip of the elongated flame are disregarded, and the acceleration of flame propagation is assumed to result solely from the increase in flame surface area. Inspired by the study of Clanet and Searby (1996) on the formation of tulip flames, the expansion of the burned gases in the flame skirt is modelled in a one-dimensional geometry introducing a mass production term in the burned gas region. This mass production term generates a backflow of burned gases towards the flame tip, which acts as a piston, pushing the flame from behind and increasing the absolute velocity of flame propagation.

##### *Nondimensional equations*

This study is performed with the scaling obtained from the ZFK asymptotic analysis for the external solution of a flame propagating in an initially unperturbed mixture with density  $\rho'_o$ , temperature  $T'_o$ , and pressure  $p'_o$ . The dimensionless spatial and time coordinates of order unity within the flame internal structure are defined as

$$r \equiv \frac{r'}{l'_{fo}} \quad \text{and} \quad t \equiv \frac{t'}{t'_{fo}}, \quad (4.63)$$

where  $l'_{fo} = D'_{Tbo}/U'_{bo}$  is the characteristic length scale of the preheat zone,  $D'_{Tbo}$  is the thermal diffusivity at the adiabatic flame temperature  $T'_{bo} = T'_o + q'_m/(c_p)$ ,  $U'_{bo}$  is the

velocity of the flame with respect to the burned gases propagating in a mixture initially at temperature  $T'_o$ , and  $t'_{fo} = l'_{fo}/U'_{bo}$  is the corresponding transit time. The physical quantities of density, flow velocity, temperature, pressure and total energy are made dimensionless using the burned state of a gas mixture that is initially unperturbed as a reference. Specifically, the dimensionless variables defined as

$$\rho \equiv \frac{\rho'}{\rho'_{bo}}, \quad u \equiv \frac{u'}{U'_{bo}}, \quad T \equiv \frac{T'}{T'_{bo}}, \quad p \equiv \frac{p'}{p'_o}, \quad E \equiv \frac{E'}{c'_p T'_{bo}} \quad (4.64)$$

where  $\rho'_{bo} = \rho'_o T'_o / T'_{bo}$  is the density of the burned gas after an isobaric expansion, and  $p'_o$  is the unperturbed pressure which remains constant in the isobaric approximation. Furthermore, the heat of reaction per unit mass is made dimensionless using the enthalpy of the burned gas  $q = q'_m / c'_p T'_{bo}$ .

The dynamics of the unsteady propagation of the one-dimensional flame tip are studied by means of the reactive Navier-Stokes equations for compressible flows, which in the introduced dimensionless form are written as follows

$$\frac{\partial \rho}{\partial t} + \frac{\partial (\rho u)}{\partial r} = 0, \quad (4.65)$$

$$\frac{\partial (\rho u)}{\partial t} + \frac{\partial (\rho u^2)}{\partial r} + \frac{1}{\gamma M_{bo}^2} \frac{\partial p}{\partial r} = \text{Pr} \frac{\partial^2 u}{\partial r^2}, \quad (4.66)$$

$$\begin{aligned} \frac{\partial (\rho E)}{\partial t} + \frac{\partial (\rho u E)}{\partial r} + \frac{\gamma - 1}{\gamma} \frac{\partial (\rho u)}{\partial r} = \\ \frac{\partial^2 T}{\partial r^2} + M_{bo}^2 \text{Pr} (\gamma - 1) \frac{\partial}{\partial r} \left( u \frac{\partial u}{\partial r} \right) + \frac{1}{\tau_{rb}} \rho q \omega, \end{aligned} \quad (4.67)$$

$$\frac{\partial (\rho Y)}{\partial t} + \frac{\partial (\rho Y u)}{\partial r} = \frac{1}{\text{Le}} \frac{\partial^2 Y}{\partial r^2} - \frac{1}{\tau_{rb}} \rho \omega \quad (4.68)$$

where  $\tau_{rb}$  is the ratio of flame transit time to characteristic reaction time, which was determined based on the thermochemical parameters of the mixture through the ZFK asymptotic analysis (Section 4.2.2)

$$\frac{1}{\tau_{rb}} = \frac{\beta^{\nu+1}}{2\nu! \text{Le}^\nu}. \quad (4.69)$$

As in the analysis of a steady flame, the thermophysical properties of kinematic viscosity  $\mu$ , thermal conductivity  $\lambda'$ , specific heat at constant pressure  $c'_p$  and constant volume  $c'_v$  are assumed to be constant. The equation of state for ideal gases in the chosen dimensional form is expressed as

$$p = \rho T, \quad (4.70)$$

and the total energy, comprising the internal thermal energy and the macroscopic kinetic energy, is written as

$$E = \frac{1}{\gamma} T + M_{bo}^2 (\gamma - 1) \frac{u^2}{2}, \quad (4.71)$$

#### 4 Deflagration-to-detonation transition at the tip of a flame in thin tubes

where  $M_{bo} \equiv U_{bo}/a_{bo} \ll 1$  represents the Mach number of a flame propagating in an unperturbed mixture with respect to the burned gases which and as shown by (4.62) is a thermochemical parameter of the mixture much smaller than unity.

The dimensionless reaction rate for a single-step reaction (4.12) of order  $\nu$  can be expressed as

$$\omega = \frac{\omega'}{1/t'_{rb}} = \rho^\nu (1 - Y)^\nu \exp \left[ \frac{E_a}{k_B T_{bo}} \left( 1 - \frac{1}{T} \right) \right]. \quad (4.72)$$

In addition to the previously introduced Zeldovich number (4.38) and Lewis number (4.31), the dimensionless Prandtl number appears in the conservation equations when the isobaric approximation is not applied. It measures the ratio of momentum diffusivity to thermal diffusivity

$$\text{Pr} \equiv \frac{\mu'}{\rho' D'_T}, \quad (4.73)$$

and is assumed to be constant throughout the analysis.

##### *Backflow of burned gases*

Considering a flame that moves along a tube with no-slip conditions on the walls, the flame surface interacts with the tube walls, causing the flame front to curve and elongate in the direction of propagation. The stability of a flame front with a convex shape towards the fresh mixture ahead of it is discussed in Zeldovich et al. (1980). The combustion process taking place at the flame skirt, which propagates almost parallel to the tube walls, induces a flow of gases that cannot be pushed radially outward due to the presence of the tube walls. The induced gas flow results in a backflow of burned gases towards the flame tip. This backflow is the main driving force for the apparent acceleration of the flame front.

In their experimental investigation of the tulip flame formation mechanism, Clanet and Searby (1996) proposed a simple geometrical model for the propagation of an elongated flame in a semi-closed tube, which produced results in close agreement with their experimental observations. During the initial stages of flame propagation, the initially hemispherical front of a flame ignited at the center of the closed end approaches the cylindrical walls of the tube. The walls block the outward running component of the induced flow, and the expansion of the combustion products results in an extension of the flame along the axis of the tube. The flame front adopts a cylindrical shape with a hemispherical cap increasing the flame surface area near the walls and, therefore, the production rate of burned gas. This configuration leads to an exponential acceleration of the velocity of the flame tip, as observed in the experimental results, until the flame skirt reaches the tube walls.

Similarly, Clavin and Tofaili (2021) proposed a self-acceleration mechanism for their one-dimensional model for elongated flames, which is produced by the piston-like effect of a backflow of burned gas towards the flame tip. Neglecting the curvature effect, the tip of the flame front is considered a planar wave perpendicular to the axis, studied in one-dimensional geometry. The region of burned gases is delimited by the closed end at

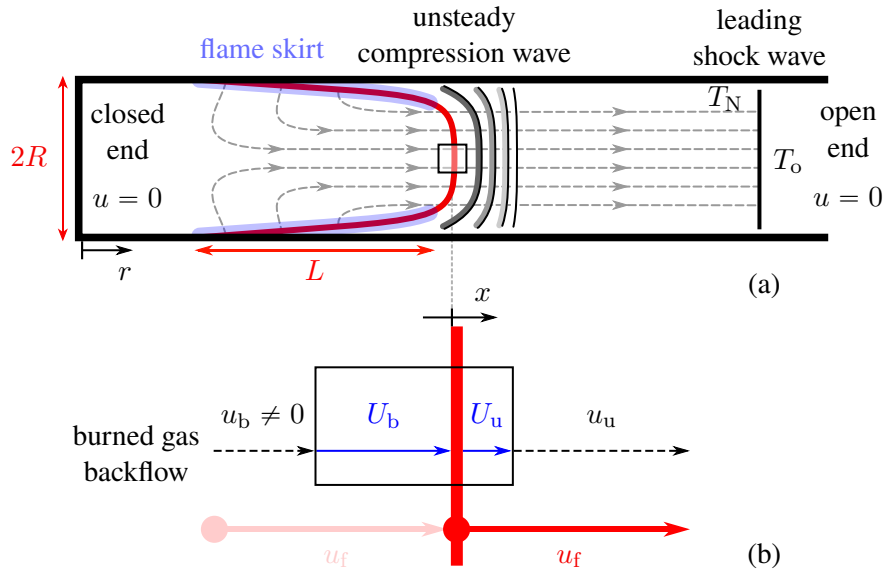


Figure 4.2: (a) Scheme of the self-accelerating elongated flame model of Clavin and Tofaili (2021). The streamlines are represented by light black lines with arrows, while the flame surface is depicted by the thick red line, with the flame skirt highlighted in light blue. (b) One-dimensional model at the tip of the flame with the absolute flow velocities in black and the flame velocities with respect to the flow in blue.

$r = 0$ , the flame skirt corresponding to the flame surface close to the wall tubes, and the flame tip at  $r = r_f$  (as shown in Figure 4.2). The expansion of the combustion products from the flame skirt in the one-dimensional geometry is modeled as a mass production term per unit of volume along the flame length  $L$ . Considering the flame skirt as a cylindrical surface as done in Clanet and Searby (1996), the mass production term is expressed as

$$\dot{m} = \begin{cases} 2 \frac{\rho_b U_b}{R} & \text{if } -L < r - r_f < 0 \\ 0 & \text{otherwise.} \end{cases} \quad (4.74)$$

When compressible and unsteady effects in the region delimited by the flame surface are neglected, integration of the mass conservation equation from the closed end  $r = 0$ , where the gases are at rest  $u(r = 0) = 0$ , to the tip of the flame  $r = r_f$ , where the gases move with a velocity denoted  $u(r = r_f) = u_b$ ,

$$\int_0^{r_f} \frac{d(\rho u)}{dr} dr = \int_0^{r_f} \dot{m} dr, \quad (4.75)$$

yields a backflow of burned gas that impinges on the flame tip from behind

$$r = r_f^- : \quad u(r) = u_b = S U_b, \quad (4.76)$$

which is proportional to an elongation parameter  $S$  and the flame burning speed  $U_b$ . The

#### 4 Deflagration-to-detonation transition at the tip of a flame in thin tubes

elongation parameter is defined as the ratio  $S \equiv 2L/R$  for a strictly cylindrical flame skirt, where the prefactor 2 may change for slightly different flame surface geometries while the flame length  $L$  to tube radius  $R$  ratio is the relevant functional dependence of the backflow. This backflow of gases drives the flame acceleration in the model of Clavin and Tofaili (2021) for elongated flames,  $R/L \ll 1$ . A similar flow field has also been observed in the two-dimensional numerical simulations of Akkerman et al. (2006) for accelerating flames in cylindrical tubes with the no-slip condition at the walls, as well as in the experimental investigation of tulip flame formation utilizing Particle Image Velocimetry by Ponizy et al. (2014).

##### *Comparison with the Sigma model*

The self-accelerating flame model based on a backflow of burned gases that pushes the flame as a piston differs significantly from the widely used Sigma model in one-dimensional simulations to reproduce the flame acceleration due to the flame surface growth (Kagan and Sivashinsky, 2003; Kagan et al., 2015; Kagan and Sivashinsky, 2017; Koksharov et al., 2018; Gordon et al., 2020a,b, 2021; Koksharov et al., 2021; Bykov et al., 2022). Both models employ a controlling parameter,  $\Sigma$  in the Sigma model and  $S$  in the backflow-based model, which provides a quantitative measure of the ratio of flame surface to tube section normal to the propagation direction.

However, the subtle yet crucial difference between these parameters lies in their impact on the flame velocity. In the Sigma model,  $\Sigma$  is employed to amplify the reaction rate resulting in a greater burning velocity  $U_b = \Sigma U_L$  with respect to the laminar flame velocity  $U_L$ . On the other hand, the  $S$  parameter in the backflow-based model introduces a backflow of burned gases that impinges on the flame tip, causing it to propagate faster  $u_b = S U_L$  by advection of the flow. Nonetheless, the burning velocity of the flame itself in the backflow-based model remains determined by the unmodified thermochemical properties of the mixture.

As a result of this difference, numerical studies based on the  $\Sigma$  model rely on an amplification of the reaction rate to model the flame acceleration. In contrast, the backflow model imposes a flow velocity behind the flame without modifying the mixture properties. Namely, the burning velocity is only modified by the temperature of the reactive mixture through the strong temperature-sensitive reaction rate.

### 4.3 Double-discontinuity model

The propagation of a flame propagating through a reactive mixture induces a movement of the surrounding gas. This motion is triggered by the difference in flow velocity on both sides of the flame, which is generated to satisfy the conservation of mass, taking into account the lower density of the hotter burned gases compared to the fresh gases at the same pressure. If the intensity of this motion is strong enough to overcome damping effects of hydraulic resistance or viscosity, it can lead to the formation of shock waves.

Unlike detonation waves, these shock waves have no relation to the combustion process and solely serve to meet the boundary conditions.

For instance, in the case of a combustion wave propagating from the close end of a tube, the velocity of the fresh mixture moving ahead of the flame relative to the burned gases is determined by the density jump at the flame and mass conservation. At the close end of the tube, the gas velocity must vanish. Consequently, the gas ahead of the flame must move relative to the tube at a constant velocity determined by the velocity jump at the flame. However, in the forward part of the tube, far enough from the flame, the gas is initially at rest. This condition can be satisfied by the presence of a shock wave, in which the gas velocity changes discontinuously from the velocity ahead of the flame to zero. This shock wave moves faster than the speed of sound, while the flame is markedly subsonic. Therefore, the distance between the flame and the shock wave grows at a rate given by the difference in velocity between the shock wave and the flame, which is significantly larger than the flame speed.

The external flow resulting from the interaction of flame with the shock wave has a characteristic length considerably greater than the flame thickness and, by extension, much greater than the shock wave thickness, which is on the order of the mean free path. As a result, both waves can be considered as discontinuities when analyzing the flow that arises from their interaction. The flame is an isobaric reactive discontinuity where conservation of mass and momentum must hold, and the increase of energy can just come from the heat released during the combustion process. On the contrary, the shock wave is a supersonic inert discontinuity.

#### *Flame as a discontinuity*

Considering the flame as a reactive discontinuity in quasi-steady state for a characteristic evolution time much larger than the transit time, mass conservation imposes the relation

$$\rho_u U_u = \rho_b U_b \quad (4.77)$$

between the density  $\rho$  and the velocities of the flame with respect to the flow of gases  $U$  ahead and behind the flame, denoted respectively by the subscript  $u$  and  $b$ . The velocity of the reactive discontinuity  $u_f$  can be defined in terms of the velocities ahead or behind the flame, resulting in the relationship

$$u_f = u_u + U_u = u_b + U_b \quad (4.78)$$

where the flow velocity behind the flame  $u_b$  in the elongated flame tip model is imposed by the backflow of burned gases (4.76).

Under the low Mach number approximation, the flame behaves as an isobaric discontinuity, with the pressure remaining constant. This provides a relationship between the density and temperature at both sides of the flame

$$p = \rho_u T_u = \rho_b T_b. \quad (4.79)$$

#### 4 Deflagration-to-detonation transition at the tip of a flame in thin tubes

Neglecting heat losses, the conservation of thermal enthalpy results in a relationship for the burned gases temperature and the temperature ahead of the flame in terms of the heat of reaction and the temperature ahead of the flame

$$T_b = T_u + q. \quad (4.80)$$

According to the asymptotic analysis of thermal flame performed by Zeldovich and Frank-Kamenetskii (1938) on thermal flame propagation in the limit of large activation energy  $\beta \rightarrow \infty$ , the laminar burning velocity is highly sensitive to temperature. In Section 4.2.2, it was shown that for a  $\nu$ -th order simple-step chemical-kinetics model with a reaction rate governed by an Arrhenius law (4.72), the laminar flame velocity depends on the burned gas temperature as follows

$$U_b(T_b) = \frac{U'_b(T'_b)}{U'_b(T'_{bo})} = T_b^{\nu+1} \exp \left[ \frac{E_a}{2k_B T_{bo}} \left( 1 - \frac{1}{T_b} \right) \right] \quad (4.81)$$

where the activation energy  $E_a$  and the heat of reaction  $q_m$  have been considered constant.

##### Shock wave

The conservation relations of Rankine-Hugoniot express the jump conditions that relate the unperturbed gas state (denoted by the subscript o) and the Neumann state behind the shock wave (denoted by the subscript N), in terms of the Mach number of the leading shock  $M_o \equiv u_s/a_o$ . Specifically, the flow velocity in the direction of propagation of the discontinuity is given by

$$\frac{u_N}{a_o} = \frac{2}{\gamma + 1} \left( M_o - \frac{1}{M_o} \right) \quad (4.82)$$

and the temperature jump is given by

$$\frac{T_N}{T_o} = \frac{[2\gamma M_o^2 - (\gamma - 1)] [(\gamma - 1) M_o^2 + 2]}{(\gamma + 1)^2 M_o^2}. \quad (4.83)$$

#### 4.3.1 Self-similar solutions

In the context of a steady regime of flame propagation, the flow between the flame and the shock is uniform and the gas found by the reactive discontinuity is at the Neumann state left behind by the shock wave. The uniformity of the flow is mathematically expressed as

$$u_N = u_u \quad \text{and} \quad T_N = T_u. \quad (4.84)$$

Under these conditions, the jump conditions on the flame (4.77), (4.79) to (4.81) and (4.86) and shock (4.82) and (4.83), as well as the relation for the backflow of burned gases (4.76), form a closed set of equations which can be solved for a particular set of thermochemical mixture properties, including  $\gamma$ ,  $q$ ,  $\beta$ ,  $\nu$ , and  $M_{bo}$ , in terms of the leading shock Mach

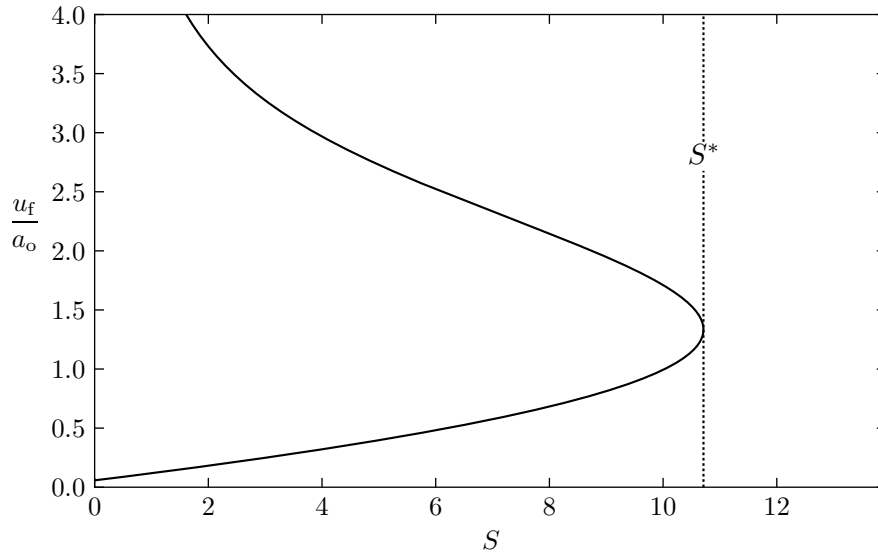


Figure 4.3: Self-similar solutions; steady flame velocity to sound speed ratio  $u_f/a_o$  as a function of the flame elongation parameter  $S$  in the double-discontinuity model for the thermochemical properties  $\gamma = 1.4$ ,  $q = 7/8$ ,  $\beta = 10$ ,  $\nu = 2$  and  $M_{bo} = 2 \cdot 10^{-4}$ .

number  $M_o$ . Thus, the external flow can be described by a self-similar solution, in which all quantities  $\rho$ ,  $T$ ,  $p$ , and  $u$  are piecewise constant, and the distances between the closed end wall, the flame, and the leading shock wave grow linearly with time.

For instance, a reactive mixture with a heat capacity ratio  $\gamma = 1.4$ , a dimensionless heat of reaction  $q = 0.875$ , a Zeldovich number  $\beta = 10$ , a flame Mach number  $M_{bo} = 2 \cdot 10^{-2}$ , and a leading shock of intensity  $M_o = 2$  can be considered. Under these conditions, the temperature jump on the shock is  $T_N/T_o = 1.69$  as given by (4.83). The burned gas temperature when the unburned gas temperature corresponds to the Neumann temperature (4.84) given by (4.80) is  $T_b = 1.09$ , and the laminar flame velocity at this temperature, as determined by (4.81), is  $U_b = 1.85$ , and by mass conservation the flame velocity with respect to the fresh gases is  $U_u = 0.36$ . The flow velocity ahead of the flame corresponding to the Neumann state for a shock wave of  $M_o = 2$  is determined by (4.82) to be  $u_N/a_o = 1.25$ . Using (4.86), the velocity of the flow behind the flame is found to be  $u_b = 19.7$ . The ratio of the backflow to laminar flame velocity then yields an elongation parameter  $S = 10.63$ , and the corresponding absolute flame velocity  $u_f = 21.6$ , which gives a flame velocity with respect to the initial sound speed of  $u_f/a_o = 1.22$ .

Considering the leading shock Mach number  $M_o$  as a parameter, the non-linear relationship between the flame velocity and the elongation parameter of the flame tip model can be established, as shown in Figure 4.3 for the specific example of thermochemical mixture properties under consideration. The curve, obtained for the self-similar solutions of the double-discontinuity model within the framework of the elongated flame tip, reveals the existence of a critical elongation parameter  $S^*$  beyond which no steady solution exists. This critical value is determined by a turning point in the curve of steady solutions, where the monotonically increasing behaviour of the



#### 4 Deflagration-to-detonation transition at the tip of a flame in thin tubes

elongation parameter with the flame velocity shifts to a decreasing function, passing through a point of infinite flame acceleration for the critical elongation value.

Deshaies and Joulin (1989) derived an analytical expression for the self-similar solutions of their model under the weak shock wave approximation  $M_o \ll 1$ , which revealed the existence of a limiting folding value for flames propagating at constant velocity. Although this approximation is not quantitatively precise since the lead shock at the turning point is not weak, it provides insights into the nature and functional dependence of the critical conditions. Clavin and Tofaili (2021) demonstrated the appearance of a turning point in the self-similar solutions for the model of elongated flames at hand using a graphical method based on the tangency of two functions of the leading shock Mach number, under the approximation  $(\gamma - 1)/(2\gamma M_o^2) \ll 1$ . The critical conditions obtained following their procedure compared favorably with the experimental and numerical findings of Kuznetsov et al. (2010) and Liberman et al. (2010) on the deflagration-to-detonation transition in highly reactive mixtures.

##### 4.3.2 Isentropic compression waves

The self-similar description of the external flow assumes uniformity in the flow between the flame and the shock wave, neglecting the dynamics of the compression waves emitted by the flame front. These compression waves travel at a speed given by the sum of the flow velocity and the local sound speed, significantly exceeding that of the flame. As such, the uniform flow assumption remains valid during the initial stage of flame acceleration when the evolution of the flame velocity is slow, allowing sufficient time for the compression waves to travel towards the shock wave, which in turn returns the corresponding acoustic and entropy waves. However, as the flame length continues to increase, the flame accelerates at a faster and faster rate, and the uniformity assumption gradually loses its accuracy. At a certain point, prior to reaching the critical conditions, the acceleration of the flame becomes too rapid, and the flow between the flame and the shock wave can solely be accurately represented by the presence of unsteady compression waves.

Once unsteady compression waves are considered in the double-discontinuity model, the temperature and flow velocity relations between the Neumann state and the flame must be found to replace the uniform flow conditions (4.84). For simplicity, the scope of the study is limited to compression waves that do not reach the leading shock wave. The shock wave propagates then at constant velocity, so the entropy production does not vary with time. Neglecting the dissipation mechanisms between the shock wave and the flame, as is customary in the study of compressible flows, the flow is said to be homentropic. That is, the entropy in the flow between the shock and the flame is uniform.

Algebraic manipulation of the Euler equations for isentropic flows leads to the Riemann invariants  $I_{\pm} = u \pm 2a/(\gamma - 1)$ . These quantities are conserved along the characteristics lines defined by  $C_{\pm} : dx/dt = u \pm a$ . The downstream running invariant  $I_-$  is determined by the Neumann state behind the steady shock wave  $I_- = u_N - 2a_N/(\gamma - 1)$ . Conservation of the Riemann invariant provides with the relationship between the flow

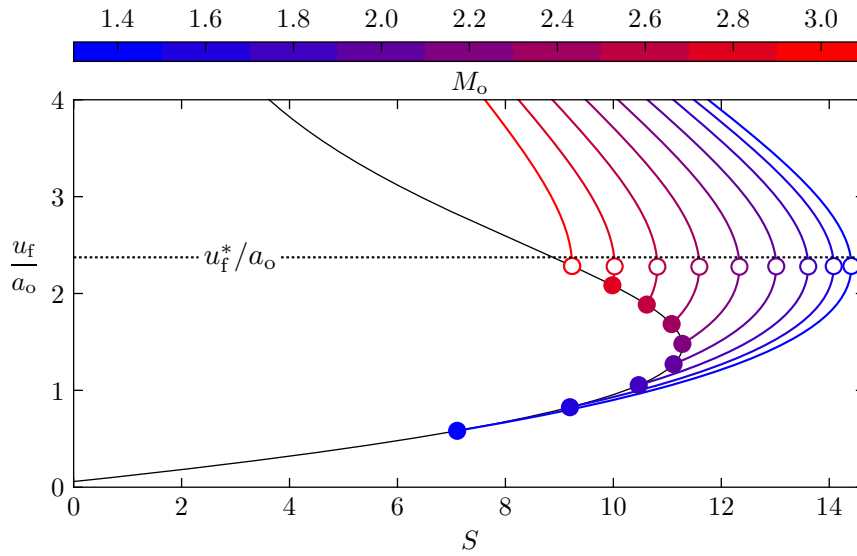


Figure 4.4: Flame velocity to sound speed ratio  $u_f/a_o$  as a function of the flame elongation parameter  $S$  in the double-discontinuity model with an isentropic compression wave between the flame and the leading shock for the thermochemical properties  $\gamma = 1.4$ ,  $q = 7/8$ ,  $\beta = 10$ ,  $\nu = 2$  and  $M_{bo} = 2 \cdot 10^{-2}$  for different values of the leading shock Mach number  $M_o$ . The full points indicate the self-similar solution for the given leading shock Mach number. The empty circle highlights the turning point of the double-discontinuity solution including an isentropic compression wave. The horizontal dotted line represents the critical flame velocity given by (4.92).

velocity and sound speed at the Neumann state and ahead of the flame  $u_N - 2a_N/(\gamma - 1) = u_u - 2a_u/(\gamma - 1)$ . Recalling that for ideal gases, the sound speed is proportional to the square root of the temperature, the conservation of the Riemann invariant can be also written as

$$\frac{T_u}{T_N} = \left[ 1 + \frac{\gamma - 1}{2} \frac{u_N}{a_N} \left( \frac{u_u}{u_N} - 1 \right) \right]^2. \quad (4.85)$$

This expression provides the relationship between the temperature ahead of the flame and behind the shock wave, which can be used to replace the uniform flow conditions (4.84).

Including this isentropic relation to link the set of jump conditions on the flame (4.77), (4.79) to (4.81) and (4.86) with those of the shock wave (4.82) and (4.83), and the relation for the backflow of burned gases (4.76), a new non-linear relationship is obtained for a given set of thermochemical properties, including  $\gamma$ ,  $q$ ,  $\beta$ ,  $\nu$  and  $M_{bo}$ , and a given leading shock Mach number  $M_o$ . Considering, in this case, the velocity of the flow ahead of the flame  $u_u$  as a parameter, the non-linear relationship between the flame velocity and the elongation parameter for the double-discontinuity model with an isentropic compression wave evolving between both discontinuities is established. This relationship is depicted in Figure 4.4 for the thermochemical properties under consideration and for a set of values of the leading shock Mach number in the range 1.4 – 3.0

The curve of solutions for the double-discontinuity model that incorporates an isentropic

#### 4 Deflagration-to-detonation transition at the tip of a flame in thin tubes

compression waves between the leading shock wave and the flame exhibits a similar turning point as the that observed for the self-similar solutions for certain values of the leading shock Mach number  $M_o$ . The critical flame propagation velocity  $u_f/a_o^*$  at which the turning point appears is independent of the intensity of the leading shock wave, while the critical elongation parameter  $S$  found at the turning point decreases as the intensity of the leading shock wave increases. For the self-similar solutions corresponding to a flame velocity  $u_f$  that exceeds the observed critical value, the curve representing the nonlinear relationship no longer displays a turning point, and the elongation parameter monotonically decreases as the flame velocity increases.

##### *Universal critical flame speed*

The complex system of nonlinear equations (4.76), (4.77), (4.79) to (4.83), (4.85) and (4.86) can be simplified under certain assumptions that apply at the critical condition in order to obtain an analytical expression for the critical flame velocity. Since the turning point is typically found for an elongation parameter larger than unity, the flame at this turning point is mainly propagated by the adjective effect of the backflow. Therefore, the flame velocity is approximately equal to the velocity of the backflow and the burning velocity is negligible compared to the backflow, resulting in both sides of the flame having approximately equal flow velocities

$$S \gg 1 : \quad u_f \approx u_u \approx u_b = SU_b. \quad (4.86)$$

In order to express the burning velocity as a function of the temperature ahead of the flame, an approximation for small variations of the burned temperature is presented as follows

$$T_b - 1 \ll 1 : \quad 1 - \frac{1}{T_b} = \left( \frac{T_u}{T_o} - 1 \right) \frac{T_o}{T_{bo}} [1 - (T_b - 1)]^{-1} \approx \left( \frac{T_u}{T_o} - 1 \right) \frac{T_o}{T_{bo}} \quad (4.87)$$

where  $T_o/T_{bo}$  represents the ratio of the fresh gas temperature to adiabatic temperature, which can be expressed in terms of the heat of reaction as  $T_o/T_{bo} = 1 - q$ . By utilizing the expression for the sensitivity of burning velocity to temperature (4.81) without the prefactor, whose impact is negligible for large activation energy, with the burned gas temperature expressed in term of temperature variation ahead of the flame (4.87), the flame velocity approximation (4.86) yields the following expression

$$S \gg 1 \text{ and } T_b - 1 \ll 1 : \quad u_f \approx S \exp \left[ \frac{E_a}{2k_B T_{bo}} \frac{T_o}{T_{bo}} \left( \frac{T_u}{T_o} - 1 \right) \right] \quad (4.88)$$

For simplicity, the temperature variation ahead of the flame is written for an isentropic compression wave between the flame and a vanishingly weak shock wave, such that  $u_N \approx 0$  and  $T_N \approx T_o$ , which results in the simplification of the isentropic relation (4.85)

to

$$M_o \ll 1 : \quad \frac{T_u}{T_N} \approx \frac{T_u}{T_o} = \left( 1 + \frac{\gamma - 1}{2} \frac{u_f}{a_o} \right)^2 \quad (4.89)$$

Under these approximations, the nonlinear relationship between the flame velocity and the elongation parameter can be written in a closed form as

$$S \gg 1, T_b - 1 \ll 1 \text{ and } M_o \ll 1 : \quad u_f \approx S \exp \left[ b \frac{\gamma - 1}{a_o} u_f + b \left( \frac{\gamma - 1}{2a_o} u_f \right)^2 \right], \quad (4.90)$$

where a parameter of thermal sensitivity  $b \equiv T_u/U_b \, dU_b/dT_u = E_a/(2k_B T_{bo}) T_o/T_{bo}$  has been introduced to simplify the notation. By taking the derivatives at both sides of this equation

$$\frac{S \, du_f}{u_f \, dS} = \left[ 1 - b \frac{\gamma - 1}{a_o} u_f - 2b \left( \frac{\gamma - 1}{2a_o} \right)^2 u_f^2 \right]^{-1}, \quad (4.91)$$

it can be observed that the change in flame velocity with respect to the evolution of the elongation parameter diverges at a certain value of flame velocity, where the denominator of the right-hand side of equation (4.91) goes to zero. This condition leads to a quadratic equation for the flame velocity whose positive root yields

$$\frac{u_f^*}{a_o} = \frac{1}{\gamma - 1} \left( \sqrt{1 + 4 \frac{k_B T_{bo}}{E_a} \frac{T_{bo}}{T_o}} - 1 \right). \quad (4.92)$$

For the set of thermochemical parameters under consideration, this expression results in a critical flame velocity of  $u_f^*/a_o = 2.37$ , which is in close agreement with the velocity at the turning point for the different curves in Figure 4.4.

A first-order expansion of the square root of (4.92) results in a more meaningful analytical expression

$$\beta \rightarrow \infty : \quad \frac{u_f^*}{a_o} = \underbrace{\frac{1}{\gamma - 1}}_{(i)} \underbrace{\frac{2k_B T_{bo}}{E_a}}_{(ii)} \underbrace{\frac{T_{bo}}{T_o}}_{(iii)} + \mathcal{O} \left( \frac{1}{\beta} \right) \quad (4.93)$$

which corresponds to the universal critical flame speed proposed by Clavin (2022). This analytical expressions allows for the identification of the dependence of the critical velocity on three distinct factors: (i) temperature sensitivity of the gaseous medium to pressure changes; (ii) laminar burning speed sensitivity to temperature; (iii) burned gas temperature sensitivity to fresh mixture temperature ahead of the flame.

Some conclusions can be drawn from this analysis. First, in the Newtonian approximation  $\gamma \rightarrow 1$  which neglects compressive heating, there is no critical velocity. The runaway mechanism for DDT requires that the temperature ahead of the gas increases due to the piston-like effect of the flame front. A highly temperature sensitive reactive mixture characterized by a large activation energy will reach the critical conditions at a

#### 4 Deflagration-to-detonation transition at the tip of a flame in thin tubes

slower velocity. In a reactive mixture with a large heat of reaction, the relative increment in burned gas temperature for a increment in the reactive mixture temperature are smaller, leading to a larger critical flame velocity.

The difference between both expressions (4.92) and (4.93) arises from the fact that the squared term in the isentropic heating (4.89) has been retained in (4.92), providing a more accurate approximation when the critical flame velocity  $u_f^*$  is close or even larger than the unperturbed sound speed  $a_o$ . Therefore, when the critical flame velocity is well below the unperturbed sound speed  $u_f/a_o \ll 1$ , both expressions yield similar results. It is important to note that the difference between the two expressions represents only a quantitative correction for large critical flame velocities. Thus, the conclusions drawn for (4.93) are expected to be equally valid for (4.92).

##### *Double-feedback mechanism and turning point*

The theoretical analysis of Deshaies and Joulin (1989) revealed that the thermal feedback of a compression wave on the velocity of the flame front leads to a singularity in flame acceleration within a finite time. This finite-time singularity is identified as a turning point in the curve of steady-state solutions for a system composed of a flame and a shock wave. The feedback loop operates as follows: an acceleration of the flame front results in the emission of compression waves in order to satisfy the boundary conditions; the compression waves slightly heat up the reactive mixture, causing an increase of the burning velocity. This feedback loop eventually leads to a critical flame velocity above which the flame accelerates limitlessly.

The backflow of burned gases in the elongated flame model of Clavin and Tofaili (2021) introduces an additional feedback mechanism, which bring forward the advent of critical conditions with respect to that obtained by Deshaies and Joulin (1989). The additional feedback mechanism works as follows: an increase in flame burning causes a larger production of burned gases in the flame skirt, which subsequently expand and generates a greater backflow of burned gases towards the flame tip. As a result, the new boundary conditions imposed behind the flame reinforce the induced flow ahead of the flame. The flow induced by the backflow of burned gases also contributes to the compressive heating of the reactive mixture, which fuels both feedback mechanisms.

Considering the steady-state flame elongation as a function of the absolute flame propagation velocity, the turning point corresponds to a local maximum in the elongation parameter. The derivative of the elongation parameter with respect to the flame velocity for steady solutions then becomes zero at the turning point

$$S = S^* : \quad \frac{1}{S} \frac{dS}{du_f} = 0 \quad (4.94)$$

By the definition of the elongation parameter  $S = u_b/U_b$ , its derivative is zero when the relative increment of the backflow of burned gases  $\delta u_b/u_b$  is equal to the relative

increment of the burning velocity  $\delta U_b/U_b$

$$S = S^* : \quad \frac{1}{S} \frac{dS}{du_f} = 0 = \frac{1}{u_b} \frac{du_b}{du_f} - \frac{1}{U_b} \frac{dU_b}{du_f} \quad \leftrightarrow \quad \frac{1}{u_b} \frac{du_b}{du_f} = \frac{1}{U_b} \frac{dU_b}{du_f}. \quad (4.95)$$

The turning point then indicates the conditions from which the most important cause of flame acceleration alternates. In the lower branch of the steady-state curve, the flame accelerates mainly due to the increase in backflow which simultaneously induces a smaller relative increment in the burning velocity. On the other hand, along the upper branch a relative increment in the backflow leads to a larger augmentation of the relative burning velocity. Therefore, the least further increase of elongation in a flame propagating at the critical velocity given by (4.92) leads to self-acceleration, or acceleration runaway, of the flame tip. In the framework of the steady solutions, this acceleration runaway corresponds to the singularity shown by the equation (4.91) according to which the flame acceleration diverges at the turning point of the steady solutions.

This divergence in flame acceleration leads to the spontaneous formation of a shock wave at the flame front that is a good candidate for blowing out the internal flame structure producing the abrupt transition of the flame to a detonation. The formation of a shock wave within the flame front considered as a discontinuity was validated through numerical simulations in Clavin and Tofaili (2021).

## 4.4 Internal flame structure

The jump conditions applied on the reactive discontinuity representing the flame in the double-discontinuity model are valid only for steady flames. Therefore, the validity of the model is limited to a characteristic time of evolution of the boundary conditions that is much greater than the transit time. In the case of a rapid acceleration of the flame front, such as that expected around the turning point, the description of the flame under the steady approximation is problematic. To address this difficulty, it is necessary to consider the internal flame structure.

In this section, a numerical integration of the unsteady conservation equations (4.1) to (4.4) that describe the internal flame structure is presented. In particular, the reactive mixture considered is characterized by the thermochemical parameters summarized in Table 4.1 is presented. The numerical method used to integrate the governing equations is described in the first subsection. Then, the numerical results obtained for the steady propagation of a flame subject to a fixed backflow of burned gases are compared with the self-similar solutions of the double-discontinuity model. Finally, the slow evolution of the elongation parameter is simulated and compared with the solutions for the double-discontinuity model containing an isentropic compression wave.

#### 4 Deflagration-to-detonation transition at the tip of a flame in thin tubes

Pr	Le	$\gamma$	$q$	$\beta$	$\nu$	$M_{bo}$
0.7	1.0	1.4	0.875	10	2	$2 \cdot 10^{-2}$

Table 4.1: Thermochemical parameters employed in the numerical study of the internal flame structure

##### 4.4.1 Numerical method

The conservation equations (4.1) to (4.4) can be written as a non-linear system of hyperbolic conservation laws with an additional dissipation flux and a source term

$$\frac{\partial \mathbf{w}}{\partial t} + \frac{\partial \mathbf{F}(\mathbf{w})}{\partial r} = \frac{\partial^2 \mathbf{D}(\mathbf{w})}{\partial r^2} + \mathbf{S}(\mathbf{w}) \quad (4.96)$$

with

$$\mathbf{w} = \begin{pmatrix} \rho \\ \rho u \\ \rho E \\ \rho Y \end{pmatrix}, \quad \mathbf{F}(\mathbf{w}) = \begin{pmatrix} \rho u \\ \rho u^2 + \frac{1}{\gamma M_{bo}^2} p \\ \rho E u + \frac{\gamma - 1}{\gamma} p u \\ \rho Y u \end{pmatrix}, \quad \mathbf{D}(\mathbf{w}) = \begin{pmatrix} 0 \\ \text{Pr } u \\ T \\ \frac{1}{\text{Le}} Y \end{pmatrix}, \quad (4.97)$$

and

$$\mathbf{S}(\mathbf{w}) = \begin{pmatrix} 0 \\ 0 \\ \rho q \omega + M_{bo}^2 (\gamma - 1) \text{Pr} \frac{\partial}{\partial r} \left( u \frac{\partial u}{\partial r} \right) \\ \rho \omega \end{pmatrix}, \quad (4.98)$$

where  $\mathbf{w}$  is the vector of conserved quantities,  $\mathbf{F}(\mathbf{w})$  is the vector of convective fluxes,  $\mathbf{D}(\mathbf{w})$  is the vector of diffusive fluxes, and  $\mathbf{S}(\mathbf{w})$  is a vector of source terms from the combustion reactions and viscous dissipation.

##### *Strang splitting*

A splitting approach is employed which divides the time interval  $\Delta t$  into two subproblems: advection and reaction-diffusion. This model has been shown to provide exact solutions for certain model inhomogeneous partial differential equations and is considered a viable approach for more general problems (Toro, 2009). Furthermore, an important advantage of splitting schemes is the ability to use optimal schemes for each subproblem. For instance, a solver for nonlinear hyperbolic equations can be used to solve the homogeneous problem, while an implicit scheme can be used to solve the reaction-diffusion problem.

In particular, a Strang splitting approach is followed, which has been proven to be second order Strang (1968). The algorithm is defined as follows

$$\mathbf{w}^{n+1} = \mathcal{D}^{(\Delta t/2)} \mathcal{C}^{(\Delta t)} \mathcal{D}^{(\Delta t/2)} (\mathbf{w}^n) \quad (4.99)$$

where the superscript  $\mathbf{w}^n$  denotes the solution at the time step  $t = t^n$ ,  $\mathcal{D}$  is the convective operator, and  $\mathcal{C}$  is the reaction-diffusion operator. The algorithm first integrates the diffusion-reaction problem for half a time step. The resulting solution is then used to integrate the conductive term. And, finally, the second half of the diffusion-reaction problem is integrated on the solution.

The same spatiotemporal discretization is applied to both subproblems. The maximum mesh grid size  $\Delta x$  is dictated by the reaction-diffusion problem to ensure that a sufficient number of mesh points are located within the reactive layer, which is the smallest relevant spatial scale of the problem. The time step, on the other hand, is constrained by the stability Courant-Friedrichs-Lewy (CFL) condition (Courant et al., 1928). For compressible flows, the CFL condition is given by

$$\text{CFL} = \max(|u| + a) \frac{\Delta t}{\Delta x} \leq 1 \quad (4.100)$$

where a conservative value of  $\text{CFL} = 0.9$  is used throughout the computations in this section.

#### *Convective subproblem*

The convective subproblem corresponds to the initial value problem given by

$$\frac{\partial \mathbf{w}}{\partial t} + \frac{\partial \mathbf{F}(\mathbf{w})}{\partial r} = 0 \quad (4.101)$$

with the initial condition

$$\mathbf{w}(r, t^n) = \bar{\mathbf{w}}^{n+1/2}. \quad (4.102)$$

This problem requires evolving the solution  $\bar{\mathbf{w}}^{n+1/2}$  at time  $t = t^n$  to the new value  $\tilde{\mathbf{w}}^{n+1}$  at  $t = t^{n+1} = t^n + \Delta t$  using the convective operator  $\mathcal{C}$ .

The convective operator  $\mathcal{C}$  is based on the high-resolution central solver for nonlinear conservation laws of Kurganov and Tadmor (2000), which employs a central difference approximation given by

$$\frac{d\mathbf{w}_j}{dt} = - \frac{\mathbf{H}_{j+1/2}(t) - \mathbf{H}_{j-1/2}(t)}{\Delta x_i}. \quad (4.103)$$



#### 4 Deflagration-to-detonation transition at the tip of a flame in thin tubes

The numerical flux  $\mathbf{H}(t)$  is defined by

$$\mathbf{H}_{j+1/2}(t) = \frac{\mathbf{F}\left(\mathbf{w}_{j+1/2}^+(t)\right) + \mathbf{F}\left(\mathbf{w}_{j+1/2}^-(t)\right)}{2} - \frac{a_{j+1/2}(t)}{2} \left[ \mathbf{w}_{j+1/2}^+(t) - \mathbf{w}_{j+1/2}^-(t) \right], \quad (4.104)$$

with the intermediate values given by

$$\mathbf{w}_{j+1/2}^+ = \mathbf{w}_{j+1}(t) - \frac{\Delta x}{2} (\mathbf{w}_x)_{j+1}(t) \quad \text{and} \quad \mathbf{w}_{j+1/2}^- = \mathbf{w}_{j+1}(t) + \frac{\Delta x}{2} (\mathbf{w}_x)_j(t). \quad (4.105)$$

The approximate derivatives are computed through the least dissipative minmod-like limiter, as shown in

$$(\mathbf{w}_x)_j = \text{minmod} \left( 2 \frac{\mathbf{w}_j - \mathbf{w}_{j-1}}{\Delta x}, \frac{\mathbf{w}_{j+1} - \mathbf{w}_{j-1}}{2\Delta x}, 2 \frac{\mathbf{w}_{j+1} - \mathbf{w}_j}{\Delta x} \right). \quad (4.106)$$

For second-order methods, such as the one proposed by Kurganov and Tadmor (2000), the application of boundary conditions follows the same fundamental approach as the Godunov method (Toro, 2009). Specifically, for a computational domain  $[0, L]$  discretized by  $J$  cells  $I_j$ , so that the cells  $j = 1, \dots, J$  lie within the computational domain, the boundary conditions are expected to provide the numerical fluxes  $\mathbf{H}_{-1/2}$ ,  $\mathbf{H}_{1/2}$ ,  $\mathbf{H}_{J+1/2}$  and  $\mathbf{H}_{J+3/2}$  required to update the extreme cells  $I_1$ ,  $I_2$ ,  $I_{J-1}$  and  $I_J$ . These numerical fluxes may be directly prescribed by the boundary conditions or obtained by prescribing fictitious data values in the fictitious cells adjacent to the extreme cells. The fictitious cells are denoted by  $j = -1$  and  $j = 0$  for the left boundary at  $x = 0$ , and by  $j = J + 1$  and  $j = J + 2$  for the right boundary at  $x = L$ . In this way, boundary Riemann problems are solved, and the corresponding fluxes are computed following the approach used for the interior cells.

Two types of boundary conditions are utilized in this problem: reflective boundary conditions are applied on the left side to account for the piston-like effect of the backflow of burned gases, and transmissive boundary conditions are applied on right side of the domain. For a reflective solid boundary at  $x = 0$  moving with velocity  $u_{\text{wall}}$ , the reflective boundary conditions for the Euler equations are applied as

$$\begin{aligned} \rho_0^n &= \rho_1^n, & u_0^n &= -u_1^n + 2u_{\text{wall}}, & p_0^n &= p_1^n, \\ \rho_{-1}^n &= \rho_2^n, & u_{-1}^n &= -u_2^n + 2u_{\text{wall}}, & p_{-1}^n &= p_2^n. \end{aligned} \quad (4.107)$$

The transmissive or transparent boundary conditions at  $x = L$  are given by

$$\mathbf{w}_{J+1}^n = \mathbf{w}_J^n, \quad \text{and} \quad \mathbf{w}_{J+2}^n = \mathbf{w}_{J-1}^n, \quad (4.108)$$

where  $\mathbf{w}$  may be the vector of conserved or primitive variables.

*Reaction-diffusion subproblem*

The reaction-diffusion subproblem corresponds to the initial value problem given by

$$\frac{\partial \mathbf{w}}{\partial t} = \frac{\partial^2 \mathbf{D}(\mathbf{w})}{\partial r^2} + \mathbf{S}(\mathbf{w}) \quad (4.109)$$

whose first integration begins from the initial condition

$$\mathbf{w}(r, t^n) = \mathbf{w}^n. \quad (4.110)$$

This integration evolves the solution  $\mathbf{w}^n$  at time  $t = t^n$  to the new value  $\bar{\mathbf{w}}^{n+1/2}$  at  $t = t^{n+1/2} = t^n + \Delta t/2$ . The second integration begins from the initial condition

$$\mathbf{w}(r, t^{n+1/2}) = \bar{\mathbf{w}}^{n+1/2}. \quad (4.111)$$

to evolve the solution  $\bar{\mathbf{w}}^{n+1/2}$  at time  $t = t^{n+1/2}$  to the new value  $\mathbf{w}^{n+1}$  at  $t = t^{n+1} = t^n + \Delta t$ .

Utilizing the first equation of (4.109), which indicates that the density remains constant during the reaction-diffusion problem, and subtracting the momentum conservation equation multiplied by  $u$  from the total energy conservation equation to obtain a equation for the conservation of thermal energy, the system of equations (4.109) can be rewritten as

$$\frac{\partial u}{\partial t} = \frac{\text{Pr}}{\rho} \frac{\partial^2 u}{\partial r^2}, \quad (4.112)$$

$$\frac{\partial T}{\partial t} = \frac{\gamma}{\rho} \frac{\partial^2 T}{\partial r^2} + M_{\text{bo}}^2 \text{Pr} (\gamma - 1) \frac{\gamma}{\rho} \left( \frac{\partial u}{\partial r} \right)^2 + \gamma \frac{q}{\tau_{\text{rb}}} \omega, \quad (4.113)$$

$$\frac{\partial Y}{\partial t} = \frac{1}{\rho \text{Le}} \frac{\partial^2 Y}{\partial r^2} + \frac{1}{\tau_{\text{rb}}} \omega \quad (4.114)$$

Considering an explicit time integration of the source terms from the dissipative and reactive effects such that their values are directly computed from the initial condition, the three equations in (4.114) become three decoupled diffusion equations with a constant source term, which can be solved independently.

The solution of the archetypal diffusion equation with a source term

$$\frac{\partial \phi}{\partial t} = \alpha \frac{\partial^2 \phi}{\partial r^2} + \sigma \quad (4.115)$$

can be approximated through a unconditionally stable implicit scheme based on the temporal backward finite difference and spatially centered finite differences as

$$\frac{\phi_j^{n+1} - \phi_j^n}{\Delta t} = \alpha_j^n \frac{\phi_{j-1}^{n+1} - 2\phi_j^{n+1} + \phi_{j+1}^{n+1}}{\Delta r^2} + \sigma_j^n \quad (4.116)$$

#### 4 Deflagration-to-detonation transition at the tip of a flame in thin tubes

leading to the tridiagonal system of linear equations

$$\alpha_j^n \frac{\Delta t}{\Delta r^2} \phi_{j-1}^{n+1} - \left(1 + 2\alpha_j^n \frac{\Delta t}{\Delta r^2}\right) \phi_j^{n+1} + \alpha_j^n \frac{\Delta t}{\Delta r^2} \phi_{j+1}^{n+1} = -\phi_j^n - \Delta t \sigma_j^n \quad (4.117)$$

which is efficiently solved by the Thomas algorithm (Hirsch, 2007).

In the resolution of the reaction-diffusion problem, identical boundary conditions are imposed on both boundaries of the domain. These boundaries are assumed to be adiabatic, thereby preventing diffusive fluxes from entering or leaving the computational domain. To achieve this, Neumann boundary conditions with a zero spatial gradient are enforced at the boundaries. This is done by modifying the first and last equations of the system (4.117). Specifically, the first equation is modified as follows

$$-\left(1 + 2\alpha_1^n \frac{\Delta t}{\Delta r^2}\right) \phi_1^{n+1} + 2\alpha_1^n \frac{\Delta t}{\Delta r^2} \phi_2^{n+1} = -\phi_1^n - \Delta t \sigma_1^n, \quad (4.118)$$

and the last equation is modified as

$$2\alpha_J^n \frac{\Delta t}{\Delta r^2} \phi_{J-1}^{n+1} - \left(1 + 2\alpha_J^n \frac{\Delta t}{\Delta r^2}\right) \phi_J^{n+1} = -\phi_J^n - \Delta t \sigma_J^n. \quad (4.119)$$

#### 4.4.2 Steady flame propagation

The influence of the backflow of burned gases in the propagation of a steady flame is analysed below when the internal flame structure is considered. For this purpose, a parametric study has been conducted by numerically integrating the conservation equations (4.65) to (4.68) for different values of the backflow of burned gases  $u_b$  in the range 0 – 30.

##### *Initial conditions*

In order to accelerate the convergence towards a steady solution, the simulation is initialized considering the solution of the double-discontinuity model and the external flow obtained from the ZFK asymptotic analysis. The initial profiles are divided into three zones: a region of burned gases for  $r < r_f$ , the preheat zone of the flame  $r_f < r < r_s$ , and the unperturbed region ahead of the leading shock wave  $r > r_s$ . The temperature and product mass concentration profiles ahead of the leading shock are set to the initial values of the unperturbed reactive mixture, while those behind the shock wave are computed from the analytical solution obtained in the ZFK analysis (4.47), using the corresponding Neumann state behind the shock and the scaled flame length

$$l_f = \frac{l'_f}{l'_{fo}} = \frac{D'_{Tb} U'_{bo}}{D'_{Tbo} U'_b} = \frac{1}{\rho_b U_b}. \quad (4.120)$$

The initial temperature and mass concentration profiles are given by the following piecewise functions

$$t = 0 : \quad T(r) = \begin{cases} T_N + q & \text{if } r < r_f, \\ T_N + q \exp\left(-\frac{r - r_f}{l_f}\right) & \text{if } r_f < r < r_s, \\ 1 - q & \text{if } r > r_s, \end{cases} \quad (4.121)$$

$$Y(r) = \begin{cases} 1 & \text{if } r < r_f, \\ \exp\left(-\text{Le} \frac{r - r_f}{l_f}\right) & \text{if } r_f < r < r_s, \\ 0 & \text{if } r > r_s. \end{cases} \quad (4.122)$$

where  $r_f = l_f$  corresponds to the initial length of the burned gas region, which is set to be equal to the flame thickness, and  $r_s = 6 l_f$  is the initial position of the leading shock, which is placed at a distance of five times the flame thickness from the reactive front. The initial pressure profile is defined as a piecewise constant function that satisfies the Rankine-Hugoniot relation at the shock wave

$$t = 0 : \quad p(r) = \begin{cases} p_N & \text{if } r < r_s, \\ 1 & \text{if } r > r_s. \end{cases} \quad (4.123)$$

The density profile is obtained by dividing the previously defined pressure profile by the temperature profile, according to the equation of state (4.70),

$$t = 0 : \quad \rho(r) = \frac{p(r)}{T(r)}. \quad (4.124)$$

The velocity profile is defined piecewise to satisfy the conservation of mass in the internal flame structure and to ensure that the flow ahead of the shock wave is at rest

$$t = 0 : \quad \begin{cases} u_b + \left[1 - \frac{\rho(r_f)}{\rho(r)}\right] U_b & \text{if } r < r_s \\ 0 & \text{if } r > r_s. \end{cases} \quad (4.125)$$

Figure 4.5 presents an example of the results obtained for the initialization of a steady flame with a fixed backflow of  $u_b = 5$ . It is observed that the initial oscillations resulting from the presence of a jump discontinuity at the shock wave and a gradient discontinuity in the reaction zone are smoothed out in a time period shorter than the transit time of the flame  $t < 1$  leading to a stable solution. A steady regime is reached which will be compared with the solutions obtained in the framework of the double-discontinuity model.

#### 4 Deflagration-to-detonation transition at the tip of a flame in thin tubes

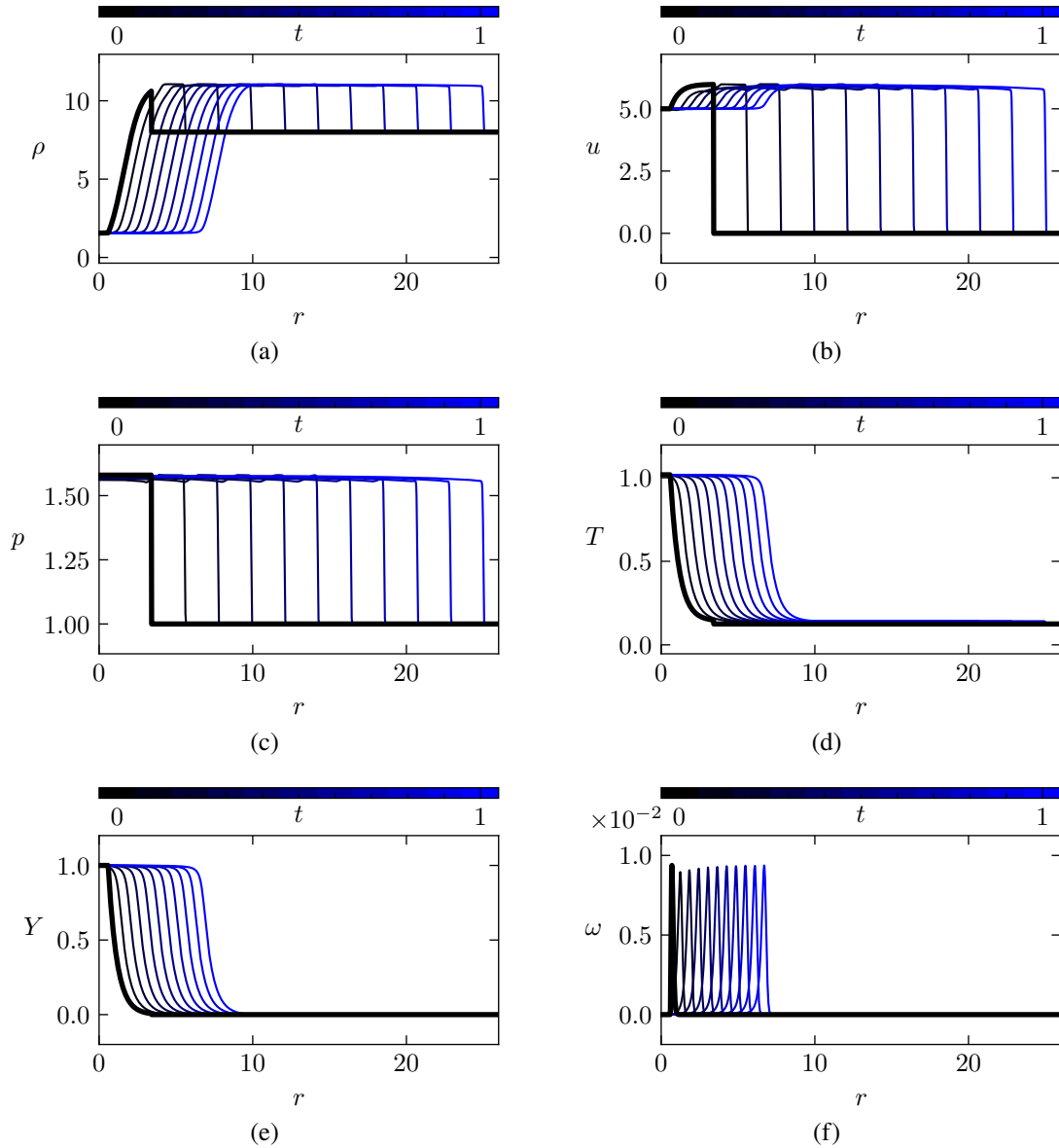


Figure 4.5: (a) Density, (b) flow velocity, (c) pressure, (d) temperature, (e) product mass fraction, (f) reaction rate profiles at evenly distributed time steps  $\Delta t = 0.1$  from the initial conditions  $t = 0$  (black) to  $t = 1$  (blue) with a burned gas backflow of  $u_b = 5$  for the set of thermochemical parameters summarized in Table 4.1.

*Self-similar solutions*

The numerical integration of the governing equations (4.65) to (4.68) successfully replicates the self-similar description of the external flow. The profiles of the physical variables at various time steps, for a backflow of burned gases of  $u_b = 20$ , are represented in Figure 4.6 in the self-similar coordinate obtained by dividing the dimensionless spatial coordinate by the time coordinate. In this regime, a flame transit time is sufficient to show the convergence towards the self-similar structure of the flow. The self-similar structure is clearly identifiable as the simulation progresses, and the distance between the leading shock and the flame becomes large enough to consider both waves as discontinuities. The shock wave is represented by the jump discontinuity on the right of the figure at  $r/t = 34.9$ , where density, velocity, temperature and pressure increase according to the Rankine-Hugoniot jump conditions. Meanwhile, the mass concentration of the products remains unchanged, as no chemical transformations take place in the shock wave. The discontinuity located approximately in the middle of the plot at  $r/t = 22.0$  corresponds to the flame internal structure, where the temperature increases due to the heat release, causing the density decreases in an isobaric process, and all the reactants are transformed into products.

It is important to note that after a certain time, specifically when the initial position becomes irrelevant, the positions of the different fronts on the self-similar coordinate represent the velocity of propagation of each front in units of the burning speed in the initial mixture  $r/t = r'/(t'U'_{bo})$ . That is, the flame-driven shock wave propagates approximately 35 times faster than the flame speed in an unperturbed medium and the absolute propagation velocity of the flame is roughly 22 times faster than its typical speed when a backflow of  $u_b = 20$  is applied behind the flame. This increase in the absolute propagation speed is the result of the combination of the advection by the backflow of burned gases and the thermal propagation speed of the flame which is increased under the effect of the thermal feedback from the shock wave.

*Parametric study*

A parametric investigation has been carried out to examine the effect of varying the backflow of burned gases  $u_b$ . The results of the study in the long time limit  $t = 10$ , are represented in Figure 4.7, which depict the self-similar profiles obtained from the parametric analysis. In these figures, it is observed the increase in intensity of the leading shock wave and the flame acceleration as the backflow of burned gases increases.

The flame elongation parameters  $S$  of the corresponding one-dimensional solution obtained by numerical integration have been computed by tracking the position of the flame. The temporal evolution of the flame positions, defined as the location of the isovalue in product mass concentration  $Y = 0.98$ , are represented in Figure 4.8a for different backflow values. The constant slope in the trajectories of the flame position confirms the steady propagation of the flame. A faster flame velocity is also evident for larger values of the backflow given the steeper slope of the flame trajectories. The velocity of the flame is determined numerically as the time derivative of the flame position,

#### 4 Deflagration-to-detonation transition at the tip of a flame in thin tubes

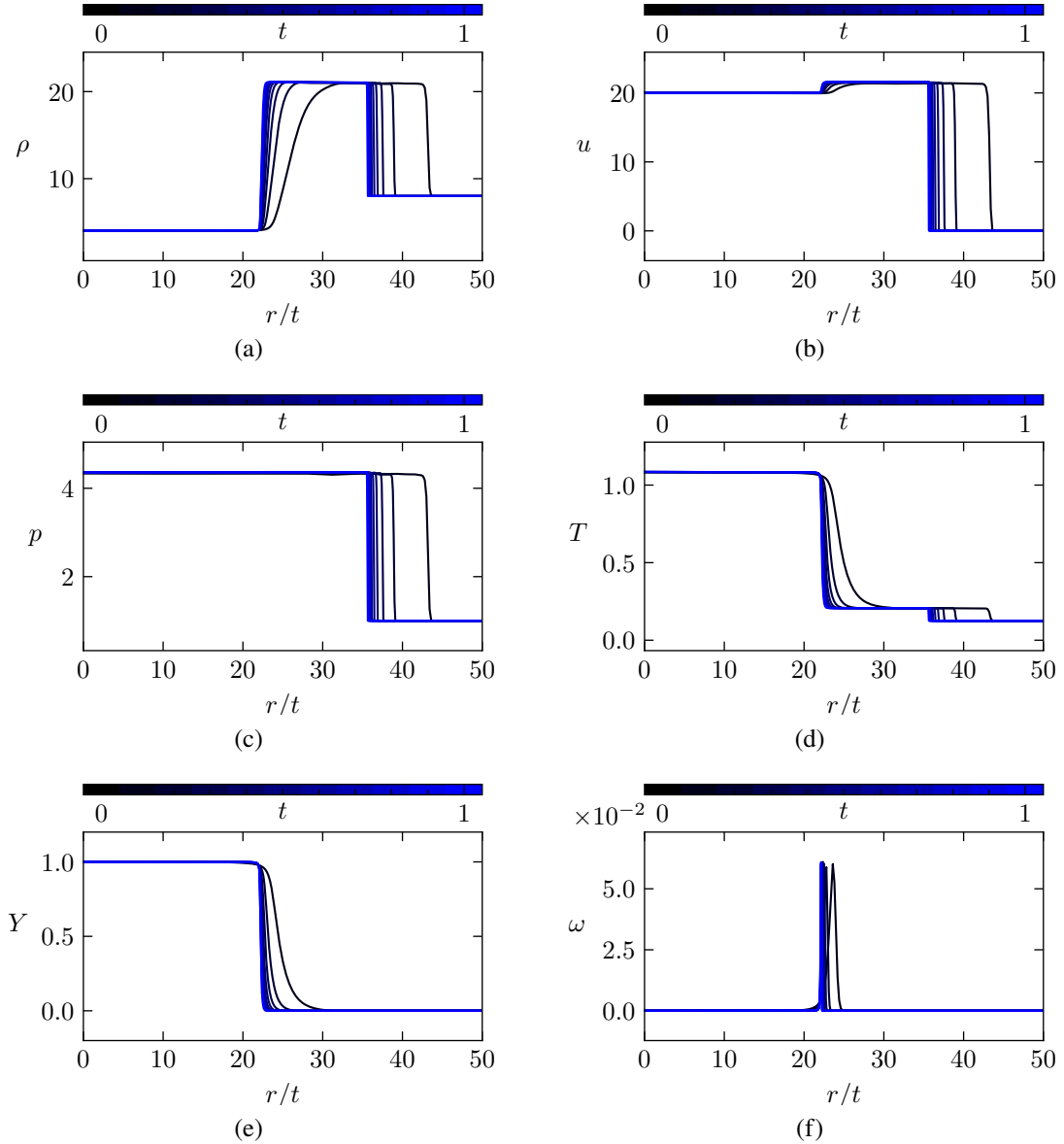


Figure 4.6: (a) Density, (b) flow velocity, (c) pressure, (d) temperature, (e) product mass fraction, and (f) reaction rate profiles at different time steps  $\Delta t = 0.1$  from the initial conditions  $t = 0$  (black) to  $t = 1$  (blue) in self-similar coordinate with a burned gas backflow of  $u_b = 20$  resulting in an elongation parameter of  $S = 10.44$ . The thermochemical properties of the flame are characterized by the parameters summarized in Table 4.1.

#### 4.4 Internal flame structure

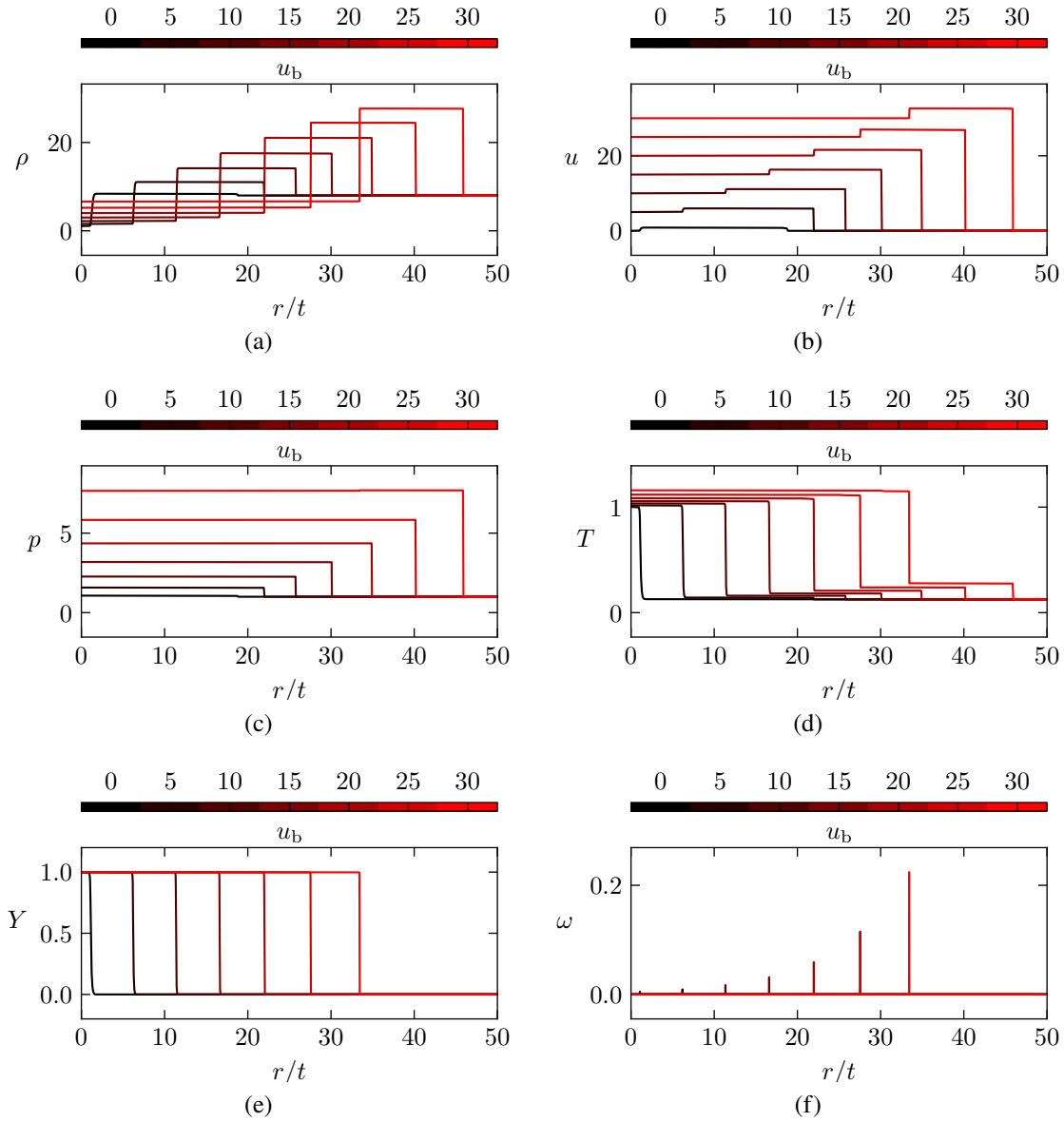


Figure 4.7: (a) Density, (b) flow velocity, (c) pressure, (d) temperature, (e) product mass fraction, and (f) reaction rate profiles in the self-similar coordinate at  $t = 10$  for different values of the burned gases backflow  $\Delta u_b = 5$  from  $u_b = 0$  (black) to  $u_b = 30$  (red). The thermochemical properties of the mixture are characterized by the parameters summarized in Table 4.1.



#### 4 Deflagration-to-detonation transition at the tip of a flame in thin tubes

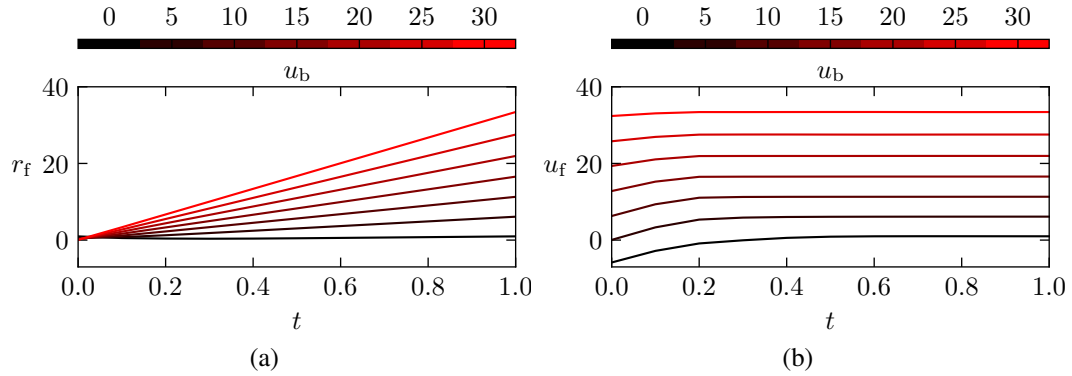


Figure 4.8: (a) Temporal evolution of the flame position, defined as the computational point with a product mass concentration isovalue of  $Y = 0.98$  for different values of the backflow of burned gases. (b) Temporal evolution of the absolute flame propagation velocity determined by numerically differentiating with respect to time its position for different values of the backflow of burned gases.

calculated using a second-order central difference approximation, which is depicted in Figure 4.8b. The different simulations, characterized by distinct values of backflow of burned gases, reach a steady regime within less than a transit time.

Once the absolute velocity of the flame  $u_f$  is established for a given backflow  $u_b$ , the burning speed, which represents the velocity of the flame relative to the burned gases, can be obtained by subtracting the backflow of burned gases from the absolute flame velocity. The numerical results for the burning speed as a function of the varying backflow are represented in Figure 4.9a, along with the relationship between the velocities obtained from the double-discontinuity model in Section 4.3.1, demonstrating good agreement.

Similarly, the absolute flame velocity is depicted in Figure 4.9b as a function of the elongation parameter  $S = u_b/U_b$  and compared with the nonlinear relationship obtained from the double-discontinuity model. The resulting elongation parameter also exhibits a turning point, indicating that there exists a critical flame length beyond which there is no steady solution for the tip of an elongated flame.

#### 4.4.3 Slow flame elongation

The results of the numerical simulation of the internal structure of the flame for a slow flame elongation are presented in this subsection. The complex dynamics in the flame skirt involving boundary layer effects combined with compressible and reactive effects are not studied here. Instead, the evolution of the flame envelope is characterized by the monotonic growth of the flame elongation parameter. The flame surface it is assumed to evolve on a timescale much larger than its characteristic time given by the transit time of a particle through the flame thickness. The flame elongation increases linearly in time,

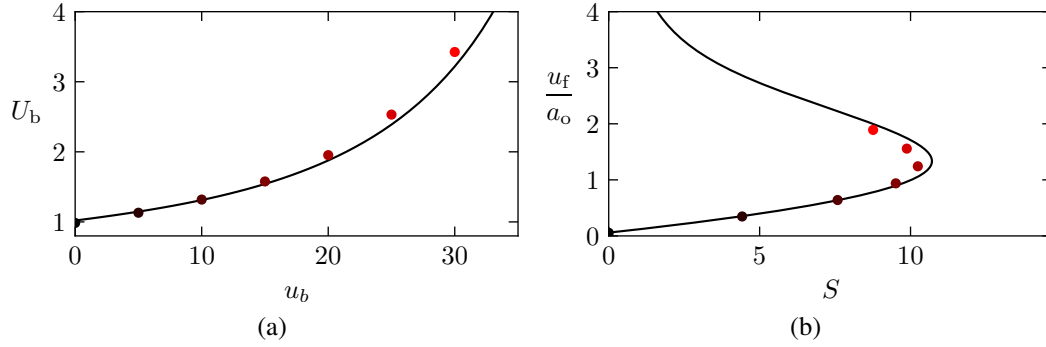


Figure 4.9: Numerical results of the parametric study for the backflow of burned gases considering the internal flame structure (colored circles) compared with the double-discontinuity model (black line). The parametric study covers the range from  $u_b = 0$  (black) to  $u_b = 30$  (red). (a) Burning velocity  $U_b$  with respect to the backflow of burned gases  $u_b$  (b) Absolute flame propagating velocity to sound speed ratio  $u_f/a_o$  as a function of the flame elongation parameter  $S$ .

with a characteristic time  $t'_S$  that is significantly larger than the flame transit time

$$S(t) = S_0(1 + \varepsilon t), \quad (4.126)$$

where  $\varepsilon = t'_f/t'_S$  represents the small, but finite, ratio of timescales, and  $S_0$  is the flame elongation parameter at time  $t = 0$ .

The numerical integration of the governing equations (4.65) to (4.68) is performed within the boundary conditions imposed by the backflow of burned gases from the elongated flame model and evolving the flame elongation in time according to the equation (4.126). The burning velocity  $U_b = \bar{U}_{\text{ZFK}}(\bar{T}_b(T_u))$ , which determines the backflow of burned gases as follows from (4.76), is computed as the steady-state burning velocity which was derived from the ZFK analysis in (4.81). The unburned gas temperature  $T_u$ , defined as the temperature at the grid point where the product mass concentration is of  $Y = 10^{-4}$

$$r = r_u : \quad Y(r) = 10^{-4}, \quad \text{and} \quad T(r) = T_u, \quad (4.127)$$

is used in the computation of the backflow of burned gases applied at the exit of the reaction zone

$$\begin{aligned} r = r_f : \quad u(r) &= u_b = S(t)U_b = S(t)\bar{U}_{\text{ZFK}}(\bar{T}_b(T_u)) \\ &= S(t)(T_u + q)^{\nu+1} \exp\left[\frac{E_a}{k_B T_{bo}} \left(1 - \frac{1}{T_u + q}\right)\right]. \end{aligned} \quad (4.128)$$

In the context of a compression wave propagating from the burned gases towards the fresh mixture, heating up the gas, the burning velocity obtained from this expression can be interpreted as the burning velocity at the flame tip, taking into account a short time delay corresponding to the time required by a fluid particle at the position  $r_u$  to reach the

#### 4 Deflagration-to-detonation transition at the tip of a flame in thin tubes

reactive zone.

The boundary conditions corresponding to the burned gases boundary condition at the exit of the reaction zone are applied to the numerical domain by following the flame. At the beginning of each time step, it is checked if the product mass concentration exceeds a threshold value of  $Y = 0.98$ . If this is the case, the grid point closest to the numerical boundary is removed, and the boundary condition is applied at the subsequent mesh point. The size of the numerical domain is kept constant, and the removal of a grid point on the burned side is compensated by the adding a mesh point on the unburned side with the same conserved variables as the neighboring grid point. This approach allows the numerical domain to follow the flame and correctly apply the boundary conditions at the exit of the reaction zone.

The initial conditions for the simulation are obtained from the numerical solutions of the propagation of a steady flame. The initial profiles of the conserved variables in the internal flame structure corresponds to the initial profiles in the same regime of backflow while the leading shock wave is removed from the numerical domain filling the domain between the shock wave and the fresh boundary with a constant profile.

##### *Flame acceleration*

An example of the numerical results obtained for the set thermochemical parameters summarized in Table 4.1, the initial conditions corresponding to a backflow  $u_b = 20$  and a flame elongation evolution characterized by the timescale ratio  $\varepsilon = 5 \cdot 10^{-2}$  is presented in Figures 4.10 to 4.12 during the phase of flame acceleration. The evolution of the physical variables across the numerical domain is depicted in Figure 4.10 in a fixed coordinate system, which corresponds to the close-end tube or laboratory reference frame. At the large scale of the problem defined by the compression wave, the flame appears as a discontinuity, where the temperature and the mass concentration of products increase sharply, while the pressure remains constant, and the absolute flow velocity decreases due to the conservation of mass throughout the flame. The propagation of the leading edge of the compression wave is observed ahead of the flame. As demonstrated by Clavin and Tofaili (2021), when the flame elongation evolves at a slow enough rate, a shock wave does not form in the compression wave before reaching the acceleration runaway.

Figure 4.11 displays the internal structure of the flame during the quasi-steady evolution in a coordinate system that is attached to the flame. The figure shows a smooth transition from the unburned to the burned states of the physical variables within the internal flame structure is observed. Despite being imperceptible in the temperature profiles, the temperature increase due to compressive heating progressively accelerates the flame up to a acceleration runaway, owing to the strong temperature sensitivity. This increase in temperature has a more noticeable impact on the thickness of the flame, which abruptly shrinks at the acceleration runaway. This sudden reduction of the flame thickness poses a significant challenge for numerical integration methods based on the discretization of the spatial domain.

In Figure 4.12, the flame velocity is represented in the reference frame of the tube and

#### 4.4 Internal flame structure

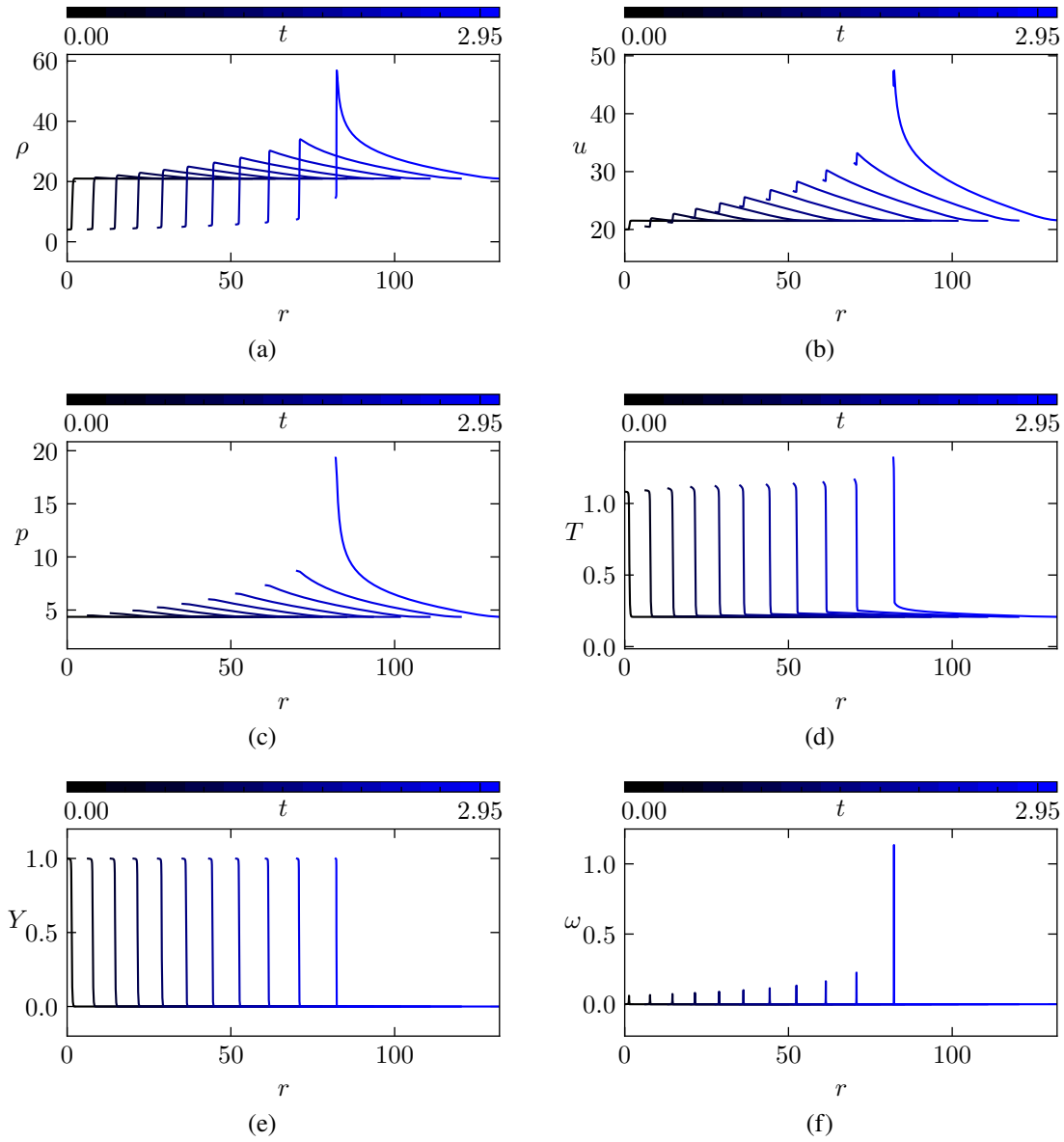


Figure 4.10: (a) Density, (b) flow velocity, (c) pressure, (d) temperature, (e) product mass fraction, and (f) reaction rate profiles in the fixed coordinate system during the quasi-steady flame acceleration. The simulation is initialized with the internal flame structure of the steady solution for a fixed backflow of burned gases  $u_b = 20$  (see Figure 4.6) at  $t = 0$ . The profiles shown evolve from  $t = 0$  (black) to  $t = 2.95$  (blue) in time steps of  $\Delta t = 0.295$  and they are represented in the fixed coordinate system of the tube with the origin at the initial position of the flame. The time-dependent flame elongation follows the law (4.126) with  $\varepsilon = 5 \cdot 10^{-2}$  and  $S_0 = 10.44$ . The thermochemical properties of the flame are characterized by the parameters summarized in Table 4.1.

#### 4 Deflagration-to-detonation transition at the tip of a flame in thin tubes

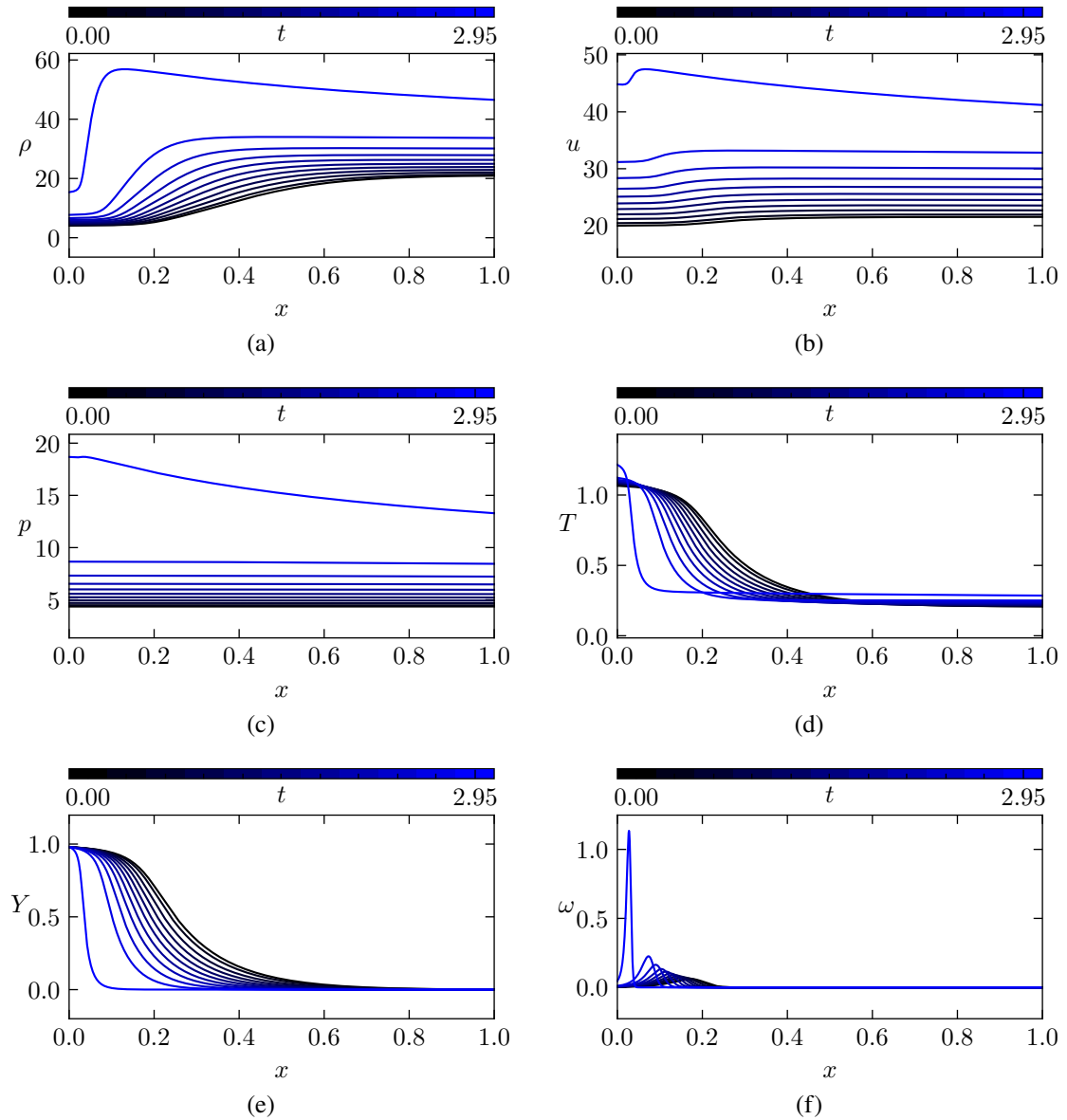


Figure 4.11: (a) Density, (b) flow velocity, (c) pressure, (d) temperature, (e) product mass fraction, and (f) reaction rate profiles in the flame-attached coordinate system during the quasi-steady flame acceleration. The simulation is initialized with the internal flame structure of the steady solution for a fixed backflow of burned gases  $u_b = 20$  (see Figure 4.6) at  $t = 0$ . The profiles shown evolve from  $t = 0$  (black) to  $t = 2.95$  (blue) in time steps of  $\Delta t = 0.295$  and they are represented in the flame attached coordinate system  $x = r - r_f(t)$  with  $r_f(t)$  defined as the position of the product mass fraction isovalue  $Y = 0.98$ . The time-dependent flame elongation follows the law (4.126) with  $\varepsilon = 5 \cdot 10^{-2}$  and  $S_0 = 10.44$ . The thermochemical properties of the flame are characterized by the parameters summarized in Table 4.1.

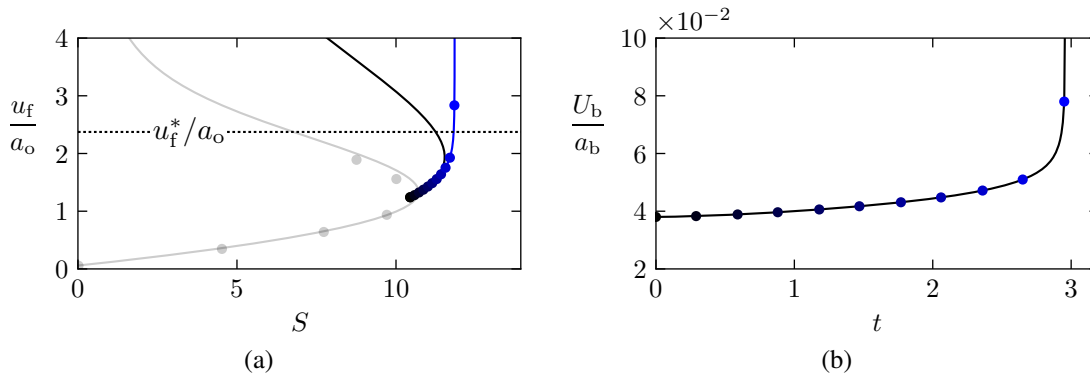


Figure 4.12: (a) Flame propagating velocity to sound speed ratio  $u_f/a_o$  as a function of the flame elongation parameter  $S$  which evolves following (4.126) with  $S_0 = 10.44$  and  $\varepsilon = 5 \cdot 10^{-2}$ . Black line: double discontinuity model with an isentropic compression wave. Blue line: flame propagating velocity to sound speed ratio obtained by numerical integration. (b) Flame velocity relative to the flow of burned gases with respect to the local sound speed. The colored circles in both figures correspond to the time steps for the profiles in Figures 4.10 and 4.11.

relative to the burned gases. The trajectory of the absolute flame velocity divided by the unperturbed sound speed against the elongation parameter is compared in Figure 4.12a with the relationship obtained for the double discontinuity model with an isentropic compression wave. Initially, the trajectory of the absolute flame velocity vs. elongation parameter closely follows the curve of the double-discontinuity model. However, as the flame velocity approaches the turning point, the flame acceleration increases, leading to a slight deviation of the trajectory of the flame velocity from the curve of double-discontinuity solutions. While in the double-discontinuity model, the reactive layer is infinitesimally thin and adapts instantaneously to the new boundary conditions, in the numerical integration of the conservation equations the thickness of the reactive layer is small but finite, causing a finite delay in the answer of the flame velocity. Once the turning point of the solutions of the double-discontinuity model is surpassed, the flame eventually undergoes an abrupt acceleration, leading to a flame acceleration runaway, which corresponds to the finite time singularity in the steady solutions anticipated by Clavin (2022). The temporal evolution of the flame velocity relative to the burned gases with respect to the local sound speed is depicted in Figure 4.12b. Despite the increase in flame velocity relative to the burned gases increases due to the temperature rise, it remains markedly subsonic, even at the divergence of the flame acceleration. Thus, the acceleration runaway occurs well before the Chapman-Jouguet marginal solution for reactive waves, characterized by the sonic condition, is reached.

#### *Influence of the timescale ratio*

To investigate the factors underlying the departure of the flame velocity trajectory from the turning point, a parametric investigation has been conducted by varying the timescale

#### 4 Deflagration-to-detonation transition at the tip of a flame in thin tubes

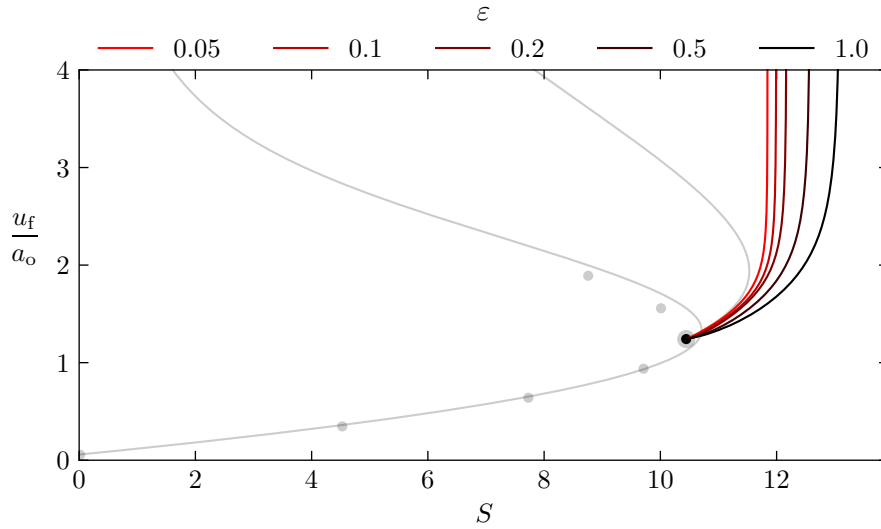


Figure 4.13: Flame propagating velocity to sound speed ratio as a function of the elongation parameter which evolves following (4.126) with  $S_0 = 10.44$  and different timescale ratios in the range  $\varepsilon = 0.05$  (red) to  $\varepsilon = 1.0$  (black).

ratio  $\varepsilon$ . This parameter governs the evolution of the elongation parameter in relation to the flame transit time, as defined in (4.126). The results of this analysis are presented in Figure 4.12. It is observed that a higher rate of growth of the elongation parameter corresponds to an increased critical flame elongation value. Conversely, a lower growth rate of the elongation parameter leads to the critical value approaching the turning point of the curve of solutions for the double-discontinuity model. A similar behaviour is observed in the dynamic saddle-node bifurcations, where a breaking time exists above which the stable steady state disappears, although a time delay must elapse before reaching a point of no return where the irreversible critical transition occurs (Peters et al., 2012; Li et al., 2019). An investigation of the influence of the flame unsteadiness on the dynamics around the turning point in the framework of the saddle-node bifurcations has been recently conducted by Clavin (2023).

#### *Onset of the detonation*

The internal structure of the flame during the acceleration runaway leading to the onset of the detonation is depicted in Figure 4.14, where the evolution of the flame is illustrated. Additionally, the propagation of the front in the fixed coordinate system of the tube is presented in Figure 4.15. As the simulation progressed from  $t = 2.985$  to  $t = 2.990$ , the flame continues to accelerate and its internal structure becoming increasingly thin. However, between  $t = 2.990$  and  $t = 2.991$ , a sudden transition in the propagating regime is observed. The flame preheat region, where the fresh mixture is gradually heated by conduction, disappears and the physical variables evolve rapidly within a few grid points from the upstream state to a state of higher temperature and pressure in chemical

equilibrium. This sharp transition can be interpreted as a discontinuity in which the mixture undergoes simultaneous compression and combustion, as in a discontinuous detonation.

It is worth mentioning that during the numerical integration, only the results obtained every  $\Delta t = 0.001$  are stored and included in these figures. However, the CFL stability condition imposes a much finer time resolution, reaching values as small as  $\Delta t = 1 \cdot 10^{-6}$  during the simulation. Therefore, the profiles shown for  $t = 2.991$  are not direct results of integrating the conservation equations at  $t = 2.990$ , but rather a large number of computational steps have taken place in between.

The transition from diffusion-controlled propagation of the flame to detonation might be explained as follows. During the acceleration runaway, as the flame experiences strong acceleration and its internal structure shrinks, the velocity gradient within the internal flame structure steepens, causing dissipation mechanisms that are negligible at ordinary flame velocities to become significant. These dissipation mechanisms eventually result in the formation of a strong shock wave within the internal structure of the flame, which rapidly increases the temperature and further accelerates the reaction rate. The reactants get consumed in a vanishingly thin reactive layer, causing the position of the isovalue  $Y = 10^{-4}$ , where the temperature is measured to calculate the backflow of burned gases, to be swept out by the reactive supersonic wave. Due to the supersonic nature of the wave, the heat released within the reactive layer cannot propagate ahead, causing the temperature at the isovalue to be determined exclusively by the upstream conditions, which become isolated from what happens behind the supersonic wave. As a result, the temperature at the isovalue does not increase further due to the effect of the compression wave, but is instead propagated into regions of fresher reactive mixture, leading to a slowdown in the backflow of burned gases. However, once the reactive supersonic wave is established it continues to propagate without the piston-like effect of the burned gas backflow.

The evolution of the velocity of the front with respect to the sound speed is plotted in Figure 4.16, with the time instants corresponding to the profiles in Figures 4.14 and 4.15 indicated by colored full points. The onset of the detonation coincides with the maximum velocity of the front. It is worth to remember that the data included in the figures does not include every time step of the simulation but just the stored solutions. Consequently, the peak velocity of the flame at the moment of shock formation may actually be significantly higher than the maximum shown in the figure.

The maximum flame velocity included in these results corresponds to the first sample stored following the regime transition. Upon the transition, the flame velocity experiences a slowdown for two reasons. On the one hand, once the front becomes supersonic it advances faster than the compression waves emitted by the flame and then it overtakes the compression waves causing the velocity of the flow ahead of it to decrease, reducing the absolute flame velocity due to the advection of the flow. On the other hand, for the same reason, the temperature of the flow ahead of the supersonic wave decreases, resulting in a reduction of the stable propagation velocity of the supersonic reactive wave.

Once the supersonic wave reaches the head of the compression wave, temperature and



#### 4 Deflagration-to-detonation transition at the tip of a flame in thin tubes

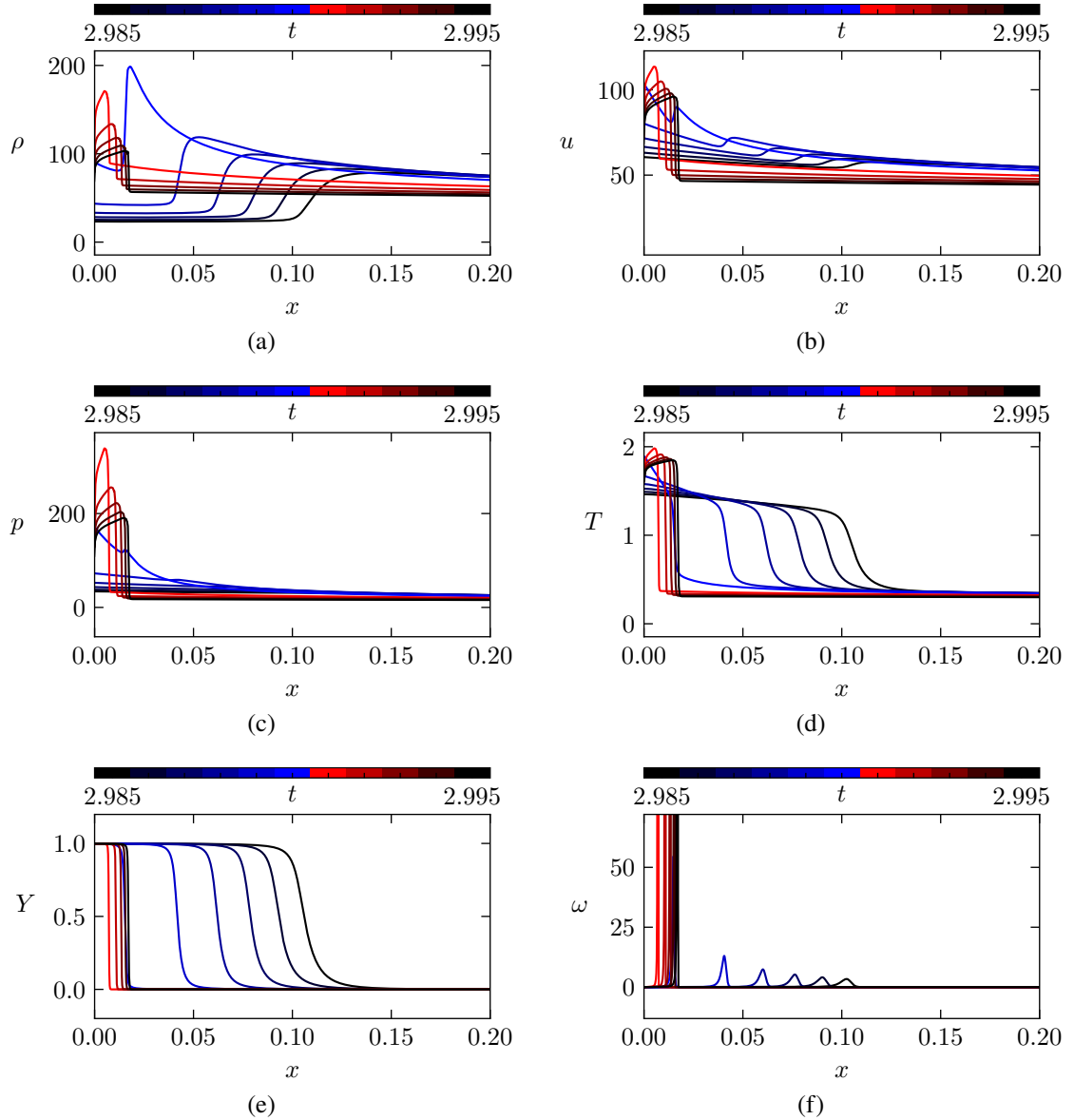


Figure 4.14: (a) Density, (b) flow velocity, (c) pressure, (d) temperature, (e) product mass fraction, and (f) reaction rate profiles in the flame-attached coordinate system during the fast flame acceleration, onset of detonation and relaxation to CJ regime. The profiles shown evolve from  $t = 2.985$  to  $t = 2.995$  in time steps of  $\Delta t = 0.001$  with the onset of the detonation taking place between  $t = 2.990$  (blue) and  $t = 2.991$  (red), and they are represented in the flame-attached coordinate system  $x = r - r_f(t)$  with  $r_f(t)$  defined as the position of the product mass fraction isovalue  $Y = 0.98$ . The thermochemical properties of the flame are characterized by the parameters summarized in Table 4.1.

#### 4.4 Internal flame structure

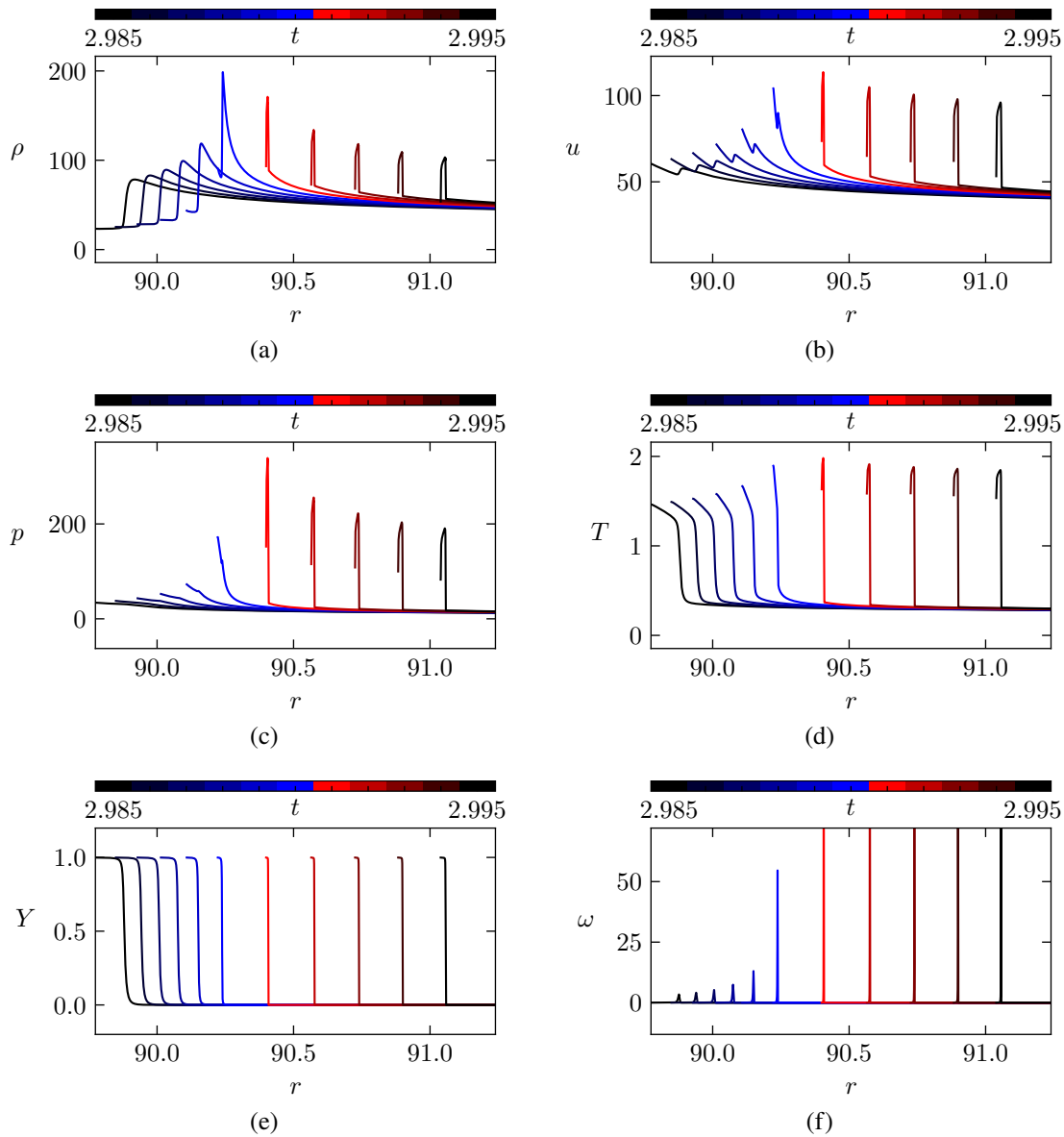


Figure 4.15: (a) Density, (b) flow velocity, (c) pressure, (d) temperature, (e) product mass fraction, and (f) reaction rate profiles in the fixed coordinate system of the tube during the fast flame acceleration, onset of the detonation and relaxation to CJ regime. The profiles shown evolve from  $t = 2.985$  to  $t = 2.995$  in time steps of  $\Delta t = 0.001$  with the onset of the detonation taking place between  $t = 2.990$  (blue) and  $t = 2.991$  (red), and they are represented in the fixed coordinate system of the tube with the origin being located at the initial position of the flame at  $t = 0$ . The thermochemical properties of the flame are characterized by the parameters summarized in Table 4.1.

#### 4 Deflagration-to-detonation transition at the tip of a flame in thin tubes

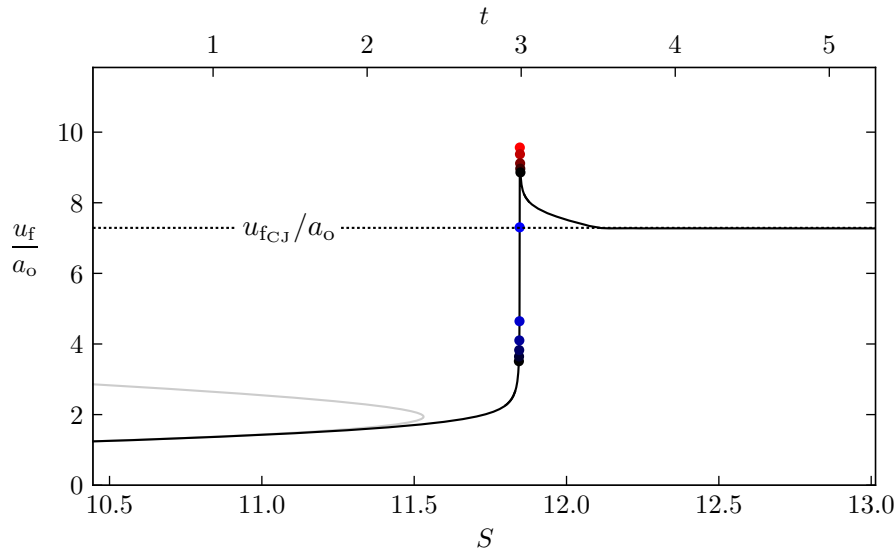


Figure 4.16: Flame propagating velocity to initial sound speed ratio as a function of the elongation parameter  $S$  (bottom axis) and time  $t$  (top axis). The colored circles in both figures correspond to the time steps for the profiles in Figures 4.14 and 4.15. The horizontal dotted line corresponds to the propagation velocity of a CJ detonation with respect to the initial sound speed considering the induced flow ahead of the wave as given by (4.129).

flow velocity ahead of it become uniform, leading to a constant propagation velocity. This constant absolute is actually equal to the CJ detonation velocity, augmented by the velocity of the flow ahead of the wave induced by the leading shock. In the notation followed in this chapter, this velocity is given by the expression

$$\frac{u_{fCJ}}{a_o} = \frac{D_{CJ}}{a_o} + \frac{u_N}{a_o} = \sqrt{\frac{\gamma+1}{2} \frac{q}{1-q} + \frac{T_N}{1-q}} + \sqrt{\frac{\gamma+1}{2} \frac{q}{1-q}} + \frac{u_N}{a_o} \quad (4.129)$$

whose result is represented by the dotted horizontal line in Figure 4.16.

### 4.5 Summary

The Deflagration-to-Detonation Transition, characterized by the sudden transformation of a diffusion-controlled flame into a supersonic reactive wave, in elongated flames propagating along thin tubes has been studied through a one-dimensional model representing the flame tip. The key element of this model is the backflow of burned gases from the flame skirt that drives initially the flame acceleration acting as a piston that pushes the reactive wave forward.

A double-discontinuity model, in which both the flame and the flame-driven shock wave were treated as discontinuities, has been investigated. Numerical solutions for the non-linear relationship between the flame velocity and the controlling elongation

parameter have been obtained in two different situations. In the first scenario, the backflow of burned gases remains constant and the flow between the flame and the shock is assumed uniform. In the second case, the backflow increases leading to the formation of compression waves ahead of the flame which do not reach the leading shock wave, so the flow between the flame and the shock remains isentropic. It has been illustrated that both situations exhibit a turning point where the acceleration of the flame becomes infinite.

Next, the internal flame structure of the flame has been considered in the study through the numerical integration of the reactive compressible conservation equations. The numerical results obtained for a constant backflow have been compared with the solution obtained from the double-discontinuity model showing satisfactory agreement and validating the existence of a turning point in the velocity ratio characterizing the elongation parameter. The results have also served to illustrate the self-similar nature of the external to the reactive and supersonic waves and to provide initial conditions for a time-dependent simulation. Finally, the evolution of the flame has been simulated by controlling the backflow of burned gases corresponding to a slowly increasing elongation parameter. The simulation results show that the relationship between the flame velocity and the elongation parameter initially follows the solutions of the double-discontinuity model. Near the turning point, the flame speed versus flame elongation trajectory moves away from the double-discontinuity solution, yet a strong acceleration is still observed after a short delay. Finally, during the strong acceleration, there is a rapid transition in the propagation regime. The reactive wave then relaxes to the corresponding CJ detonation regime.



---

## Conclusions and perspectives

---

In this chapter, the key findings and insights gained from the study the direct initiation of gaseous detonations in the small heat release asymptotic limit and the deflagration-to-detonation transition at the tip of elongated flames propagating along thin tubes are brought together. This chapter not only provides a summary of the research but also a discussion of the significance of the findings. Furthermore, this chapter outlines the limitations of the study and suggests possible directions for future research. Overall, this chapter concludes the thesis and highlights the contributions made to the understanding of the initiation of gaseous detonations.

### 5.1 Direct Initiation

In the small heat release limit coupled with the Newtonian approximation, the problem of the long time dynamics of the detonation initiation is reduced to a single hyperbolic equation. This asymptotic limit highlights the two-time-scale nature of the problem, which is also a characteristic of real detonations since the regime at the exit of the reaction zone is nearly sonic. The simplification is made possible since, in the limit of small heat release, the Mach number of the flow relative to the leading shock is close to unity throughout the detonation structure and the technical difficulty of the sound speed variation is avoided. In real detonations near the CJ regime, the nearly sonic condition is satisfied at the end of the reaction zone, but not close to the leading shock. The small heat release limit extends this condition to the entire internal structure of the detonation. Besides, the sound speed only changes slightly with temperature under the typical conditions found in detonations. The definition of the precise sonic plane, where

## 5 Conclusions and perspectives

the flow speed relative to the leading shock equals the local sound speed, may pose a greater challenge in real detonations. However, due to the weaker spatial change in sound speed compared to the flow speed, a small region where the flow speed with respect to the shock is significantly close to the local sound speed will still exist. Therefore, the fundamental physical mechanisms in detonations close to the CJ regime are retained in the asymptotic approximation.

Concerning the evolution of the leading shock propagating velocity in direct initiation, the limit of small heat release introduces differences that are mainly quantitative. The asymptotic limit yields analytical expressions for both the rarefaction flow in the discontinuous model of detonation and the combustion waves whose internal structure is in steady-state. Remarkably, these asymptotic solutions exhibit the same characteristic properties as those found in the opposite limit of large Mach number of propagation, reinforcing the relevance of the limit of small heat release in enhancing our understanding of detonation dynamics.

The analysis of the dynamics of the detonation considering the internal structure reveals that the evolution of the sonic plane inside the rarefaction wave is the key element of the overall dynamics. The time delay of the response of the detonation internal structure to the burnt-gas flow results in a slowdown mechanism when the sonic point, originally located in the burnt-gas away from the reaction wave in overdriven regimes, moves closer to the exit of the reaction zone. This mechanism explains the dynamics of the trajectories “propagation velocity vs. front radius” observed in direct numerical simulations for critical conditions of initiation. The detonation velocity drops below the CJ velocity and reaches a minimum associated with the onset of the sonic condition. This deceleration phase is followed by a re-acceleration back to the CJ regime, corresponding to an isolated combustion wave whose internal structure is out of equilibrium. During this nonlinear relaxation, the sonic point remains within the internal structure of the combustion wave, near the end of the reaction zone. Failure occurs if the deceleration of the detonation wave is so significant that the chemical-kinetics quenching takes place in the overdriven regime before the sonic point reaches the end of the reaction zone. The likelihood of failure increases as the radius at which the overdriven detonation velocity first crosses the CJ velocity decreases. Furthermore, this analysis clarifies how the self-similar solution for the rarefaction wave behind a CJ wave is reached in the long-time limit, showing a behaviour similar to the discontinuous model.

The detailed analysis of the critical dynamics has been limited to spherical geometries. Results from the discontinuous model and the leading shock trajectories considering the internal structure indicate that planar overdriven waves approach asymptotically the CJ regime in the long-time limit without exhibiting a critical condition or singular dynamics. With the physical mechanisms retained in this study the initiation of planar detonations with reduced activation energies of order unity are consistently successful. The longitudinal instability observed for larger values of activation energy has been extensively explored in the previous literature (see, for instance, Clavin and Williams (2002) and Tofaili et al. (2021)). Regarding cylindrical waves, the discontinuous model and the trajectories of the leading shock considering the internal structure reveal that the

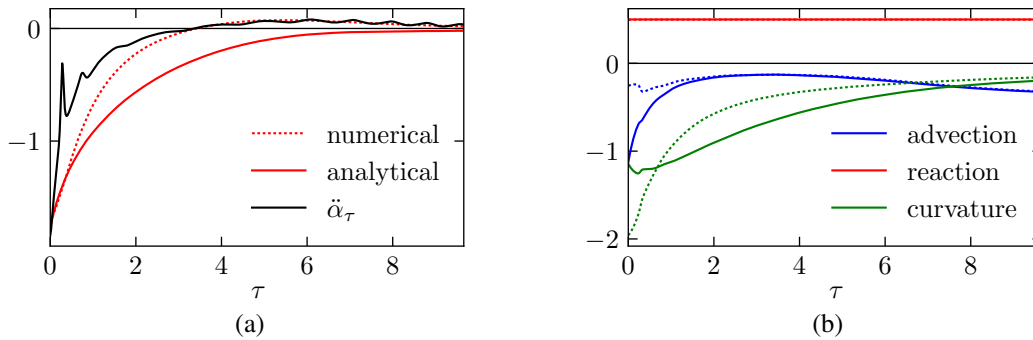


Figure 5.1: Analysis of the numerical results through numerical integration of (3.105). (a) The red line represents the evolution of the deviation from the steady-state solution obtained by integration of (3.105) using the analytical approximations that lead to (3.114) in solid line and through numerical integration of the results in dotted line. The black line represents the evolution of the time derivative of the propagation velocity  $\ddot{\alpha}_\tau \equiv d\dot{\alpha}_\tau/d\tau$  obtained numerically. (b) Term by term integration of (3.105) on the numerical results through analytical approximation in solid line and numerical integration in dotted line.

dynamics are qualitatively similar to those of spherical waves. The only distinction is quantitative, with the curvature effect of cylindrical waves being halved for equivalent front radii in spherical geometry. As a result, the curvature-induced decay is slower in cylindrical detonations and the predicted curvature-induced quenching is expected to occur at a radius that is half the critical radius for spherical detonations. The dynamics of the sonic point within the rarefaction wave plays similarly a essential role in both geometries.

### 5.1.1 Future work

A successful theory for direct initiation should provide an analytic expression that allows to compute the critical initiation energy based on the properties of the reactive mixture. In the small heat release limit, the steady-state curves obtained for an overdriven regime and a self-sustained regime provide an estimate of the critical radius at which the detonation should not decrease below the chemical-kinetics quenching velocity. A preliminary analysis of the numerical results (as illustrated in Figure 5.1) can help to elucidate the discrepancy found between the critical radius and the quasi-steady regime observed at the onset of the sonic condition.

The integration of the quasi-steady description of a self-sustained wave (3.105) on the internal structure using the numerical results reveals that a steady state is well established at the minimum of propagation velocity (as shown in Figure 5.1a). However, the approximations used to derive the analytic expression fail to predict a steady state solution in the corresponding front radius. An analysis of each term in the integration of (3.105) shows that the advection term is well approximated as the sonic point approaches



## 5 Conclusions and perspectives

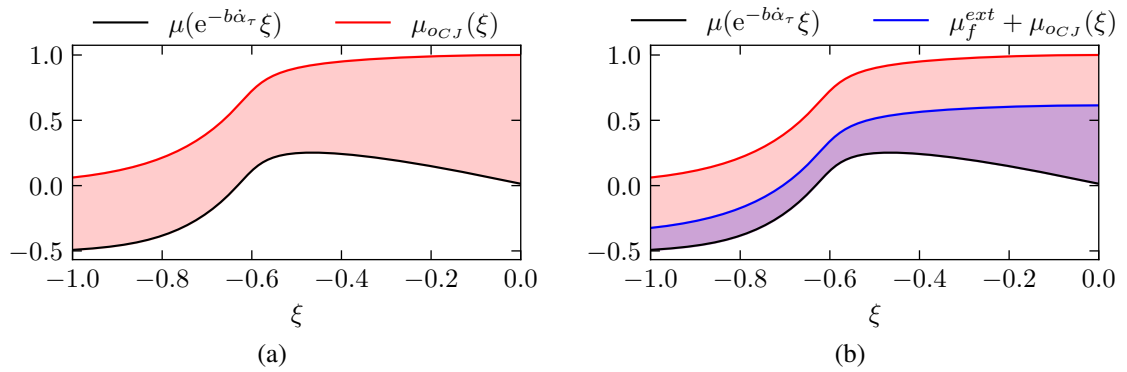


Figure 5.2: Flow velocity profile at  $\tau_s$  when the sonic point reaches the exit of the reaction zone

the exit of the reaction zone and the discrepancy is negligible around the steady state. The integration of the reaction term is straightforward due to the scaling law, thus the numerical results match precisely the analytical value. On the other hand, the approximation of curvature term yields a value that is twice the result obtained from the numerical calculations.

Examining the velocity profile at the onset of the sonic condition sheds light on the source of this discrepancy (as depicted in Figure 5.2a). In the overdriven regime, before the sonic condition isolates the internal structure of the detonation from the external rarefaction flow, the flow velocity at the exit of the reaction zone is well below the flow velocity at the exit of the reaction zone of the planar CJ wave. The difference between the CJ wave and the actual velocity profile at the onset of the sonic condition is quantified by the red area in Figure 5.2a.

An improvement of this approximation could be achieved by adding the burnt-gas flow velocity  $\mu_f^{\text{ext}}$  to the velocity profile of the CJ wave leading to a reduction in the error as shown in Figure 5.2b. This approximation may be useful in predicting the critical front radius at which the sonic condition is reached. However, it is important to note that this approximation will not be valid once the sonic point enters the reaction zone and the internal detonation structure becomes isolated from the external flow.

Moreover, the analysis of the critical dynamics has been restricted to a reduced activation energy of order unity due to the challenges in examining strongly unstable detonations in the limit of small heat release using a scaling law for the chemical kinetics, as pointed out by Clavin and Denet (2020). This approach, unfortunately, prevents the investigation of the curvature-induced quenching, which is predicted through a quasi-steady approximation for a large activation energy for a single-step kinetics rate law without cross-over temperature.

It is noteworthy that the radius at which the sonic condition is satisfied at the exit of a reaction zone in the overdriven regime is of the same order of magnitude as the critical radius for steady-state self-sustained waves. Future research will aim to explore the potential relationship between these two conditions and provide more accurate prediction

for the detonation radius where the sonic condition is verified. This will require the use of unsteady reaction rates different from the scaling law used in the present analysis.

Additionally, efforts will be made to improve the asymptotic analysis in the limit of small heat release in order to provide a more accurate quantitative analysis in relation to actual detonations. Furthermore, the phenomenon of shock wave re-ignition, observed when the propagation velocity approaches the acoustic regime yet the chemical kinetics continue to release heat of combustion deserves further investigation.

## 5.2 Deflagration-to-Detonation Transition

The one-dimensional model for elongated flames propagating from the closed end of a tube proposed by Clavin and Tofaili (2021) provides a relationship between the flame elongation and the flow that advects the flame from the burned gases side. Considering the flame as a discontinuity, the relationship between the flame elongation and the absolute flame velocity behind a flame-driven shock wave is determined by a closed set of nonlinear equations. The flame speed sensitivity to temperature introduces a thermal feedback loop between the leading shock and the flame speed. Furthermore, the backflow of burned gases that advects the flame in the Clavin and Tofaili (2021) model introduces an additional feedback loop between the burning velocity and the induced flow ahead of the flame. These two feedback effects combined give rise to a turning point in the steady solutions. For a set of thermochemical parameters characteristic of hydrogen-oxygen mixtures, the turning point corresponds to an absolute flame speed close to the speed of sound in the initial mixture. The turning point defines a critical flame elongation. Beyond this critical value, the double-discontinuity model has no solution.

The thermal feedback of the leading shock wave on the flame speed is the cause of the turning point in the steady solutions as was first recognized by Deshaies and Joulin (1989) using a somewhat different one-dimensional model. As Deshaies and Joulin stated, the existence of a turning point “follows from the faster-than-linear increase with reaction temperature of the local laminar burning velocity”. At the beginning of the flame acceleration process, the increase in burning velocity due to the increase in temperature induced by the compressive heating is negligible. However, given the exponential nature of the sensitivity with temperature, the relative increase in burning velocity eventually becomes equal to the relative increase in the advection flow of burned gases. It is then that the flame elongation parameter that links both velocities reaches a maximum value. Beyond this critical condition, a slight further increase in flame speed requires reducing the flame elongation to reach a stable solution.

The critical condition appears whether the flow between the flame and the leading shock is uniform, or whether the development of an isentropic compression wave between a steady leading shock wave and the flame is considered. Both scenarios correspond to two limiting cases between which the actual conditions are found. The compression wave issued from the flame actually develops at the same time as the shock wave accelerates and is therefore not isentropic. The critical flame elongation conditions in the second

## 5 Conclusions and perspectives

scenario vary with the intensity of the leading shock. The critical flame elongation decreases with the intensity of the precursor shock as it was mathematically formulated by Clavin (2022). The absolute flame velocity at critical conditions however is universal for a given reactive mixture.

An analytical expression for the critical flame velocity considering an isentropic compression has been obtained. This expression yields a value of critical velocity that is in reasonable good agreement with the critical speed defined by the turning point obtained numerically. Simplifying the expression for a critical flame velocity significantly lower than the sound speed, the analytic expression given by Clavin (2022) is recovered.

A more precise study of the critical conditions would have to consider the entropy increase in the compression wave when the shock wave is accelerate. However, this situation would correspond to an intermediate case between the uniform flow approach where the compression occurs within the shock wave and the consideration of an isentropic compression wave ahead of the flame. Therefore, the critical conditions in the more realistic conditions can be expected to lie between the critical condition defined for both situations.

The numerical study of the flame internal structure shows that when the flame elongation exceeds the critical value for a sufficient amount of time to allow the flame to adjust to the new conditions, the flame undergoes an abrupt violent acceleration. This strong acceleration corresponds to the singularity of the acceleration obtained in the solutions for a steady flame. During the strong acceleration, the flame thickness also shrinks abruptly, so that the velocity gradient within the internal flame structure becomes large enough for dissipative effects to become important. Dissipation mechanisms transform the macroscopic kinetic energy of the flow into internal thermal energy where steep velocity gradients develop. It can then be said that a shock wave develops within the internal flame structure. The temperature then rises rapidly and abruptly also due to the dissipation of kinetic energy. Under these conditions, autoignition of the reactive gases occurs and the onset of the detonation occurs.

As the detonation front propagates from the flame tip towards the tube walls, it blows away the flame envelope and the model of a backflow of burned gases from the flame skirt is no longer justified. However, once the strong detonation is initiated, it relaxes to the Chapman-Jouguet regime. In this regime, the detonation is isolated from the downstream conditions and the backflow of burned gases does not affect its propagation. The supersonic detonation wave catches the compression waves previously emitted by the flame. The reactive mixture through which the detonation propagates becomes less and less hot, resulting in a slowing of the propagation velocity. Once the detonation wave passes the leading edge of the compression wave, the reactive front propagates along a uniform flow with constant velocity. Thereafter, the propagation velocity coincides with the sum of the Chapman-Jouguet velocity and the flow velocity that advects the front.

The Deflagration-to-Detonation process concludes when the detonation wave reaches the precursor shock wave. In this study, the precursor shock wave has not been included in the simulations with a time-dependent flame elongation in order to reduce the computational cost. Therefore, a complete description of the process through which a

deflagration wave becomes a single detonation wave propagating in a uniform medium also requires the study of a detonation wave that catches form behind a shock wave.

In a strict sense, the relevance of numerical simulations based on the integration of the Navier-Stokes conservation equations during the onset of the detonation must be questioned. The formation of a shock wave involves spatiotemporal scales corresponding to the mean free path and the elastic collision frequency, where the continuum and local equilibrium assumptions are no longer accurate. Thus, the numerical results presented cannot provide an accurate description of the process of detonation onset due to the formation of a strong shock wave within the internal flame structure. Within the framework of the Navier-Stokes equations, it can only be concluded that the thermal feedback of the compression waves on the flame speed enhanced by the piston effect of a backflow of burned gases, leads to the finite-time singularity analyzed in Clavin (2022), which is likely to result in the formation of a shock wave at the flame tip. If true, this conjecture would mean that the condition  $S > S^*$  is sufficient for the onset of a detonation in the DDT process, and that the predetonation time should be close to the time needed by the flame elongation to exceed its critical value.

### 5.2.1 Future work

During the acceleration runaway, the burning velocity attains values that are comparable to the local sound speed. This calls into question the hypothesis that unsteadiness and compressibility are negligible in the region of burned gases, as previously assumed when deriving the expression for the flow burned gases impinging the flame tip  $u_b$  (4.76).

For instance, the analysis of the transient effects by Deshaies and Joulin (1989) was focused on the acoustic dynamics within the burned gas region. Deshaies and Joulin derived an evolution equation that accounts for the delay in the flame response to the boundary condition imposed at the closed end of the tube. The numerical solution to this equation revealed a ladder-like behavior in flame velocity, which aligns more closely with experimental observations.

The transient dynamics of the acoustic waves within the burned gas region, which is delimited by the point of contact of the flame with the tube and the flame tip, could be incorporated into the double-discontinuity model by introducing a time-delay in the backflow of burned gases. This time delay corresponds to the transit time of acoustic waves along the flame length, which is determined by the ratio of flame length to sound speed in the burned gases. A comprehensive analysis of the implications of such delay is currently under revision (Clavin, 2023).

The numerical study of the internal structure of the flame by integrating the full set of conservation equations can be performed including the burned gas region. In this way, the dynamics of the burned gases enclosed between the closed end of the tube and the flame envelope could be included in the study. This would also eliminate the approximation of constant density in this region. The integration domain would then be limited on the burned gas side by the closed end of the tube which imposes the condition of zero velocity. The increase of the flame surface would be considered in the numerical

## 5 Conclusions and perspectives

integration by adding the mass production rate corresponding to the burned gases in the flame skirt (4.74) to the mass conservation equation. The continuity equation would then be expressed as

$$\frac{\partial \rho}{\partial t} + \frac{\partial (\rho u)}{\partial r} = \dot{m}, \quad (5.1)$$

where  $\dot{m}$  is the mass production rate per volume unit given by (4.74).

Such simulation would include the unsteady and compressible gas dynamics in the region of burned gases. During the initial phase of slow flame acceleration, the acoustic time is much shorter than the characteristic time of flame acceleration so that the steady approximation for the burned gases is accurate. A similar backflow towards the reactive zone should be observed in this phase. Near the turning point however the acoustic and flame acceleration characteristic times could become comparable and the results may differ. Results obtained in such a study would help to confirm whether the backflow of burned gases is sufficient to reach the conditions that can promote the formation of a shock wave within the flame structure.

The main difficulty anticipated for this numerical study lies on the large domain that must be considered due to the large flame propagation speed around the critical point. More elaborate numerical integration strategies, such as adaptive mesh refinement or code parallelization, may be required to obtain results in a reasonable time.

Another aspect that has not been addressed in this study and is expected to play an important role in the DDT is related to the chemical-kinetics of the reactive mixture. The reaction rate has been modeled with a single Arrhenius-type law that describes well the thermal runaway that characterizes in general the reactions of combustion. However, it is known that the dominant elementary reactions for flames are typically not the same in detonations. In flames, which propagate at subsonic velocities over the reactive mixture, the diffusion of reactive radicals can contribute to the overall reaction mechanism, whereas in detonations this diffusion flux is limited by the supersonic character of the wave. Temperatures in the reactive zone are also higher in detonation than in deflagration, which modifies the balance of dominant elementary reactions. Therefore, the chemical-kinetics model should also consider a transition as a function of the front propagation conditions to include a more realistic description of combustion reactions.

---

## Bibliography

---

- Akkerman, V., V. Bychkov, A. Petchenko, and L.-E. Eriksson (2006). “Accelerating Flames in Cylindrical Tubes with Nonslip at the Walls”. *Combustion and Flame* 145.1-2, 206–219. DOI: 10.1016/j.combustflame.2005.10.011.
- Anderson, J. D. (2003). *Modern Compressible Flow: With Historical Perspective*. 3rd ed. McGraw-Hill Series in Aeronautical and Aerospace Engineering. McGraw-Hill.
- Bach, G. G., R. Knystautas, and J. H. Lee (1969). “Direct Initiation of Spherical Detonations in Gaseous Explosives”. *Symposium (International) on Combustion* 12.1, 853–864. DOI: 10.1016/S0082-0784(69)80466-2.
- Ballossier, Y. (2021). “Topologies de l’accélération de Flamme d’H<sub>2</sub>-O<sub>2</sub>-N<sub>2</sub> Dans Des Canaux Étroits : De l’allumage Jusqu’à La Détonation”. These de doctorat. Poitiers, France: Ecole nationale supérieure de mécanique et d’aérotechnique.
- Ballossier, Y., F. Virot, and J. Melguizo-Gavilanes (2021). “Strange Wave Formation and Detonation Onset in Narrow Channels”. *Journal of Loss Prevention in the Process Industries* 72, 104535. DOI: 10.1016/j.jlp.2021.104535.
- Bender, C. M. and S. A. Orszag (1999). *Advanced Mathematical Methods for Scientists and Engineers I*. New York, NY: Springer New York. DOI: 10.1007/978-1-4757-3069-2.
- Berthelot, M. and P. Vieille (1881). “On the Velocity of Propagation of Explosive Processes in Gases”. *CR Hebd. Seances Acad. Sci* 93.2, 18–21.
- Boivin, P., M. Le Boursicaud, A. Millan-Merino, S. Taieb, J. Melguizo-Gavilanes, and F. Williams (2022). “Hydrogen Ignition and Safety”. In: *Hydrogen for Future Thermal Engines*.
- Boulal, S., P. Vidal, and R. Zitoun (2016). “Experimental Investigation of Detonation Quenching in Non-Uniform Compositions”. *Combustion and Flame* 172, 222–233. DOI: 10.1016/j.combustflame.2016.07.022.
- Brailovsky, I., L. Kagan, and G. Sivashinsky (2012). “Combustion Waves in Hydraulically Resisted Systems”. *Philosophical Transactions of the Royal Society A: Mathematical, Physical and Engineering Sciences* 370.1960, 625–646. DOI: 10.1098/rsta.2011.0341.

## Bibliography

- Brailovsky, I. and G. I. Sivashinsky (2000). “Hydraulic Resistance as a Mechanism for Deflagration-to-Detonation Transition”. *Combustion and Flame* 122.4, 492–499. DOI: 10.1016/S0010-2180(00)00157-7.
- Bush, W. B. and F. E. Fendell (1970). “Asymptotic Analysis of Laminar Flame Propagation for General Lewis Numbers”. *Combustion Science and Technology* 1.6, 421–428. DOI: 10.1080/00102206908952222.
- Bychkov, V. V. and M. A. Liberman (2000). “Dynamics and Stability of Premixed Flames”. *Physics Reports* 325.4, 115–237. DOI: 10.1016/S0370-1573(99)00081-2.
- Bykov, V., A. Koksharov, M. Kuznetsov, and V. P. Zhukov (2022). “Hydrogen-Oxygen Flame Acceleration in Narrow Open Ended Channels”. *Combustion and Flame* 238, 111913. DOI: 10.1016/j.combustflame.2021.111913.
- Carnasciali, F., J. H. S. Lee, R. Knystautas, and F. Fineschi (1991). “Turbulent Jet Initiation of Detonation”. *Combustion and Flame* 84.1, 170–180. DOI: 10.1016/0010-2180(91)90046-E.
- Chamberlain, G., E. Oran, and A. Pekalski (2019). “Detonations in Industrial Vapour Cloud Explosions”. *Journal of Loss Prevention in the Process Industries* 62, 103918. DOI: 10.1016/j.jlp.2019.103918.
- Chapman, D. L. (1899). “VI. On the Rate of Explosion in Gases”. *The London, Edinburgh, and Dublin Philosophical Magazine and Journal of Science* 47.284, 90–104. DOI: 10.1080/14786449908621243.
- Charignon, C. and J.-P. Chièze (2013). “Deflagration-to-Detonation Transition by Amplification of Acoustic Waves in Type Ia Supernovae”. *Astronomy & Astrophysics* 550, A105. DOI: 10.1051/0004-6361/201220483.
- Charignon, C. (2013). “Transition Déflagration-Détonation dans les supernovae thermonucléaires”. PhD thesis. Université Paris Sud - Paris XI.
- Chaumeix, N., S. Pichon, F. Lafosse, and C. -. Paillard (2007). “Role of Chemical Kinetics on the Detonation Properties of Hydrogen /Natural Gas/Air Mixtures”. *International Journal of Hydrogen Energy*. ICHS-2005 32.13, 2216–2226. DOI: 10.1016/j.ijhydene.2007.04.008.
- Cheikhravat, H., N. Chaumeix, A. Bentaib, and C.-E. Paillard (2012). “Flammability Limits of Hydrogen-Air Mixtures”. *Nuclear Technology* 178.1, 5–16. DOI: 10.13182/NT12-A13543.
- Ciccarelli, G., N. Chaumeix, A. Z. Mendiburu, K. N’Guessan, and A. Comandini (2019). “Fast-Flame Limit for Hydrogen/Methane-Air Mixtures”. *Proceedings of the Combustion Institute* 37.3, 3661–3668. DOI: 10.1016/j.proci.2018.06.045.
- Clanet, C. and G. Searby (1996). “On the “Tulip Flame” Phenomenon”. *Combustion and Flame* 105.1, 225–238. DOI: 10.1016/0010-2180(95)00195-6.
- Clarke, J. F., D. R. Kassoy, N. Riley, and E. G. Broadbent (1986). “On the Direct Initiation of a Plane Detonation Wave”. *Proceedings of the Royal Society of London. A. Mathematical and Physical Sciences* 408.1834, 129–148. DOI: 10.1098/rspa.1986.0113.

- Clavin, P. and M. Champion (2022). “Asymptotic Solutions of Two Fundamental Problems in Gaseous Detonations”. *Combustion Science and Technology* 0.0, 1–32. DOI: 10.1080/00102202.2022.2041612.
- Clavin, P. (1985). “Dynamic Behavior of Premixed Flame Fronts in Laminar and Turbulent Flows”. *Progress in Energy and Combustion Science* 11.1, 1–59. DOI: 10.1016/0360-1285(85)90012-7.
- Clavin, P. (2019). “Advances in the Analytical Study of the Dynamics of Gaseous Detonation Waves”. *Comptes Rendus Mécanique*. Patterns and Dynamics: Homage to Pierre Couillet / Formes et Dynamique: Hommage à Pierre Couillet 347.4, 273–286. DOI: 10.1016/j.crme.2019.03.008.
- Clavin, P. (2022). “Finite-Time Singularity Associated with the Deflagration-to-Detonation Transition on the Tip of an Elongated Flame-Front in a Tube”. *Combustion and Flame* 245, 112347. DOI: 10.1016/j.combustflame.2022.112347.
- Clavin, P. (2023). “One-Dimensional Mechanism of Gaseous Deflagration-to-Detonation Transition”. *Journal of Fluid Mechanics, Under Review*.
- Clavin, P. and B. Denet (2018). “Decay of Plane Detonation Waves to the Self-Propagating Chapman–Jouguet Regime”. *Journal of Fluid Mechanics* 845, 170–202. DOI: 10.1017/jfm.2018.237.
- Clavin, P. and B. Denet (2020). “Analytical Study of the Direct Initiation of Gaseous Detonations for Small Heat Release”. *Journal of Fluid Mechanics* 897. DOI: 10.1017/jfm.2020.359.
- Clavin, P. and L. He (1996). “Stability and Nonlinear Dynamics of One-Dimensional Overdriven Detonations in Gases”. *Journal of Fluid Mechanics* 306, 353–378. DOI: 10.1017/S0022112096001334.
- Clavin, P., R. Hernández Sánchez, and B. Denet (2021a). “Asymptotic Analysis of the Critical Dynamics of Spherical Gaseous Detonations”. *Journal of Fluid Mechanics* 915, A122. DOI: 10.1017/jfm.2021.196.
- Clavin, P., R. Hernández Sánchez, and B. Denet (2021b). “Study of the Direct Initiation of Spherical Detonations”. XXV International Congress of Theoretical and Applied Mechanics (ICTAM). Milano, Italy.
- Clavin, P. and G. Searby (2016). *Combustion Waves and Fronts in Flows: Flames, Shocks, Detonations, Ablation Fronts and Explosion of Stars*. Cambridge University Press. 723 pp.
- Clavin, P. and H. Tofaili (2021). “A One-Dimensional Model for Deflagration to Detonation Transition on the Tip of Elongated Flames in Tubes.” *Combustion and Flame* 232, 111522. DOI: 10.1016/j.combustflame.2021.111522.
- Clavin, P. and F. A. Williams (2002). “Dynamics of Planar Gaseous Detonations near Chapman–Jouguet Conditions for Small Heat Release”. *Combustion Theory and Modelling* 6.1, 127–139. DOI: 10.1088/1364-7830/6/1/307.
- Courant, R., K. Friedrichs, and H. Lewy (1928). “On the Partial Difference Equations of Mathematical Physics”. *Mathematische Annalen* 100, 32–74. DOI: 10.1147/rd.112.0215.



## Bibliography

- Courant, R. and K. O. Friedrichs (1948). *Supersonic Flow and Shock Waves*. New York: Interscience Publishers, Inc. 488 pp.
- Crabtree, G. W., M. S. Dresselhaus, and M. V. Buchanan (2004). “The Hydrogen Economy”. *Physics Today* 57.12, 39–44. DOI: 10.1063/1.1878333.
- Cuadra, A., C. Huete, and M. Vera (2020). “Effect of Equivalence Ratio Fluctuations on Planar Detonation Discontinuities”. *Journal of Fluid Mechanics* 903, A30. DOI: 10.1017/jfm.2020.651.
- Darrieus, G. (1938). “Propagation d’un Front de Flamme”. La Technique Moderne and Congrès de Mécanique Appliquée Paris.
- Deshaies, B. and G. Joulin (1989). “Flame-Speed Sensitivity to Temperature Changes and the Deflagration-to-Detonation Transition”. *Combustion and Flame* 77.2, 201–212. DOI: 10.1016/0010-2180(89)90037-0.
- Döring, W. (1943). “On Detonation Processes in Gases”. *Annals of Physics* 43.421-436, 9.
- Dorofeev, S. B. (2011). “Flame Acceleration and Explosion Safety Applications”. *Proceedings of the Combustion Institute* 33.2, 2161–2175. DOI: 10.1016/j.proci.2010.09.008.
- Eckett, C. A., J. J. Quirk, and J. E. Shepherd (2000). “The Role of Unsteadiness in Direct Initiation of Gaseous Detonations”. *Journal of Fluid Mechanics* 421, 147–183. DOI: 10.1017/S0022112000001555.
- Faria, L. M. and A. R. Kasimov (2015). “Qualitative Modeling of the Dynamics of Detonations with Losses”. *Proceedings of the Combustion Institute* 35.2, 2015–2023. DOI: 10.1016/j.proci.2014.07.006.
- Faria, L. M., A. R. Kasimov, and R. R. Rosales (2015). “Theory of Weakly Nonlinear Self-Sustained Detonations”. *Journal of Fluid Mechanics* 784, 163–198. DOI: 10.1017/jfm.2015.577.
- Fickett, W. (1985). *Introduction to Detonation Theory*. Berkeley.
- Fickett, W. and W. C. Davis (2000). *Detonation: Theory and Experiment*. Courier Corporation. 420 pp.
- Gordon, P. V., L. Kagan, and G. Sivashinsky (2020a). “Parametric Transition from Deflagration to Detonation Revisited: Planar Geometry”. *Combustion and Flame* 211, 465–476. DOI: 10.1016/j.combustflame.2019.10.011.
- Gordon, P. V., L. Kagan, and G. Sivashinsky (2020b). “Parametric Transition from Deflagration to Detonation Revisited: Spherical Geometry”. *Combustion and Flame* 219, 405–415. DOI: 10.1016/j.combustflame.2020.05.015.
- Gordon, P. V., L. Kagan, and G. Sivashinsky (2021). “Parametric Transition from Deflagration to Detonation in Stellar Medium”. *Physical Review E* 103.3, 033106. DOI: 10.1103/PhysRevE.103.033106.
- Grosseuvres, R., A. Comandini, A. Bentaib, and N. Chaumeix (2019). “Combustion Properties of H<sub>2</sub>/N<sub>2</sub>/O<sub>2</sub>/Steam Mixtures”. *Proceedings of the Combustion Institute* 37.2, 1537–1546. DOI: 10.1016/j.proci.2018.06.082.

- He, L. (1996). “Theoretical Determination of the Critical Conditions for the Direct Initiation of Detonations in Hydrogen-Oxygen Mixtures”. *Combustion and Flame* 104.4, 401–418. DOI: 10.1016/0010-2180(96)00141-1.
- He, L. and P. Clavin (1994). “On the Direct Initiation of Gaseous Detonations by an Energy Source”. *Journal of Fluid Mechanics* 277, 227–248. DOI: 10.1017/S0022112094002740.
- Hernández Sánchez, R. and B. Denet (2023a). “Numerical Analysis of a Flame Acceleration Runaway Model for Thin Tubes”. *Combustion and Flame, Under Review*.
- Hernández Sánchez, R. and B. Denet (2023b). “Numerical Study of a 1D Model for DDT at the Tip of a Flame in Narrow Channels”. 11th European Combustion Meeting (ECM). Rouen, France.
- Hernández Sánchez, R., B. Denet, and P. Clavin (2022). “Critical Dynamics of Direct Initiation of Spherical Detonations”. 28th International Colloquium on the Dynamics of Explosions and Reactive Systems (ICDERS). Naples, Italy.
- Hirsch, C. (2007). *Numerical Computation of Internal and External Flows: Fundamentals of Computational Fluid Dynamics*. 2nd ed. Vol. 1. Oxford ; Burlington, MA: Elsevier/Butterworth-Heinemann. 656 pp.
- Hof, B., C. W. H. van Doorne, J. Westerweel, F. T. M. Nieuwstadt, H. Faisst, B. Eckhardt, H. Wedin, R. R. Kerswell, and F. Waleffe (2004). “Experimental Observation of Nonlinear Traveling Waves in Turbulent Pipe Flow”. *Science* 305.5690, 1594–1598. DOI: 10.1126/science.1100393.
- Huang, K. (1987). *Statistical Mechanics*. 2nd Edition.
- Huete, C., A. L. Sánchez, and F. A. Williams (2013). “Theory of Interactions of Thin Strong Detonations with Turbulent Gases”. *Physics of Fluids* 25.7, 076105. DOI: 10.1063/1.4816353.
- Ivanov, M. F., A. D. Kiverin, and M. A. Liberman (2011). “Hydrogen-Oxygen Flame Acceleration and Transition to Detonation in Channels with No-Slip Walls for a Detailed Chemical Reaction Model”. *Physical Review E* 83.5, 056313. DOI: 10.1103/PhysRevE.83.056313.
- Johnson, D. M. (2010). “The Potential for Vapour Cloud Explosions – Lessons from the Buncefield Accident”. *Journal of Loss Prevention in the Process Industries*. Papers Presented at the 2009 International Symposium of the Mary Kay O’Connor Process Safety Center 23.6, 921–927. DOI: 10.1016/j.jlp.2010.06.011.
- Jouguet, E. (1905). “Sur La Propagation Des Réactions Chimiques Dans Les Gaz”. *J. Maths. Pure Appl.* 7, 347.
- Kagan, L., P. Gordon, and G. Sivashinsky (2015). “An Asymptotic Study of the Transition from Slow to Fast Burning in Narrow Channels”. *Proceedings of the Combustion Institute* 35.1, 913–920. DOI: 10.1016/j.proci.2014.06.096.
- Kagan, L. and G. Sivashinsky (2003). “The Transition from Deflagration to Detonation in Thin Channels”. *Combustion and Flame* 134.4, 389–397. DOI: 10.1016/S0010-2180(03)00138-X.

## Bibliography

- Kagan, L. and G. Sivashinsky (2008). “Autoignition Due to Hydraulic Resistance and Deflagration-to-Detonation Transition”. *Combustion and Flame* 154.1, 186–190. DOI: 10.1016/j.combustflame.2007.11.007.
- Kagan, L. and G. Sivashinsky (2017). “Transition to Detonation of an Expanding Spherical Flame”. *Combustion and Flame* 175, 307–311. DOI: 10.1016/j.combustflame.2016.06.001.
- Kamenskihs, V., H. D. Ng, and J. H. S. Lee (2010). “Measurement of Critical Energy for Direct Initiation of Spherical Detonations in Stoichiometric High-Pressure H<sub>2</sub>–O<sub>2</sub> Mixtures”. *Combustion and Flame* 157.9, 1795–1799. DOI: 10.1016/j.combustflame.2010.02.014.
- Kasimov, A. R., L. M. Faria, and R. R. Rosales (2013). “Model for Shock Wave Chaos”. *Physical Review Letters* 110.10, 104104. DOI: 10.1103/PhysRevLett.110.104104.
- Kasimov, A. R. and D. S. Stewart (2005). “Asymptotic Theory of Evolution and Failure of Self-Sustained Detonations”. *Journal of Fluid Mechanics* 525, 161–192. DOI: 10.1017/S0022112004002599.
- Knystautas, R. and J. H. Lee (1976). “On the Effective Energy for Direct Initiation of Gaseous Detonations”. *Combustion and Flame* 27, 221–228. DOI: 10.1016/0010-2180(76)90025-0.
- Knystautas, R., J. H. Lee, I. Moen, and H. GG. Wagner (1979). “Direct Initiation of Spherical Detonation by a Hot Turbulent Gas Jet”. *Symposium (International) on Combustion*. Seventeenth Symposium (International) on Combustion 17.1, 1235–1245. DOI: 10.1016/S0082-0784(79)80117-4.
- Koksharov, A., V. Bykov, L. Kagan, and G. Sivashinsky (2018). “Deflagration-to-Detonation Transition in an Unconfined Space”. *Combustion and Flame* 195, 163–169. DOI: 10.1016/j.combustflame.2018.03.006.
- Koksharov, A., L. Kagan, and G. Sivashinsky (2021). “Deflagration-to-Detonation Transition in an Unconfined Space: Expanding Hydrogen-Oxygen Flames”. *Proceedings of the Combustion Institute* 38.3, 3505–3511. DOI: 10.1016/j.proci.2020.08.051.
- Korobeinikov, V. P. (1971). “Gas Dynamics of Explosions”. *Annual Review of Fluid Mechanics* 3.1, 317–346. DOI: 10.1146/annurev.fl.03.010171.001533.
- Kurdyumov, V., A. L. Sánchez, and A. Liñán (2003). “Heat Propagation from a Concentrated External Energy Source in a Gas”. *Journal of Fluid Mechanics* 491, 379–410. DOI: 10.1017/S0022112003005664.
- Kurganov, A. and E. Tadmor (2000). “New High-Resolution Central Schemes for Nonlinear Conservation Laws and Convection–Diffusion Equations”. *Journal of Computational Physics* 160.1, 241–282. DOI: 10.1006/jcph.2000.6459.
- Kuznetsov, M., M. Liberman, and I. Matsukov (2010). “Experimental Study of the Preheat Zone Formation and Deflagration to Detonation Transition”. *Combustion Science and Technology* 182.11-12, 1628–1644. DOI: 10.1080/00102202.2010.497327.
- Laffitte, P. (1925). “Recherches expérimentales sur l’onde explosive et l’onde de choc”. *Annales de Physique* 10.4 (4), 587–694. DOI: 10.1051/anphys/192510040587.
- Landau, L. D. (1944). “Slow Combustion Theory”. *Zhurnal Éksperimentalnoi i Teoreticheskoi Fiziki* 14.6, 240–244.

- Landau, L. D. and E. M. Lifshitz (1987). *Fluid Mechanics*. 2nd ed. Vol. 6.
- Lee, J. H., R. Knystautas, and N. Yoshikawa (1978). “Photochemical Initiation of Gaseous Detonations”. *Acta Astronautica* 5.11, 971–982. DOI: 10.1016/0094-5765(78)90003-6.
- Lee, J. H. S. and A. J. Higgins (1999). “Comments on Criteria for Direct Initiation of Detonation”. *Philosophical Transactions of the Royal Society of London. Series A: Mathematical, Physical and Engineering Sciences* 357.1764. Ed. by K. N. C. Bray and N. Nikiforakis, 3503–3521. DOI: 10.1098/rsta.1999.0506.
- Lee, J. H. S. (1977). “Initiation of Gaseous Detonation”. *Annual Review of Physical Chemistry* 28.1, 75–104. DOI: 10.1146/annurev.pc.28.100177.000451.
- Lee, J. H. S. (1984). “Dynamic Parameters of Gaseous Detonations”. *Annual Review of Fluid Mechanics* 16.1, 311–336.
- Lee, J. H. S. (2008). *The Detonation Phenomenon*. Cambridge University Press.
- Lee, J. H. S. (2016). *The Gas Dynamics of Explosions*. Cambridge University Press.
- Lee, J. H. S., B. H. K. Lee, and R. Knystautas (1966). “Direct Initiation of Cylindrical Gaseous Detonations”. *The Physics of Fluids* 9.1, 221–222. DOI: 10.1063/1.1761523.
- Li, J. H., F. X. Ye, H. Qian, and S. Huang (2019). “Time-Dependent Saddle–Node Bifurcation: Breaking Time and the Point of No Return in a Non-Autonomous Model of Critical Transitions”. *Physica D: Nonlinear Phenomena* 395, 7–14. DOI: 10.1016/j.physd.2019.02.005.
- Liberman, M., M. Ivanov, A. Kiverin, M. Kuznetsov, A. Chukalovsky, and T. Rakhimova (2010). “Deflagration-to-Detonation Transition in Highly Reactive Combustible Mixtures”. *Acta Astronautica* 67.7-8, 688–701. DOI: 10.1016/j.actaastro.2010.05.024.
- Liñán, A., V. N. Kurdyumov, and A. L. Sánchez (2012). “Initiation of Reactive Blast Waves by External Energy Sources”. *Comptes Rendus Mécanique. Out of Equilibrium Dynamics* 340.11, 829–844. DOI: 10.1016/j.crme.2012.10.033.
- Liñán, A., M. Vera, and A. L. Sánchez (2015). “Ignition, Liftoff, and Extinction of Gaseous Diffusion Flames”. *Annual Review of Fluid Mechanics* 47.1, 293–314. DOI: 10.1146/annurev-fluid-010814-014711.
- Liu, D., Z. Liu, and H. Xiao (2022). “Flame Acceleration and Deflagration-to-Detonation Transition in Narrow Channels Filled with Stoichiometric Hydrogen-Air Mixture”. *International Journal of Hydrogen Energy* 47.20, 11052–11067. DOI: 10.1016/j.ijhydene.2022.01.135.
- Mallard, E. and H. Le Chatelier (1881). “Sur Les Vitesses de Propagation de l’inflammation Dans Les Mélanges Gazeux Explosifs”. *Comptes Rendus Hebdomadaires des Séances de l’Académie des Sciences* 93, 145–148.
- Manson, N. (1987). “Historique de la découverte de l’onde de detonation”. *Le Journal de Physique Colloques* 48.C4, C4–37. DOI: 10.1051/jphyscol:1987401.
- Mazaheri, B. K. (1997). “Mechanism of the Onset of Detonation in Blast Initiation.” PhD thesis. Montreal, Canada: McGill University.
- Mazzali, P. A., F. K. Röpkke, S. Benetti, and W. Hillebrandt (2007). “A Common Explosion Mechanism for Type Ia Supernovae”. *Science* 315.5813, 825–828. DOI: 10.1126/science.1136259.

## Bibliography

- Melguizo-Gavilanes, J., Y. Ballossier, and L. Faria (2021a). “Experimental and Theoretical Observations on DDT in Smooth Narrow Channels”. *Proceedings of the Combustion Institute* 38.3, 3497–3503. DOI: 10.1016/j.proci.2020.07.142.
- Melguizo-Gavilanes, J., V. Rodriguez, P. Vidal, and R. Zitoun (2021b). “Dynamics of Detonation Transmission and Propagation in a Curved Chamber: A Numerical and Experimental Analysis”. *Combustion and Flame* 223, 460–473. DOI: 10.1016/j.combustflame.2020.09.032.
- Mével, R., S. Javoy, F. Lafosse, N. Chaumeix, G. Dupré, and C. -. Paillard (2009). “Hydrogen–Nitrous Oxide Delay Times: Shock Tube Experimental Study and Kinetic Modelling”. *Proceedings of the Combustion Institute* 32.1, 359–366. DOI: 10.1016/j.proci.2008.06.171.
- Mével, R., J. Sabard, J. Lei, and N. Chaumeix (2016). “Fundamental Combustion Properties of Oxygen Enriched Hydrogen/Air Mixtures Relevant to Safety Analysis: Experimental and Simulation Study”. *International Journal of Hydrogen Energy* 41.16, 6905–6916. DOI: 10.1016/j.ijhydene.2016.03.026.
- Mével, R., D. Davidenko, F. Lafosse, N. Chaumeix, G. Dupré, C.-É. Paillard, and J. E. Shepherd (2015). “Detonation in Hydrogen–Nitrous Oxide–Diluent Mixtures: An Experimental and Numerical Study”. *Combustion and Flame* 162.5, 1638–1649. DOI: 10.1016/j.combustflame.2014.11.026.
- Mikhel’son, V. A. (1893). “On the Normal Ignition Velocity of Explosive Gaseous Mixtures”. *Scientific Papers of the Moscow Imperial University on Mathematics and Physics* 10, 1–93.
- Ng, H. D. and J. H. S. Lee (2003). “Direct Initiation of Detonation with a Multi-Step Reaction Scheme”. *Journal of Fluid Mechanics* 476, 179–211. DOI: 10.1017/S0022112002002872.
- Ng, H. D. and J. H. S. Lee (2008). “Comments on Explosion Problems for Hydrogen Safety”. *Journal of Loss Prevention in the Process Industries. Hydrogen Safety* 21.2, 136–146. DOI: 10.1016/j.jlp.2007.06.001.
- Oran, E. S. (2015). “Understanding Explosions – From Catastrophic Accidents to Creation of the Universe”. *Proceedings of the Combustion Institute* 35.1, 1–35. DOI: 10.1016/j.proci.2014.08.019.
- Oran, E. S. and J. P. Boris (2005). *Numerical Simulation of Reactive Flow*. Cambridge University Press. 553 pp.
- Oran, E. S., G. Chamberlain, and A. Pekalski (2020). “Mechanisms and Occurrence of Detonations in Vapor Cloud Explosions”. *Progress in Energy and Combustion Science* 77, 100804. DOI: 10.1016/j.pecs.2019.100804.
- Oran, E. S. and V. N. Gamezo (2007). “Origins of the Deflagration-to-Detonation Transition in Gas-Phase Combustion”. *Combustion and Flame* 148.1-2, 4–47. DOI: 10.1016/j.combustflame.2006.07.010.
- Oriani, R. A. (1978). “Hydrogen Embrittlement of Steels”. *Annual Review of Materials Science* 8.1, 327–357. DOI: 10.1146/annurev.ms.08.080178.001551.
- Ott, J. D., E. S. Oran, and J. D. Anderson (2003). “A Mechanism for Flame Acceleration in Narrow Tubes”. *AIAA Journal* 41.7, 1391–1396. DOI: 10.2514/2.2088.

- Peters, R. D., M. Le Berre, and Y. Pomeau (2012). “Prediction of Catastrophes: An Experimental Model”. *Physical Review E* 86.2, 026207. DOI: 10.1103/PhysRevE.86.026207.
- Poinsot, T. and D. Veynante (2005). *Theoretical and Numerical Combustion*. 2nd ed.
- Poludnenko, A. Y., J. Chambers, K. Ahmed, V. N. Gamezo, and B. D. Taylor (2019). “A Unified Mechanism for Unconfined Deflagration-to-Detonation Transition in Terrestrial Chemical Systems and Type Ia Supernovae”. *Science* 366.6465. DOI: 10.1126/science.aau7365.
- Pomeau, Y., M. Le Berre, P.-H. Chavanis, and B. Denet (2014). “Supernovae: An Example of Complexity in the Physics of Compressible Fluids”. *The European Physical Journal E* 37.4, 26. DOI: 10.1140/epje/i2014-14026-1.
- Pomeau, Y. and P. Manneville (1980). “Intermittent Transition to Turbulence in Dissipative Dynamical Systems”. *Communications in Mathematical Physics* 74.2, 189–197. DOI: 10.1007/BF01197757.
- Ponizy, B., A. Claverie, and B. Veyssi re (2014). “Tulip Flame - the Mechanism of Flame Front Inversion”. *Combustion and Flame* 161.12, 3051–3062. DOI: 10.1016/j.combustflame.2014.06.001.
- Radulescu, M. I. and J. Tang (2011). “Nonlinear Dynamics of Self-Sustained Supersonic Reaction Waves: Fickett’s Detonation Analogue”. *Physical Review Letters* 107.16, 164503. DOI: 10.1103/PhysRevLett.107.164503.
- Radulescu, M. I., A. J. Higgins, J. H. S. Lee, and S. B. Murray (2000). “On the Explosion Length Invariance in Direct Initiation of Detonation”. *Proceedings of the Combustion Institute* 28.1, 637–644. DOI: 10.1016/S0082-0784(00)80264-7.
- Rankin, B. A., M. L. Fotia, A. G. Naples, C. A. Stevens, J. L. Hoke, T. A. Kaemming, S. W. Theuerkauf, and F. R. Schauer (2017). “Overview of Performance, Application, and Analysis of Rotating Detonation Engine Technologies”. *Journal of Propulsion and Power* 33.1, 131–143. DOI: 10.2514/1.B36303.
- Rayleigh, J. (1910). “Aerial Plane Waves of Finite Amplitude”. *Proceedings of the Royal Society of London. Series A, Containing Papers of a Mathematical and Physical Character* 84.570, 247–284. DOI: 10.1098/rspa.1910.0075.
- Ronney, P. D. (1995). “Some Open Issues in Premixed Turbulent Combustion”. *Modeling in Combustion Science*. Ed. by J. Buckmaster and T. Takeno. Lecture Notes in Physics. Berlin, Heidelberg: Springer, 1–22. DOI: 10.1007/3-540-59224-5\_1.
- R pke, F. K. and W. Hillebrandt (2005). “Full-Star Type Ia Supernova Explosion Models”. *Astronomy & Astrophysics* 431.2 (2), 635–645. DOI: 10.1051/0004-6361:20041859.
- Roy, G. D., S. M. Frolov, A. A. Borisov, and D. W. Netzer (2004). “Pulse Detonation Propulsion: Challenges, Current Status, and Future Perspective”. *Progress in Energy and Combustion Science* 30.6, 545–672. DOI: 10.1016/j.pecs.2004.05.001.
- S nchez, A. L. and F. A. Williams (2014). “Recent Advances in Understanding of Flammability Characteristics of Hydrogen”. *Progress in Energy and Combustion Science* 41, 1–55. DOI: 10.1016/j.pecs.2013.10.002.
- Sedov, L. I. (1946). “Propagation of Strong Shock Waves”. *Journal of Applied Mathematics and Mechanics* 10, 241–250.

## Bibliography

- Shchelkin, K. I. (1940). “Influence of Tube Roughness on Detonation Formation and Propagation in Gases”. *Sov. Phys.–JETP* 10, 823.
- Shelkin, K. I. (1940). “Influence of the Wall Roughness on Initiation and Propagation of Detonation in Gases”. *Zhurnal Éksperimentalnoi i Teoreticheskoi Fiziki* 10, 823.
- Shen, H. and M. Parsani (2017). “The Role of Multidimensional Instabilities in Direct Initiation of Gaseous Detonations in Free Space”. *Journal of Fluid Mechanics* 813, R4. DOI: 10.1017/jfm.2017.5.
- Sorin, R., R. Zitoun, and D. Desbordes (2006). “Optimization of the Deflagration to Detonation Transition: Reduction of Length and Time of Transition”. *Shock Waves* 15.2, 137–145. DOI: 10.1007/s00193-006-0007-4.
- Strang, G. (1968). “On the Construction and Comparison of Difference Schemes”. *SIAM Journal on Numerical Analysis* 5.3, 506–517. DOI: 10.1137/0705041.
- Taylor, G. (1941). “The Formation of a Blast Wave by a Very Intense Explosion I. Theoretical Discussion”. *Proceedings of the Royal Society of London. Series A. Mathematical and Physical Sciences* 201.1065, 159–174. DOI: 10.1098/rspa.1950.0049.
- Taylor, G. (1950a). “The Dynamics of the Combustion Products behind Plane and Spherical Detonation Fronts in Explosives”. *Proceedings of the Royal Society of London. Series A. Mathematical and Physical Sciences* 200.1061, 235–247. DOI: 10.1098/rspa.1950.0014.
- Taylor, G. (1950b). “The Formation of a Blast Wave by a Very Intense Explosion. II. The Atomic Explosion of 1945”. *Proceedings of the Royal Society of London. Series A, Mathematical and Physical Sciences* 201.1065, 175–186.
- Tofaili, H. (2022). “Revisiting Deflagration-to-Detonation Transition in the Context of Carbon-Free Energy”. PhD thesis. INSA de Rouen Normandie.
- Tofaili, H., G. Lodato, L. Vervisch, and P. Clavin (2021). “One-Dimensional Dynamics of Gaseous Detonations Revisited”. *Combustion and Flame* 232, 111535. DOI: 10.1016/j.combustflame.2021.111535.
- Toro, E. F. (2009). *Riemann Solvers and Numerical Methods for Fluid Dynamics: A Practical Introduction*. 3rd ed. Dordrecht ; New York: Springer. 724 pp.
- Treffers, R. R., A. V. Filippenko, S. D. van Dyk, M. W. Richmond, A. Martel, and R. W. Goodrich (1994). “Supernova 1994D in NGC 4526”. *International Astronomical Union Circular* 5946, 2.
- Urtiew, P. A., A. K. Oppenheim, and S. O. Saunders (1966). “Experimental Observations of the Transition to Detonation in an Explosive Gas”. *Proceedings of the Royal Society of London. Series A. Mathematical and Physical Sciences* 295.1440, 13–28. DOI: 10.1098/rspa.1966.0223.
- Urzay, J. (2018). “Supersonic Combustion in Air-Breathing Propulsion Systems for Hypersonic Flight”. *Annual Review of Fluid Mechanics* 50.1, 593–627. DOI: 10.1146/annurev-fluid-122316-045217.
- Veiga-López, F., M. Kuznetsov, D. Martínez-Ruiz, E. Fernández-Tarrazo, J. Grune, and M. Sánchez-Sanz (2020). “Unexpected Propagation of Ultra-Lean Hydrogen Flames in

- Narrow Gaps”. *Physical Review Letters* 124.17, 174501. DOI: 10.1103/PhysRevLett.124.174501.
- Veynante, D. and L. Vervisch (2002). “Turbulent Combustion Modeling”. *Progress in Energy and Combustion Science* 28.3, 193–266. DOI: 10.1016/S0360-1285(01)00017-X.
- Vidal, P. (2009). “Critical Slow Dynamics of Detonation in a Gas with Non-Uniform Initial Temperature and Composition: A Large-Activation-Energy Analysis”. *International Journal of Spray and Combustion Dynamics* 1.4, 435–471. DOI: 10.1260/175682709789685822.
- Vieille, M. (1900). “Étude Sur Le Role Des Discontinuités Dans Les Phénomènes de Propagation”. *J. Phys. Theor. Appl.* 9.1, 621–644. DOI: 10.1051/jphystap:0190000900062100.
- Von Neumann, J. (1942). *Theory of Detonation Waves*. Progress Report OSRD-549. National Defense Research Committee Div. B.
- Weng, Z., R. Mével, Z. Huang, F. Cai, and J. Xu (2021). “Direct Detonation Initiation: A Comparison between the Critical Curvature and Critical Decay Rate Models”. *Physics of Fluids* 33.9, 096110. DOI: 10.1063/5.0062506.
- Williams, F. A. (1985). *Combustion Theory*. CRC Press.
- Wolański, P. (2013). “Detonative Propulsion”. *Proceedings of the Combustion Institute* 34.1, 125–158. DOI: 10.1016/j.proci.2012.10.005.
- Wu, M. H., M. P. Burke, S. Son, and R. Yetter (2007). “Flame Acceleration and the Transition to Detonation of Stoichiometric Ethylene/Oxygen in Microscale Tubes”. *Proceedings of the Combustion Institute* 31.2, 2429–2436. DOI: 10.1016/j.proci.2006.08.098.
- Wu, M. H. and C.-Y. Wang (2011). “Reaction Propagation Modes in Millimeter-Scale Tubes for Ethylene/Oxygen Mixtures”. *Proceedings of the Combustion Institute* 33.2, 2287–2293. DOI: 10.1016/j.proci.2010.07.081.
- Yanez, J., M. Kuznetsov, and A. Souto-Iglesias (2015). “An Analysis of the Hydrogen Explosion in the Fukushima-Daiichi Accident”. *International Journal of Hydrogen Energy* 40.25, 8261–8280. DOI: 10.1016/j.ijhydene.2015.03.154.
- Zeldovich, I. B., G. I. Barenblatt, V. B. Librovich, and G. M. Makhviladze (1985). “Mathematical Theory of Combustion and Explosions”.
- Zeldovich, Y. and D. A. Frank-Kamenetskii (1938). “A Theory of Thermal Flame Propagation”. *Acta Phys. Chim.* 9, 341–350.
- Zeldovich, Y. B. (1940). “On the Theory of Detonation Propagation in Gaseous Systems”. *Journal of Experimental and Theoretical Physics* 1, 411–451.
- Zeldovich, Y. B. (1942). “On the Distribution of Pressure and Velocity in Products of Detonation Blasts, in Particular for Spherical Propagating Detonation Waves”. *Journal of Experimental and Theoretical Physics* 12, 389–406.
- Zeldovich, Ya. B., A. G. Istratov A. G., N. I. Kidin, and V. B. Librovich (1980). “Flame Propagation in Tubes: Hydrodynamics and Stability”. *Combustion Science and Technology* 24.1-2, 1–13. DOI: 10.1080/00102208008952419.



## *Bibliography*

- Zeldovich, Ya. B., S. M. Kogarko, and N. N. Simonov (1956). “An Experimental Investigation of Spherical Detonation of Gases”. *Soviet physics. Technical physics*. 1.8, 1689–1731.
- Zhang, B., H. D. Ng, and J. H. S. Lee (2012). “The Critical Tube Diameter and Critical Energy for Direct Initiation of Detonation in C<sub>2</sub>H<sub>2</sub>/N<sub>2</sub>O/Ar Mixtures”. *Combustion and Flame* 159.9, 2944–2953. DOI: 10.1016/j.combustflame.2012.06.010.
- Zhang, B., H. D. Ng, R. Mével, and J. H. S. Lee (2011). “Critical Energy for Direct Initiation of Spherical Detonations in H<sub>2</sub>/N<sub>2</sub>O/Ar Mixtures”. *International Journal of Hydrogen Energy* 36.9, 5707–5716. DOI: 10.1016/j.ijhydene.2011.01.175.
- Zitoun, R., D. Desbordes, C. Gueraud, and B. Deshaies (1995). “Direct Initiation of Detonation in Cryogenic Gaseous H<sub>2</sub>-O<sub>2</sub> Mixtures”. *Shock Waves* 4.6, 331–337. DOI: 10.1007/BF01413875.